Scuola Normale Superiore di Pisa
Faculty of Mathematical and Natural Sciences

PhD Course in

Neurobiolgy

RISC-mediated control of selected chromatin regulators stabilizes ground state pluripotency of mouse embryonic stem cells

Thesis of

Luca Pandolfini

Tutor:

Prof. Federico Cremisi

Academic Year 2014/2015

Contents

List of Figures

Abstract

Embryonic stem (ES) cells are intrinsically unstable, spontaneously differentiating if they are not shielded from external stimuli. Although the nature of such instability is still controversial, growing evidence suggests that protein translation control may play a crucial role. We performed an integrated analysis of RNA and proteins at the transition between naïve ES cells and cells primed to differentiate. During this transition, mRNAs coding for chromatin regulators were specifically released from translational inhibition mediated by RNA-Induced Silencing Complex (RISC). This suggests that, prior to differentiation, the propensity of ES cell to change their epigenetic status is hampered by RNA interference. The expression of these chromatin regulators was reinstated following acute inactivation of RISC, and it correlated with loss of stemness markers and activation of early cell differentiation markers in treated ES cells. We propose that RISC-mediated inhibition of specific sets of chromatin regulators is a primary mechanism of preserving ES cell pluripotency while maintaining cells in a metastable state.

Introduction

1.1 Mouse Embryonic Stem Cells

Stem cells may be functionally defined as cells having the capacity to generate daughter cells identical to their mother (self-renewal) as well as the ability to produce progeny with more restricted potential (differentiated cells; Smith, 2001). If a cell, upon differentiation, is able to produce all three germ layers (endoderm, mesoderm and ectoderm), thus giving rise to all fetal or adult cell types, that cell is said to be pluripotent. Different types of pluripotent stem cells have been derived from mouse embryos so far. Mouse embryonic stem (ES) cells are derived from the inner cell mass (ICM) of preimplantation embryos (Figure 1.1). These cells can be indefinitely cultured *in vitro* without loss of developmental potency, as demonstrated by their ability to generate cell and tissue types of all three germ layers *in vitro*. The observation that no bias can be detected in the colonization pattern of ES cell in diploid host embryos is another proof that ES cells are able to produce functional differentiated progeny in all tissues and organs (Beddington and Robertson, 1989). Moreover, the definition of embryonic stem cell comprises the ability to form chimeras when injected into tetraploid host embryos. Tetraploid embryos are generated by treatment of cleavage-stage mouse eggs with the mitotic drug Cytochalasin B. These embryos are capable of developing extraembryonic tissues but fail to generate fetal lineages. Consequently, chimeras of tetraploid and diploid cells give rise to embryos composed almost exclusively of diploid cells (Tarkowski et al., 1977),

provided that diploid cells are pluripotent. A further assay to test pluripotency is the formation of teratomas, which are tumors naturally occurring as germ line neoplasms, composed by tissues belonging to all three germ layers. The ability to give rise to teratomas when grafted into immunocompromised mice is a key feature of pluripotent cells.

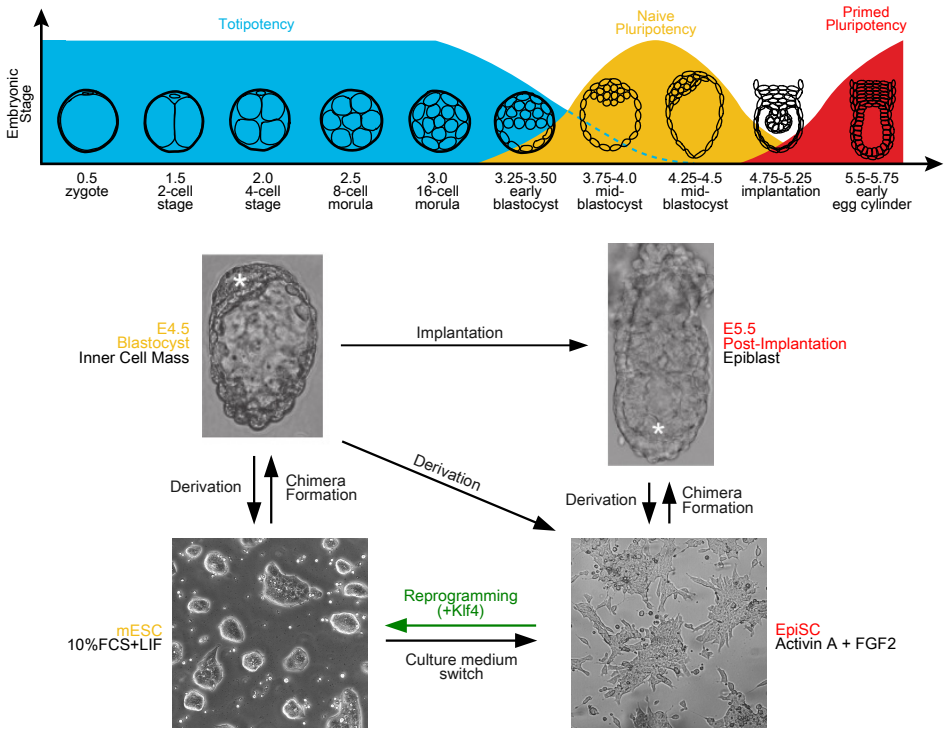

Figure 1.1: Different flavours of pluripotency

Upper graph shows the progression of the very early stages of mouse embryogenesis and the corresponding pluripotency states. Numbers indicate days *post-coitum*. Lower diagram shows the relationships between *in vitro* and *in vivo* populations of stem cells. Adapted from Nichols and Smith, 2009,2012.

1.2 Molecular circuits of pluripotency

Mouse ES cells were first isolated and cultured on a feeder layer of mouse embryonic fibroblasts that were mitotically inactivated by treatment with mitomycin C or γ-irradiation. The presence of a feeder layer then proved to be

necessary as a source of cytokine leukemia inhibitory factor (LIF), which addition to culture medium can replace the requirement for feeders. LIF, a member of the interleukin-6 family of cytokines, activates the gp130 receptor, directing ES cell self-renewal and the retention of undifferentiated phenotype through the activation of the transcription factor STAT3 (Matsuda et al., 1999; Niwa et al., 1998). In serum-free cultures, however, LIF is insufficient to block neural differentiation and to maintain pluripotency; indeed, bone morphogenetic proteins (BMPs), which induce the expression of Id genes via the Smad pathway, are required to propagate ES cells without serum or feeders in combination with LIF (Ying et al., 2003). The ES cell state is characterized by a defined network of transcription factors, orchestrated by Oct3/4 (Pou5f1). Oct-3/4 is a POU family transcription regulator whose expression is restricted to early embryos, germ line cells, and ES cells (Pesce et al. 1998). Oct-3/4 is necessary for both the development of ICM (Nichols et al. 1998) and the maintenance of ES cells (Niwa et al. 2000). The Sry-related HMG box transcription factor Sox2 (Ambrosetti et al. 1997) is a well-known partner of Oct-3/4, with which is co-expressed in the ICM of pre-implantation embryos, ES cells, and germ cells. HMG box in Sox2 interacts with the minor groove of the DNA helix and induces strong bending in the DNA molecule. This elicits transcriptional activation mediated by the functional association with Oct3/4.

Another important factor is the divergent NK2-class homeobox protein Nanog, named after the mythological celtic land of the ever young Tir nan Og (Chambers et al., 2003). Nanog is expressed *in vivo* in the ICM or epiblast of a preimplantation blastocyst, and in postmigratory germ cells. The interplay of Oct3/4 and Nanog has a crucial role in maintaining the core circuitry of pluripotent stem cells: while Oct3/4 safeguards the stemness blocking differentiation into trophoblast but tending to trigger differentiation into primitive endoderm and germ layers, Nanog may support the expression of Oct4 counteracting its differentiation effects. The instructive and permissive signals that control the binary

choice of self-renewal and differentiation of ES cells are constituted by both growth the factors provided by the microenvironment (or "stem cell niche") and autocrine signals produced by stem cells themselves. In this regard a pivotal role of FGF signaling in destabilizing the pluripotency has been elucidated (Kunath et al., 2007). Indeed, BMP/Smad/Id and LIF/STAT3 signalling do not instruct self-renewal but rather act to preserve the pluripotent state shielding the cells from differentiation-inducing clues: as a result of this, ES cells insulated from mitogen-activated protein kinase (ERK1/2) pathway signalling, which is normally activated by the autoinductive stimulation of fibroblast growth factor-4 (FGF4), remain undifferentiated even in a minimal medium devoid of BMP and serum (Ying et al., 2008; Figure 1.2).

On the other hand, the Erk cascade directs the conversion of ES cells to a transient state, corresponding to egg cylinder epiblast, which is called a "primed" state of pluripotency, distinct from the former "ground" or "naïve" pluripotency. Primed cells intrinsically tend to undergo a neural fate differentiation as a response of ongoing FGF and Notch signalling (Lowell et al., 2006), but remain prone to receive the instructions by other morphogens as TGF-β superfamily members, which are able to steer their fate to other lineages, starting from an endo-mesodermal identity. Cells in this competent state are able to rapidly evolve toward the generation of the three germ layers, nevertheless they can be captured and halted by the derivation of a population of stem cells *in vitro*, namely epiblast stem cells.

1.3 Epiblast stem cells

Epiblast stem cells (EpiSCs) are a type of pluripotent cells derived from the columnar epithelial epiblast of postimplantation (E5.5-E7.5) mouse embryos. Like ES cells, EpiSCs are considered to be pluripotent, as they pass the teratoma formation test, but they are not able to contribute to tetraploid blastocyst complementation. (Guo et al., 2009; Tesar et al., 2007). Mouse ES cells

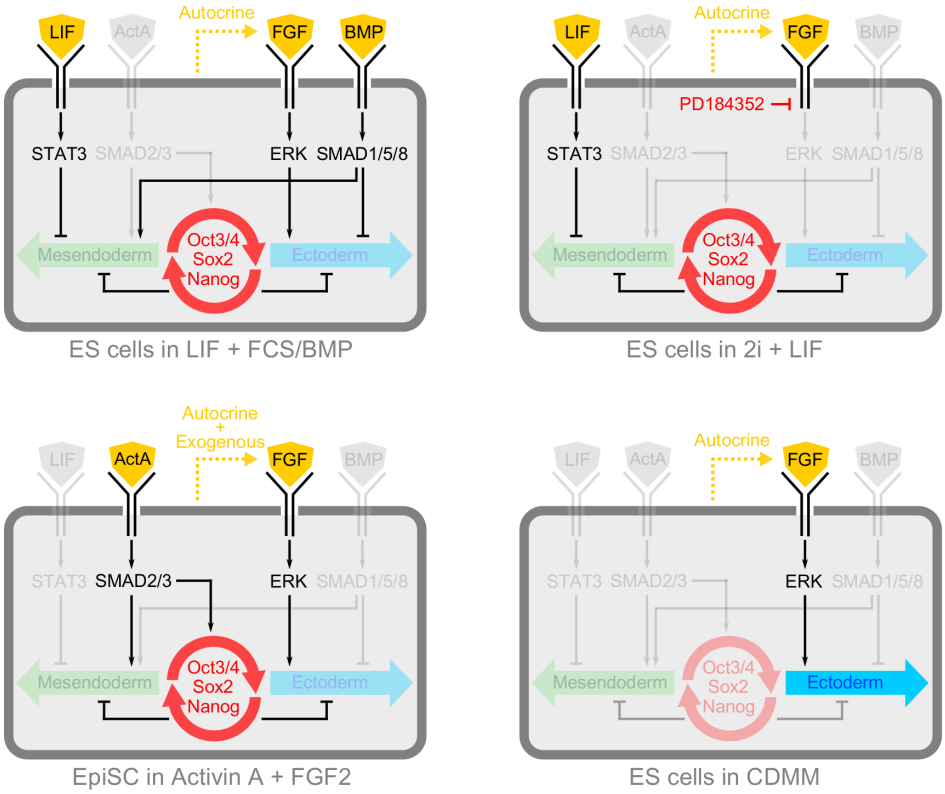

Figure 1.2: Signaling pathways of pluripotency

LIF, BMP, Activin and FGF act, in different pluripotency states, to maintain the molecular equilibrium which ensures cell self-renewal. 2iL: dual inibition of FGF receptor and GSK-3.

and EpiSCs display a different morphology, which takes account of the different developmental origin of the two populations: while ES cell grow as dome-shaped, light-refracting colonies that can be replated clonally, EpiSCs form adherent colonies with spindle-like cells at the borders, and they need to be dissociated as small clumps in order to overcome their low clonogenicity. These two states of pluripotency are distinguished also from the metabolic point of view: in fact, ES cells utilize oxidative phosphorylation, dynamically switching from glycolysis to mitochondrial respiration according to their needs, whereas EpiSC are almost entirely glycolytic, with very low mitochondrial respiration activity (Zhou et al., 2012).

1.4 Molecular dissection of primed pluripotency state

These divergent, macroscopic features are likely explained by the differences in the signaling pathways required for self-renewal: while ES need LIF and direct or indirect inhibition of MAPK activity, EpiSCs require FGF and Activin/Nodal signalling to be derived and sustain their self-renewal. In particular, Activin stimulation of Smad2/3 pathway is a strong activator of Nanog expression in EpiSCs. In turn, Nanog prevents neuroectoderm differentiation induced by FGF signalling. At the same time Nanog dampens the transcriptional activity of Activin/Nodal pathway on the progression of mesendoderm differentiation, through a direct interaction with Smad2/3. This feedback loop produces a stasis of both neuroectoderm and mesendoderm development, resulting in pluripotency of hES and mouse EpiSCs (Vallier et al., 2009). EpiSCs express high levels of Oct3/4 and Sox2, but activate the transcription of the epiblast-specific marker Fgf5 and other early differentiation markers according to the developmental stage in which cells have been derived (Bernemann et al., 2011). Conversely, they display intermediate levels of Nanog (Chambers et al., 2003), and very low amounts of Klf4, Rex1, Dax1 and Essrb, which compose a signature of ground-state ICM-specific pluripotency genes. Klf4 is one of the members of the Krüppel-like factor family and is remarkably down-regulated during transition from ES cells to EpiSCs. Klf4 has been implicated in the maintenance of ES cell pluripotency (Jiang et al., 2008), since it shares many common targets of Nanog, which is also a direct target of Klf4, suggesting a close functional relationship between the two factors. Klf4 is induced by Lif/Stat3 signalling in ES cells, but not in EpiSCs. Rex1 (Zfp-42) gene, which encodes a zinc finger protein, is expressed at high levels in the inner cell mass (ICM) of the day 4.5 mouse blastocyst, but fails to be detected in day 7.5 to 12.5 mouse embryo, and is down-regulated *in vitro* upon differentiation (Pelton et al., 2002; Hosler et al., 1989). A region required for Rex-1 promoter activity contains an octamer motif which serves as a binding site for POU domain transcription factors, and it is

sufficient to drive expression of the bacterial lacZ gene in mouse embryos at the morula stage (Hosler et al., 1989). Dax1 (dosage-sensitive sex reversal, adrenal hypoplasia critical region, on chromosome X, gene 1; Nr0b1) and Esrrb (estrogen-related receptor beta) are two orphan nuclear receptor genes displaying a ground-state specific expression (restricted to ES cells and ICM). Dax1 is able to form a complex with the POU-specific domain of Oct3/4; as a result, it can repress the transcription of Oct3/4: since too high levels of this key gene trigger differentiation, Dax1 serves as a rheostat for Oct3/4 expression, in order to maintain self-renewal of ES cells (Sun et al. 2009). Esrrb interacts with Oct3/4, and the association of Esrrb and Oct3/4 enhances the promoter activity of the Nanog gene. Conversely, Esrrb is a diret downstream target of Nanog, being necessary and sufficient to confer cytokine-independent self-renewal and pluripotency (Festuccia et al., 2012). Despite being characterized by distinct features and molecular circuits, ES and EpiSCs represent two subsequent states of pluripotency naturally evolving one into the other, as observed both *in vivo* and *in vitro*. Indeed, ES cells transferred into EpiSC culture medium maintain their self-renewal, becoming EpiSC-like. On the other hand, the overexpression of Klf4 in ground state culture conditions is sufficient to revert the priming of EpiSC, yelding undifferentiated colonies with ICM-like properties and capable to contribute to chimera formation (Guo et al., 2009). This strongly supports the idea that the restriction of pluripotency occuring in the early phases of mammalian embryogenesis is a rather gradual process, during which ES cells display a highly dynamic behaviour, as they continuously fluctuate between a ground-state and a primed phenotype (Hayashi et al., 2008). Intriguingly, human embryonic stem cells (hES; Thomson et al. 1998), although derived from preimplantation embryos, appear to be more close to EpiSCs than to mouse ES cells (Brons et al. 2007; Tesar et al. 2007). This seems likely to be due to the inherent different stage in developmental time of derivation than the result of species-specific differences. As a matter of fact, the overexpression of Nanog

and Klf2 and the inhibition of ERK and protein kinase C in hES cells restores the molecular network which supports ground-state pluripotency in mouse ES cells, resulting in the conversion of hES cells to a state closely resembling naïve pluripotency (Takashima et al., 2015).

1.5 Epigenetic remodelling during priming

One key feature distinguishing ES cells from EpiSCs is the presence of two active X chromosomes in female cells. In female embryos, the paternally inherited X chromosome is silenced during cleavage and remains silent in extraembryonic lineages. Reactivation occurs transiently in the pluripotent lineage prior to implantation (Heard, 2004), and this is the status which is captured following derivation of mouse ES cells. Conversely, immunocytodetection of female-derived EpiSCs shows nuclear staining for the repressive histone modification trimethylated H3 lysine 27 (me3H3K27), that is diagnostic of a silent X chromosome (Silva et al., 2003), the inactive Barr body. This represent a macroscopic epigenetic modification, that accompanies many global changes in the regulation of chromatin during the transition from ground to primed pluripotent state. In fact, electron spectroscopic imaging permitted to observe that ES cells have less heterochromatin and less condensed constitutive heterochromatin than differentiated cells, as a result of massive compaction of chromatin during priming. This accounts for the massive ultrastructural changes which parallel lineage commitment (Ahmed et al., 2010). A common feature of both naïve and primed pluripotency is the inherent proliferation, necessary for cell self-renewal. Nevertheless, detailed analysis of the topology of genome replication timing reveals that exit from the ground state is characterized by the consolidation of smaller replication domains into larger units with differing replication timing, a process which is accompanied by rearrangements in the subnuclear position of replication and transcriptional units (Hiratani et al., 2008). Overall these changes point to the evidence of a reorganization of higher-order chromosome structure

and function during differentiation. In fact, it is becoming clear that nuclear architecture and three-dimensional spatial positioning contribute to gene regulation. Microscopic observations of sub-nuclear gene localization showed a spatial compartmentalization of chromosomal domains: ES cell locate gene-enriched regions of DNA in the center of the nucleus, while gene-depleted regions or centromeres are found in the nuclear periphery. Upon differentiation, pluripotency genes are relocated from the center of the nucleus to the nuclear lamina to become silenced (Peric-Hupkes et al., 2010; Figure 1.3).

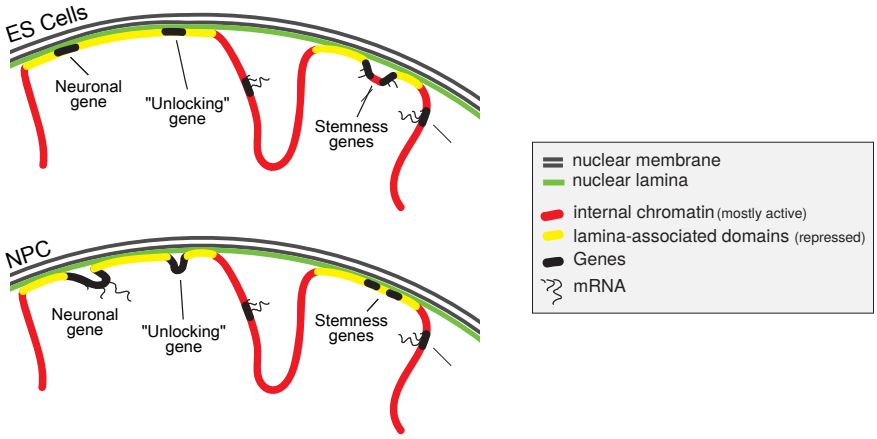

Figure 1.3: Dynamic reshaping of nuclear localization during differentiation
Scheme of gene localization and chromatin domain conformation in ES cells and neural cells. Adapted from Peric-Hupkes et al., 2010.

Nuclear architecture can be altered by a number of distinct mechanisms which include DNA modifications (e.g., cytosine methylation and cytosine hydroxymethylation), post-translational modifications of histones (e.g.,, phosphorylation, acetylation, methylation and ubiquitylation), the incorporation of histone variants, ATP-dependent chromatin remodelling and non-coding RNA (ncRNA)-mediated pathways. During early embryonic development, genomic methylation profiles rapidly change, defining distinct epigenetic levels (Reik et al., 2001). Experimental depletion of both Dnmt3a and Dnmt3b activity results in lethality of early postimplantation embryos, demonstrating that de novo methylation is an

essential process for mammalian development (Okano et al., 1999). Extensive reprogramming of global methylation pattern is a key event in ES cell priming; indeed, several pluripotency-related genes as well as widespread genomic loci are hypomethylated in ICM embryos and ground-state stem cells (Farthing et al., 2008; Leitch et al., 2013), and global DNA hypermethylation occurs in epiblast cells (Smith et al., 2014).

Genome-wide maps of epigenetic modifications permitted to highlight the presence in ES cells of widespread active chromatin domains, which are distinguished by the enrichment of both histone acetylation and H3K4me3 (Roh et al., 2005; Barski et al.,2007). Enhancers of both pluripotency genes and developmental commitment genes are marked by H3K4me1 modification and histone acetyltransferase p300. The presence of H3K27ac defines enhancers of pluripotency genes as active, whereas enhancers of developmental genes are in a "poised" state, being enriched in H3K27me3 and lacking H3K27ac. Transcriptional elongation is prevented at these genes by promoter-proximal RNA polymerase II (Pol II) pausing. Following priming, lineage-specific genes acquire chromatin modifications marking active promoter and enhancer regions, and Pol II pausing is released to permit the elongation of the transcript. Conversely, promoters of genes of other lineages gain H3K27me3, which results in transcriptional repression. Pluripotency genes aquire H3K9 methylation and DNA methylation, becoming stably silenced. Upon differentiation, heterochromatic regions, characterized by H3K9me2 and H3K9me3 marks, binding of HP1 (heterochromatin protein 1) and DNA methylation at CpG sites, start to expand and become more condensed. H3K27me3 signature is also expanded in both intergenic regions and repressed genes, to form large domains featuring the differentiated lineage (Chen and Dent, 2014; Figure 1.4).

For successful differentiation of ES cells, active enhancers which control ES cell-specific genes must be inactivated. Histone H3K4/K9 demethylase Lsd1 (Kdm1a) has been reported to modulate the inactivation of ES cell-specific

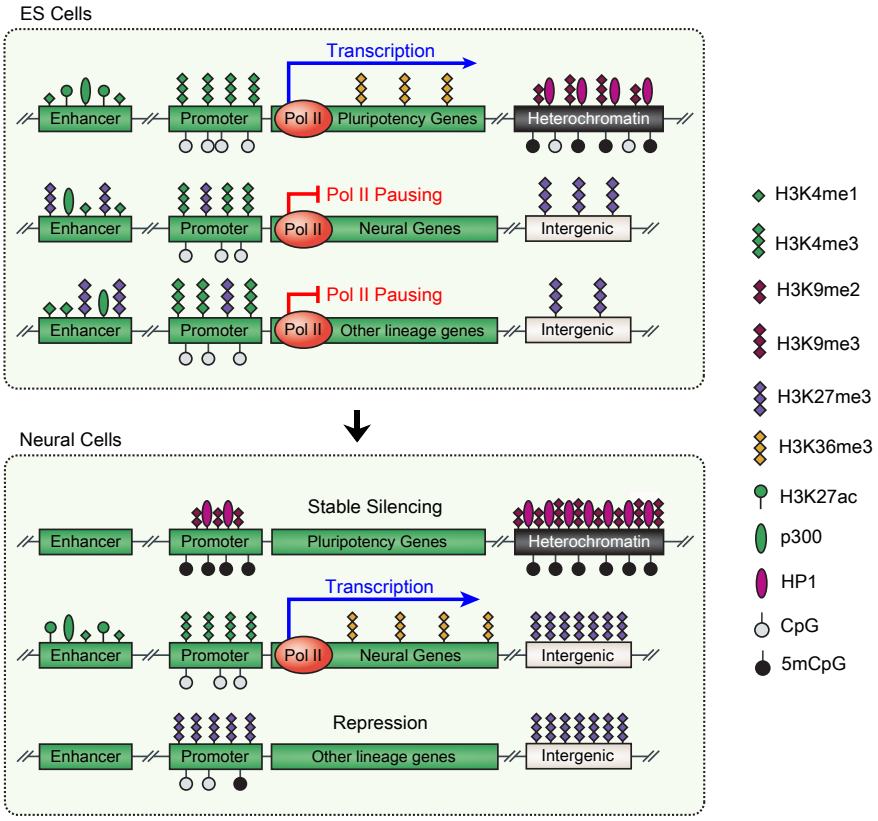

Figure 1.4: Epigenetic rearrangement during differentiation

Scheme shows how epigenetic features evolve upon exit from ground pluripotent state. Adapted from Chen and Dent, 2014.

enhancers (Whyte et al., 2012). Nucleosome remodelers are required for establishing and maintaining the overall structure and long-range interactions of chromatin, which have clear functional impact on the molecular networks of pluripotency. For example, mammalian SWI/SNF family (orthologue of yeast SWItch/Sucrose Non-Fermentable cluster, one of the most-studied families of ATP-dependent chromatin-remodelling factors), occupy the loci of many pluripotency transcription factors like Oct4, Sox2 and Nanog (Lessard and Crabtree, 2010). It has been proposed that the role of SWI/SNF member Brg1 (SmarcA4) is to "tonically" repress these genes in order to maintain expression within optimal limits. More strikingly, SWI/SNF appears important for

turning off pluripotency genes on differentiation, as well as for facilitating chromatin compaction (Schaniel et al., 2009). Another example of key acivity of SWI/SNF in defining the status of pluripotent cells is the Nucleosome Remodeling and Deacetylation (NuRD) corepressor complex, a transcriptional repressor which embeds the chromatin remodelling factor Mi2α/β (Chd3/4). NuRD is required in both peri-implantation stage embryos and ESCs, where and its activity controls the transcription of a set of pluripotency gene (McDonel et al., 2009). In self-renewing conditions the activity of NuRD contribute to the metastability of pluripotent cells, as it appears to be counter-balanced by the pluripotency-sustaining growth factors. Upon differentiation, NuRD activity down-regulates the core network of ES transcription factors, allowing cells to exit self-renewal (Reynolds et al., 2012). Although the control of NuRD activity appears crucial in the transition between pluripotency and differentiation, its modulation is poorly understood (Nichols and Smith, 2012).

1.6 ES cell metastability and transcriptional noise

It has been proposed that fluctuations in transcripion factor expression may represent an important feature of pluripotency which allows the exploration of different transcriptional and epigenetic states for lineage commitment: at the extremes of this variation, cells display identifiable features of ES cells or EpiSCs, respectively. These states are interchangeable, reflecting both the metastability and plasticity of ES cells in serum-containing medium (Hayashi et al., 2008; Figure 1.5). The lack of heterogeneity in 2i medium, on the other side, indicates that metastability is not a general feature of pluripotency (Marks et al., 2012). In any instances, a role of metastability as a developmental prerequisite cannot be excluded: as a matter of fact ES cells in epiblast-like status are more prompt to respond to retinoic acid-induced neuralization or trophectoderm differentiation. Moreover, *ex vivo* observation of 3.25 day *post-coitum* ICM cells do not show a uniform gene expression profile, but on the contrary it reveals a mixture

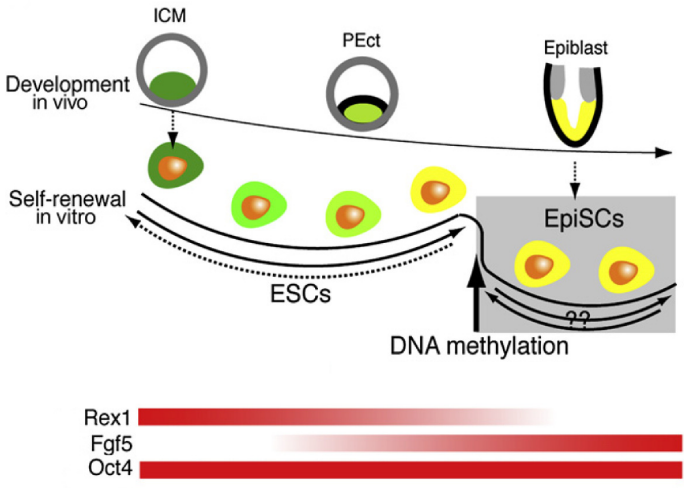

Figure 1.5: Model of metastability as a developmental continuum

Scheme shows the dynamic equilibrium of cells in different states, ranging between the ICM and epiblast-like phenotypes. Massive epigenetic, long-term rearrangements, including DNA methylation, distinguish ES cells from EpiSCs. Adapted from Hayashi et al., 2008.

of cells with stochastic gene expression variability, as demonstrated by single-cell analysis (Guo et al., 2010).

A recent work performed by means of a data-constrained computational approach has defined a minimum set of molecular components and interactions which explain ES cell identity, revealing that pluripotency can be reduced to a relatively simple process of molecular computation (Dunn et al., 2014). A network of 16 interactions, 12 components and three inputs results to satisfy all prior specifications for self-renewal in different culture conditions and defines a program which is unchanging under the action of different inputs, but computes the appropriate stable state as a consequence of these inputs.

If this model certainly applies to the steady-state of ES cell ground state self-renewal, the mechanisms underlying pluripotency destabilization and cell heterogeneity both *in vivo* and *in vitro* are far to be coherently integrated in a general model. ES cells have a globally relaxed and dynamic chromatin state, which is believed to provide rapid genomic readaptation upon differentiation, in order to

promote the progression of specific genetic programs. This clearly indicates that lineage specification during early embryonic development is driven by reduction of the transcribed portion of the genome, but it also poses the question of how pluripotency can accommodate the transcription of tissue-specific genes, expected to be silent in undifferentiated cells. In fact, the chromatin plasticity of ES cells may be the source of some degree of transcriptional "leakage" (Efroni et al., 2008; Marks et al., 2012), that is a semi-permissive transcriptional state. The proteasome has a role in limiting this process by increasing the turnover of transcription factors and Pol II at the promoters of developmentally regulated genes; in this way the transcriptional activity of these gene remains restricted, but they result to be in a poised state for a prompt later activation (Szutorisz et al. 2006).

1.7 Translation repression, miRNAs and stemness

A tight inhibitory control at the post-transcriptional level could provide a downstream backup system for reducing the production of proteins from unwanted transcripts and, definitely, to maintain pluripotency. In fact, protein synthesis is parsimonious during ES self-renewal, whereas upon differentiation an anabolic switch occurs, which triggers a global increase in polysome loading and protein synthesis. Restricted translation in pluripotent state and translational up-regulation during differentiation, due to the activity of several factors like mTOR, 4EBP1, and RNA-binding proteins, may represent an important quality control system for both cell identity maintenance and fate determination in embryonic stem cells (Sampath et al., 2008). The inhibition of protein translation through microRNA (miRNA) and the RNA-Interference Silencing Complex (RISC; Bartel, 2009) might represent another strategy to avoid a "transcriptional paradox". Indeed, miRNA-mediated mechanisms of regulation have been shown to be involved in limiting the protein translational noise in ES cells (Schmiedel et al., 2015). Moreover there is an established body of evidence indicating that a

release from RISC-mediated translational inhibition, produced through the disruption of components of miRNA maturation pathway such as Dgcr8 (Melton et al., 2010) or Dicer (Bernstein et al., 2003) severely impairs self-renewal in ES cells. Indeed, knock-out of Dicer1 results in early embryonic lethality due to depletion of the stem cell population, as demonstrated by the reduction of Oct4 staining in the Dicer1 mutant embryos. Moreover, inactivation of Dicer compromises the proliferation of ES cells *in vitro*, possibly explaining the mouse developmental phenotype (Murchison et al., 2005). Finally, a functional connection between RISC activity modulation and the switch between ground and primed pluripotent state is suggested by the evidence that ES cells and EpiSCs are characterized by very different miRNA profiles, with one third of miRNAs being differentially expressed between the two cell types (Jouneau et al., 2012).

1.8 Aims and goals of the thesis

While a general involvement of RISC in the maintenance of pluripotency is established, the experimental evidences in the literature do not provide details on the extent to which miRNA-mediated inhibition of protein translation contributes to the stabilization of ground-state pluripotency and its role in the switch to primed state. Moreover, little is known about the families of genes subject to this control and the overall effects of this inhibition. At the same time, the availability of monoclonal antibodies that recognize human and mouse Ago proteins offer the possibility to efficiently immunoprecipitate miRNAs and mRNAs which are associated to RISC (Nelson et al., 2007), in order to dissect the molecular pathways and functions under the control of RISC-mediated inhibition. Remarkably, this startegy would allow to evaluate dynamic changes in the strength of miRNA post-transcriptional control during priming and differentiation. In the present work, we developed an experimental and analytical framework to evaluate and integrate the high-throughput profiling of mRNA, miRNA, protein, RISC loading and ribosome occupancy levels, with the aim to

get a more comprehensive and robust view of the transition from ground to primed pluripotent state. On the front of the functional validation of the role of RISC in preserving pluripotency, many published studies have analyzed Dicer or DGCR8 knock-out ES cell lines after extensive cell culture selection and stabilization (Kanellopoulou et al., 2005; Murchison et al., 2005; Melton et al., 2008; Wang et al., 2007,2008,2013). This type of approach hardly permits to assay the immediate effect of global miRNA inactivation in ES cells and hampers the observation of the changes occurring during cell priming. In the present work we set up and employed alternative strategies for achieving conditional impairment of RISC function, to assess the acute effects of the suppression of miRNA function in ground-state embryonic stem cells.

Materials and methods

2.1 ES culture and Neuralization

Murine embryonic stem (ES) cell lines E14Tg2A, 46C and TNG-A (transgenic Sox1-GFP and Nanog-GFP ES cells, kindly gifted by A. Smith, University of Cambridge, UK;(Chambers et al., 2007b; Ying et al., 2003), and Dicer flox/null ES cell line, generously provided by G. Hannon (Cancer Research UK Cambridge Institute; Murchison et al., 2005), were cultured on gelatin-coated tissue culture dishes at a density of 40,000 cells/cm^2. ES cell medium, which was changed daily, contained GMEM (Sigma), 10% Fetal Calf Serum, 2mM Glutamine, 1mM sodium Pyruvate, 1mM non-essential amino acids, 0.05mM β-mercaptoethanol, 100 U/mL Penicillin/Streptomycin and 1000 U/mL recombinant mouse LIF (Invitrogen). For ground state reprogramming of ES cells, medium was switched for 3-5 passages to 2iL medium: GMEM (Sigma) supplemented with N2/B27 (no vitamin A; Invitrogen), 2mM Glutamine, 1mM sodium Pyruvate, 1mM non-essential amino acids, 0.05mM β-mercaptoethanol, 100 U/mL Penicillin/Streptomycin; MEK inhibitor PD0325901 (1μM); GSK3 inhibitor CHIR99021 (3μM); 1000 U/mL recombinant mouse LIF (Ying et al., 2008). Chemically defined minimal medium (CDMM) for neural induction consisted of DMEM/F12 (Invitrogen), 2mM Glutamine, 1mM sodium Pyruvate, 0.1mM non-essential amino acids, 0.05mM β-mercaptoethanol, 100 U/mL Penicillin/Streptomycin supplemented with N2/B27 (no vitamin A; Invitrogen). The protocol of ES neuralization consisted of three steps (Figure 2.1A; 3.1A). Dur-

ing Step-I, dissociated ES cells were washed with DMEM/F12, aggregated in agar-coated culture dishes (65,000 cells per cm^2) and cultured as floating aggregates in CDMM for 2 days. The second day, 75% of CDMM was renewed. In Step-II, ES cell aggregates were dissociated and cultured in adhesion (65,000 cells per cm^2) on Poly-ornithine (Sigma; 20 μg/ml in sterile water, 24 hours coating at 37°C) and natural mouse Laminin (Invitrogen; 2.5 μg/ml in PBS, 24 hours coating at 37°C) for 4 days, changing CDMM daily. In Step-III, after a second dissociation, ES cells were cultured 4 additional days in CDMM devoid of B27 supplement to drive terminal differentiation, using the same type of seeding density and coated surface described for Step II. For long-term neuronal cultures, cells were splitted again ad 10DIV and reseeded on coated dishes as above. At 12DIV medium was switched to Neurobasal supplemented with B27 to sustain neuron survival.Serum employed for Trypsin inactivation was carefully removed by washing with DMEM/F12. LIF-serum withdrawal coupled to culturing as cell aggregates for the first two days results in a very low amount of cell death (Bertacchi et al., 2013). Cell viability, which was monitored by trypan blue exclusion test and cell counting, was more than 90% and did not vary significantly between different steps of the differentiation protocol. Analysis of global gene expression on GO terms of apoptosis between ES and ELA cells showed no significant change (GO: 0006917 induction of apoptosis, p=0.668; GO: 1900117 regulation of execution phase of apoptosis, p= 0.373; GO: 0097194, execution phase of apoptosis, p= 0.559). The following factors were tested by addition during Step-I: 5-Azacytidine (Sigma-Aldrich; 50 nM) and 5-Carboxy-8-hydroxyquinoline (Sigma-Aldrich; 100 μM).

2.2 Calcium Imaging

In order to monitor intracellular Ca^{2+} levels in response to depolarization and/or neurotrasmitter signaling, we employed cell-permeant dye Fluo-4AM. Loading solution was composed by 3 μM Fluo-4AM, 0.1% Pluronic F-127 surfactant

in Hank's Balanced Salt Solution (Gibco). Neurons in adhesion on a Willco Chamber were washed with HBSS, incubated 1 hour at 37°C in loading solution ad washed again with HBSS. Imaging was performed with a confocal laser scanning microscope (DM IRE2, Leica) with excitation at 488nm.

2.3 Argonaute-bound RNA immunoprecipitation

In order to isolate cellular mRNAs that are incorporated into RISC we used "RIP-Assay Kit for microRNA" (MBL Japan), according to the protocol described by the manufacturer. Anti pan-Ago Antibody, clone 2A8 (Ago*; Millipore; Nelson et al., 2007), mouse total IgG (Millipore) or Anti-Ago2 Antibody, clone 9E8.2 (Millipore) were used for IP. For each single experiment, we started from 10^7 cells collected pooling 3 to 10 different samples. The binding of RNP with the beads was confirmed after immunoprecipitation by Western blot with anti-Ago* antibody (Figure 2.1B). The global screening of RISC-RNAs by microarray analysis was performed follwing IP with Anti-pan Ago Antibody (see next section). Three independent experiments were performed. IP with Anti-Ago2 Antibody was used to validate association of selected mRNAs to RISC by RT-PCR, using a spike-in as a reference (Figure 2.1C; 3.8B). 8ng of Tol2 transposase mRNA synthesized *in vitro* were added to each pellet as a spike-in before IP. Mouse total IgG were always used as IP negative control. Two independent experiments were performed.

2.4 Microarray hybridization and data analysis

Total RNA was extracted with NucleoSpin RNA II columns (Macherey-Nagel). RNA quality was assessed with Agilent Bioanalyzer RNA 6000 Nano kit; 200 ng of RNA were labeled with LowInput QuickAmp Labeling Kit One-Color (Agilent Technologies, purified and hybridized overnight onto an Agilent SurePrint G3 Mouse Gene Expression Array (8x60K) before detection, according to the man-

ufacturer's instructions. Agilent DNA Microarray scanner was used for slide acquisition and spot analysis was performed with Feature Extraction software (Agilent Technologies). Data were background-corrected and quantile normalized among arrays by means of Bioconductor package limma (Smyth and Speed, 2003). In order to sort out RISC-released or RISC-loaded mRNAs, we employed the following analysis pipeline, schematized in Figure 2.1E.

i) For a gene probe to be considered significantly bound to RISC, we assumed that the distribution of signal is bimodal, with a fraction of genes not bound (first peak, background) and another displaying a heterogeneous degree of binding. In fact this is what we observed in the distribution of Fluorescence Intensity (Figure 2.1D). After fitting the distribution to a gaussian mixture model (Benaglia et al., 2009) we set a threshold T_1 equal to ($\mu_1 + 3\sigma_1$), which corresponds to p=0.001 of false positive bound mRNA. Only mRNAs above this threshold were taken into account.

ii) For each step, RISC Enrichment (En) was evaluated by log_2 ratio between RISC-RNA and total-RNA levels after quantile normalization, and an arbitrary threshold of $T_2 > 2$ was applied in order to capture only the most enriched genes. Conversely, genes with enrichment less than 0.5 were considered not significantly enriched (T_3; this value was relaxed to 1.2 for subsequent analyses; e.g. GO Analysis).

iii) For each transition, genes released from RISC have $E_n > T_2$ and $E_{n+1} < T_3$ (as depicted in Figure 2.1F, right panel), while conversely genes loaded by RISC have $E_n < T_3$ and $E_{n+1} > T_2$.

iv) Finally, a threshold on the differential enrichment between steps ($\Delta E = E_{n+1} - E_n$) was used as a filter to sort out top regulated genes ($|\Delta E| > 1.5$).

Gene Ontologies over-represented in the subset of RISC-released genes during ES/ELA transition were evaluated using the web service Database for An-

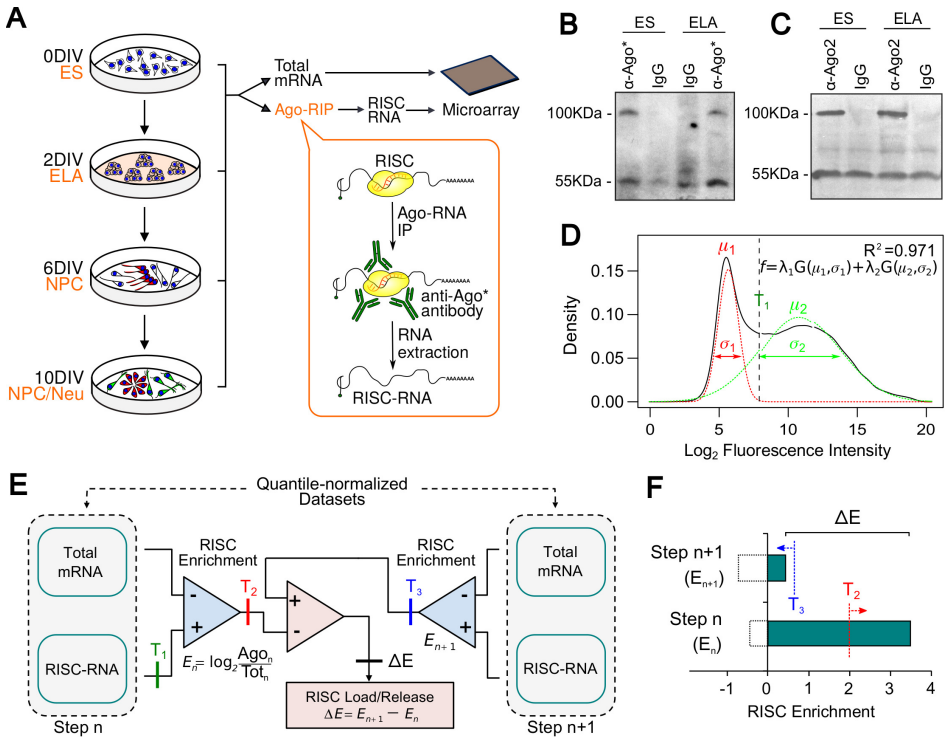

Figure 2.1: RISC Enrichment Analysis

A, Scheme of ES cell *in vitro* neuralization and RNA analysis. DIV, days of *in vitro* differentiation. **B**,**C**, Western blot of protein immunoprecipitation with anti pan-Ago antibody (α-Ago*, A), with anti Ago2 antibody (Ago2, B) or with total mouse IgG (A,B), in ES and ELA cells. Arrohwhead indicates Ago proteins. IgG are large bands migrating at about 50 KDa. **D**, fluorescence intensity distribution (black curve) is fitted by a linear combination of two gaussian functions (dashed red and green curves, respectively) of mean μ_n , standard deviation σ_n and relative weight λ_n . T_1 is set equal to $\mu_1 + 3\sigma_1$. R^2 is the coefficient of determination. **E**, scheme of the experimental workflow of mRNA analysis. **F**, scheme of the thresholds used for RISC enrichment evaluation.

notation, Visualization and Integrated Discovery (DAVID; Huang et al., 2009). Genes that were differentially expressed between ES and ELA cells with $|log_2 FC| > 1$, corrected p-value< 0.05 and mean log_2 expression > 7.5 (n=1207) were used for hierarchical clustering, in order to assess the effect of manipulations. RNA from two to three different sets of treatments was pooled. We have changed cutoffs for different analyses of global mRNA expression, because the dynamic range of mRNA change was different in the the experimental settings: we used $log_2 > 2.5$ when comparing ES, ELA, NPC and Neuron cells, which are

very different from each other, while we used $log_2 > 1$ when comparing ES cells to ELA cells, which are more similar. Euclidean distance and complete linkage algorithm were employed for clustering.

To assay the concordance of gene modulation between different conditions and obtain the statistical significance, we used sign test. Sign test was performed comparing the fold change of ES/ELA cells to the fold change of treated/control ELA cells for each gene. Randomized sets of data used as control were obtained by substituting the fold changes of treated/control datasets with fold changes of random genes (randomization 1), or by scrambling the order of treated/control ELA cells values (randomization 2).

2.5 Profiling of ribosome-associated RNA (Ribo-Seq)

For the pull-down of ribosome-associated RNA we were inspired by the TRAP protocol (translating ribosome affinity purification) developed in the laboratory of Dr. Nathaniel Heintz (Heiman et al., 2008; 2014). In short, this protocol is based on the pull-down of ribosomes using the large subunit protein Rpl10a, which is fused with GFP. We modified this protocol in order to pull-down the endogenous Rpl10a protein, as this would allow us to sample translation without altering the endogenous translational machinery. Immediately before the analysis, ES ELA cells were trypsinized and resuspended in the appropriate growth medium supplemented with 100 μg/mL cycloheximide in order to stall ribosomes. After a 15' incubation at 37°C, cells were recovered and washed with ice-cold PBS + 100μg/mL cycloheximide to remove traces of serum and medium. Each sample (both for ELA and for ES) included approximately 20 million cells, and we conducted all experiments in duplicate. The samples were resuspended in 1ml ice-cold lysis buffer (20 mM HEPES/KOH pH 7.3; 150 mM KCl; 10 mM $MgCl_2$; 1% IGEPAL CA 630, Sigma; 0.5 mM DTT; 100 μg/mL Cycloheximide, 1 pill/10mL Complete MINI EDTA free protease inhibitor, Roche; 3 μL/mL RNAsin RNAse inhibitor, Promega; 3 μL/mL SUPERA-

SEin RNAse inhibitor, Life Techologies) and incubated on ice for 10 minutes, before being triturated in a chilled dounce homogenizer with approximately 20 strokes. After lysis was completed, cellular debris (mostly formed by nuclei and fragments of cell membrane) was removed by centrifugation at 2000 RCF for 10 minutes. After centrifugation, 0.1 volumes of 300 mM 1,2-diheptanoyl-sn-glycero-3-phosphocholine (DHPC, Generon Ltd) were added to each sample to further solubilize ribosomes, followed by a 10' incubation on ice and by a second centrifugation at 20000 RCF for 10'. The final clarified lysate was transferred to new low-retention tube and $1/10^{th}$ volume were removed to be used as "input" sample for the measurements of total RNA levels. To immunoprecipitate ribosomes, 16 μg of anti-Rpl10a antibody (Sigma, cat.no WH0004736M1) or an equivalent amount of anti-GFP antibody (control, Sigma cat. No. G1544) were added to each sample, and incubated overnight with end-to-end agitation at 4°C. The following day, 200μL of 30mg/mL Protein-G Dynabeads (Life Technologies) were washed in PBS+0.1% Tween 20 (PBST), blocked in PBST + 1% BSA for 1 hour, and added to the lysate/antibody mix. Beads were incubated overnight at 4°C with end-to-end agitation. The following day the precipitated ribosomes were washed 4 times in 1mL high-salt buffer (20 mM HEPES/KOH pH 7.3; 350 mM KCl; 10 mM $MgCl_2$; 1% IGEPAL CA 630, Sigma; 0.5 mM DTT; 100 μg/mL Cycloheximide), and RNA was extracted using the RNEasy Micro kit (Qiagen) as per supplier's protocol. The results were quantified by spectrophotometry (Nanodrop) and capillary electrophoresis (Bioanalyzer RNA Nano kit; Figure 2.2B). 2 μg of RNA were used to prepare each RNA-seq library. Purified RNA was ribosome-depleted using the RIBO-Zero Gold kit (Illumina), which uses magnetic beads conjugated to rRNA-specific oligonucleotides to remove ribosomal RNA. The final purified RNA was analysed by capillary electrophoresis (Bioanalyzer Pico Kit), and was retro-transcribed and cloned into a sequencing library using the SCRIPTSeq v2 library preparation kit (Illumina) according to the supplier's protocol. Sequencing libraries were evaluated by bioanalyzer (to

verify the size distribution of fragments) and quantified by qPCR using primers specific for Illumina adaptors (KAPA library quantification kit). All the 8 libraries (2 replicates for ELA and ES cells, both IP and input) were mixed at a similar final concentration before cluster generation and sequencing on a HiSeq 2500 instrument.

2.6 Ribo-Seq data analysis

All the libraries were sequenced in a multiplexed lane using v4 chemistry on a Illumina HiSeq instrument, producing approximately 250M reads of raw data. After demultiplexing, each library produced between 20M and 50M of data, with the input library overall producing fewer reads than the Ribo-IP libraries. This effect was most likely due to an unequal loading and to the different nature of the input RNA samples (including a variety of RNA and small RNA types, while the Ribo-IP were mostly composed by messenger RNAs), and raised no concern for the subsequent analysis (Figure 2.2A). All the datasets were subject to quality control using the fastx-toolkit software through the following analyses:

i) quality score per cycle

ii) nucleotide distribution per cycle

iii) PCR duplicates (estimated by collapsing the reads)

All libraries yielded good quality data, with the exception of one of the replicates for the ELA input sample, which showed a lower complexity and higher amount of duplication (resulting in lower mapping to the transcriptome during the later steps of the analysis, data not shown). Reads contained in each of the remaining libraries were mapped to the Mouse transcriptome (USCS mm10 release) using the software Tophat2 (Kim et al., 2013), which accounts for spliced transcripts. Repeated regions (i.e. transposable elements) were excluded, and a maximum of 2 hits on the genome and 2 mismatches were allowed

during mapping. Mapped reads were assigned to genes using the htseq-count script (Anders et al., 2014), which counts features overlapping each gene in the released transcriptome. Counts were calculated for each gene_id, collapsing eventual splicing isoforms. The resulting raw counts were normalized using the DESeq2 R package (Love et al., 2014).

The DESeq scaling factor for a given lane is computed as the median of the ratio, for each gene, of its read count over its geometric mean across all samples. It is important to notice that this normalization (and, effectively, any other normalization applicable to our data) is based on the assumption that the majority of genes are not differentially expressed among samples. This is not necessarily true during differentiation, as there are reports indicating a massive upregulation of the translational machinery (Sampath et al., 2008), which would imply a higher read number for most genes during the ES to ELA transition. Unfortunately, it is impossible for any "internal" normalization method to account for global changes. As a consequence, our analysis of differential translation only indicates as significant genes that vary above or below the overall change level. We believe that this further increases the significance of our findings, since our results include genes subject to a specific regulation rather than a global effect.

After normalization, we analysed our results to assess correlation among datasets and among conditions (through hierarchical clustering and principal component analysis; Figure 2.1D-E). The results indicated that one of the replicates for the ELA input sample showed poor correlation with both the other input replicate and the other datasets (ELA.input.1). This, together with the lower mappability, lower read quality and increased amount of PCR duplicates (as described above), lead us to exclude this replicate from further processing. While this reduces the statistical power of our analysis, the fact that we are filtering our results to include only genes presenting high expression and high degree of change in their ribosome enrichment makes us confident that our conclusions are still significant.

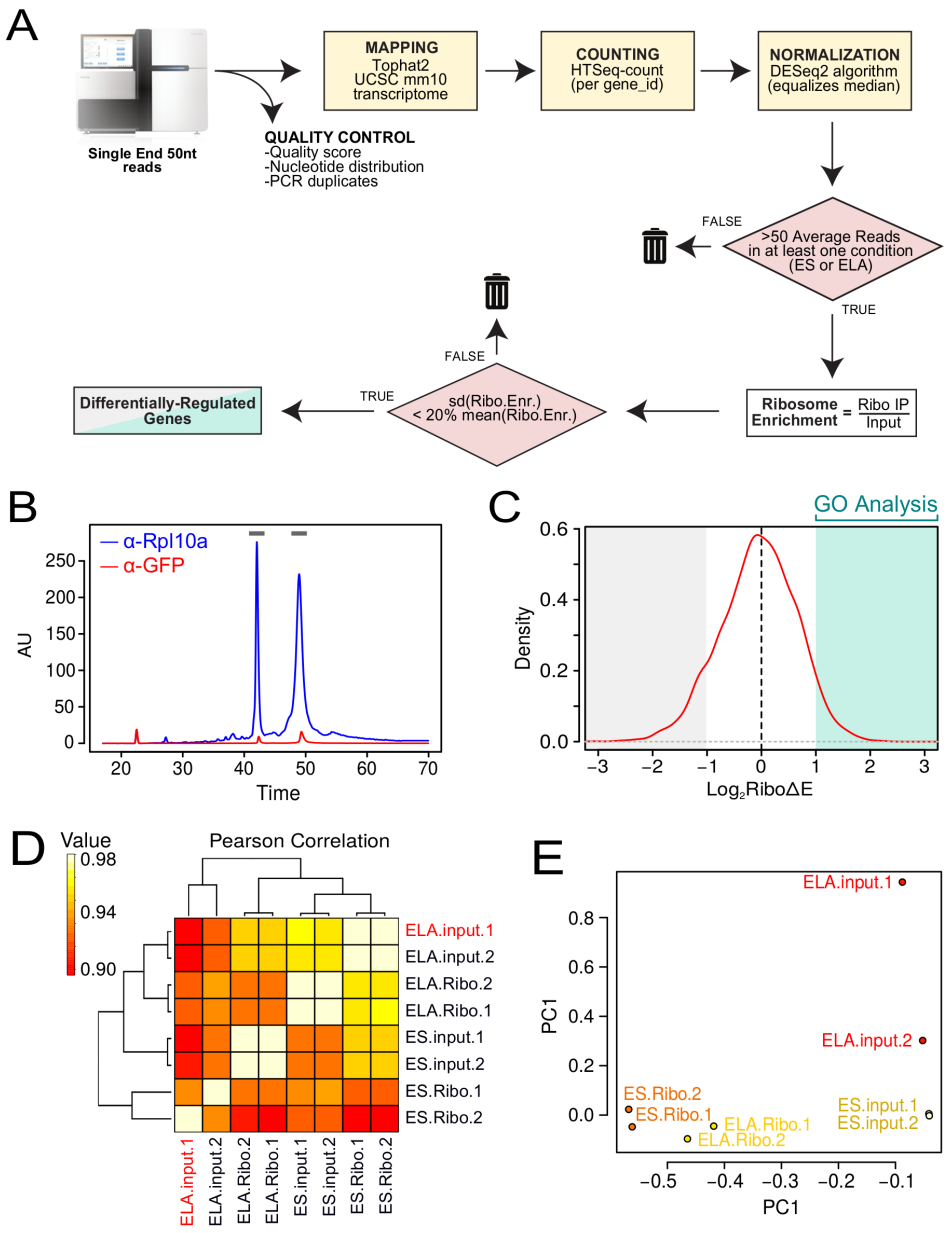

Figure 2.2: Ribo-Seq Analysis

A, flow-chart of Ribo-Seq analysis. **B**, Capillary electropherogram (Bioanalyzer) of RNA after pull down with antibody against Rpl10a (blue) or GFP (red). Gray bars show peaks for 18S (left) and 28S (right) ribosomal RNAs. **C**, graph shows the distribution of log_2 Ribosome Enrichment variation ($Ribo\Delta E$) during ES/ELA transition. **D**,**E**, hierarchical clustering of Pearson correlation (D) and PCA (E) of Ribo-Seq samples.

The remaining libraries were filtered to only include genes with an average of 50 counts in at least one of the two conditions (ES or ELA). This threshold

was chosen to exclude less-expressed genes, which would be the most affected by the inherent noise of our method. For all the genes passing this first filter, Ribosome Enrichment was calculated by dividing the average Ribo IP count by the Input count. A second filter was then applied, excluding genes for which the standard deviation of the counts accounted for more than 20% of the average value. This filtering produced a list of approximately 5000 genes, for which we calculated a $log2$ fold change in ribosome Enrichment (ELA average Enrichment / ES average Enrichment; $log_2 Ribo\Delta E$). For our GO enrichment analysis, we considered only genes with $log_2 Ribo\Delta E > 1$ during differentiation, producing a final list of 400 differentially regulated genes. While the GO categories enrichment results we obtained were all highly significant according to multiple statistic tests, we couldn't properly assess the significance of changes in the ribosome enrichment of individual genes due to our decision to remove the faulty replicate in the ELA input dataset. We nevertheless filtered our data to exclude genes with high replicate-to-replicate variation and low expression, and reported those with the highest changes, in both directions, in our raw data. Some of the genes individuated by our other analyses (Ago IP and protein MS) fell short of matching our filter in the ribosome enrichment data, nevertheless they showed a clear increase in enrichment, which was consistent with the modulation highlighted by the other techniques. We decided to show these results, since we believe that the fact that we obtained similar results through multiple and complementary analysis types constitute a strong proof of significance.

2.7 Semiquantitative real-time PCR

Total RNA was extracted from ES cell or tissue samples with NucleoSpin RNA II columns (Macherey-Nagel). ES cells from at least two-three different wells of 24-well plates were always pooled together to compensate for variability in cell seeding. RNA quantity and RNA quality were assessed by gel electrophoresis. For each sample, 200 ng of total RNA were reverse-transcribed (Eurogentech,

RT Core kit). Amplified cDNA was quantified using GoTaq qPCR Master Mix (Promega) on Rotor-Gene 6000 (Corbett). Primers used for amplification which were not previously reported (Bertacchi et al., 2013) were taken from PrimerBank (Spandidos et al., 2010). Amplification take-off values were extracted using the built-in Rotor-Gene 6000 relative quantitation analysis function, and relative expression was calculated with the $2^{-\Delta\Delta Ct}$ method, normalizing to the housekeeping gene β-Actin. Standard errors shown as error bars in all histograms were obtained from the error propagation formula as described in (Nordgård et al., 2006); statistical significance of 3 indipendent experiments was probed with randomization test, taking advantage of REST Software (Pfaffl et al., 2002).

2.8 Immunocytodetection

Cells prepared for immunocytodetection experiments were cultured on Poly-ornithine/Laminin-coated round glass coverslips. Cells were fixed using 2% paraformaldehyde for 10-15 minutes, washed twice with PBS, permeabilized using 0.1% Triton X100 in PBS and blocked using 0.5% BSA in PBS. Primary antibodies used for microscopy included Oct3/4 (1:200; Santa Cruz), Nanog (1:300; Novus Biologicals), acetylated N-Tubulin (1:500; Sigma), Neuronal Class III β-Tubulin (1:500; Covance), Nestin (1:200; Millipore), Pax6 (1:400; Covance) and GFP (1:1000, Life Technologies). Primary antibodies were incubated 2 hours at room temperature; cells were then washed three times with PBS (10' each). Alexa Fluor 488 and Alexa Fluor 568 anti-mouse or anti-rabbit IgG conjugates (Molecular Probes, 1:500) were incubated 1 hr at RT in PBS containing 0.5% BSA for primary antibody detection, followed by three PBS washes (10' each). Nuclear staining was obtained with DAPI (2μg/mL; Sigma). The same protocol was applied on sections of embryoid bodies after fixation (2 hours at 4°C in 2% PFA), dehydration (overnight at 4°C in 30% sucrose/PBS), inclusion in Tissue-Tek OCT compound (Sakura) and cryostat sectioning (12-16 μm) on SuperFrost glass slides (Thermo).

2.9 Proteomics sample pre-processing

About 10^7 cells per sample were dissociated, washed with ice-cold PBS and re-suspended in 400 μL of nuclear extraction buffer (50mM Tris-Hcl pH 7.9, 10mM KCl, 0.2% NP40, 10% glycerol and 1mM PMSF) for 3' in ice, then nuclei were pelleted by centrifugation at 6000RPM for 3' at 4°C. Nuclei were washed twice with 1 mL of nuclear extraction buffer devoid of NP40; before proceeding to mass spectrometry analysis, a small aliquot was lysed in loading buffer and used for western blot to confirm that the enrichment in nuclear fraction was homogeneous between samples. Nuclear extracts were lysed using lysis buffer containing TRIS HCl 50 mM pH=8.1, Triton X-100 0.5% and Deoxycholic Na 0.25% and sonicated. Samples were centrifuged at 10000 g for 10' at 4°C to discard cell debris, and buffer detergent was removed using detergent removal spin column (Pierce, Thermo Scientific, USA). Protein concentration was determined by bicinchoninic acid assay (Pierce, Thermo Scientific, USA). 100 μg of protein were diluted in 25 mM of ammonium hydrogen carbonate (pH=8) and reduction was obtained by adding 5 mM dithiothreitol with an incubation of 20 min at 80°C. Iodoacetamide was added to the samples to a final concentration of 10 mM and incubated in the dark for 30 min at 37°C. Digestion was performed incubating overnight with 100:1 substrate:trypsin (Roche, Germany) at 37°C. Nucleic acid contaminants were removed with Amicon Ultra-3K centrifugal devices (Merck Millipore, Germany), then flow-through containing peptides was loaded on a C18 cartridge in order to eliminate debris and filtered with 0.22 μm filter.

2.10 LC-MS/MS analysis

Chromatographic separation of peptides was performed using a nano-HPLC system (Eksigent, ABSciex, USA). The loading pump pre-concentrated the sample in a pre-column cartridge (PepMap-100 C18 5 μm 100 A, 0.1 x 20 mm, Thermo Scientific, USA). Chromatographic separation of peptides was performed using

a C18 PepMap-100 column (3 μm, 75 μm x 150 mm, Thermo Scientific, USA) at a flow rate of 300 nL min^{-1}. Runs were performed with eluent A (Ultrapure water, 0.1% Formic acid) under 60 min linear gradient from 25 to 40% of eluent B (Acetonitrile (Romil, UK), 0.1% Formic acid) followed by 10 min of a purge step and 20 min re-equilibration step. The column was directly coupled to TripleTOF 5600 System (ABSciex, USA), equipped with a DuoSpray ion source (ABSciex, USA). Peptides eluted from chromatography were directly processed using TripleTOF 5600 mass spectrometer (ABSciex, USA). The mass spectrometer was controlled by Analyst TF 1.6.1 software (ABSciex, USA). For information dependent acquisition (IDA) analysis, survey scans were acquired in 250 ms and 25 product ion scans were collected if exceeding a threshold of 125 counts per second (counts/s). Dynamic exclusion was set for 1/2 of peak width ($\sim$8 s), then the precursor was refreshed off the exclusion list. MS/MS data were processed with ProteinPilot Software (ABSciex, USA), using the Paragon and Pro Group Algorithms and UniProt 2013 as protein database for Mus musculus species. The false discovery rate (FDR) analysis was done using the integrated tool in ProteinPilot software and a confidence level of 95% was set. Label free statistical comparative analysis (Zhu et al., 2010) was performed using MarkerView (ABSciex, USA). The ion chromatograms of high confidence peptides identified by ProteinPilot were extracted using PeakView Software (ABSciex, USA), then MS peak areas and identifications were imported into MarkerView Software. Normalization of the total plaque area (plaque size) was done using a global normalization of profiles (total protein content). Principal Component Analysis (PCA, data not shown) was performed in order to evidence groupings among the data set. The two groups (ES and ELA, n=3) were compared with t-test using a threshold of p-value$<$0.05 and fold change$>$2.

2.11 Western Blot

Cells were lysed with RIPA buffer (50mM Tris-Hcl ph=7.6, 1% NP40, 0.5% Deoxycholic Acid, 150 mM NaCl, 1mM EDTA, 1mM PMSF, 1% SDS) supplemented with C0mplete Protease Inhibitor Cocktail (Roche); lysate was incubated 30' on ice and sonicated 3x10" at medium power in order to reduce viscosity. Supernatant was harvested by centrifugation (10' at 13,000RPM, 4°C) and quantified with Micro BCA Protein Assay Kit (Thermo Scientific). Samples were denatured by adding sample buffer (LDS Sample Buffer, Thermo Scientific) and boiled 10' on thermal block at 99°. 10 to 50 μg of total protein extract were resolved on 8-10% acrylamide gels, transferred on a nitrocellulose membrane (Hybond-c Extra, GE Healthcare), blocked with 5% milk proteins in TBST (50 mM Tris pH7.6; 150 mM NaCl; 0.05% Tween-20) and probed with primary antibodies, including Dnmt3b (1:2000, Imgenex), SmarcA4 (1:1000, Abcam), Kdm2b (1:2000, Merck Millipore), PolII (1:1000, Millipore), α-tubulin (1:5000, Sigma-Aldrich), Ago* (1:250, Millipore) and Ago2 (1:2000, Millipore). After 1h of incubation, membrane was washed 3 times with TBST (15' each) and probed with a HRP-coniugated secondary anti-mouse or anti-rabbit antibody for 1h (Santa Cruz Biotechnology). After three more washes, signal was revealed by means of an enhanced chemiluminescence kit (G&E Healthcare) on a BioMax XAR Film (Kodak).

2.12 FACS analysis

Cells were detached by trypsinization, washed and resuspended in PBS at RT, then analyzed with a FACSCalibur cytometer (BD). At least 25,000 events per sample were collected. Data were processed with Bioconductor package flowCore (Hahne et al., 2009).

2.13 Lentiviral Vector Construction and use

Knock-down vectors against SmarcA4 or luciferase (shSA4 and shCtrl, respectively) were constructed in order to sustain high expression of shRNAs both in ES and in differentiating conditions: IRES-PuroR-shRNA cassette from pGIPZ vectors (Open Biosystems) was excised by double restriction with NotI and MluI (NEB), filled-in with T4 DNA polymerase (NEB) and inserted into a modified pWPXLd vector (Addgene number: 12258; original GFP was swapped with DsRed with restriction sites MluI/XmaI) which was cut with NdeI and blunted as above. This resulted into a self-inactivating transfer plasmid carrying a DsRed-IRES-Puromycin resistance cassette with the shRNA of interest, driven by the strong ubiquitous promoter EF1α (Figure 2.3A). As a reporter of human nanog promoter activity we employed PL-SIN-Nanog-EGFP vector (Hotta et al., 2009; Addgene number: 21321).

CRISPR/Cas9 vectors were based on LentiCRISPR v2 (Sanjana et al., 2014; Addgene number: 52961) and constructed following manufacturer instructions. Briefly, vector was linearized with BsmBI (NEB), dephosphorilated with Calf Intestinal Phosphatase (NEB) and ligated with an oligo duplex obtained by annealing two ssDNA synthesized *in vitro* and 5'-phosphorylated by T4 Polynucleotide Kinase (NEB). The following oligos were designed and synthesized for Ago1-2 and CTRL guides, respectively: Ago1-2_fw: `CAC CGC GCA TCA TCT TCT ACC GCG A`; Ago1-2_rev: `AAA CTC GCG GTA GAA GAT GAT GCG C`; CTRL_fw: `CAC CGG CGA GGT ATT CGG CTC CGC G`; CTRL_rev: `AAA CCG CGG AGC CGA ATA CCT CGC C`. For CRE-GFP vector construction, CRE-NLS-IRES cassette from CRE-PuroR vector (Addgene Number: 30205) was excised by double restriction with NotI and NdeI (NEB), filled-in with T4 DNA polymerase (NEB) and inserted into pWPXLd vector (Addgene number: 12258) which was cut with MluI and blunted as above. This resulted into a self-inactivating transfer plasmid carrying a CRE-IRES-EGFP cassette driven by the strong ubiquitous promoter EF1α.

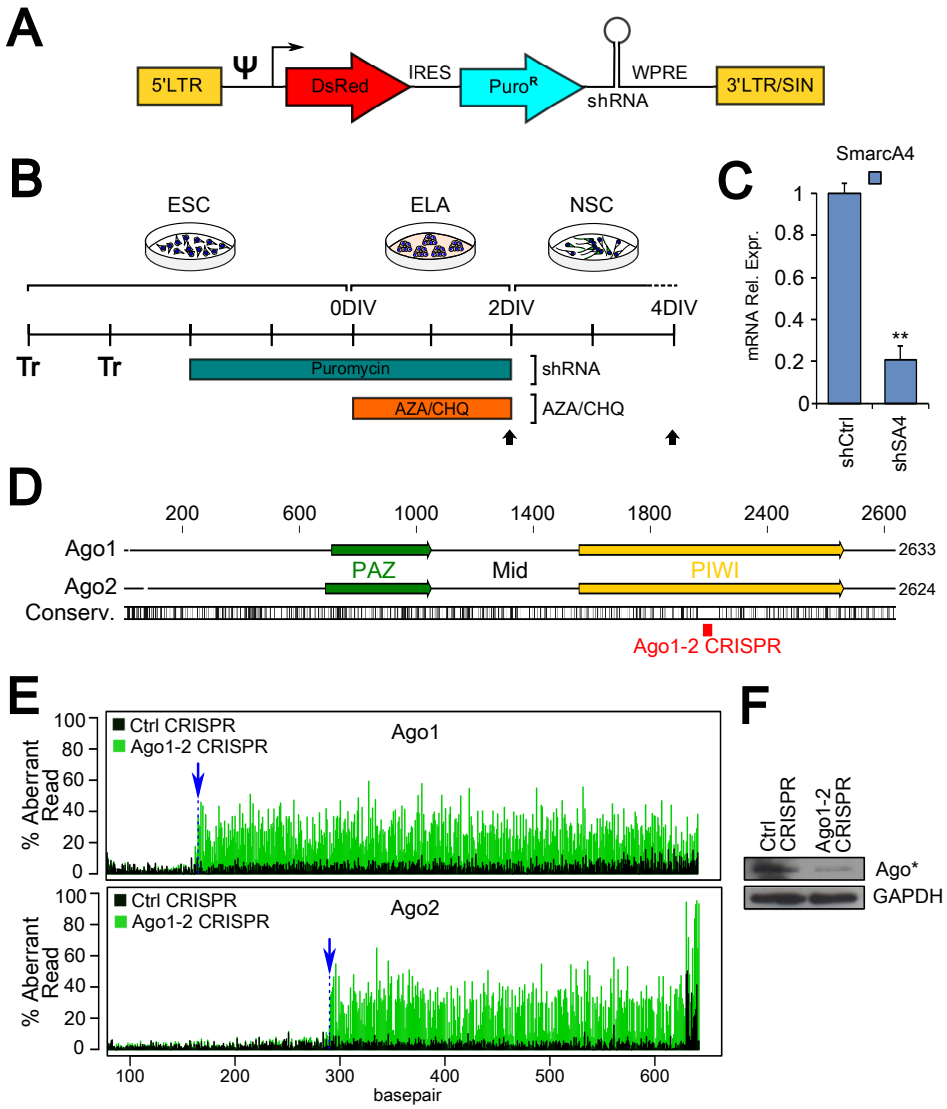

Figure 2.3: Lentiviral-mediated functional manipulations

A, scheme of the lentiviral vector employed for knock-down of SmarcA4. LTR: Long Terminal Repeats; ψ: packaging sequence; IRES: Internal Ribosome Entry Site; WPRE: Woodchuck Hepatitis Virus (WHP) Posttranscriptional Regulatory Element; shRNA: short-hairpin RNA. **B**, scheme of the protocol for functional interference with chromatin remodelers. **C**, RT-PCR analysis showing mRNA expression of SmarcA4 in shCtrl- and shSA4-transduced cells. Values are relative to β-actin mRNA expression, with shCtrl level normalized to 1. **D**, Position of guide RNA of Ago1-2 CRISPR. PAZ: Piwi/Argonaute/Zwille domain; mid: middle domain; PIWI: Piwi domain. **E**, Aberrant reads (y axis) along the genomic sequence of Ago1 (top panel) or Ago2 (bottom panel) in cells transduced with control CRISPR lentiviral vector (dark green) or Ago1-2 CRISPR lentiviral vector (light green). This analysis was carried by Sanger sequence trace decomposition (Brinkman et al., 2014). **F**, Western blot of Ago* in control (Ctrl) or Ago1-2 CRISPR ES cells 4 days after transduction.

Lentiviral vectors were produced by transient transfection of 293T cells by using 150 nM polyethylenimine (PEI) reagent (Sigma) with either PL-SIN-Nanog-EGFP, shCtrl or shSA4 plasmids, together with the Δ8.91 packaging and a VSV-G envelope expressing plasmids (Zufferey et al., 1997) in a ratio of 20μg:15μg:5μg respectively per single 100mm dish. Transfection medium was discarded 24h after transfection, then viral particles were collected at 48h and 72h, pooled and frozen at -80°C. For shRNA-mediated knock-down experiments, ES cells underwent two rounds of spinoculation (1h, 1100RCF at RT; O'Doherty et al., 2000), then transduced cells were selected in puromycin (0.75μg/mL) for 48h before embryoid body formation (Figure 2.3B). By 0DIV more than 90% of cells resulted to be DsRed+, achieving a knock-down of SmarcA4 mRNA level to 21.2% of expression in shCtrl-infected cells (Figure 2.3C).

For CRISPR/Cas9 experiments, cells were transduced and selected as above and maintained in ES medium (either serum and LIF or 2i+LIF), achieving genomic editing (Figure 2.3E) and strong downregulation of Ago* protein levels (Figure 2.3F) by 4 days after transduction. Rapamycin (100nM, Abcam) or MG-115 (1μM; Sigma-Aldrich) activity was tested adding the drugs to the culture medium 48h after transduction.

For Dicer conditional knock-out experiments, Dicer flox/null ES cell line was transduced with CRE-GFP lentiviral vector then, after 48h, GFP-positive cells were sorted by cytofluorimetry and reseeded for culturing in ES medium. Control (not excised) cells were transduced with pWPXLd vector devoid of CRE recombinase.

2.14 HNP cell line generation

For the generation of a mouse ES cell line carrying human nanog proximal promoter (Figure 2.4A), E14Tg2A cells in FCS+LIF were infected with PL-SIN-Nanog-EGFP lentiviral vector. After 6 passages from transduction cells were detached by trypsinization, washed and resuspended in PBS, 2% FBS, 2mM

EDTA and kept on ice. Nanog::GFP+ population (Figure 2.4B) was sorted on FACS Aria II Flow Cytometer (BD Biosciences) and reseeded as a polyclonal line for amplification (HNP: Human Nanog Promoter) to average positional effects of promoter insertion. The resulting cell line remains GFP+ after multiple passages in 2iL (data not shown) but promptly switches off fluorescence upon differentiation (Figure 2.4C), with a kinetics consistent with developmental nanog regulation. EGFP mRNA levels correlate well with that of endogenous nanog, as seen by real-time PCR (Figure 2.4D).

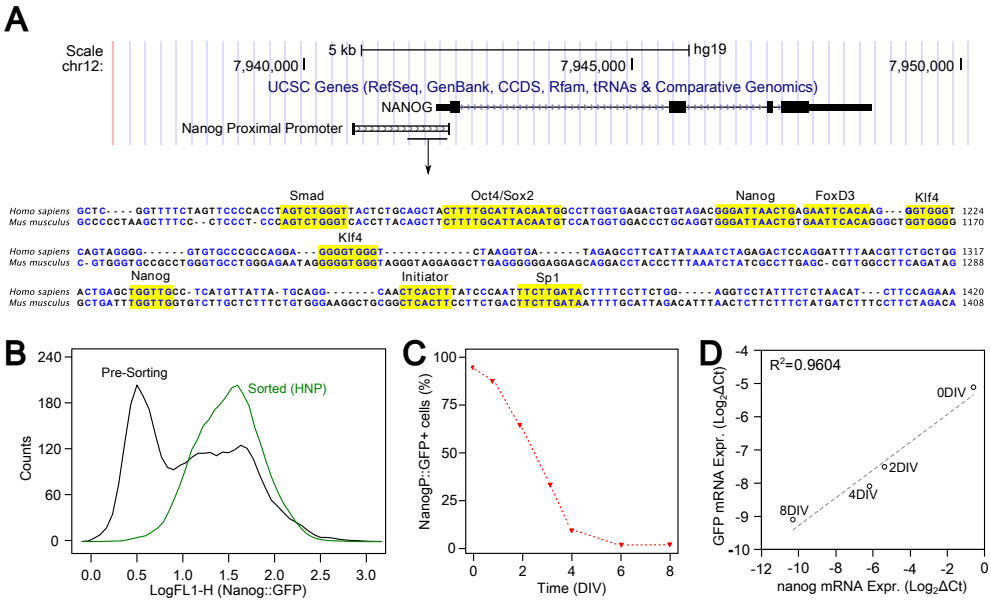

Figure 2.4: Generation of HNP ES cell line

A, Nanog proximal promoter region and sequence conservation. The scheme represents the region of human nanog promoter driving the reporter vector PL-SIN-Nanog-EGFP, as obtained by the UCSC genome browser (http://genome.ucsc.edu/). Kb, kilobases; chr, chromosome. The lower part shows the alignment of a portion of human and mouse sequences: although the overall degree of homology is not high, the core regulatory modules (yellow boxes) are conserved. **B**, green fluorescence distribution (FL1-H) of cells transduced with lentiviral vectors carrying PL-SIN-Nanog-EGFP, before (black curve) and after (green curve) cell-sorting of the EGFP-positive population. **C**, time-course of EGFP-positive cell percentage during differentiation (DIV: days of *in vitro* differentiation). **D**, Diagram showing the correlated expression of EGFP (y axis) and nanog (x axis) mRNA at different DIV. Values are expressed as $log_2\Delta Ct$ of RT-PCR assay; R_2 is the coefficient of determination.

2.15 Nanog promoter methylation assay

For the characterization of nanog promoter methylation status, we extracted genomic DNA with Wizard SV Genomic DNA purification System (Promega). 500ng of DNA were bisulphite-treated using EZ DNA Methylation-Lightning Kit (Zymo Research) and the region of proximal nanog promoter (Figure 3.11C) was amplified by PCR with a primer set from (Lienert et al., 2011) and cloned into pGEM-T Easy vector (Promega).
For each experiment, DNA obtained from 10 to 15 different colonies transformed with plasmid was sequenced on ABI3730 DNA analyzer (Applied Biosystems) and data were analyzed with software BiQ Analyzer (Bock et al., 2005).

2.16 Small RNA-seq and analysis

Sequencing procedure was done using Illumina Seqeuncing By Synthesis technology (Bentley et al., 2008). 1 μg of total RNA extracted with miRNeasy Mini kit (Qiagen) was used for library preparation (Illumina, TruSeq Small RNA Sample Prep Kit) following the manufacturer's description. Libraries were sequenced on a miSeq (Illumina) running in 50 bp single-read mode using sequencing chemistry v3, and demultiplexed in FASTQ format using CASAVA v.1.8 (Illumina). Library adaptors were trimmed with Trimmomatic (Bolger et al., 2014) and reads were mapped to mouse genome (NCBI37/mm9) with Bowtie (Langmead et al., 2009). miRNAs reads were annotated according to miRbase20 (Kozomara and Griffiths-Jones, 2014) and summarized using featureCounts (Liao et al., 2014). Normalization was performed as Reads per Million (RPM) and differential expression was evaluated with R package edgeR (Robinson et al., 2010).

2.17 In silico analysis of 3'UTR binding

We predicted the affinity of the specific miRNA subset which is expressed in ES cells and is down-regulated during ES/ELA transition (log_2 mean count per million > 5; $log_2 FoldChange < -1$) towards different mRNA families. For this purpose, we took advantage of UCSF Table Browser data retrieval tool (Karolchik et al., 2004), which allows batch downloading of the 3'UTR sequences of the genes of interest; when genes had several 3'UTR variants, the longest one was taken into account. We employed miRanda algorithm, which searches for complementarity matches between miRNAs and 3' UTRs using dynamic programming alignment and thermodynamic calculation (Enright et al., 2003). We set a minimum score of 140 and a maximum energy of -10 Kcal/mol as thresholds. For each gene, miRNA scores were summed, and the distributions of sums in different families were tested for statistically significant difference with Wilcoxon test. 3'UTR randomization was obtained by scrambling the 3'UTR sequences (Stothard, 2000). Global miRNA/mRNA binding prediction was performed using the miRVestigator framework (Plaisier et al., 2011) submitting as inputs the lists of either the top RISC-released ($\Delta E < -2$) or RISC-loaded ($\Delta E > 2$) mRNAs during ES/ELA transition. Only miRNA with a p-value < 0.002 were retained in the z-score analysis.

Results

3.1 In vitro differentiation of functional neurons

As a cell differentiation model, we employed a protocol of mouse ES cell neuralization that has been show to reproduce the main steps of early embryonic neural development (Bertacchi et al., 2013), while minimizing the influence of exogenous signals. This method consists of a three-step procedure of culture in a chemically defined minimal medium (CDMM) devoid of serum or morphogens but allowing cell survival (Figure 3.1A). Upon LIF and serum withdrawal, dissociated ESCs were initially grown as aggregates (Figure 3.1B) in CDMM for 2 days. ESC aggregates (ELA) were subsequently dissociated and cultured in adhesion, progressively yelding neural progenitor cells (NPC), neural precursors (NPC/Neu) and neurons (Figure3.1B-E). At the end of the protocol, cells obtained show immunostaining for mature neuron markers Map2 and NeuN (Figure 3.1F,G) and display many feature of functional neurons. In fact, stimulation of 25DIV ES cell-derived neurons with glutamate elicits istantaneous cell depolarization, as shown by Fluo-4AM intracellular calcium imaging (Figure 3.1H) and causes a robust overexpression of immediate-early genes c-fos and Egr1 30' after glutamate delivery (Figure 3.1I). More strikingly, unstimulated neurons show calcium waves which propagate from cell to cell spontaneously (Figure 3.1J,K). Overall these observations indicate that our *in vitro* protocol leads to the differentiation of functional neurons from ES cells.

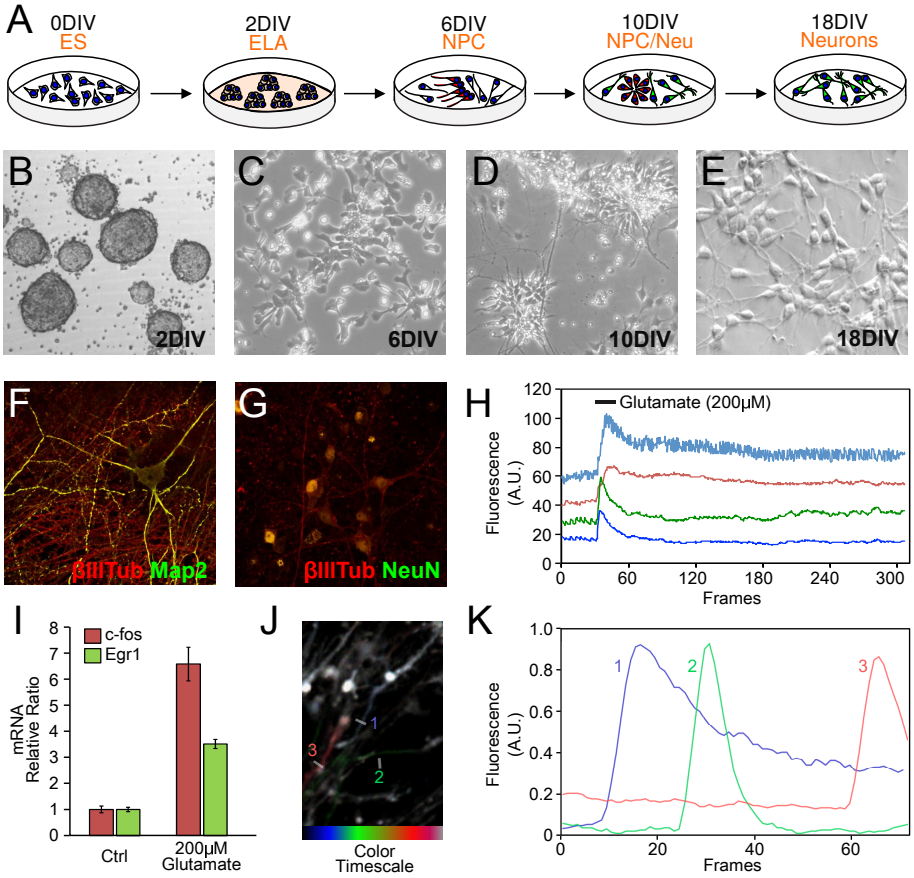

Figure 3.1: *In vitro* differentiation protocol produces functional neurons

A, Scheme of ES cell *in vitro* neuralization; **B**-**E**, bright-field micrographies of ES cells at different steps of differentiation (DIV); **F**,**G**, immunocytodetection of βIIITubulin and Map2 (F) or NeuN (G) in mature neurons at 18DIV. **H**, Fluo-4AM fluorescence levels of single 25DIV neurons stimulated with glutamate (200μM). **I**, RT-PCR of immediate-early genes c-fos and Egr1 in control neurons and after stimulation with glutamate. **J**, Micrograph showing spontaneous waves of intracellular Ca^{2+} represented with a pseudo-color time scale. **K**, fluorescence levels measured in neurons 1-3 in J demonstrate consequential depolarization of the neurons in this net.

Nerve cells generated with this protocol seem genuine neurons, as they activate gene expression profiles typical of distinct brain regions (Figure 3.2A-C). Notably, they are sensitive to the activation of specific signaling, to which they respond initiating programs of neuronal patterning. ES cells neuralized in CDMM express a gene expression pattern typical of midbrain cells, whereas they turn on the expression of hinbrain genes when treated with retinoic acid (Figure 3.2D).

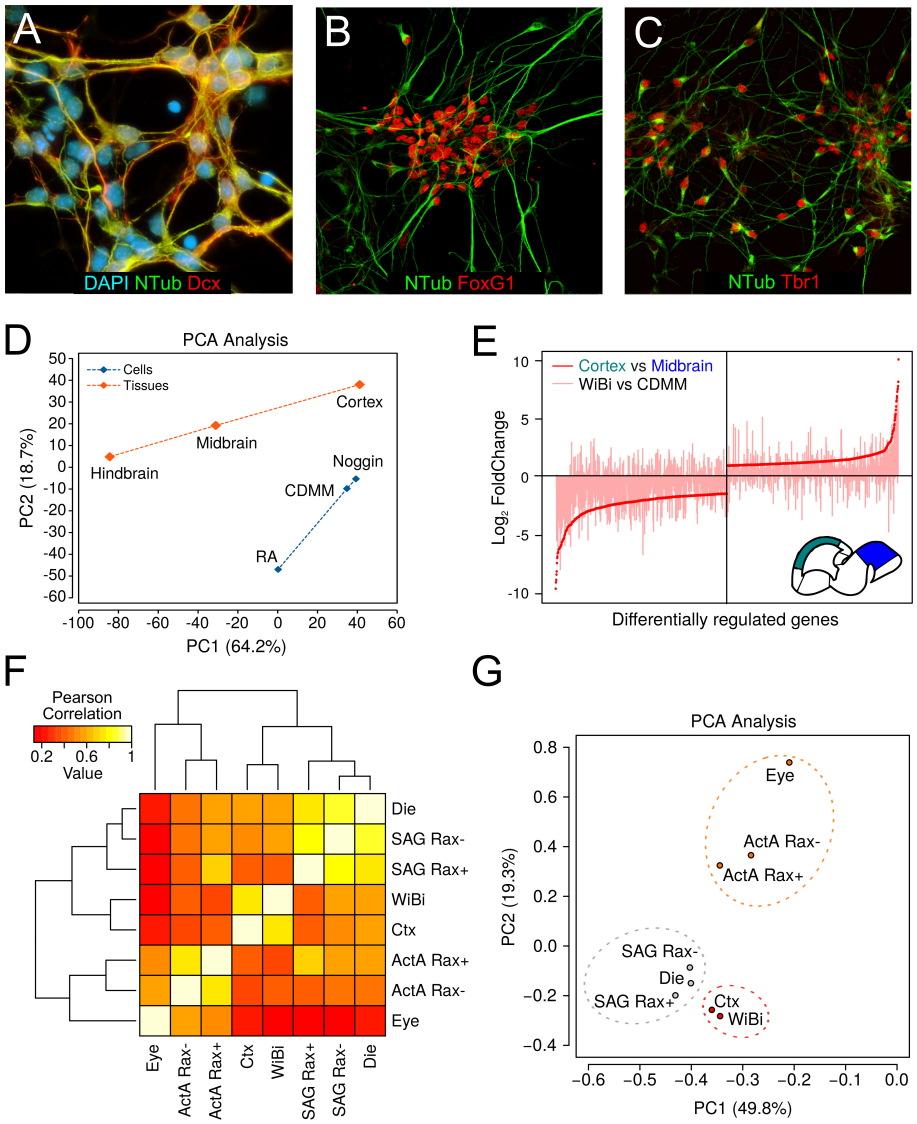

Figure 3.2: Neurons respond to patterning cues

A-**C**, immunocytochemistry showing Ntub (green) and Doublecortin (A; Dcx), FoxG1 (B) or Tbr1 (C) staining of 10DIV neural cells. Blue marks nuclei (DAPI). **D** Principal Component Analysis (PCA) of DIV10 cells in CDMM and treated with retinoic acid (RA) or BMP inhibitor Noggin. Cells display the same anterior/posterior identity as samples of E12 neural tissue dissected from hindbrain, midbrain and forebrain regions. **E** Genes differentially expressed between embryonic cortex and midbrain show the same modulation in the comparison of BMP and Wnt-inhibited cells (WiBi) with control cells (CDMM). **F**, hierarchical clustering based on Pearson Correlation between cells treated with Wnt inhibitor and Activin A (ActA), Wnt inhibitor and Sonic Hedgehog Agonist (SAG) or Wnt Inhibitor and BMP inhibitor (WiBi). Different patterning cues steer the cells toward specific positional identities of the forebrain, as demonstrated by the relative distance from embryonic tissues (Ctx, cortex; Die, diencephalon). **G**, PCA of cells and embryonic samples as in (F).

However, when blocking BMP and Wnt signaling, which are elicited during early in vitro nerualization by the endogenous production of BMP and Wnt ligands in ES cultures, cells acquire a cortical identity (Bertacchi et al., 2015a; Figure 3.2D,E). The mechanisms by which neuralizing ES cells acquire distinct regional identities involve cell competence (intended as the special status in which a cells is able to respond to a given stimulus by activating a specific genetic program), and temporal windows of sensitivity, similarly to what it occurs during embryonic development. For instance, only anterior neural progenitor cells, and not midbrain cells, when derived from ES cell cultures, can be specified as retinal or hypothalamic cells when exposed to Activin or Shh agonist (SAG), respectively (Bertacchi et al., 2015b; Figure 3.2F,G). Overall, these observations indicate that ES cell differentiation performed in controlled culture medium is a reliable model of early embryonic development.

3.2 Dissection of RISC activity during differentiation

To perform a global survey of the mRNAs that interact with RISC during the first steps of in vitro differentiation, we isolated RISC-interacting RNAs by immunoprecipitating Argonaute proteins (Ago*; Nelson et al., 2007), which are the main RISC components (Bartel, 2009). We isolated either RISC-interacting RNA (RISC-RNA) or total RNA from both mouse ES cells and cells at 2, 6 and 10 days of in vitro differentiation (DIV). RISC-RNA and total-RNA were hybridized to gene expression microarrays. The release of mRNA from RISC at the transition between sequential steps was evaluated as the variation of the ratio between RISC-RNA and total-RNA levels, after normalization (RISC Enrichment). While most of the transcriptional regulation occurred at the ELA/NPC transition (Figure 3.3A), the highest release of mRNA from RISC was observed at the ES/ELA transition (Figure 3.3B), with more than 100 mRNA species significantly released from RISC binding. We verified that this could not be explained by either a different efficiency in Ago immunoprecipitation (see Figure

2.1B,C in Materials and Methods), or a differential expression of Ago proteins in the two conditions (Figure 3.3C). The variation of RISC enrichment was coherently correlated with the variation of total RNA level at the ES/ELA transition for 82.4% of genes (Figure 3.3D), confirming a predominant effect of RISC in mRNA destabilization (Eichhorn et al., 2014).

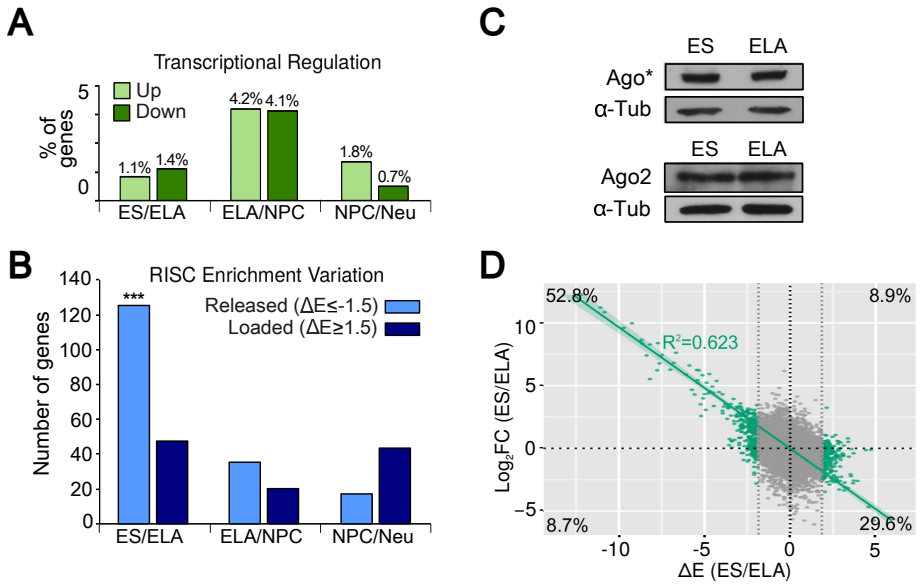

Figure 3.3: Kinetics of mRNA-RISC interaction

A, bar histogram shows the fraction of total mRNAs that are up- or down-regulated between consecutive steps of differentiation, with a threshold of $|log_2 FC| > 2.5$. **B**, number of genes whose mRNA is significantly released by (or loaded onto) the RISC (see Experimental Procedures); $***$p=0.001 (χ^2-test). **C**, Western blot of Ago* and Ago2 in ES and ELA cells. **D**, Scatter plot shows linear regression between log_2 ES/ELA mRNA expression fold-change (y axis) and ES/ELA ΔE (x axis) of green dots, reporting mRNAs with $|\Delta E| > 2$. Percentages indicate the fraction of mRNAs in each quadrant over total green population.

3.3 ELA are equivalent to primed pluripotent cells

Focusing on the biological relevance of this observation, we better characterized the nature of ELA cells. General markers of pluripotency, Oct4 and Sox2, were only marginally affected in ELA cells (Figure 3.4A), indicating an undifferentiated condition. However, epiblast markers FGF5 (Pelton et al., 2002) and

eomesodermin (Bernemann et al., 2011) were upregulated. FGF4, Klf4, Rex1, Esrrb and Dax1, which are markers of ground-state pluripotency (Brons et al., 2007; Tesar et al., 2007), were highly down-regulated, and Nanog was also expressed at a lower level (Figure 3.4A-C). This is similar to that observed in post-implantation epiblast stage embryos (Chambers et al., 2003) or in mouse ES cell-derived epiblast stem cells (EpiSCs; Ye et al., 2013). Therefore, we speculated that ELA cells are equivalent to post-implantation epiblast cells.

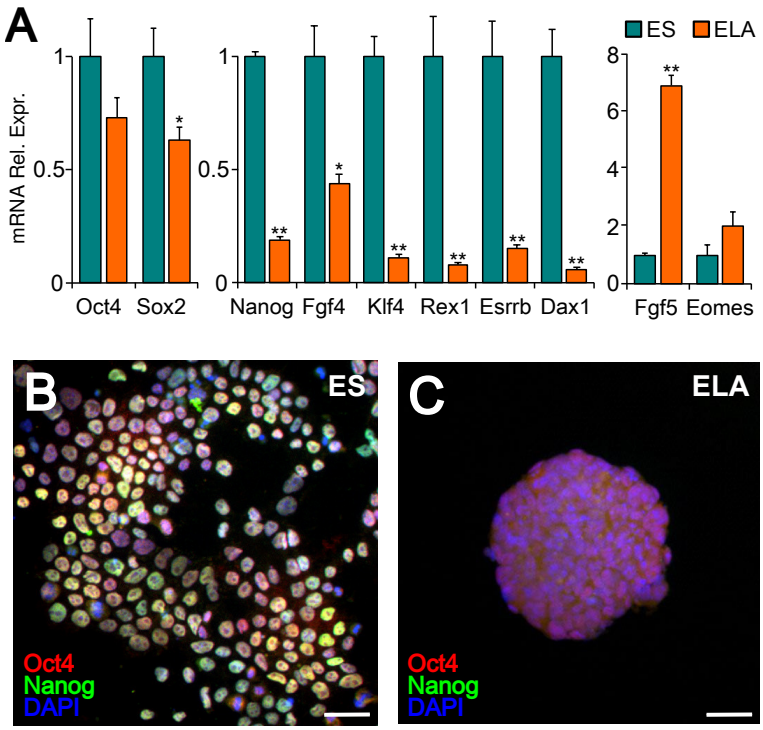

Figure 3.4: ELA cells are transient primed stem cells

A, RT-PCR gene expression analysis. Values are relative to β-actin mRNA expression. Highest and lowest expression levels were normalized to 1 in left/middle and in right histogram, respectively. **B**,**C**, Oct4 and Nanog immunodetection in ES cells (B) or ELA cells (C). Error bars show standard error. $*p=0.05$, $**p=0.01$ (REST randomization test). Scale bars are 30 microns.

Mouse epiblast cells can be maintained in a pluripotent state similar to that of human ES cells (hESCs; Thomson, 1998; Vallier et al., 2005) by FGF2/Activin A treatment (Brons et al., 2007; Tesar et al., 2007). Ground-state ES cells cultured for several passages in FGF2/Activin-containing medium (Figure 3.5A)

acquire a flattened morphology (Figure 3.5D) retaining a gene expression profile similar to ELA cells and consistent with epiblast identity (Guo et al., 2009).

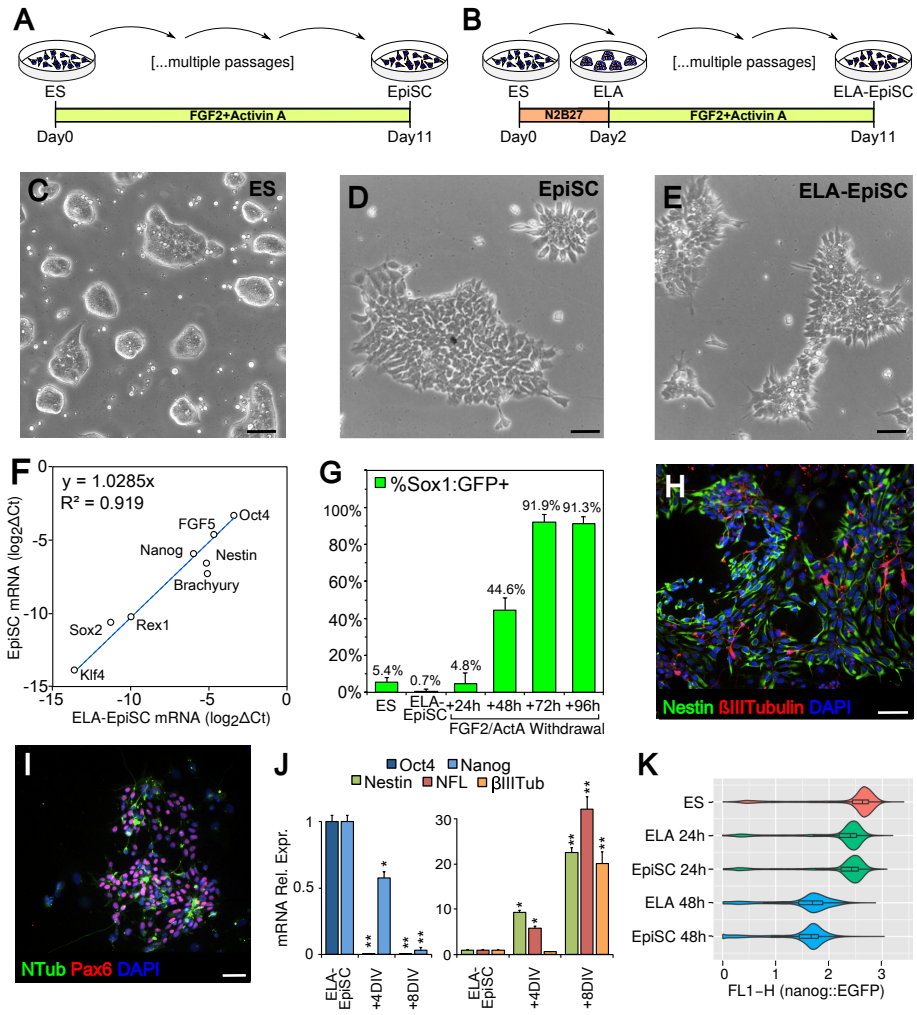

Figure 3.5: ELA correspond to EpiSC

A,**B**, Derivation of EpiSC and ELA-EpiSC from ES and ELA cells, respectively. **C**-**E**, ES, EpiSC and ELA-EpiSC cell bright-field imaging. **F**, Expression correlation of markers of pluripotency and priming between EpiSC (y axis) and ELA-EpiSC (x axis). Values are expressed as $log_2 \Delta Ct$ of RT-PCR assay; R^2, coefficient of determination. **G**, flow cytofluorimetric analysis of Sox1::GFP cells (46C line). **H**,**I**, Immunodetection of neural markers at 7 days of ELA-EpiSC neuralization. **J**, RT-PCR gene expression analysis in ELA-EpiSC after 4 (+4DIV) or 8 (+8DIV) days from FGF2/Activin A withdrawal. **K**, violin plot showing the distribution of GFP intensity in TNG-A Nanog::GFP line (Chambers et al.,2007a) in LIF/serum (ES cells, red), and 24h (green) or 48h (blue) after LIF/serum withdrawal (ELA), or Activin/FGF2 induction (EpiSC), respectively. Error bars in G,J show standard error. $*$p=0.05, $**$p=0.01 (REST randomization test). Scale bars are 40 microns.

Accordingly, ELA-derived cells could be dissociated and maintained in an EpiSC-like state by adding FGF2/Activin A to culture medium (Figure 3.5B). The resulting cells (ELA-EpiSC; Figure 3.5E) displayed a high level of correlation with the gene expression profile of mouse ES cell-derived EpiSC (Figure 3.5F). As well as ground-state ES cells, pluripotent stem cells derived from the epiblast spontaneously neuralize when deprived of FGF2 and Activin A. Similarly, more than 90% of ELA-EpiSCs induced the early marker of neuralization Sox1 72 hours after FGF2/Activin A withdrawal (Figure 3.5G). These cells became nestin-positive neural progenitor cells (Figure 3.5H) and differentiated as neurons positive positive to N-tubulin and Pax6 (Figure 3.5I) by down-regulating Oct4 and Nanog and up-regulating neuronal differentiation markers (Nestin, β-III-Tubulin and NFL; Figure 3.5J). Finally, the distribution of Nanog::GFP intensity during ES/ELA transition, while shifting from high to low level, maintains a narrow peak and is almost superimposable to the distribution during ES/EpiSC cell transition (Figure 3.5K) supporting the idea that ELA cells represent an homogenous population similar to EpiSCs.

Overall our results indicate that ELA cells are equivalent to epiblast stem cells, and therefore ES/ELA transition could be used as an in vitro model of the transition from inner mass cells to primed post-implantation epiblast cells. Using ELA instead of EpiSCs for studying priming allowed us to avoid the requirement for exogenous FGF and Activin, whose action could not parallel the autocrine signaling of the developing embryo. Moreover, since ELA cells are not steady-state cultures as EpiSCs are, they retain the transient nature of epiblast cells *in vitro* and could provide a better model than EpiSCs for investigating rapidly occurring molecular changes during this developmental transition.

3.4 RISC occupancy of selected chromatin regulators

We investigated the nature of the mRNAs released by RISC during priming by analyzing the distribution of Gene Ontology (GO) terms in our Ago-RIP res-

ults. Genes whose mRNAs were mainly associated to RISC in ES cells belong to gene ontologies related to DNA repair, replication, chromatin organization and modification, and embryonic development (Figure 3.6A). The release from RISC of mRNAs involved in DNA repair and replication in ELA cells is consistent with the marked enhancement of replication observed in epiblast following implantation (Snow, 1977).

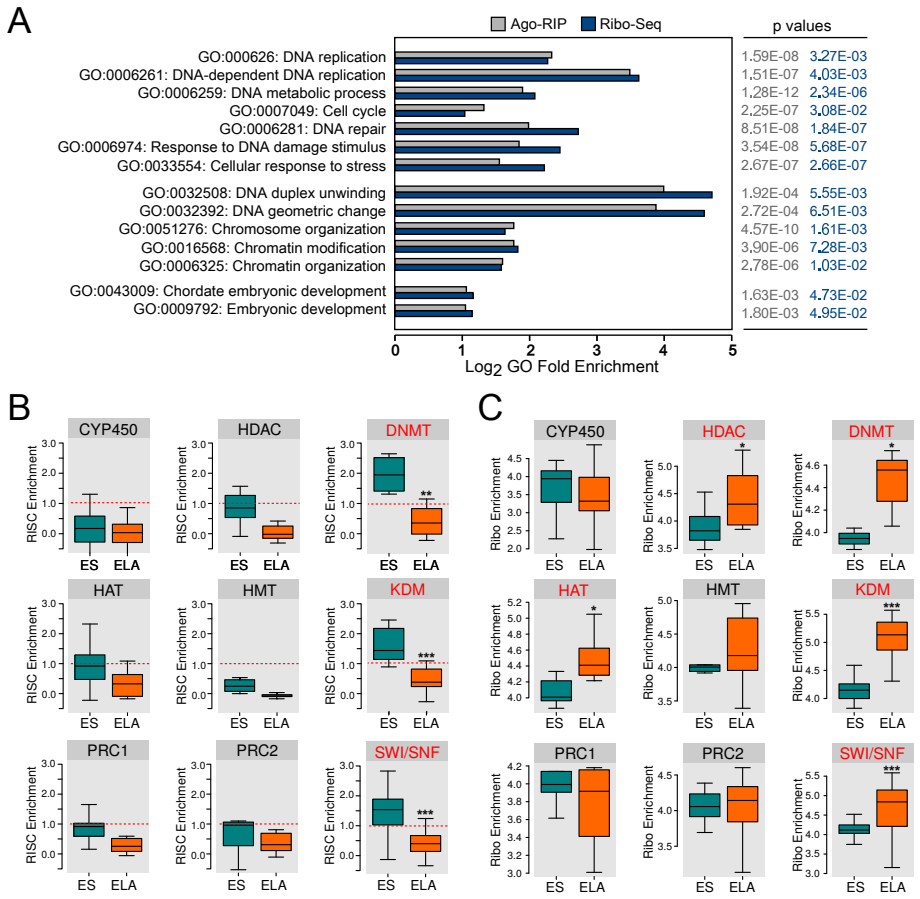

Figure 3.6: Selected chromatin regulators are regulated by RISC

A, GO terms significantly enriched in both gene sets of mRNAs released from RISC (Ago-RIP, gray), and of mRNAs significantly loaded on ribosomes (Ribo-Seq, dark blue) at ES/ELA transition, as obtained by DAVID. **B**,**C**, Box plots of RISC Enrichment (B) and log_2 Ribosome Enrichment (Ribo Enrichment, C) of mRNAs belonging to distinct classes of chromatin regulators. HDAC, Histone Deacetylases; HAT, Histone Acetyl-Transferases; HMT, Histone Methyl-Transferases; PRC1/2, Polycomb Repressor Complex 1/2. $*$p=0.05, $**$p=0.01, $***$p=0.001 (Wilcoxon test)

Chromatin modifications are postulated to play a crucial role in priming (Ahmed et al., 2010; Navarro et al., 2010; Song et al., 2012), but miRNA-mediated translational control of chromatin regulators has never been extensively described. Therefore, we focused our attention on the release from RISC of distinct families of chromatin modifiers (Khare et al., 2012). While the families of mRNAs coding for de novo DNA methyltransferases (DNMT), histone lysine demethylases (KDM) and SWitch/Sucrose NonFermentable nucleosome remodeling complex (SWI/SNF) showed more than two fold increase of RISC enrichment in ES cells compared to ELA cells, other families of chromatin regulators showed little or no increase, similarly to what was observed for families of mRNAs with unrelated functions such as Cytochrome P450 (CYP450; Figure 3.6B).

To evaluate changes in protein translation at ES/ELA transition, we evaluated ribosome occupancy by means of ribosome profiling (Ribo-Seq; Heiman et al., 2008; 2014), adapting the Translating Ribosome Affinity Purification protocol (TRAP) for our purposes. We measured the amount of mRNAs loaded on translating ribosomes, and calculated Ribosome Enrichment as an estimate of ribosome occupancy. Our analysis showed that the GO categories of genes showing increased ribosome loading during the ES/ELA transition were almost superimposable to those found for genes released from RISC (Figure 3.6A). Strikingly, DNMT, KDM and SWI/SNF families showed a Ribosome Enrichment essentially specular to their RISC Enrichment (Figure 3.6C).

3.5 Proteomic validation of translational regulation

To further verify our findings, we carried out label-free mass spectrometry (MS) of protein nuclear extracts. Notably, we observed a general correspondence of protein level variation with both the Ago-RIP and Ribosome profiling data (Figure 3.7A). This observation indicates that our method of evaluation of RISC Enrichment is quite predictive of protein translation inhibition. Using MS, we identified two DNMT members (Dnmt1 and Dnmt3b), two KDM mem-

bers (Kdm2b and Kdm5b) and three SWI/SNF members (Chd4, SmarcA4 and SmarcD1) as significantly increased during the transition to ELA. In all these cases, the increase in overall mRNA level was modest, strongly indicating a post-transcriptional effect (Figure 3.7B-D).

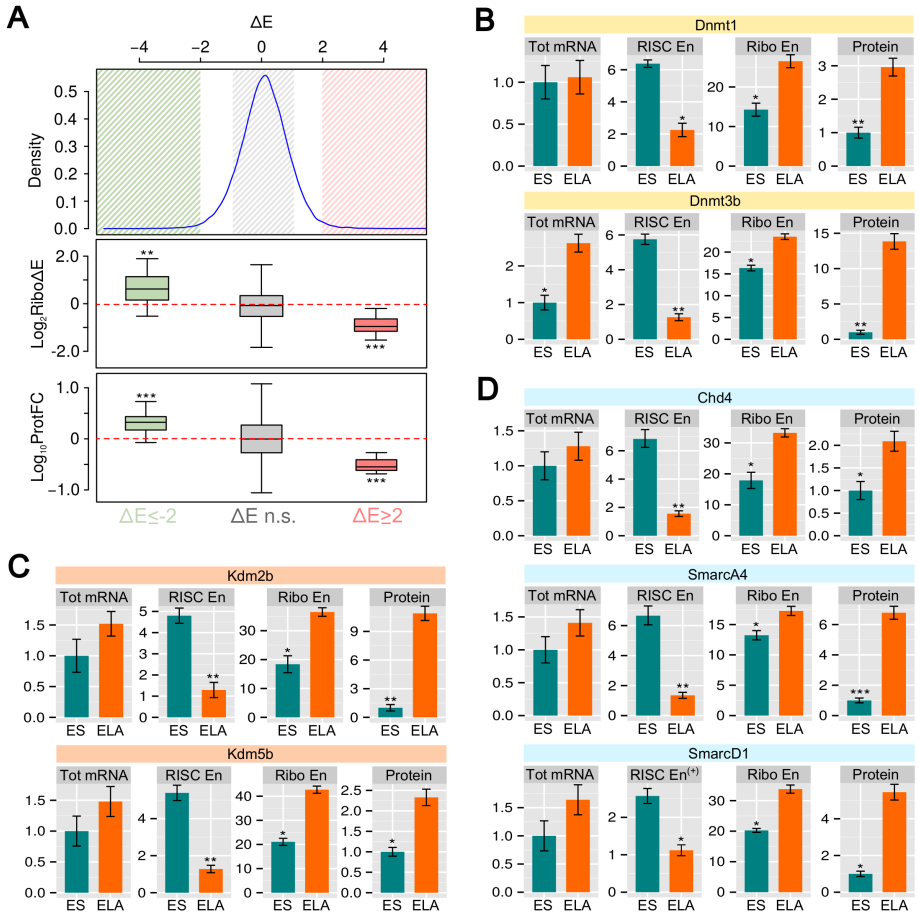

Figure 3.7: RISC Enrichment is predictive of protein translation activity

A, upper panel shows the distribution of RISC Enrichment variation (ΔE) during ES/ELA transition. Medium and lower panel show comparison between log_2 variation of Ribosome Enrichment ($Ribo\Delta E$, medium panel), or log_{10} protein fold-changes (lower panel), of three subsets of genes displaying significant RISC release ($\Delta E < -2$, green), significant RISC loading ($\Delta E > 2$, pink) or non-significant change of RISC Enrichment ($-1 < \Delta E < 1$, gray). Asterisks indicate the p of Student's t-test ($***$, 0.001) against null hypothesis of mean equal to 0. **B**-**D**, Total-mRNA fold change (Tot mRNA), linear RISC Enrichment (RISC En), Ribosome Enrichment (Ribo En) and Mass Spect. fold change (Protein) for the members of DNMT, KDM and SWI/SNF classes of chromatin regulators detected in ES and ELA nuclear cell extracts. $**$p=0.01, $***$p=0.001 (Wilcoxon test). Error bars show standard error.

Dnmt3b, SmarcA4 and Kdm2b proteins were barely detectable in the cytoplasm of ES cells (Figure 3.8A), arguing against a switch in cytoplasmic to nuclear localization as explanation for the protein changes observed. Indeed, this phenomenon could most likely be explained by the dramatic drop of RISC Enrichment displayed by these specific mRNA families during the ES/ELA cell transition. Furthermore, it would likely be not due to a general drop in RISC activity, as the bulk of variation of RISC Enrichment is symmetrical and zero-centered (Figure 3.7A, upper panel). Intriguingly, the modest increase in total mRNA levels suggests either that these specific mRNAs undergo a lower RISC-mediated decay than that of the majority of RISC-loaded mRNAs (see paragraph 3.1), or that an additional transcriptional modulation is occurring.

To confirm the specificity of Ago-RIP, which was performed with an α-Ago* antibody, we repeated RNA-immunoprecipitation with a different antibody (α-Ago2), obtaining a high and specific enrichment of several members of the selected chromatin regulator families taken into account.

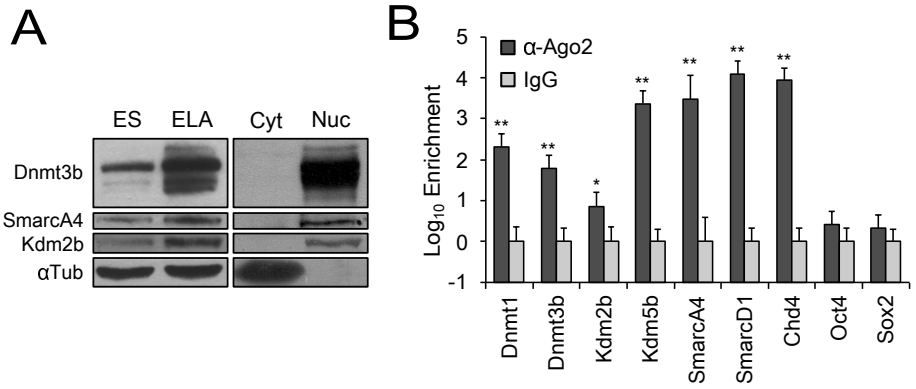

Figure 3.8: Validation of protein detection and immunoprecipitation

A, Western blot of Dnmt3b, SmarcA4 and Kdm2b in total extracts of ES and ELA cells, or in cytoplasmic (Cyt) and nuclear (Nuc) extracts of ES cells. **B**, RT-PCR analysis of mRNAs after immunoprecipitation with an α-Ago2 antibody or mouse IgG. Values were obtained by $\Delta\Delta Ct$ analysis using Tol2 spike-in mRNA as reference and then normalized to IgG. $*$p=0.05, $**$p=0.01 (REST randomization test).

3.6 DNMT, KDM and SWI/SNF activities are required to repress Nanog

We assayed the impact of the functional inhibition of chromatin regulators on the expression of Nanog, which is down-regulated during priming (Silva et al., 2009). Using the mouse TNG-A Nanog::GFP line (Chambers et al., 2007) as a model, we inhibited our target genes using either drugs, 5-Azacytidine (AZA; Santi et al., 1984) for DMNT and 5-Carboxy-8-hydroxyquinoline (CHQ; King et al., 2010) for KDM, or lentiviral-mediated transduction of shRNAs against SmarcA4 (shSA4), and measured the effect on Nanog expression at 0, 2 or 4DIV (Figure 3.9). AZA, CHQ and shSA4 significantly increased the ratio of GFP-positive cells at 4DIV compared to control (Figure 3.9B), maintaining a high median content of fluorescence (Figure 3.9C). A similar analysis was performed using a mouse ES cell line carrying GFP under the control of the human Nanog promoter (HNP; Figure 2.4). This analysis produced similar results (Figure 3.9E-H), indicating that DNMT, KDM and SWI/SNF activity is necessary for Nanog down-regulation during priming and that such requirement has been conserved in mice and humans.

3.7 Block of chromatin regulators impedes priming

In addition to Nanog, markers of pluripotency such as Klf4, Rex1 and Dax1 were up-regulated in cells treated with AZA, CHQ or shSA4 compared to control at 4 DIV, while the priming marker Fgf5 was down-regulated (Figure 3.10A,B). We investigated the role of DNMT in silencing Nanog expression more directly by monitoring its promoter methylation, which was consistently inhibited by AZA treatment at 2DIV as compared to control (Figure 3.10C). Interestingly, CHQ treatment and shSA4 transduction blocked the methylation of the Nanog promoter as well, indicating the requirement of KDM and SWI/SNF activities in this modification, in agreement with previous reports (Schaniel et al., 2009).

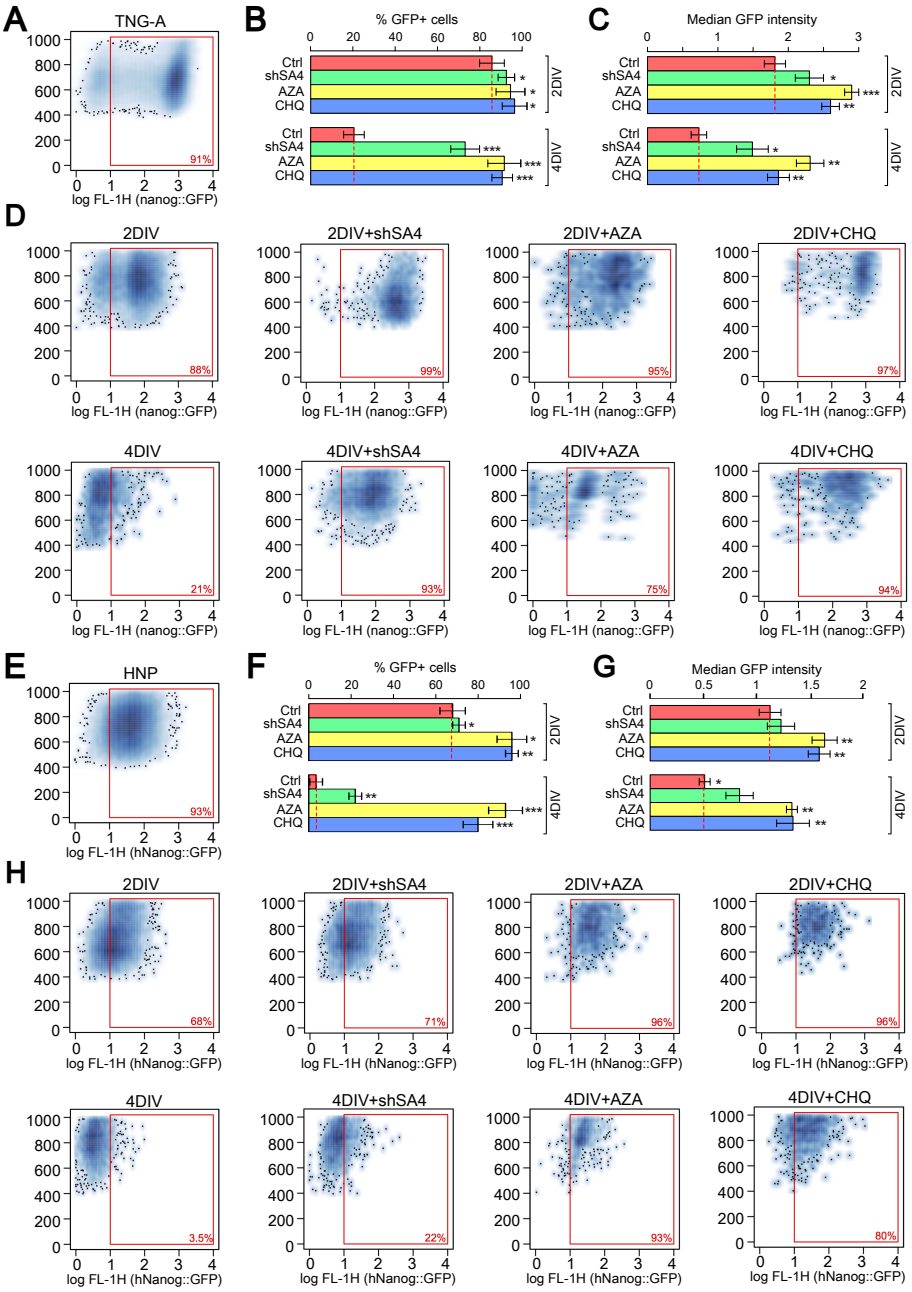

Figure 3.9: Nanog repression requires DNMT, KDM and SWI/SNF

A-**H**, Flow cytofluorimetry analysis of TNG-A Nanog::GFP cells (A-D) and Human Nanog promoter murine ES cells (HNP; E-H) in different conditions. **B**,**F**, GFP-positive cell ratios and **C**,**G**, median GFP intensity at 2DIV and 4DIV after inhibition of SmarcA4 (shSA4), DNMT (AZA) or KDM (CHQ) compared to control (Ctrl).

At 2DIV, cells treated with AZA and CHQ showed a global mRNA expression profile, evaluated by microarray hybridization, almost identical to that of ES cells, as evaluated by hierarchical clustering and fold change analysis (Figure 3.10D-J). Cells transduced with shSA4 showed a modulation of their profile consistent with that of AZA and CHQ (Figure 3.10H), but in this case gene expression clustered with that of ELA cells (Figure 3.10D), suggesting that the combined action of several SWI/SNF members might be necessary to control ES/ELA cell transition.

3.8 RISC impairment destabilizes pluripotency

In order to evaluate the impact of global miRNA activity in ES cells we performed acute RISC functional inactivation. We used a CRISPR/Cas9 lentivector with a RNA guide targeting both Ago1 and 2 (Figure 2.3D-F), which are the only Argonaute genes expressed in ES cells (Figure 3.11A). RISC downregulation resulted in a dramatic increase in Dnmt3b, SmarcA4 and Kdm2b protein levels without significantly affecting mRNA expression (3.11B,C). This increase was also observed when the mTOR pathway, or the protein degradation pathway, were pharmacologically inhibited, although with a lower extent due to the general decrease/increase of protein levels (Figure 3.11F). This indicates that a RISC-mediated control of these proteins exists and is independent from their rate of translation/degradation. In addition, RISC inactivation in ES cells cultured in 2i-medium caused downregulation of pluripotency markers and upregulation of early neural markers including Zfp521, which is essential and sufficient for driving the intrinsic neural differentiation of mouse ES cells (Kamiya et al., 2011; Figure 3.11D,E), and Sox1, as validated also by immunocytodetection and FACS analysis (Figure 3.11I-L). Similar results were obtained using a conditional Dicer flox/null cell line upon Dicer excision with a CRE-carrying lentiviral vector (Figure 3.11G,H). These data indicate that acute global miRNA downregulation results in pluripotency destabilization.

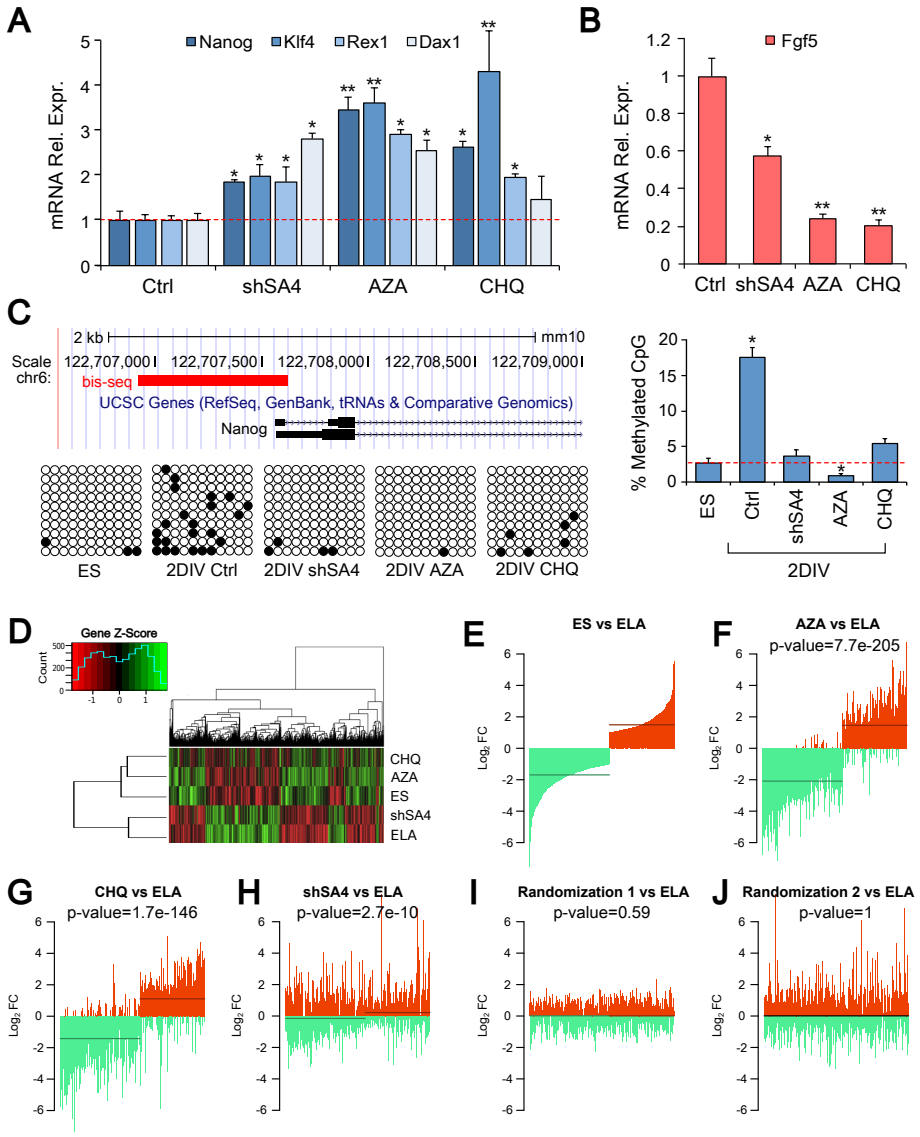

Figure 3.10: DNMT, KDM and SWI/SNF impairment blocks priming

A,**B**, RT-PCR gene expression analysis. Values are relative to β-actin mRNA expression. Lowest and highest expression levels were normalized to 1 in left and in right histogram, respectively. **C**, Nanog proximal promoter methylation. Black circles in grid rows indicate CpG methylation sites. Bar histogram shows the percentage of CpG methylation in different culture conditions as above. **D**, Hierarchical clustering analysis of mRNA expression of ES cells (ES) and of ELA cells in control medium (ELA) or treated as indicated. Inset shows the distribution of genes (count) with respect to their z-score. **E**-**J**, bar plots indicating the distribution of log_2 fold changes (log_2FC in y axis) of mRNA expression of genes whose expression is mostly changed between ES and ELA cells. Lines show the median fold change of up- (red) or down- (green) regulated genes. p-value refers to sign test. Randomization 1/2, datasets of values randomized as explained in Materials and Methods. AZA and CHQ treated cells show a gene expression fold change profile almost identical to that of ES cells. shSA4 cells, although showing a more different profile, have a significant tendency toward ES cell identity. $*$p=0.05, $**$p=0.01, $***$p=0.001 (A,B; REST randomization test; C, Student's t-test).

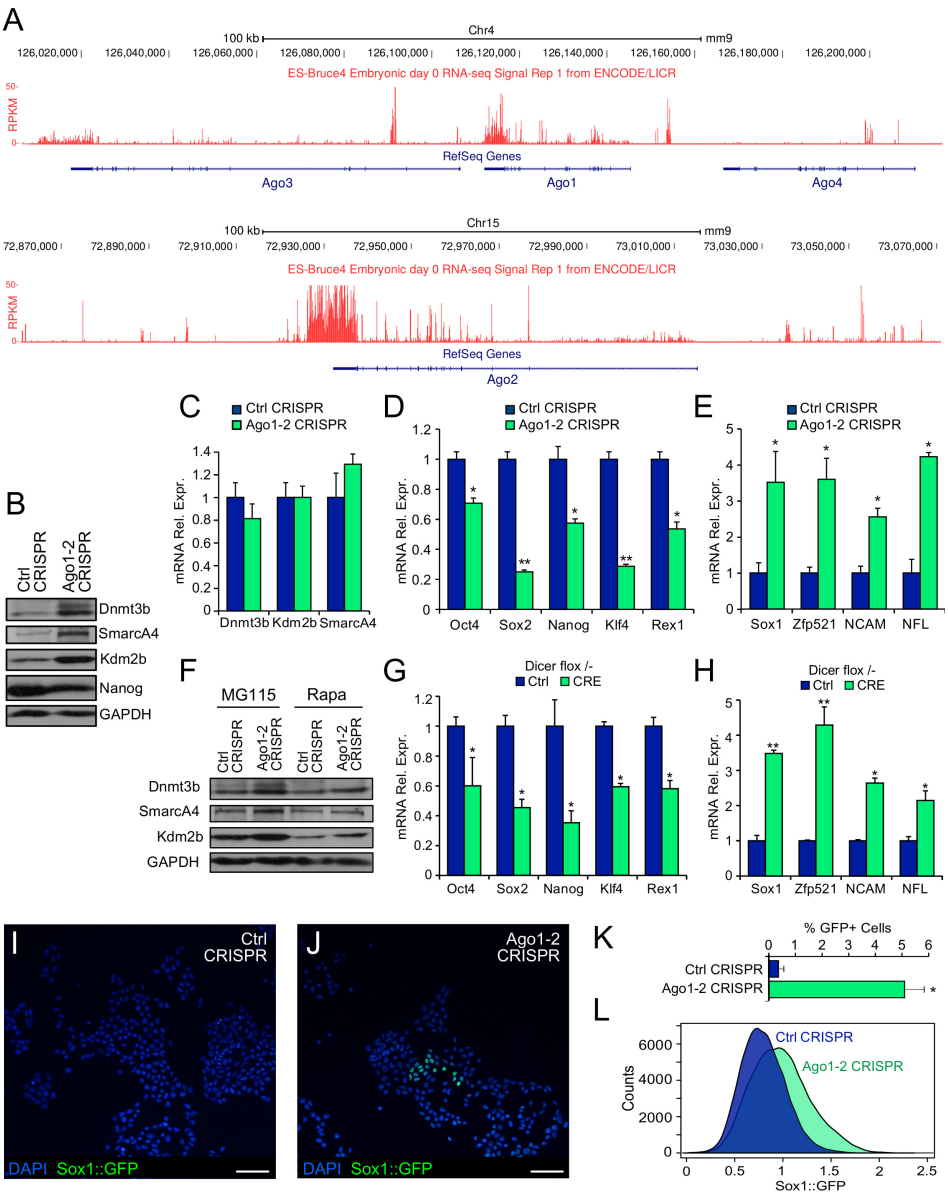

Figure 3.11: Impairment of RISC function destabilizes pluripotency

A, Gene plots show RNA-seq profiles of Argonaute genes in mouse ES cells as reported in dataset ES-Bruce4 (UCSC Genome Browser; Mortazavi et al., 2008). y axis shows the distribution of reads per kilobase per million on (RPKM). **B**, Western blot shows Dnmt3b, SmarcA4, Kdm2b, Nanog and GAPDH protein levels in ES cells cultured in 2i medium, 4 days after transduction with Ago1-2 CRISPR lentiviral vector, compared to control cells transduced with non-targeting CRISPR vector (Ctrl CRISPR). **C**, mRNA levels of Dnmt3b, SmarcA4 and Kdm2b of cells as in B. **D**,**E**, mRNA levels of pluripotency (D) or early neural commitment (E) in cells as in A,B, 8 days after transduction. **F**, Western blot of Dnmt3b, SmarcA4 and Kdm2b in in control (Ctrl) or Ago1-2 CRISPR ES cells cultured in the presence of inhibitors of proteasome (MG115; 1μM) or mTOR pathway (rapamycin, Rapa, 100nM). **G**,**H**, mRNA levels of pluripotency (G) or early neural commitment (H) markers in Dicer flox/null conditional ES cells (Murchison et al., 2005) 8 days after transduction with CRE-GFP carrying lentiviral vector. **I**,**J**, GFP immunodetection in 46C Sox1::GFP mouse ES cell line cultured in 2i medium, 8 days after transduction with Ctrl CRISPR (I) or Ago1-2 CRISPR lentiviral vector (J). Scale bars, 50 microns. **K**, Cell count of GFP-positive cells as in I,J. **L**, Cytofluorimetric analysis of cells as in I,J.

3.9 miRNA signature of ground state pluripotency

To get a better insight in the mechanisms of RISC targeting, we performed small RNA-seq of cells during ES/ELA transition. This experiment had the additional advantage of allowing us to validate the robustness of Ago-RIP as a method to measure RISC-mediated inhibition of mRNAs.

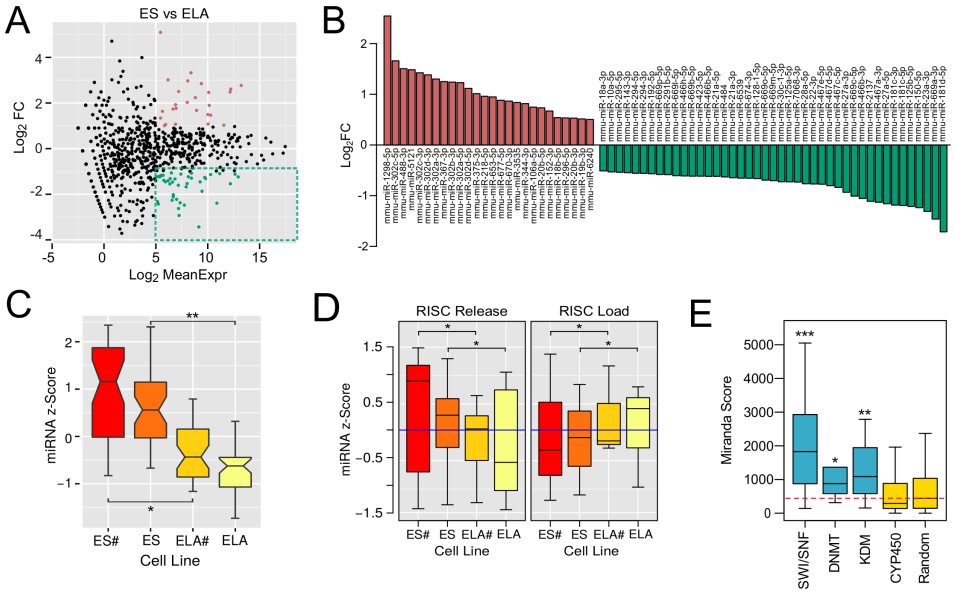

Figure 3.12: miRNA signature of ground pluripotent state

A, Scatter plot shows $log_2FoldChange$ (FC; y axis) and mean value of miRNA expression (x axis) between ES and ELA cells. Green dashed box indicates miRNAs significantly downregulated (mean $log_2RPM > 5$ and $log_2FoldChange < -1$) during priming. **B**, Selection of top-regulated miRNAs ($|log_2FoldChange| > 1$) at ES/ELA cell transition. **C**, Box plots show z-scores of expression (RPM) of miRNAs selected in the green box in I, in ES cells cultured in 2i medium and LIF (ES#), ES cells cultured in LIF/serum (ES), ELA cells obtained from ES in 2iL (ELA#) and ELA obtained from ES (ELA). **D**, box plots show z-scores of the expression of miRNAs predicted to bind top RISC-released ($\Delta E < -2$; left panel) or top RISC-loaded ($\Delta E > 2$; right panel) mRNAs at ES/ELA transition. Global miRNA/mRNA binding prediction was performed by the miRVestigator framework, which is designed to take as input a list of co-expressed genes and return the miRNA most likely regulating these genes (Plaisier et al., 2011). **E**, box plot shows the distribution of predicted binding affinity, calculated as cumulative Miranda scores of miRNAs in green box of A, in the 3'UTR of genes from the indicated families. Dashed red line marks the median score of a random gene set. $*$p=0.05, $**$p=0.01, $***$p=0.001. C-E, Wilcoxon test between pairs of conditions (C,D) or between each family and a randomized set of 3'UTRs (E).

Indeed, we observed that the expression of a set of miRNAs predicted to regulate the mRNAs resulting most RISC-enriched or depleted was significantly up or down-regulated during the ES/ELA transition (Figure 3.12A). This result suggests that our method of analysis of mRNA/RISC Enrichment is indeed predictive of miRNA/mRNA interactions. More interestingly, the analysis of global miRNA expression at the ES/ELA cell transition highlighted a number of up- and down-regulated miRNAs (3.12B) consistent with the differential pattern of expression observed in naïve and primed pluripotent cells (Jouneau et al., 2012). Specifically, the level of expression of these miRNAs is higher in naïve pluripotent cells and lower in ELA generated from ES cells (Figure 3.12C), making them part of a signature of ground-state pluripotency. We found that the 3'UTRs of genes coding for DNMT, KDM and SWI/SNF are significantly enriched in predicted binding sites for the miRNAs down-regulated at the ES/ELA cells transition compared to control 3'UTRs (Figure 3.12E). This observation suggests a direct role of these miRNAs in inhibiting the translation of DNMT, KDM and SWI/SNF in ES cells.

Discussion

4.1 RISC-mRNA interaction profiling

Taking advantage of the spontaneous differentiation program that ES cells undergo when deprived of pluripotency-maintaining signals, we set up a protocol of in vitro neural differentiation which recapitulates the early steps of nervous system development and patterning (Bertacchi et al., 2013; 2015a; 2015b).
This model allowed us to isolate and study cells that are primed to differentiation (ELA) just after their escape from the ground-state pluripotency. This is a transient population which closely resembles the stem cells derived from post-implantation mouse epiblast. Thus, comparing ES to ELA cells allowed us to investigate the molecular mechanisms at the bases of cell priming to differentiation.
Although many papers in the recent past have highlighted the role of miRNAs in the maintenance of pluripotency, the direct mRNA targets of miRNAs and their overall functions remained to be elucidated. To fill this gap, we performed Argonaute RIP as a way to estimate RISC-mediated inhibition of gene expression (Nelson et al., 2007). Through an integrated analysis at many different "omic" levels (total mRNAs, RISC-interacting mRNAs, miRNAs, ribosome loading and mass spectrometry of nuclear proteins) we evaluated RISC-mRNA interactions at the bases of cell pluripotency. Notably the intersection of RISC Enrichment with datasets of ribosome occupancy or mass spectrometry was crucial for a large-scale cross-validation of our experimental results. We observed that the

strongest variation, in terms of number of mRNAs changing their association with RISC, occurred at the ES/ELA transition, whereas the main modification in term of number of genes changing their transcriptional level was observed at the ELA/NPCs passage. We found a relatively small number of genes (about 120) whose mRNA is subject to significant RISC release at the ES/ELA transition. This observation suggests that cell priming might be initiated by the translational regulation of few regulatory master genes and implies that transcriptional control should not be the primary type of control in ES/ELA transtion, rather it might account for most of the first step of cell differentiation (early neuralization, in our protocol). In this view, the characterization of the genes involved in translational control at the ES/ELA transition was crucial to understand the rationale of cell priming. Discovering that, in addition to cell cycle regulators, chromatin remodelers are primarily represented in the set of translationally regulated genes at this transition strongly supported the notion that cell priming is indeed a step permissive, but not sufficient, to the subsequent changes resulting in cell differentation. This is well consistent with the maintenance of pluripotency in ELA/EpiSCs/epiblast cells and their capacity to differentiate in all the three embryonic layers. Although it is not immediate to deduce the role of cell priming in the very first steps of cell differentiation, the observation that chromatin regulators are primarily involved indicates that this step prepares the chromatin to respond to the major changes required for the establishment of the three embryonic layers. The fact that translational control accounts for most of this step suggests that priming must occur more rapidly than expected if regulated by a pure transcriptional control.

4.2 Chromatin remodeling and priming

A number of mRNAs released by RISC are related to DNA repair and replication. As ES cells and ELA correspond to inner cell mass (ICM) and post-implantation cells, respectively, the requirement of increased proliferation during priming is

consistent with the higher cell division rate occurring after embryo implantation, when cells shorten their cell cycle duration (Snow, 1977).

Chromatin regulators are the other main class of mRNAs released from RISC at the ES/ELA transition. There is large evidence that the activity of chromatin remodelers is necessary for cell priming (Chen and Dent, 2014). Nonetheless, we found that DNMT, KDM and SWI/SNF mRNAs are already present in ground-state pluripotent cells, though their translation is either inhibited or kept at lower levels. We found this observation of interest, since an activity of chromatin regulators would not be expected in ES cells, as they are stably maintained in a state of pluripotency and are not prone to undergo spontaneous differentiation when cultured in the appropriate conditions.

A number of observations indicate specific requirements of distinct chromatin regulators in cell priming. The nucleosome remodeling and deacetylase (NuRD) corepressor complex, which core enzymatic activities are expleted, among the others, by proteins of DNMT, KDM and SWI/SNF families, plays a critical role in the exit from pluripotency. In fact, lack of NuRD activity in ES cells leads to inefficient differentiation and failure to silence pluripotency genes (Kaji et al. 2006), while in embryos causes cellular disorganization soon after implantation (Kaji et al. 2007). However, despite the important role in the exit from pluripotency, how NuRD activity is modulated in nave ES cells was to date unclear (Nichols and Smith, 2012). Indeed, the presence in undifferentiated cells of many chromatin regulators which have a strong role in pluripotency destabilization poses the question of how the cell can avoid a "transcriptional paradox".

During early embryonic development, DNMT activity contributes to establish different genomic methylation patterns, which characterize somatic differentiated cells (Reik et al., 2001). The observations that a number of pluripotency-related genes are hypomethylated in stem cells (Farthing et al., 2008) and that global DNA hypermethylation occurs in epiblast cells (Smith et al., 2014) sug-

gest that the extensive reprogramming of genomic methylation pattern is a key event in ES cell priming. Global DNA hypomethylation is associated with ground-state pluripotency (Ficz et al., 2011, 2013; Habibi et al., 2013; Leitch et al., 2013) but, surprisingly, appreciable levels of DNMTs are transcribed in naïve ES cells (Faddah et al., 2013). Our finding that Dnmt1/3 mRNAs are significantly released by RISC and that Dnmt1/3 protein translation is enhanced at the ES/ELA transition might contribute both to explain the presence of DNMT mRNAs in ESCs and to suggest a mechanism of NuRD regulation in the naive pluripotent state.

The same consideration holds for the members of the KDM and SWI/SNF families that we found released from RISC at ES/ELA transition, which can act as well as transcriptional repressors. Kdm2b (Jhdm1b) is responsible for the demethylation of H3K36 (He et al., 2008), which marks the transcribed region of active genes (Barski et al., 2007), while SmarcA4 is part of a complex that is believed to be necessary to silence Nanog upon differentiation (Schaniel et al., 2009). Indeed, inhibiting the increase of SmarcA4 impedes ES/ELA transition when LIF and serum are removed from the culture medium. This, in spite of not being in contrast with the requirement of SmarcA4 for the maintenance of pluripotency (Ho et al., 2009), confirms and accounts for the evidence that increase of SmarcA4 activity is necessary for ES neuralization (Efroni et al., 2008). Overall, although some of these chromatin remodellers are important for the maintenance of pluripotency, we found that their up-regulation is crucial for the control of priming.

4.3 miRNA and stemness

Naïve and primed mouse embryonic stem cells have distinct miRNA signatures, with few genomic clusters accounting for the majority of the difference in miRNA expression profiles (Jouneau et al., 2012). miRNA expression analysis of our *in vitro* model confirmed a consistent modulation during the transition from ES to

ELA cells, with members of miR-302/367 and miR-290/295 clusters resulting up and down-regulated, respectively. Although several mRNAs targeted by miRNAs of the pluripotency signature were described in hES cells (Lipchina et al., 2011), since human embryonic stem cells represent a more advanced differentiation step, the dynamics of RISC-mediated regulation during priming are completely unknown. Our integrated analysis indicated that few distinct classes of genes are indeed modulated by miRNAs in the exit from ground pluripotent state. The role of miRNAs in ES cell cycle regulation, self-renewal and ability to differentiate has been extensively assayed using cell lines in which the key components of miRNA processing were inactivated (Kanellopoulou et al., 2005; Murchison et al., 2005; Melton et al., 2008; Wang et al., 2007, 2008, 2013). However, as these studies were performed in cell lines obtained through extensive cell culture selection and stabilization, they neither permit to assay the immediate effect of global miRNA inactivation in ES cells nor allow to analyze the changes "naturally" occurring during cell priming. By acutely inactivating Dicer or RISC, we found that global miRNA activity is required to maintain pluripotency, and that its perturbation triggers the beginning of a differentiation program even in ES cell culture conditions.

ES cells self-renewal is controlled by a small gene regulatory circuitry made of a dozen of interacting key transcription factors, which activity seems sufficient to maintain ground state pluripotency (Dunn et al., 2014). Nevertheless, other players different from transcription factors are likely to control the choice between self-renewal and differentiation of ES cells. For instance, global increase of protein translation enforced by a hierarchy of translational regulators is a feature of the switch between stem cell self-renewal and differentiation (Sampath et al., 2008). This observation, together with the evidence of pervasive transcription occurring in ES cells (Efroni et al., 2008), supports the hypothesis that a tight control of protein translation, in addition to transcriptional regulation, might account for ground state pluripotency. This is consistent also with the

observation that RNAi impairement produced by Dicer inactivation dramatically downregulated Oct4 in the epiblast, causing the loss of stem cells possibly due to their premature differentiation (Bernstein et al., 2003). Our findings of functional inactivation of miRNA pathway (namely Dicer or Argonaute1-2 loss of function) show how RISC activity is required for the maintenance of pluripotency, possibly suggesting that the phenotype obtained in vivo after Dicer inactivation could be caused by the dis-regulated translation of key chromatin regulators.

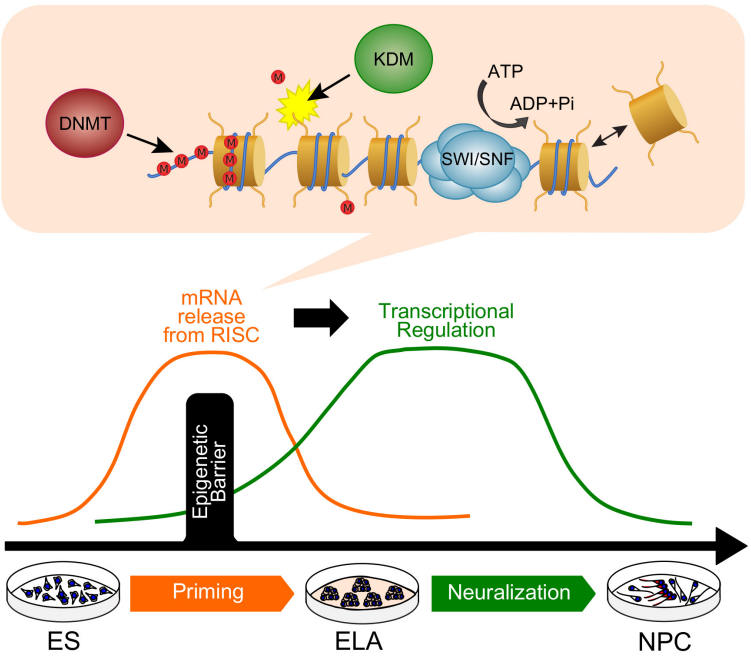

Figure 4.1: Two-layer model of priming

During ES to ELA transition there is a bulk release from RISC. Then transcriptional regulation occurs, thus distingushing priming and neuralization. Our data suggest a causal link between the two phenomena, as the pool of derepressed genes contains distinct chromatin remodelers which could overcome the epigenetic barrier between primed an ground-state pluripotency.

4.4 Conclusions

Our results suggest that the release of selected chromatin regulators from RISC inhibition during priming may serve to reduce the pervasive transcription observed in ES cells (Efroni et al., 2008) by reshaping the nuclear landscape of the cell (Ahmed et al., 2010). Moreover, the release from RISC inhibition of DNMT, KDM and SWI/SNF members could explain the intrinsic tendency of ES cells to begin differentiating in the absence of external signals (Ying et al., 2003).

Altogether, our model poses the RISC-mediated control of protein translation among the key switches of pluripotency states. If this suggests a primary mechanism for preserving ES cell pluripotency, on the other hand miRNA-mediated control of translation could maintain cells in a metastable state, rapidly converted into a differentiation program upon the removal of stemness-sustaining factors both *in vitro* and in the embryo. Accordingly, priming can be seen as a process in which two epigenetic mechanisms are layered one on the other: a first, microRNA-mediated layer, on which lies chromatin-based modulation of transcription (Figure 4.1).

Bibliography

[Ahmed et al., 2010] Ahmed, K., Dehghani, H., Rugg-Gunn, P., Fussner, E., Rossant, J. and Bazett-Jones, D. P. (2010). Global chromatin architecture reflects pluripotency and lineage commitment in the early mouse embryo. PLoS ONE *5*, e10531.

[Ambrosetti et al., 1997] Ambrosetti, D. C., Basilico, C. and Dailey, L. (1997). Synergistic activation of the fibroblast growth factor 4 enhancer by Sox2 and Oct-3 depends on protein-protein interactions facilitated by a specific spatial arrangement of factor binding sites. Molecular and cellular biology *17*, 6321–6329.

[Anders et al., 2014] Anders, S., Pyl, P. T. and Huber, W. (2014). HTSeq A Python framework to work with high-throughput sequencing data. bioRxiv *31*, 002824.

[Barski et al., 2007] Barski, A., Barski, A., Cuddapah, S., Cuddapah, S., Cui, K., Cui, K., Roh, T.-y., Roh, T.-y., Schones, D. E., Schones, D. E., Wang, Z., Wang, Z., Wei, G., Wei, G., Chepelev, I., Chepelev, I., Zhao, K. and Zhao, K. (2007). High-Resolution Profiling of Histone Methylations in the Human Genome. Cell *129*, 823–837.

[Bartel, 2009] Bartel, D. P. (2009). MicroRNAs: Target Recognition and Regulatory Functions. Cell *136*, 215–233.

[Beddington and Robertson, 1989] Beddington, R. S. and Robertson, E. J. (1989). An assessment of the developmental potential of embryonic stem

cells in the midgestation mouse embryo. Development (Cambridge, England) *105*, 733–737.

[Benaglia et al., 2009] Benaglia, T., Chauveau, D., Hunter, D. R. and Young, D. S. (2009). mixtools: An R Package for Analyzing Finite. Journal of Statistical Software *32*, 1–29.

[Bentley et al., 2008] Bentley, D. R., Balasubramanian, S., Swerdlow, H. P., Smith, G. P., Milton, J., Brown, C. G., Hall, K. P., Evers, D. J., Barnes, C. L., Bignell, H. R., Boutell, J. M., Bryant, J., Carter, R. J., Keira Cheetham, R., Cox, A. J., Ellis, D. J., Flatbush, M. R., Gormley, N. a., Humphray, S. J., Irving, L. J., Karbelashvili, M. S., Kirk, S. M., Li, H., Liu, X., Maisinger, K. S., Murray, L. J., Obradovic, B., Ost, T., Parkinson, M. L., Pratt, M. R., Rasolonjatovo, I. M. J., Reed, M. T., Rigatti, R., Rodighiero, C., Ross, M. T., Sabot, A., Sankar, S. V., Scally, A., Schroth, G. P., Smith, M. E., Smith, V. P., Spiridou, A., Torrance, P. E., Tzonev, S. S., Vermaas, E. H., Walter, K., Wu, X., Zhang, L., Alam, M. D., Anastasi, C., Aniebo, I. C., Bailey, D. M. D., Bancarz, I. R., Banerjee, S., Barbour, S. G., Baybayan, P. a., Benoit, V. a., Benson, K. F., Bevis, C., Black, P. J., Boodhun, A., Brennan, J. S., Bridgham, J. a., Brown, R. C., Brown, A. a., Buermann, D. H., Bundu, A. a., Burrows, J. C., Carter, N. P., Castillo, N., Chiara E Catenazzi, M., Chang, S., Neil Cooley, R., Crake, N. R., Dada, O. O., Diakoumakos, K. D., Dominguez-Fernandez, B., Earnshaw, D. J., Egbujor, U. C., Elmore, D. W., Etchin, S. S., Ewan, M. R., Fedurco, M., Fraser, L. J., Fuentes Fajardo, K. V., Scott Furey, W., George, D., Gietzen, K. J., Goddard, C. P., Golda, G. S., Granieri, P. a., Green, D. E., Gustafson, D. L., Hansen, N. F., Harnish, K., Haudenschild, C. D., Heyer, N. I., Hims, M. M., Ho, J. T., Horgan, A. M., Hoschler, K., Hurwitz, S., Ivanov, D. V., Johnson, M. Q., James, T., Huw Jones, T. a., Kang, G.-D., Kerelska, T. H., Kersey, A. D., Khrebtukova, I., Kindwall, A. P., Kingsbury, Z., Kokko-Gonzales, P. I.,

Kumar, A., Laurent, M. a., Lawley, C. T., Lee, S. E., Lee, X., Liao, A. K., Loch, J. a., Lok, M., Luo, S., Mammen, R. M., Martin, J. W., McCauley, P. G., McNitt, P., Mehta, P., Moon, K. W., Mullens, J. W., Newington, T., Ning, Z., Ling Ng, B., Novo, S. M., O'Neill, M. J., Osborne, M. a., Osnowski, A., Ostadan, O., Paraschos, L. L., Pickering, L., Pike, A. C., Pike, A. C., Chris Pinkard, D., Pliskin, D. P., Podhasky, J., Quijano, V. J., Raczy, C., Rae, V. H., Rawlings, S. R., Chiva Rodriguez, A., Roe, P. M., Rogers, J., Rogert Bacigalupo, M. C., Romanov, N., Romieu, A., Roth, R. K., Rourke, N. J., Ruediger, S. T., Rusman, E., Sanches-Kuiper, R. M., Schenker, M. R., Seoane, J. M., Shaw, R. J., Shiver, M. K., Short, S. W., Sizto, N. L., Sluis, J. P., Smith, M. a., Ernest Sohna Sohna, J., Spence, E. J., Stevens, K., Sutton, N., Szajkowski, L., Tregidgo, C. L., Turcatti, G., Vandevondele, S., Verhovsky, Y., Virk, S. M., Wakelin, S., Walcott, G. C., Wang, J., Worsley, G. J., Yan, J., Yau, L., Zuerlein, M., Rogers, J., Mullikin, J. C., Hurles, M. E., McCooke, N. J., West, J. S., Oaks, F. L., Lundberg, P. L., Klenerman, D., Durbin, R. and Smith, A. J. (2008). Accurate whole human genome sequencing using reversible terminator chemistry. Nature *456*, 53–59.

[Bernemann et al., 2011] Bernemann, C., Greber, B., Ko, K., Sterneckert, J., Han, D. W., Araúzo-Bravo, M. J. and Schöler, H. R. (2011). Distinct developmental ground states of epiblast stem cell lines determine different pluripotency features. Stem Cells *29*, 1496–1503.

[Bernstein et al., 2003] Bernstein, E., Kim, S. Y., Carmell, M. a., Murchison, E. P., Alcorn, H., Li, M. Z., Mills, A. a., Elledge, S. J., Anderson, K. V. and Hannon, G. J. (2003). Dicer is essential for mouse development. Nature genetics *35*, 215–217.

[Bertacchi et al., 2015a] Bertacchi, M., Lupo, G., Pandolfini, L., Casarosa, S., D'Onofrio, M., Pedersen, R., Harris, W. A. and Cremisi, F. (2015a). Activin/Nodal signaling supports retinal progenitor specification in a narrow time

window during pluripotent stem cell differentiation to anterior neuroectoderm. Cell Reports , in press.

[Bertacchi et al., 2015b] Bertacchi, M., Pandolfini, L., D'Onofrio, M., Brandi, R. and Cremisi, F. (2015b). The double inhibition of endogenously produced BMP and Wnt factors synergistically triggers dorsal telencephalic differentiation of mouse ES cells. Developmental neurobiology *75*, 66–79.

[Bertacchi et al., 2013] Bertacchi, M., Pandolfini, L., Murenu, E., Viegi, A., Capsoni, S., Cellerino, A., Messina, A., Casarosa, S. and Cremisi, F. (2013). The positional identity of mouse ES cell-generated neurons is affected by BMP signaling. Cellular and Molecular Life Sciences *70*, 1095–1111.

[Bock et al., 2005] Bock, C., Reither, S., Mikeska, T., Paulsen, M., Walter, J. and Lengauer, T. (2005). BiQ Analyzer: Visualization and quality control for DNA methylation data from bisulfite sequencing. Bioinformatics *21*, 4067–4068.

[Bolger et al., 2014] Bolger, a. M., Lohse, M. and Usadel, B. (2014). Trimmomatic: A flexible read trimming tool for Illumina NGS data. Bioinformatics *30*, 2114–2120.

[Brinkman et al., 2014] Brinkman, E. K., Chen, T., Amendola, M. and van Steensel, B. (2014). Easy quantitative assessment of genome editing by sequence trace decomposition. Nucleic Acids Research *42*, e168–e168.

[Brons et al., 2007] Brons, I. G. M., Smithers, L. E., Trotter, M. W. B., Rugg-Gunn, P., Sun, B., Chuva de Sousa Lopes, S. M., Howlett, S. K., Clarkson, A., Ahrlund-Richter, L., Pedersen, R. a. and Vallier, L. (2007). Derivation of pluripotent epiblast stem cells from mammalian embryos. Nature *448*, 191–195.

[Chambers et al., 2003] Chambers, I., Colby, D., Robertson, M., Nichols, J., Lee, S., Tweedie, S. and Smith, A. (2003). Functional expression cloning of

Nanog, a pluripotency sustaining factor in embryonic stem cells. Cell *113*, 643–655.

[Chambers et al., 2007] Chambers, I., Silva, J., Colby, D., Nichols, J., Nijmeijer, B., Robertson, M., Vrana, J., Jones, K., Grotewold, L. and Smith, A. (2007). Nanog safeguards pluripotency and mediates germline development. Nature *450*, 1230–1234.

[Chen and Dent, 2014] Chen, T. and Dent, S. Y. R. (2014). Chromatin modifiers and remodellers: regulators of cellular differentiation. Nature reviews. Genetics *15*, 93–106.

[Dunn et al., 2014] Dunn, S.-J., Martello, G., Yordanov, B., Emmott, S. and Smith, a. G. (2014). Defining an essential transcription factor program for naïve pluripotency. Science (New York, N.Y.) *344*, 1156–60.

[Efroni et al., 2008] Efroni, S., Duttagupta, R., Cheng, J., Dehghani, H., Hoeppner, D. J., Dash, C., Bazett-Jones, D. P., Le Grice, S., McKay, R. D. G., Buetow, K. H., Gingeras, T. R., Misteli, T. and Meshorer, E. (2008). Global Transcription in Pluripotent Embryonic Stem Cells. Cell Stem Cell *2*, 437–447.

[Enright et al., 2003] Enright, A. J., John, B., Gaul, U., Tuschl, T., Sander, C. and Marks, D. S. (2003). MicroRNA targets in Drosophila. Genome biology *5*, R1.

[Faddah et al., 2013] Faddah, D. a., Wang, H., Cheng, A. W., Katz, Y., Buganim, Y. and Jaenisch, R. (2013). Single-cell analysis reveals that expression of nanog is biallelic and equally variable as that of other pluripotency factors in mouse escs. Cell Stem Cell *13*, 23–29.

[Farthing et al., 2008] Farthing, C. R., Ficz, G., Ng, R. K., Chan, C. F., Andrews, S., Dean, W., Hemberger, M. and Reik, W. (2008). Global mapping

of DNA methylation in mouse promoters reveals epigenetic reprogramming of pluripotency genes. PLoS Genetics *4*, e1000116.

[Festuccia et al., 2012] Festuccia, N., Osorno, R., Halbritter, F., Karwacki-Neisius, V., Navarro, P., Colby, D., Wong, F., Yates, A., Tomlinson, S. R. and Chambers, I. (2012). Esrrb is a direct Nanog target gene that can substitute for Nanog function in pluripotent cells. Cell Stem Cell *11*, 477–490.

[Ficz et al., 2011] Ficz, G., Branco, M. R., Seisenberger, S., Santos, F., Krueger, F., Hore, T. a., Marques, C. J., Andrews, S. and Reik, W. (2011). Dynamic regulation of 5-hydroxymethylcytosine in mouse ES cells and during differentiation. Nature *473*, 398–402.

[Guo et al., 2010] Guo, G., Huss, M., Tong, G. Q., Wang, C., Li Sun, L., Clarke, N. D. and Robson, P. (2010). Resolution of cell fate decisions revealed by single-cell gene expression analysis from zygote to blastocyst. Developmental cell *18*, 675–85.

[Guo et al., 2009] Guo, G., Yang, J., Nichols, J., Hall, J. S., Eyres, I., Mansfield, W. and Smith, A. (2009). Klf4 reverts developmentally programmed restriction of ground state pluripotency. Development (Cambridge, England) *136*, 1063–1069.

[Habibi et al., 2013] Habibi, E., Brinkman, A. B., Arand, J., Kroeze, L. I., Kerstens, H. H. D., Matarese, F., Lepikhov, K., Gut, M., Brun-Heath, I., Hubner, N. C., Benedetti, R., Altucci, L., Jansen, J. H., Walter, J., Gut, I. G., Marks, H. and Stunnenberg, H. G. (2013). Whole-genome bisulfite sequencing of two distinct interconvertible DNA methylomes of mouse embryonic stem cells. Cell Stem Cell *13*, 360–369.

[Hahne et al., 2009] Hahne, F., LeMeur, N., Brinkman, R. R., Ellis, B., Haaland, P., Sarkar, D., Spidlen, J., Strain, E. and Gentleman, R. (2009). flow-

Core: a Bioconductor package for high throughput flow cytometry. BMC bioinformatics *10*, 106.

[Hayashi et al., 2008] Hayashi, K., Chuva, S. M. and Lopes, D. S. (2008). Supplemental Data Dynamic Equilibrium and Heterogeneity of Mouse Pluripotent Stem Cells with Distinct Functional and Epigenetic States. Cell stem cell *3*.

[He et al., 2008] He, J., Kallin, E. M., Tsukada, Y.-I. and Zhang, Y. (2008). The H3K36 demethylase Jhdm1b/Kdm2b regulates cell proliferation and senescence through p15(Ink4b). Nature structural & molecular biology *15*, 1169–1175.

[Heard, 2004] Heard, E. (2004). Recent advances in X-chromosome inactivation. Current Opinion in Cell Biology *16*, 247–255.

[Heiman et al., 2014] Heiman, M., Kulicke, R., Fenster, R. J., Greengard, P. and Heintz, N. (2014). Cell type-specific mRNA purification by translating ribosome affinity purification (TRAP). Nature protocols *9*, 1282–91.

[Heiman et al., 2008] Heiman, M., Schaefer, A., Gong, S., Peterson, J. D., Day, M., Ramsey, K. E., Suárez-Fariñas, M., Schwarz, C., Stephan, D. a., Surmeier, D. J., Greengard, P. and Heintz, N. (2008). A Translational Profiling Approach for the Molecular Characterization of CNS Cell Types. Cell *135*, 738–748.

[Hiratani et al., 2008] Hiratani, I., Ryba, T., Itoh, M., Yokochi, T., Schwaiger, M., Chang, C. W., Lyou, Y., Townes, T. M., Schübeler, D. and Gilbert, D. M. (2008). Global reorganization of replication domains during embryonic stem cell differentiation. PLoS Biology *6*, 2220–2236.

[Ho et al., 2009] Ho, L., Ronan, J. L., Wu, J., Staahl, B. T., Chen, L., Kuo, A., Lessard, J., Nesvizhskii, A. I., Ranish, J. and Crabtree, G. R. (2009). An embryonic stem cell chromatin remodeling complex, esBAF, is essential

for embryonic stem cell self-renewal and pluripotency. Proceedings of the National Academy of Sciences of the United States of America *106*, 5181–5186.

[Hosler et al., 1989] Hosler, B. a., LaRosa, G. J., Grippo, J. F. and Gudas, L. J. (1989). Expression of REX-1, a gene containing zinc finger motifs, is rapidly reduced by retinoic acid in F9 teratocarcinoma cells. Molecular and cellular biology *9*, 5623–5629.

[Hotta et al., 2009] Hotta, A., Cheung, A. Y. L., Farra, N., Vijayaragavan, K., Séguin, C. a., Draper, J. S., Pasceri, P., Maksakova, I. a., Mager, D. L., Rossant, J., Bhatia, M. and Ellis, J. (2009). Isolation of human iPS cells using EOS lentiviral vectors to select for pluripotency. Nature methods *6*, 370–376.

[Huang et al., 2009] Huang, D. W., Sherman, B. T. and Lempicki, R. a. (2009). Systematic and integrative analysis of large gene lists using DAVID bioinformatics resources. Nature protocols *4*, 44–57.

[Jiang et al., 2008] Jiang, J., Chan, Y.-S., Loh, Y.-H., Cai, J., Tong, G.-Q., Lim, C.-A., Robson, P., Zhong, S. and Ng, H.-H. (2008). A core Klf circuitry regulates self-renewal of embryonic stem cells. Nature cell biology *10*, 353–360.

[Jouneau et al., 2012] Jouneau, A., Ciaudo, C., Sismeiro, O., Brochard, V., Jouneau, L., Vandormael-Pournin, S., Coppée, J.-Y., Zhou, Q., Heard, E., Antoniewski, C. and Cohen-Tannoudji, M. (2012). Naive and primed murine pluripotent stem cells have distinct miRNA expression profiles. RNA (New York, N.Y.) *18*, 253–64.

[Kaji et al., 2006] Kaji, K., Caballero, I. M., MacLeod, R., Nichols, J., Wilson, V. A. and Hendrich, B. (2006). The NuRD component Mbd3 is required for pluripotency of embryonic stem cells. Nature cell biology *8*, 285–92.

[Kaji et al., 2007] Kaji, K., Nichols, J. and Hendrich, B. (2007). Mbd3, a component of the NuRD co-repressor complex, is required for development of pluripotent cells. Development (Cambridge, England) *134*, 1123–32.

[Kamiya et al., 2011] Kamiya, D., Banno, S., Sasai, N., Ohgushi, M., Inomata, H., Watanabe, K., Kawada, M., Yakura, R., Kiyonari, H., Nakao, K., Jakt, L. M., Nishikawa, S.-i. and Sasai, Y. (2011). Intrinsic transition of embryonic stem-cell differentiation into neural progenitors. Nature *470*, 503–509.

[Kanellopoulou et al., 2005] Kanellopoulou, C., Muljo, S. a., Kung, A. L., Ganesan, S., Drapkin, R., Jenuwein, T., Livingston, D. M. and Rajewsky, K. (2005). Dicer-deficient mouse embryonic stem cells are defective in differentiation and centromeric silencing. Genes and Development *19*, 489–501.

[Karolchik et al., 2004] Karolchik, D., Hinrichs, A. S., Furey, T. S., Roskin, K. M., Sugnet, C. W., Haussler, D. and Kent, W. J. (2004). The UCSC Table Browser data retrieval tool. Nucleic acids research *32*, D493–D496.

[Khare et al., 2012] Khare, S. P., Habib, F., Sharma, R., Gadewal, N., Gupta, S. and Galande, S. (2012). HIstome - A relational knowledgebase of human histone proteins and histone modifying enzymes. Nucleic Acids Research *40*, D337–42.

[Kim et al., 2013] Kim, D., Pertea, G., Trapnell, C., Pimentel, H., Kelley, R. and Salzberg, S. L. (2013). TopHat2: accurate alignment of transcriptomes in the presence of insertions, deletions and gene fusions. Genome biology *14*, R36.

[Kozomara and Griffiths-Jones, 2014] Kozomara, A. and Griffiths-Jones, S. (2014). MiRBase: Annotating high confidence microRNAs using deep sequencing data. Nucleic Acids Research *42*, D68–73.

[Kunath et al., 2007] Kunath, T., Saba-El-Leil, M. K., Almousailleakh, M., Wray, J., Meloche, S. and Smith, A. (2007). FGF stimulation of the Erk1/2

signalling cascade triggers transition of pluripotent embryonic stem cells from self-renewal to lineage commitment. Development (Cambridge, England) *134*, 2895–2902.

[Landmead et al., 2009] Landmead, B., Trapnell, C., Pot, M. and Salzberg, S. (2009). Ultrafast and memory-efficient alignment of short DNA sequences to the human genome. Genome Biology *10*, R25.

[Leitch et al., 2013] Leitch, H. G., McEwen, K. R., Turp, A., Encheva, V., Carroll, T., Grabole, N., Mansfield, W., Nashun, B., Knezovich, J. G., Smith, A., Surani, M. A. and Hajkova, P. (2013). Naive pluripotency is associated with global DNA hypomethylation. Nature structural & molecular biology *20*, 311–6.

[Lessard and Crabtree, 2010] Lessard, J. a. and Crabtree, G. R. (2010). Chromatin regulatory mechanisms in pluripotency. Annual review of cell and developmental biology *26*, 503–532.

[Liao et al., 2014] Liao, Y., Smyth, G. K. and Shi, W. (2014). FeatureCounts: An efficient general purpose program for assigning sequence reads to genomic features. Bioinformatics *30*, 923–930.

[Lienert et al., 2011] Lienert, F., Wirbelauer, C., Som, I., Dean, A., Mohn, F. and Schübeler, D. (2011). Identification of genetic elements that autonomously determine DNA methylation states. Nature Genetics *43*, 1091–1097.

[Lipchina et al., 2011] Lipchina, I., Elkabetz, Y., Hafner, M., Sheridan, R., Mihailovic, A., Tuschl, T., Sander, C., Studer, L. and Betel, D. (2011). Genome-wide identification of microRNA targets in human ES cells reveals a role for miR-302 in modulating BMP response. Genes & development *25*, 2173–86.

[Love et al., 2014] Love, M. I., Huber, W. and Anders, S. (2014). This Provisional PDF corresponds to the article as it appeared upon acceptance . Fully

formatted Moderated estimation of fold change and dispersion for RNA-seq data with DESeq2. Genome biology *15*, 550.

[Lowell et al., 2006] Lowell, S., Benchoua, A., Heavey, B. and Smith, A. G. (2006). Notch promotes neural lineage entry by pluripotent embryonic stem cells. PLoS Biology *4*, 805–818.

[Marks et al., 2012] Marks, H., Kalkan, T., Menafra, R., Denissov, S., Jones, K., Hofemeister, H., Nichols, J., Kranz, A., Francis Stewart, a., Smith, A. and Stunnenberg, H. G. (2012). The transcriptional and epigenomic foundations of ground state pluripotency. Cell *149*, 590–604.

[Matsuda et al., 1999] Matsuda, T., Nakamura, T., Nakao, K., Arai, T., Katsuki, M., Heike, T. and Yokota, T. (1999). STAT3 activation is sufficient to maintain an undifferentiated state of mouse embryonic stem cells. EMBO Journal *18*, 4261–4269.

[McDonel et al., 2009] McDonel, P., Costello, I. and Hendrich, B. (2009). Keeping things quiet: Roles of NuRD and Sin3 co-repressor complexes during mammalian development. International Journal of Biochemistry and Cell Biology *41*, 108–116.

[Melton et al., 2010] Melton, C., Judson, R. L. and Blelloch, R. (2010). Opposing microRNA families regulate self-renewal in mouse embryonic stem cells. Nature *463*, 621–626.

[Murchison et al., 2005] Murchison, E. P., Partridge, J. F., Tam, O. H., Cheloufi, S. and Hannon, G. J. (2005). Characterization of Dicer-deficient murine embryonic stem cells. Proceedings of the National Academy of Sciences of the United States of America *102*, 12135–12140.

[Navarro et al., 2010] Navarro, P., Oldfield, A., Legoupi, J., Festuccia, N., Dubois, A., Attia, M., Schoorlemmer, J., Rougeulle, C., Chambers, I. and

Avner, P. (2010). Molecular coupling of Tsix regulation and pluripotency. Nature *468*, 457–460.

[Nelson et al., 2007] Nelson, P. T., De Planell-Saguer, M., Lamprinaki, S., Kiriakidou, M., Zhang, P., O'Doherty, U. and Mourelatos, Z. (2007). A novel monoclonal antibody against human Argonaute proteins reveals unexpected characteristics of miRNAs in human blood cells. RNA (New York, N.Y.) *13*, 1787–1792.

[Nichols and Smith, 2012] Nichols, J. and Smith, A. (2012). Pluripotency in the embryo and in culture. Cold Spring Harbor Perspectives in Biology *4*, a008128.

[Nichols et al., 1998] Nichols, J., Zevnik, B., Anastassiadis, K., Niwa, H., Klewe-Nebenius, D., Chambers, I., Schöler, H. and Smith, A. (1998). Formation of pluripotent stem cells in the mammalian embryo depends on the POU transcription factor Oct4. Cell *95*, 379–391.

[Niwa et al., 1998] Niwa, H., Burdon, T., Chambers, I. and Smith, a. (1998). Self-renewal of pluripotent embryonic stem cells is mediated via activation of STAT3. Genes & development *12*, 2048–2060.

[Niwa et al., 2000] Niwa, H., Miyazaki, J. and Smith, a. G. (2000). Quantitative expression of Oct-3/4 defines differentiation, dedifferentiation or self-renewal of ES cells. Nature genetics *24*, 372–376.

[Nordgå rd et al., 2006] Nordgå rd, O., Kvalø y, J. T., Farmen, R. K. and Heikkilä, R. (2006). Error propagation in relative real-time reverse transcription polymerase chain reaction quantification models: The balance between accuracy and precision. Analytical Biochemistry *356*, 182–193.

[O'Doherty et al., 2000] O'Doherty, U., Swiggard, W. J. and Malim, M. H. (2000). Human immunodeficiency virus type 1 spinoculation enhances infection through virus binding. Journal of virology *74*, 10074–10080.

[Okano et al., 1999] Okano, M., Bell, D. W., Haber, D. a. and Li, E. (1999). DNA methyltransferases Dnmt3a and Dnmt3b are essential for de novo methylation and mammalian development. Cell *99*, 247–257.

[Pelton et al., 2002] Pelton, T. a., Sharma, S., Schulz, T. C., Rathjen, J. and Rathjen, P. D. (2002). Transient pluripotent cell populations during primitive ectoderm formation: correlation of in vivo and in vitro pluripotent cell development. Journal of cell science *115*, 329–339.

[Peric-Hupkes et al., 2010] Peric-Hupkes, D., Meuleman, W., Pagie, L., Bruggeman, S. W. M., Solovei, I., Brugman, W., Gräf, S., Flicek, P., Kerkhoven, R. M., van Lohuizen, M., Reinders, M., Wessels, L. and van Steensel, B. (2010). Molecular Maps of the Reorganization of Genome-Nuclear Lamina Interactions during Differentiation. Molecular Cell *38*, 603–613.

[Pesce et al., 1998] Pesce, M., Wang, X., Wolgemuth, D. J. and Schöler, H. R. (1998). Differential expression of the Oct-4 transcription factor during mouse germ cell differentiation. Mechanisms of Development *71*, 89–98.

[Pfaffl et al., 2002] Pfaffl, M. W., Horgan, G. W. and Dempfle, L. (2002). Relative expression software tool (REST) for group-wise comparison and statistical analysis of relative expression results in real-time PCR. Nucleic acids research *30*, e36.

[Plaisier et al., 2011] Plaisier, C. L., Bare, J. C. and Baliga, N. S. (2011). MiRvestigator: Web application to identify miRNAs responsible for co-regulated gene expression patterns discovered through transcriptome profiling. Nucleic Acids Research *39*, W125–31.

[Reik et al., 2001] Reik, W., Dean, W. and Walter, J. (2001). Epigenetic reprogramming in mammalian development. Science (New York, N.Y.) *293*, 1089–1093.

[Reynolds et al., 2012] Reynolds, N., Latos, P., Hynes-Allen, A., Loos, R., Leaford, D., O'Shaughnessy, A., Mosaku, O., Signolet, J., Brennecke, P., Kalkan, T., Costello, I., Humphreys, P., Mansfield, W., Nakagawa, K., Strouboulis, J., Behrens, A., Bertone, P. and Hendrich, B. (2012). NuRD suppresses pluripotency gene expression to promote transcriptional heterogeneity and lineage commitment. Cell Stem Cell *10*, 583–594.

[Robinson et al., 2009] Robinson, M. D., McCarthy, D. J. and Smyth, G. K. (2009). edgeR: A Bioconductor package for differential expression analysis of digital gene expression data. Bioinformatics *26*, 139–140.

[Roh et al., 2005] Roh, T.-Y., Cuddapah, S. and Zhao, K. (2005). Active chromatin domains are defined by acetylation islands revealed by genome-wide mapping. Genes & development *19*, 542–52.

[Sampath et al., 2008] Sampath, P., Pritchard, D. K., Pabon, L., Reinecke, H., Schwartz, S. M., Morris, D. R. and Murry, C. E. (2008). A Hierarchical Network Controls Protein Translation during Murine Embryonic Stem Cell Self-Renewal and Differentiation. Cell Stem Cell *2*, 448–460.

[Sanjana et al., 2014] Sanjana, N. E., Shalem, O. and Zhang, F. (2014). Improved vectors and genome-wide libraries for CRISPR screening. bioRxiv *11*, 006726.

[Schaniel et al., 2009] Schaniel, C., Ang, Y.-S., Ratnakumar, K., Cormier, C., James, T., Bernstein, E., Lemischka, I. R. and Paddison, P. J. (2009). Smarcc1/Baf155 couples self-renewal gene repression with changes in chromatin structure in mouse embryonic stem cells. Stem cells *27*, 2979–2991.

[Schmiedel et al., 2015] Schmiedel, J. M., Klemm, S. L., Zheng, Y., Sahay, a., Bluthgen, N., Marks, D. S. and van Oudenaarden, a. (2015). MicroRNA control of protein expression noise. Science *348*, 128–132.

[Silva et al., 2003] Silva, J., Mak, W., Zvetkova, I., Appanah, R., Nesterova, T. B., Webster, Z., Peters, A. H. F. M., Jenuwein, T., Otte, A. P. and Brockdorff, N. (2003). Establishment of histone H3 methylation on the inactive X chromosome requires transient recruitment of Eed-Enx1 polycomb group complexes. Developmental Cell *4*, 481–495.

[Smith, 2001] Smith, A. G. (2001). : Of Mice and Men. Annual Review of Cell and Developmental Biology *17*, 435–462.

[Smith et al., 2014] Smith, Z. D., Chan, M. M., Humm, K. C., Karnik, R., Mekhoubad, S., Regev, A., Eggan, K. and Meissner, A. (2014). DNA methylation dynamics of the human preimplantation embryo. Nature *511*, 611–615.

[Smyth and Speed, 2003] Smyth, G. K. and Speed, T. (2003). Normalization of cDNA microarray data. Methods *31*, 265–273.

[Snow, 1977] Snow, M. H. L. (1977). Gastrulation in the mouse: growth and regionalization of the epiblast. Journal of Embryology and Experimental Morphology *Vol. 42*, 293–303.

[Song et al., 2012] Song, J., Saha, S., Gokulrangan, G., Tesar, P. J. and Ewing, R. M. (2012). DNA and chromatin modification networks distinguish stem cell pluripotent ground states. Molecular & cellular proteomics : MCP *11*, 1036–47.

[Spandidos et al., 2009] Spandidos, A., Wang, X., Wang, H. and Seed, B. (2009). PrimerBank: A resource of human and mouse PCR primer pairs for gene expression detection and quantification. Nucleic Acids Research *38*, D792–9.

[Stothard, 2000] Stothard, P. (2000). The sequence manipulation suite: JavaScript programs for analyzing and formatting protein and DNA sequences. BioTechniques *28*, 1102, 1104.

[Sun et al., 2009] Sun, C., Nakatake, Y., Akagi, T., Ura, H., Matsuda, T., Nishiyama, A., Koide, H., Ko, M. S. H., Niwa, H. and Yokota, T. (2009). Dax1 binds to Oct3/4 and inhibits its transcriptional activity in embryonic stem cells. Molecular and cellular biology *29*, 4574–4583.

[Szutorisz et al., 2006] Szutorisz, H., Georgiou, A., Tora, L. and Dillon, N. (2006). The Proteasome Restricts Permissive Transcription at Tissue-Specific Gene Loci in Embryonic Stem Cells. Cell *127*, 1375–1388.

[Takashima et al., 2014] Takashima, Y., Guo, G., Loos, R., Nichols, J., Ficz, G., Krueger, F., Oxley, D., Santos, F., Clarke, J., Mansfield, W., Reik, W., Bertone, P. and Smith, A. (2014). Resetting Transcription Factor Control Circuitry toward Ground-State Pluripotency in Human. Cell *158*, 1254–69.

[Tarkowski et al., 1977] Tarkowski, a. K., Witkowska, a. and Opas, J. (1977). Development of cytochalasin in B-induced tetraploid and diploid/tetraploid mosaic mouse embryos. Journal of embryology and experimental morphology *41*, 47–64.

[Tesar et al., 2007] Tesar, P. J., Chenoweth, J. G., Brook, F. a., Davies, T. J., Evans, E. P., Mack, D. L., Gardner, R. L. and McKay, R. D. G. (2007). New cell lines from mouse epiblast share defining features with human embryonic stem cells. Nature *448*, 196–199.

[Thomson et al., 1998] Thomson, J. a., Itskovitz-Eldor, J., Shapiro, S. S., Waknitz, M. a., Swiergiel, J. J., Marshall, V. S. and Jones, J. M. (1998). Embryonic stem cell lines derived from human blastocysts. Science (New York, N.Y.) *282*, 1145–1147.

[Vallier et al., 2005] Vallier, L., Alexander, M. and Pedersen, R. a. (2005). Activin/Nodal and FGF pathways cooperate to maintain pluripotency of human embryonic stem cells. Journal of cell science *118*, 4495–4509.

[Vallier et al., 2009] Vallier, L., Mendjan, S., Brown, S., Chng, Z., Teo, A., Smithers, L. E., Trotter, M. W. B., Cho, C. H.-H., Martinez, A., Rugg-Gunn, P., Brons, G. and Pedersen, R. a. (2009). Activin/Nodal signalling maintains pluripotency by controlling Nanog expression. Development (Cambridge, England) *136*, 1339–1349.

[Wang et al., 2008] Wang, Y., Baskerville, S., Shenoy, A., Babiarz, J. E., Baehner, L. and Blelloch, R. (2008). Embryonic stem cell-specific microRNAs regulate the G1-S transition and promote rapid proliferation. Nature genetics *40*, 1478–1483.

[Wang et al., 2007] Wang, Y., Medvid, R., Melton, C., Jaenisch, R. and Blelloch, R. (2007). DGCR8 is essential for microRNA biogenesis and silencing of embryonic stem cell self-renewal. Nature genetics *39*, 380–385.

[Wang et al., 2013] Wang, Y., Melton, C., Li, Y. P., Shenoy, A., Zhang, X. X., Subramanyam, D. and Blelloch, R. (2013). MiR-294/miR-302 Promotes Proliferation, Suppresses G1-S Restriction Point, and Inhibits ESC Differentiation through Separable Mechanisms. Cell Reports *4*, 99–109.

[Whyte et al., 2012] Whyte, W., Bilodeau, S., Orlando, D., Hoke, H., Frampton, G., Young, R., Whyte, W., Hoke, H., Frampton, G., Young, R., Foster, C., Foster, C. and Cowley, S. (2012). Enhancer decommissioning by LSD1 during embryonic stem cell differentiation. Nature *482*, 221–5.

[Ye et al., 2013] Ye, S., Li, P., Tong, C. and Ying, Q.-L. (2013). Embryonic stem cell self-renewal pathways converge on the transcription factor Tfcp2l1. The EMBO journal *32*, 2548–60.

[Ying et al., 2003a] Ying, Q. L., Nichols, J., Chambers, I. and Smith, A. (2003a). BMP induction of Id proteins suppresses differentiation and sustains embryonic stem cell self-renewal in collaboration with STAT3. Cell *115*, 281–292.

[Ying et al., 2003b] Ying, Q.-L., Stavridis, M., Griffiths, D., Li, M. and Smith, A. (2003b). Conversion of embryonic stem cells into neuroectodermal precursors in adherent monoculture. Nature biotechnology *21*, 183–186.

[Ying et al., 2008] Ying, Q.-L., Wray, J., Nichols, J., Batlle-Morera, L., Doble, B., Woodgett, J., Cohen, P. and Smith, A. (2008). The ground state of embryonic stem cell self-renewal. Nature *453*, 519–523.

[Zhou et al., 2012] Zhou, W., Choi, M., Margineantu, D., Margaretha, L., Hesson, J., Cavanaugh, C., Blau, C. A., Horwitz, M. S., Hockenbery, D., Ware, C. and Ruohola-Baker, H. (2012). HIF1α induced switch from bivalent to exclusively glycolytic metabolism during ESC-to-EpiSC/hESC transition. The EMBO Journal *31*, 2103–2116.

[Zhu et al., 2010] Zhu, W., Smith, J. W. and Huang, C. M. (2010). Mass spectrometry-based label-free quantitative proteomics. Journal of Biomedicine and Biotechnology *2010*, 1–6.

[Zufferey et al., 1997] Zufferey, R., Nagy, D., Mandel, R. J., Naldini, L. and Trono, D. (1997). Multiply attenuated lentiviral vector achieves efficient gene delivery in vivo. Nature biotechnology *15*, 871–875.

Cell. Mol. Life Sci. (2013) 70:1095–1111
DOI 10.1007/s00018-012-1182-3

Cellular and Molecular Life Sciences

RESEARCH ARTICLE

The positional identity of mouse ES cell-generated neurons is affected by BMP signaling

Michele Bertacchi · Luca Pandolfini · Elisa Murenu · Alessandro Viegi · Simona Capsoni · Alessandro Cellerino · Andrea Messina · Simona Casarosa · Federico Cremisi

Received: 11 July 2012 / Revised: 24 September 2012 / Accepted: 25 September 2012 / Published online: 16 October 2012

Abstract We investigated the effects of bone morphogenetic proteins (BMPs) in determining the positional identity of neurons generated in vitro from mouse embryonic stem cells (ESCs), an aspect that has been neglected thus far. Classical embryological studies in lower vertebrates indicate that BMPs inhibit the default fate of pluripotent embryonic cells, which is both neural and anterior. Moreover, mammalian ESCs generate neurons more efficiently when cultured in a minimal medium containing BMP inhibitors. In this paper, we show that mouse ESCs produce, secrete, and respond to BMPs during in vitro neural differentiation. After neuralization in a minimal medium, differentiated ESCs show a gene expression profile consistent with a midbrain identity, as evaluated by the analysis of a number of markers of anterior–posterior and dorsoventral identity. We found that BMPs endogenously produced during neural differentiation mainly act by inhibiting the expression of a telencephalic gene profile, which was revealed by the treatment with Noggin or with other BMP inhibitors. To better characterize the effect of BMPs on positional fate, we compared the global gene expression profiles of differentiated ESCs with those of embryonic forebrain, midbrain, and hindbrain. Both Noggin and retinoic acid (RA) support neuronal differentiation of ESCs, but they show different effects on their positional identity: whereas RA supports the typical gene expression profile of hindbrain neurons, Noggin induces a profile characteristic of dorsal telencephalic neurons. Our findings show that endogenously produced BMPs affect the positional identity of the neurons that ESCs spontaneously generate when differentiating in vitro in a minimal medium. The data also support the existence of an intrinsic program of neuronal differentiation with dorsal telencephalic identity. Our method of ESC neuralization allows for fast differentiation of neural cells via the same signals found during in vivo embryonic development and for the acquisition of cortical identity by the inhibition of BMP alone.

Keywords Noggin · BMP · Cortical identity · Embryonic stem cells

Electronic supplementary material The online version of this article (doi:10.1007/s00018-012-1182-3) contains supplementary material, which is available to authorized users.

M. Bertacchi · L. Pandolfini · A. Viegi · S. Capsoni · A. Cellerino · F. Cremisi (✉)
Scuola Normale Superiore di Pisa, Piazza dei Cavalieri 7, 56100 Pisa, Italy
e-mail: f.cremisi@sns.it

E. Murenu · A. Messina · S. Casarosa
CIBIO, Università di Trento, Trento, Italy

A. Cellerino
Leibniz Institute for Age Research – Fritz Lipmann Institute, Jena, Germany

Introduction

Neural inducing signals are proposed to impart both neural and anterior identity to the ectoderm, while the generation of the full range of CNS structures would be the result of later events that posteriorize anterior neural tissue. According to this view, bone morphogenetic proteins (BMPs) play a key role by antagonizing a neural anterior default differentiation program. Antagonists of BMP signaling such as Noggin would ensure low levels of BMPs in the presumptive neuroectoderm thus allowing forebrain development in the absence of posteriorizing signals [67].

The dissection of diffusible signals that orchestrate neural induction has recently been made easier by the study of embryonic stem cells (ESCs) in vitro differentiation. In recent years, several reports have described methods for the generation of neural cells from mouse ESCs [5, 15, 19, 65, 66]. Using defined growth media, it has been possible to investigate the diffusible factors that affect anterior–posterior (A/P) as well as dorsoventral (D/V) identity of in vitro-generated neurons. Among these, retinoic acid (RA), BMPs, Wnts, fibroblast growth factors (FGFs) and sonic hedgehog (SHH) have been described [10, 15, 18, 28, 65].

Conversely, the use of factor-free chemically defined media has allowed for the investigation of the differentiation fate of ESCs in the absence of exogenous signals, showing that it is predominantly neural [19, 20, 63]. Effects of factors endogenously produced by ESCs have also been suggested. BMPs sustain self-renewal and inhibit neural differentiation of ESCs [70]. The BMP inhibitor Noggin triggers in vitro neuronal differentiation of mammalian ESCs cultured in growth factor-free chemically defined medium [9, 22]. It was recently shown that the cell-intrinsic expression of the zinc-finger nuclear protein Zfp521, which is inhibited by BMPs, plays a pivotal role in promoting a default neural state of ESCs. Furthermore, a role of Zfp521 in supporting an anterior identity of neurons generated by ESCs was hypothesized [33]. These data suggest that ESCs produce and are sensitive to BMPs with an autocrine/paracrine mechanism. However, to our knowledge, there is no direct measurement of BMP production by differentiating ESCs.

Early studies in lower vertebrates suggested that BMP plays a key role in anterior/posterior patterning. BMP antagonism on pluripotent cells of *Xenopus* animal caps induces cement glands, which are the most anterior ectodermal structures in *Xenopus*, and anterior brain markers such as the fore-midbrain marker Otx2, but not hindbrain or spinal cord markers [26, 38, 56]. More recent studies highlight that Noggin has a dose-dependent patterning effect on *Xenopus* animal caps. At lower doses, Noggin supports neuralization without the expression of diencephalic markers, which are instead activated at higher doses [39]. Moreover, in *Xenopus* embryos, the specification of the forebrain requires isolation of its cells from BMP, Activin/Nodal, and Wnt signaling by high concentrations of Noggin produced in cells at the anterior margin of the neural plate [4]. These observations suggest that, in vivo, the concentration of endogenous BMPs might be relevant in the control of the positional identity of neurons. It has also been proposed that BMPs play a role in the regional morphogenesis of mouse dorsal telencephalon, by the control of specific gene expression, cell proliferation, and local cell death [17]. Forebrain truncations were found in double-mutant mice for both BMP antagonists Noggin and Chordin [3]. BMP signaling specifies telencephalic progenitor cells toward the most dorsal fate, the choroid plexus [27], but earlier effects on the anterior–posterior patterning are not well characterized.

The aim of the present work is to directly show the endogenous production of BMP by differentiating ESCs and to characterize the effects of BMP on the differentiation and positional identity of ESC-generated neurons. We, therefore, established an in vitro differentiation protocol that minimizes exogenous signals and analyzed ESCs differentiation by performing a genome-wide expression analysis. We report that mouse ESCs produce and release BMPs, which act on their differentiation in such a minimal medium. Blocking the BMP pathway by Noggin or by other inhibitors selectively affects the A/P positional identity of the generated neurons. At the highest doses of Noggin that we tested, the fate of neurons produced by ESCs is predominantly dorsal telencephalic. These neurons have a gene expression profile that clusters with that of early cerebral cortical cells and express telencephalic differentiation markers.

Materials and methods

Cells cultures

Murine embryonic stem cell (ESC) lines E14Tg2A (passages 25–38) and 46 C (transgenic Sox1-GFP ESC kindly provided by A. Smith, University of Cambridge, UK, passages 33–39) were cultured on gelatin-coated tissue culture dishes at a density of 40,000 cells/cm^2. ESC medium, which was changed daily, contained GMEM (Sigma), 10 % Fetal Calf Serum, 2 mM Glutamine, 1 mM sodium Pyruvate, 1 mM non-essential amino acids, 0.05 mM β-mercaptoethanol, 100 U/ml Penicillin/Streptomycin and 1,000 U/ml recombinant mouse LIF (Invitrogen). Cells were passaged using Trypsin dissociation and re-plated at a dilution of 1:3–1:4, to avoid cell confluence and to maintain pluripotency. RAW 264.7 (mouse leukemic monocyte macrophage cell line, kindly supplied by Diana Boraschi, Institute of Medical Biotechnology, CNR of Pisa) were cultured in Dulbecco's modified Eagle's Medium with 4 mM L-glutamine and 4.5 g/L glucose, supplemented with 10 % fetal bovine serum. Cells were split every 2 days at a confluence of approximately 10 % (1×10^6 and 3×10^6 cells in 100- and 150-mm plates, respectively) and grown to a confluence of approximately 80 %. Mouse mesenchymal stromal cells (MSCs) primary cultures (kindly supplied by Cristina Magli, CNR of Pisa) were established from B6D2F1 (BDF1) mice (Charles River) as described [44].

Neural induction

Chemically defined minimal medium (CDMM) consisted of DMEM/F12 (Invitrogen), 2 mM Glutamine, 1 mM sodium Pyruvate, 0.1 mM non-essential amino acids, 0.05 mM β-mercaptoethanol, 100 U/ml Penicillin/Streptomycin supplemented with N2/B27 (no vitamin A; Invitrogen). Step I: dissociated ESCs were washed with DMEM/F12, aggregated in agar-coated culture dishes (65,000 cells per cm^2) and cultured as floating aggregates in CDMM for 2 days. The second day 70 % of CDMM was renewed. Step II: ESCs aggregates were dissociated and cultured in adhesion (65,000 cells per cm^2) on Poly-ornithine (Sigma; 20 µg/ml in sterile water, 4 h coating at 37 °C) and natural mouse Laminin (Invitrogen; 5 µg/ml in PBS, 4 h coating at 37 °C) for 4 days, changing CDMM daily. Step III: After a second dissociation, ESCs were cultured 4 additional days in CDMM devoid of B27 supplement to drive terminal differentiation, using the same type of seeding density and coated surface. Serum employed for trypsin inactivation was carefully removed by several washes in DMEM/F12. The following factors were tested by addition during step II: Recombinant Mouse Noggin (R&D; ranging from 5 to 400 nM), BMP4 (R&D; 50 ng/ml), Recombinant Mouse BMPRIA/Fc Chimera (R&D; 3.75 and 37.5 nM), Dorsomorphin (Sigma-Aldrich; 5 µM), Retinoic Acid (Sigma-Aldrich; 0.1–10 µM), Cyclopamine (Sigma-Aldrich; 10 µM), SAG (Santa Cruz Biotechnology; 100 nM), SB431542 (Sigma-Aldrich; 10 µM). Cell viability and proliferation, which were monitored by trypan blue exclusion test and cell counting, respectively, were not significantly affected by treatments.

Semiquantitative real-time PCR

For each sample, 500 ng of total RNA were reverse-transcribed. Amplified cDNA was quantified using GoTaq qPCR Master Mix (Promega) on Rotor-Gene 6000 (Corbett) with the primers listed in Supplemental Table 1. Amplification take-off values were evaluated using the built-in Rotor-Gene 6000 "relative quantitation analysis" function, and relative expression was calculated with the $2^{-\Delta\Delta Ct}$ method, normalizing to the housekeeping gene β-Actin. Standard errors were obtained from the error propagation formula as described in [46], and statistical significance was probed with randomization test, taking advantage of REST Software [51].

Immunocytodetection

Cells prepared for immunocytodetection experiments were cultured on Poly-ornithine/Laminin coated round glass coverslips. Cells were fixed using 2 % paraformaldehyde for 15 min, washed twice with PBS, permeabilized using 0.1 % Triton X100 in PBS and blocked using 0.5 % BSA in PBS. Primary antibodies used for microscopy included Oct3/4 (1:200; Santa Cruz DBA), Nanog (1:300; Novus Biologicals), acetylated N-Tubulin (1:500; Sigma), Neuronal Class III β-Tubulin (1:500; Covance), Doublecortin (1:500; Abcam), Musashi-1 (1:200; Cell Signaling), Nestin (1:200; Millipore), Synaptophysin (1:100; Santa Cruz DBA), α-Internexin (1:100; Santa Cruz DBA), phospho-Smad1/5/8 (1:100; Millipore), FoxG1 (1:200; Abcam), Tbr1 (1:400; Millipore), Satb2 (1:200; Abcam), VGlut2 (1:300; Abcam), GAD65 (1:500; Chemicon), Pax6 (1:400; Covance), Nkx2.1 (1:400; Abcam) and GFAP (1:100; Dako). Primary antibodies were incubated 2 h at room temperature; cells were then washed three times with PBS (10′ each). Alexa Fluor 488 and Alexa Fluor 568 anti-mouse or anti-rabbit IgG conjugates (Molecular Probes, 1:500) were incubated 1 h at RT in PBS containing 0.1 % Triton X100 and 0.5 % BSA for primary antibody detection, followed by three PBS washes (10′ each). Nuclear staining was obtained with DAPI. The protocol varied for Tbr1, Satb2 and FoxG1, the antibodies of which were incubated overnight at 4 °C using 0.3 % Triton X100.

FACS analysis

Adherent cells were detached by trypsinization, washed and resuspended in PBS at RT, then analyzed with a FACSCalibur cytometer (BD). At least 10,000 events per sample were collected. Data were processed with the free software WinMDI 2.9 (The Scripps Research Institute).

BMP2 ELISA

Cells were seeded into 24-well plates and cultured as described. When cells reached 70–80 % confluence, each well was washed with PBS and fresh medium (DMEM/F12 containing 2 mM Glutamine and 1 mM sodium Pyruvate) was replaced. After 24 h, supernatant was collected, centrifuged (10,000g, 5 min) to remove particulates and assayed for BMP2 content with a commercially available ELISA kit (Quantikine, BMP-2 Immunoassay; R&D Systems, Minneapolis, MN, USA), according to the manufacturer's instructions. This assay could measure BMP-2 concentrations as low as 50 pg/ml in a linear range (Pearson correlation coefficient of linear regression $R^2 = 0.999$; see Supplemental Figure SF1). A 1.2 % cross-reactivity was observed with 50 ng/mL recombinant human BMP-4. BMP-2 concentrations of triplicate samples were determined from the optical densities at 450 nm in relation to standard curves of the recombinant antigen provided in the kit.

Microarray hybridization and data analysis

Cortex, midbrain and hindbrain were dissected from $n = 3$ mouse embryos (C57BL/6 strain) at embryonic day (E)16. Total RNA was extracted with NucleoSpin RNA II columns (Macherey–Nagel). RNA from three different sets of experiment was pooled. RNA quality was assessed with Agilent Bioanalyzer RNA 6000 Nano kit; 500 ng of RNA were labeled with One Color Quick amp labeling kit (Agilent), purified and hybridized overnight onto an Agilent Mouse Gene Expression Microarray chip (4 × 44 Kv2) before detection, according to the manufacturer's instructions. Three slides were hybridized with Noggin-treated ESCs RNA and two slides were hybridized with RNA from all the other conditions. Agilent DNA Microarray scanner was used for slide acquisition and spot analysis was performed with Feature Extraction software (Agilent).

For GSEA analysis, genes differentially expressed between Noggin treatment and CDMM (Supplemental Table 2), or between RA treatment and CDMM (Supplemental Table 3; fold-change ≥2), were analyzed by the GeneSpring GX11.0 software using BROAD Gene Ontology collection (C5; http://www.broadinstitute.org/gsea). A complete GSEA list with enrichment scores of gene sets with q value <0.3 is shown in Supplemental Table 4.

To select a gene set representing the anterior-posterior regionalization of the developing brain, we compared gene expression profiles of E16 cortex and hindbrain using Genespring GX11.0 software (Agilent). A set of 592 genes with an absolute fold-change greater or equal than 10 ($p < 0.05$) was selected (see Supplemental Table 5). Significance of the data was proven by one-way ANOVA and Tukey post hoc test with Bonferroni correction for multiple comparisons. The content of this set of genes was explored by hierarchical clustering and principal component analysis, taking advantage of Cluster software [16]. Single linkage algorithm was employed for hierarchical clustering. Trees were generated using absolute correlation for genes and Euclidean distance for arrays, and visualized with java TreeView [55].

Results

A chemically defined minimal medium (CDMM) induces neurogenesis of ESCs

In order to investigate the default positional identity of neurons generated from ESCs, we established a culture method that promotes neurogenesis minimizing the influence of exogenous signals. This method consists of a three-step procedure of culture in a chemically defined minimal medium (CDMM; see "Materials and methods"; Fig. 1a) devoid of serum or morphogens but allowing cell survival by insulin.

Upon LIF and serum withdrawal, dissociated ESCs were initially grown as aggregates (Fig. 1b) in CDMM for 2 days. This step (step I), which minimizes cell death, follows a procedure adapted from previously described methods [5, 40, 65]. As many protocols use serum-containing medium (SCM) during ESCs aggregation, we also assayed this condition in the preliminary set-up of our protocol. As additional control, we used undifferentiated ESCs cultured in LIF + serum (ESC medium).

ESC aggregates were subsequently dissociated and cultured in adhesion for 4 days on Poly-ornhitine/Laminin-coated wells in CDMM (step II). All additional treatments (e.g., Noggin), when applied, were performed during this step (Fig. 1a), unless specified. During step II, ESCs turned off the expression of the stem cell marker Oct4 [45] and activated the expression of the pan-neuronal markers β-Tubulin-III and Ncam, as seen by RT-PCR (Fig. 1c). This activation was higher in ESCs aggregated in CDMM than in ESCs aggregated in SCM, as the latter still expressed high levels of Oct4 and activated the mesodermal marker GATA4 (Fig. 1c). Immunostaining showed much higher expression of the neural progenitor cell marker Musashi-1 [47] and robust downregulation of Oct4 in ESCs cultured in CDMM (Fig. 1d) compared to ESCs cultured in SCM (Fig. 1e). Whereas ESCs aggregated in CDMM started expressing β-Tubulin-III at step II, ESCs aggregated in SCM failed to show β-Tubulin-III labeling (Supplemental Figure SF2A, B). Similar results were obtained when analyzing ESCs aggregates cultured for 5 days (Supplemental Figure SF2C, D). Our observations indicate that aggregation (step I) in the absence of serum facilitates loss of stem cell pluripotency and induces rapid neural differentiation (as evaluated at the end of step II).

After a second dissociation, cells were cultured for 4 days in CDMM. This additional step (step III) allowed cells to undergo terminal differentiation. Notably, the presence of serum during step I profoundly affected the fate of cells produced at the end of step III, as the ratio of neural progenitor cells immunostained by Nestin antibody was lower in cells aggregated in SCM (8 ± 4.8 %;) compared to cells aggregated in CDMM (44.3 ± 8.7 %; Supplemental Figure SF2E–G). Consistently, mRNA expression of Nestin and of pan-neuronal markers Ncam and β-Tubulin-III was significantly lower at the end of step III in cells that were aggregated in SCM than in cells that were aggregated in CDMM (Supplemental Figure SF2H). Moreover, cells cultured in CDMM formed rosette-like structures at the end of step III, which are typical of neural progenitors in vitro ([73]; Supplemental Figure SF2F), and generated high proportions of neuronal cells

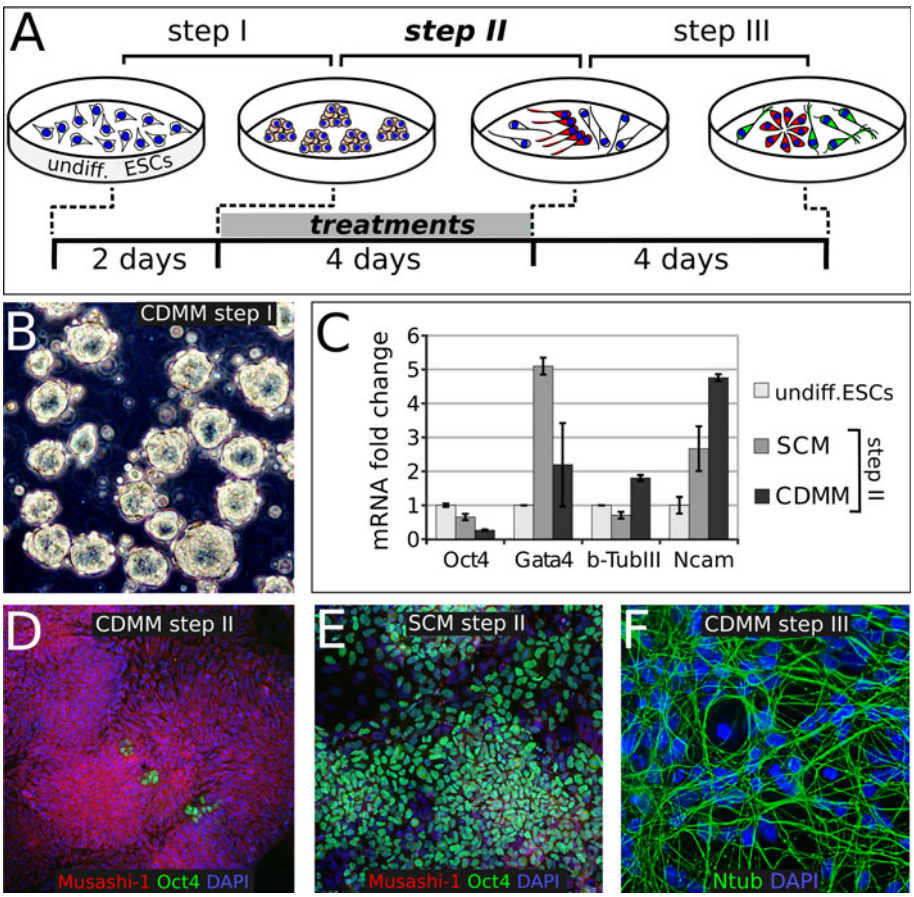

Fig. 1 Three-step protocol of ESCs neuronal differentiation: **a** ESCs differentiation protocol outline; *undiff* undifferentiated. **b** ESCs aggregates at step I. **c** RT-PCR mRNA analysis of expanding ESCs (undifferentiated), or of ESCs at the end of step II, initially (step I) aggregated in two diverse conditions (SCM and CDMM), normalized on ESCs. **d**, **e** Oct4 (*green*) and Musashi-1 (*red*) immunocytodetection of ESCs at the end of step II, after CDMM (**d**) or SCM (**e**) aggregation in step I. **f** immunocytodetection for anti-acetylated-Tubulin antibody (Ntub, *green*) of ESCs aggregated and differentiated in CDMM, at the end of step III. *Error bars* standard error; $p < 0.001$ (Randomization test, REST software) for all SCM and CDMM values compared to ESCs values, except for Gata4 in CDMM, which was not significant

immunostained by anti-acetylated-Tubulin (Ntub, Fig. 1f) and β-Tubulin-III antibody (Supplemental Figure SF2I).

We further characterized the nature of the differentiated ESCs by immunocytodetection. Neuronal morphology was heterogeneous, as we found multipolar cells, pyramidal-like cells, bipolar and unipolar cells (Supplemental Figure SF2J–M). ESC-generated neurons showed processes with varicosities positive to the neuronal intermediate filament α-Internexin that are typical of neurons forming synapses (Supplemental Figure SF2N). Moreover, ESC-derived neurons showed a punctate staining of the synaptic marker Synaptophysin (Supplemental Figure SF2O). We failed to detect GFAP-positive cells by immunostaining and GFAP mRNA levels were very low compared to the levels of P0 embryonic cortex, as evaluated by RT-PCR (not shown). This is consistent with an early differentiation state of the cells, as gliogenesis is the latest step in ESCs neural differentiation protocols [19].

We concluded that a short exposure to serum in the first days of differentiation cultures (step I) inhibits the acquisition of a neuronal fate and that ESCs cultured in the absence of any added morphogen efficiently differentiate into neuronal cells, which is consistent with previous observations [19, 59].

Effects of Noggin as a neural inducer in ESCs culture

The ability of Noggin to support neuronal differentiation of ESCs has been reported in different in vitro differentiation protocols [12, 22, 43]. Consistently, we found that adding increasing doses of Noggin (5–400 nM) to CDMM during step II supported the expression of the pan-neuronal markers Ncam and Pax6, as compared to cells grown in CDMM without Noggin (Fig. 2a). Notably, Noggin did not significantly affect pan-neuronal markers expression when added at step I or III (not shown).

At the end of step III, ESCs treated with Noggin during step II slightly increased the expression of Doublecortin (Dcx, a general marker of migrating neuroblasts; [36]) and of acetylated-Tubulin (Ntub, pan-neuronal marker) compared to ESCs cultured in CDMM (ctrl; Fig. 2b, c).

We directly compared the neural inducing activity of Noggin to SCM and CDMM conditions in terms of percentage of neural progenitors generated by ESCs. We took advantage of a Sox1-GFP knock-in ES cell line (46 C, [70]), analyzing GFP expression by flow cytometry. This analysis showed that CDMM culture conditions induced a massive increase of Sox1-GFP-positive neural progenitors at mid-step II (day 2; 68.2 %) compared to SCM condition

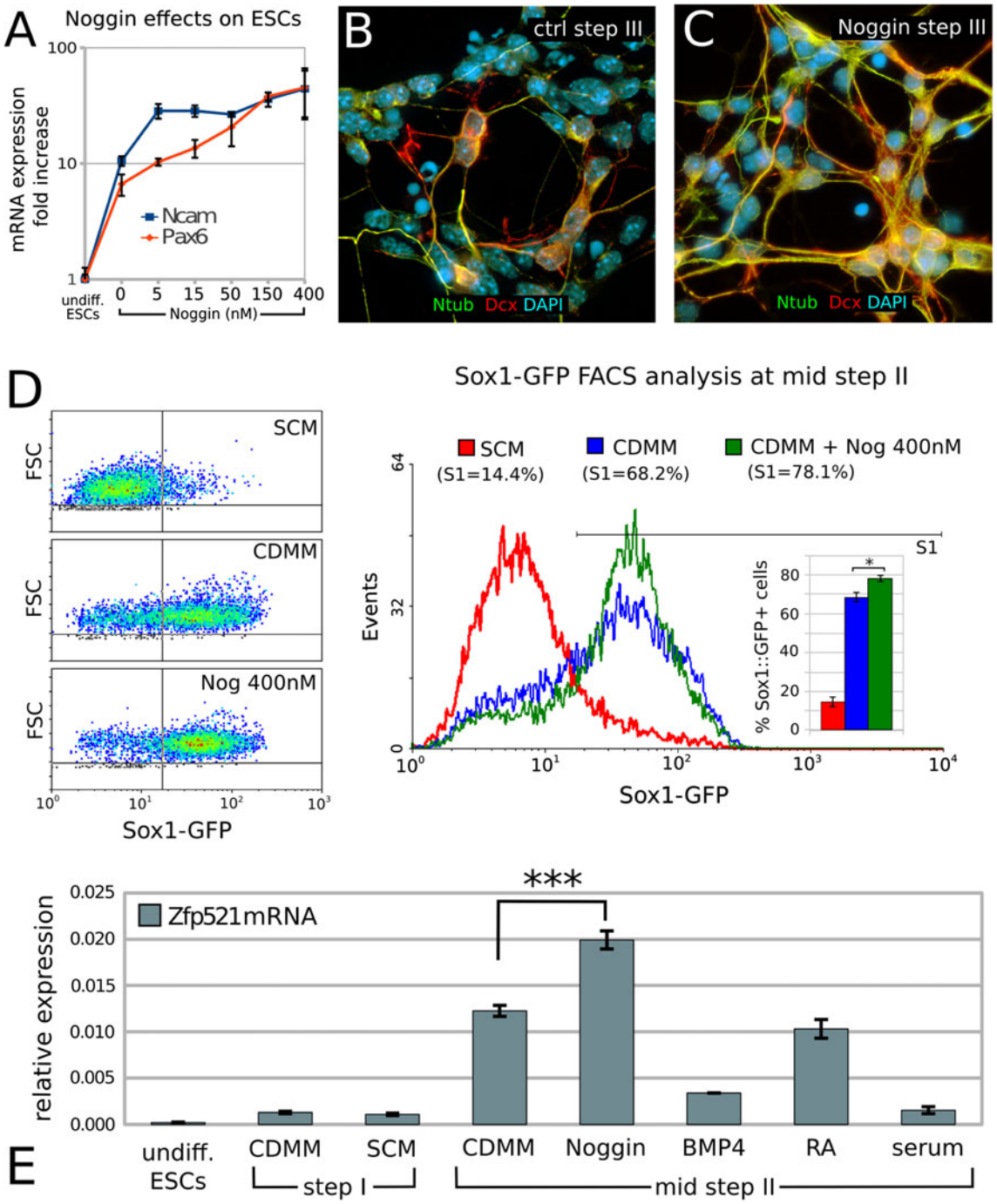

Fig. 2 Effects of Noggin as a neural inducer on ESCs differentiation:**a** RT-PCR mRNA quantification of pan-neuronal markers Ncam and Pax6 in expanding ESCs (undifferentiated) and ESCs at the end of step III after differentiation in CDMM (0) or in CDMM plus 5–400 nM Noggin (expression normalized on undifferentiated ESCs). **b**, **c** Doublecortin (Dcx, *red*) and acetylated-Tubulin (Ntub, *green*) immunocytodetection of ESCs at the end of step III after differentiation in CDMM (**b**, ctrl) or in CDMM containing 150 nM Noggin (**c**). **d** Flow-cytometry analysis of Sox1-GFP ESCs at day 2 of step II after culture in different conditions. SCM: ESCs were aggregated (step I) in serum-containing medium and differentiated (2 days, step II) without serum. CDMM: both ESCs aggregation (step I) and differentiation (2 days, step II) were carried out without serum. CDMM + Nog 400 nM: as CDMM condition, plus Noggin treatment during the first two days of step II. **e** RT-PCR mRNA quantification (ratio over β-Actin) of Zfp521 at different time points and after culture in different conditions, as indicated; treatments with Noggin (400 nM), BMP4 (50 ng/ml), RA (10 nM) and serum (10 %) were performed at step II. In (**a**, **d**, **e**), *error bars* show standard error; $*p < 0.05$, $***p < 0.001$ (two-tailed Student's *t* test)

(14.4 %), whereas Noggin (400 nM) induced a modest, although significant, increase compared to CDMM (78.1 %; Fig. 2d). A similar trend was also observed at early-step II (day1; SCM, 6.4 %; CDMM, 27.9 %; Noggin, 31.1 %; not shown). Ratios of Sox1-GFP positive neural progenitors obtained in the different culture conditions are consistent with a differential expression of the key transcription factor of neural commitment Zfp521, which is highest in cultures with Noggin (400 nM; Fig. 2e). We concluded that the majority of ESCs cultured in CDMM or in CDMM plus Noggin become neural progenitors at step II and established CDMM culture condition as control for subsequent investigations on BMP inhibition.

CDMM-differentiating ESCs produce and respond to BMPs

As Noggin affects ESCs neuralization, but BMPs were not added to culture medium, we assayed for the presence of BMPs that were endogenously produced by ESCs during differentiation. We thus compared the mRNA expression levels of BMP2/4 in proliferating ESCs, in CDMM-differentiating ESCs (during step II), in cells that express high BMP levels (primary mouse mesenchymal stromal cells, MSCs) or in cells that express low BMP2/4 levels (macrophage cell line RAW 264.7; [52]). We found that both undifferentiated and differentiating ESCs express high BMP2/4 levels (Fig. 3a).

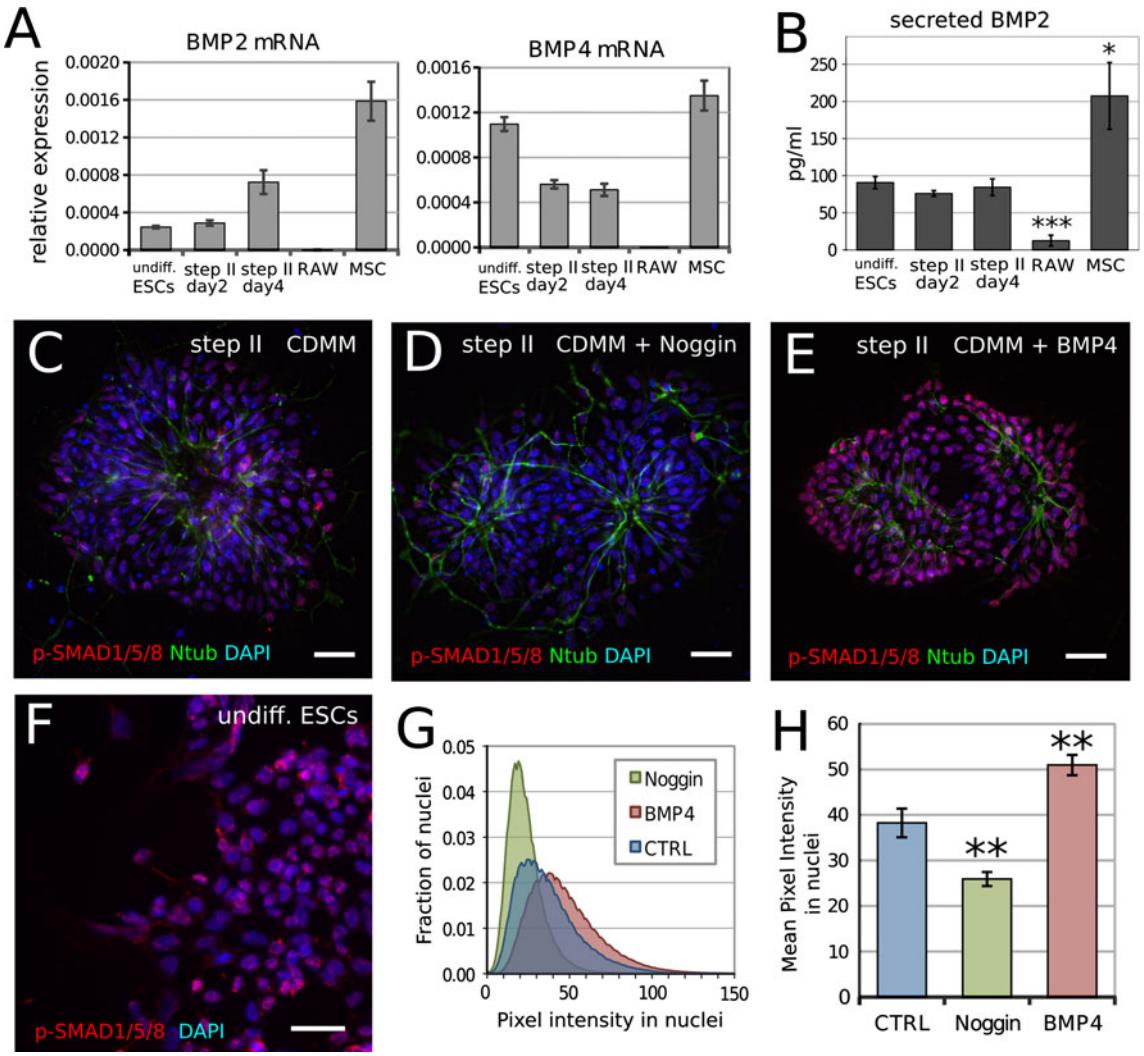

Fig. 3 Endogenous BMP production and BMP activity during ESCs differentiation in CDMM: **a** RT-PCR mRNA quantification (ratio over β-Actin) of BMP2 and BMP4 in expanding ESCs (undifferentiated), ESCs at the second and fourth day of step II, expanding RAW 264.7 cell line (RAW) and mouse mesenchymal stromal cells (MSCs, passage 3). **b** Secreted BMP2 quantification by ELISA in cells as in (**a**). **c–e** Ntub (*green*) and phospho-SMAD1/5/8 immunodetection (nuclear red staining over DAPI nuclear counterstaining) in ESCs at step II (day 2) in CDMM (**c**), 5 h after the addition of 400 nM Noggin to CDMM (**d**) and 5 h after the addition of 50 ng/ml BMP4 to CDMM (**e**). **f** Phospho-SMAD1/5/8 immunodetection (*red* staining over DAPI) in undifferentiated ESCs. *Scale bars* 30 µm. **g, h** Pixel intensity distribution (fraction of nuclei with given pixel intensity (**g**) and mean pixel intensity (**h**) of immunodetection in nuclei as in (**c–e**), respectively. *Error bars* standard error; $*p < 0.05$, $**p < 0.01$, $***p < 0.001$ (Student's t test)

Notably, ESCs transcribe BMP2/4 also at step II, when Noggin addition to CDMM exerts its effect on neuronal differentiation. Moreover, ELISA showed that CDMM-differentiating ESCs secrete approximately 50 % of the BMP2 protein secreted by MSCs, but almost ten times more than the amount secreted by RAW cells (Fig. 3b).

We found that CDMM-differentiating ESCs during step II express functional BMP receptors. In fact, ESCs at step II expressed higher levels of BMPR1a-b mRNA than MSCs, which depend on the binding of BMP2/4 to BMPR1a-b receptors for osteoblastogenesis [1] (Supplemental Figure SF3A). Interestingly, Noggin decreased the expression of ID1, a downstream effector of the BMP-responsive pathway [30] in a dose-dependent manner (Supplemental Figure SF3B). This is in line with the ability of noggin to block the BMP-responsive pathway in ESCs.

We further investigated the activation of intracellular transduction pathway in response to BMP signaling by analyzing SMAD1/5/8 phosphorylation (phospho-SMAD; Fig. 3c–h). Undifferentiated ESCs were used as a positive control (Fig. 3f). Most nuclei of both undifferentiated ESCs and ESCs at step II in different conditions showed phospho-SMAD immunostaining, with different degrees of intensity. Figure 3g shows the distribution of the immunostaining intensity and Fig. 3h reports the mean immunostaining intensity. We found that control CDMM-differentiating ESCs show intermediate levels of the phosphorylated form of SMAD1/5/8 during step II, as compared to ESCs in other culture conditions (Fig. 3c). This confirms the presence of an endogenous BMP production and activity. Acute 5 h treatment with Noggin (400 nM) or BMP4 (50 ng/ml) during step II significantly decreased or increased SMAD phosphorylation, respectively (Fig. 3d–g). The pattern of phospho-SMAD immunodetection showed that virtually all cells responded to BMP4 addition (Fig. 3e).

Consistently, BMP4 added exogenously to CDMM throughout step II (50 ng/ml), dramatically repressed the expression of the pan-neuronal markers Nestin, NFL, β-Tubulin-III and Pax6 (Supplemental Figure SF3C), thus confirming the ability of ESCs to specifically respond to BMP signaling during step II.

Our data thus show that ESCs produce and are sensitive to BMPs during neuronal differentiation in vitro.

In the absence of exogenous signals, ESCs generate neurons expressing midbrain dorsal markers

In order to investigate the effect of endogenous BMPs on ESCs positional identity, we characterized our control culture (ESCs differentiated in CDMM), by analyzing the expression of the FoxG1 [69], Wnt7b [49], Six3 [48], Otx2 [2], and En1 [68] genes at the end of step III. These genes display an ordered (A/P) expression that covers the most anterior aspect of forebrain (FoxG1, Emx2), entire forebrain (Six3), forebrain/midbrain (Otx2), and midbrain (En1). We also analyzed the expression of HoxB4 [53] and HoxB9 [11], which mark hindbrain and spinal cord, respectively (Fig. 4a). We compared the mRNA levels of these genes in CDMM-differentiated ESCs to the mRNA levels found in cortex (rostral–dorsal forebrain), mesencephalon (midbrain), rombencephalon (hindbrain), spinal cord of embryonic day 16 (E16) mouse, and undifferentiated ESCs. Compared to mouse brain, CDMM-differentiated ESCs expressed very high levels of Otx2 and En1, low levels of Wnt7b and Six3, and very low levels of both telencephalic (FoxG1), and posterior markers (HoxB4 and HoxB9) (Fig. 4b).

As ESCs cultured in CDMM failed to express high levels of hindbrain/spinal cord specific genes, we wanted to assay their ability to turn on these genes upon induction with the posteriorizing factor RA. As expected, ESCs treated with RA during step II, and analyzed at the end of step III, turned on the posterior markers HoxB4 and HoxB9 and downregulated the anterior markers FoxG1, Six3 and Otx2 in a dose-dependent fashion (Supplemental Figure SF4A).

We then analyzed the dorso-ventral (D/V) identity of ESCs generated cells at the end of step II by comparing the relative ratios of the cells expressing the dorsal marker Pax6 [60] or the ventral marker Nkx2.1 [50]. A large fraction (53.1 $\pm$ 7.6 %) of control CDMM ESCs expressed Pax6 protein and virtually no cells expressed Nkx2.1 protein (Fig. 4c, d). As the Pax6/Nkx2.1 D/V gradient is generated in response to a gradient of sonic hedgehog (Shh) activity [7], we assayed the effects of a SHH agonist (SAG, [13]) or of an antagonist (Cyclopamine; [62]) on ESCs. Drugs were added to CDMM throughout step II. SAG treatment dramatically repressed Pax6 (3.9 $\pm$ 1.1 %) and activated Nkx2.1 protein expression in a very large fraction of cells (79 $\pm$ 2.9 %), whereas Cyclopamine affected neither Pax6 nor Nkx2.1 (Fig. 4c, d). RT-PCR analysis confirmed these results (Supplemental Figure SF4B). Notably, the lack of any effect of Cyclopamine is consistent with the observation that Step II ESCs produced very low level of endogenous SHH (Supplemental Figure SF4C).

These data suggest that in our protocol of differentiation ESCs change the expression of A/P and D/V markers accordingly to treatments with morphogens, but mostly adopt a midbrain dorsal identity when cultured in CDMM (see "Discussion").

BMP inhibition during differentiation supports the expression of telencephalic markers

We subsequently investigated if endogenously produced BMPs can affect the regional identity of ESC-generated

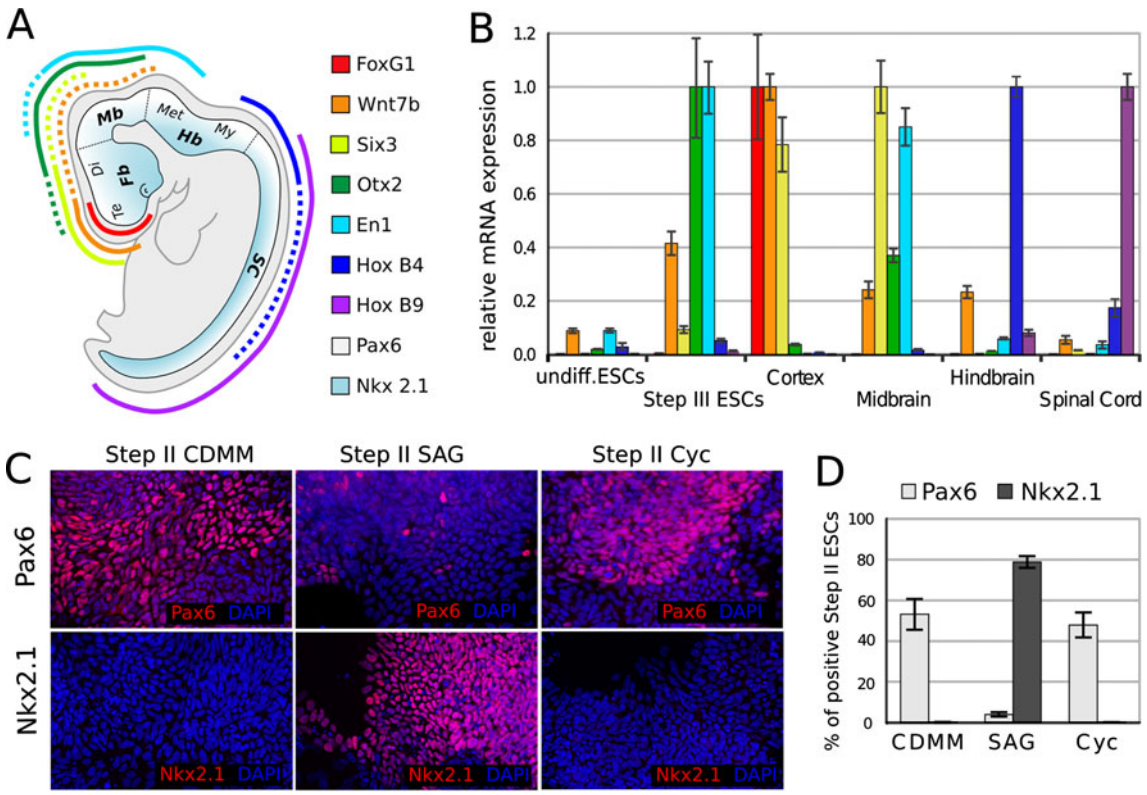

Fig. 4 Regional identity of ESCs differentiated in CDMM: **a** A/P (*color code*) and D/V (*white-cyan code*) patterning of mouse embryo as identified by the expression of key patterning genes, elaborated from EMAP (http://www.emouseatlas.org/emap/home.html) and articles cited in text. *Fb* forebrain, *Mb* midbrain, *Hb* hindbrain, *SC* spinal cord, *Te* telencephalon, *Di* diencephalon, *Met* metencephalon, *My* myelencephalon. **b** mRNA relative expression of A/P genes (as evaluated by RT-PCR, normalized on maximum expression) in brain tissues of E16 embryos, undifferentiated ESCs and ESCs at the end of step III. **c** Immunocytodetection of Pax6 and Nkx2.1 (nuclear *red* staining over DAPI nuclear counterstaining) at the end of step II in ESCs differentiated as indicated. Numbers in (**d**) show fractions of Pax6-positive cells (*light gray bars*) and Nkx2.1-positive cells (*dark gray bars*), in ESCs differentiated as in (**c**). *Cyc* cyclopamine. *Error bars* standard error

neurons. Compared to control, the treatment with increasing doses of Noggin (5–400 nM) during step II induced the telencephalic marker FoxG1 and repressed the more posterior markers Otx2 and En1 (Fig. 5a) in a dose-dependent manner, as evaluated at the end of step III. Moreover, Noggin induced the expression of Wnt7b (a forebrain marker; [49]), Six3 (prosencephalic marker), Emx2 (early cortical marker; [58]), Tbr1 and α-CamK-II (late cortical markers; [8]; [35]; Fig. 5b), and repressed the expression of the posterior marker Irx3, which is present in midbrain and more posterior regions ([6]; Fig. 5c). Noggin was ineffective on the hindbrain/spinal cord markers Gbx2, HoxB4 and HoxB9, leaving their low expression levels almost unchanged (Fig. 5c). As similar results were obtained when analyzing cells at earlier or later times of differentiation (end of step II or step III plus 4 days, respectively; Supplemental Fig. 5), we excluded the possibility that the effect of Noggin on positional identity may be the result of an enhancement/acceleration in neural fate induction.

To confirm the specificity of action of Noggin, we used the chimeric protein BMPR1A-Fc, a BMP inhibitor that binds to a BMP epitope outside the region recognized by Noggin ([23, 34]; see Supplemental Figure SF6A) and Dorsomorphin, a selective inhibitor of the BMP type I receptors ALK2, ALK3 and ALK6 that blocks BMP-mediated SMAD1/5/8 phosphorylation ([72]; Supplemental Figure SF6B). BMPR1A-Fc induced an increase of Sox1-GFP positive neural progenitors at mid-step II (day 2; 77.6 %; Supplemental Figure SF6D) that is comparable to the increase induced by Noggin (78.1 %; Fig. 2d). Dorsomorphin or BMPR1A-Fc treatment during step II also mimicked Noggin action by inhibiting ID1 expression (Supplemental Figures SF3B and SF6C), by supporting FoxG1 expression and by repressing Otx2 and En1 (Supplemental Figure SF6E, F). The specificity of BMPs in affecting ESCs differentiation fate is also suggested by the effects exerted by treatment at step II with SB431542. While Dorsomorphin selectively inhibits the BMP2/4 pathway, SB431542 suppresses the Activin/Tgf-β receptors ALK4, ALK5 and ALK7 and prevents BMP-independent, Activin/Tgf-β mediated, SMAD2/3 phosphorylation (Supplemental Figure SF6B; [9]). Compared to Noggin and

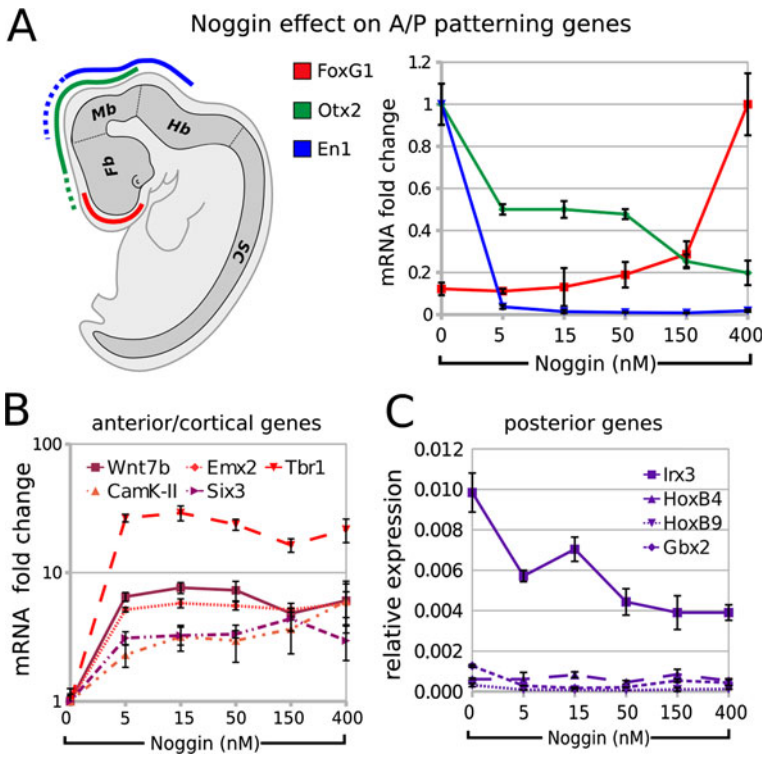

Fig. 5 Effects of BMP inhibition on the expression of A/P patterning genes: **a** A/P (*color code*) patterning of mouse embryonic brain by FoxG1, Otx2 and En1. *Fb* forebrain, *Mb* midbrain, *Hb* hindbrain, *SC* spinal cord. Graph shows RT-PCR mRNA quantification of FoxG1, Otx2 and En1 in ESCs at the end of step III after differentiation in CDMM (0) or in CDMM plus 5–400 nM Noggin (normalized on maximum expression). **b**, **c** RT-PCR mRNA quantification of forebrain/cortical markers (**b**) or hindbrain/spinal cord markers (**c**), in cells as in A (ratio over *β*-Actin). *Error bars* standard error

Dorsomorphin, SB451243 acted by repressing, rather than by inducing, FoxG1, slightly inhibited En1 and left Otx2 expression almost unchanged (Supplemental Figure SF6E).

Our results indicate that the inhibition of endogenously produced BMPs alters the A/P positional identity of the ESC-generated neurons.

BMP inhibition induces a mixed population of neural progenitor cells and differentiated neurons expressing cortical markers

We further investigated the nature of cells generated by Noggin-treated ESCs. At the end of step II, we found 79.2 % Nestin-positive neural progenitors in CDMM-differentiating ESCs, while Noggin treatment (150 nM) increased this ratio to 90.5 %. Notably, of the Nestin-positive progenitors in CDMM cultures only 1.2 % were positive for FoxG1, while Noggin treatment (150 nM) increased this ratio to 18.2 % (Fig. 6a–c). This implies that the majority of ESCs in CDMM become neural progenitors also without Noggin, but Noggin is necessary to acquire a telencephalic identity (see "Discussion").

The ratio of *β*-III-Tubulin positive neurons in cultures treated with Noggin (400 nM) was slightly higher than the ratio in control cultures at the end of Step III (Fig. 6d). In both conditions, the majority of cells negative for *β*-III-Tubulin staining were Nestin-positive progenitors (not shown). Both control and Noggin-treated ESCs generated high ratios of VGlut2-positive glutamatergic neurons (Fig. 6d, e), whereas the ratios of GAD65-positive GABAergic neurons either in control or in Noggin-treated ESCs were lower (Fig. 6d, f). Noggin induced the expression of a number of genes coding for the isoforms of receptors for many different neurotransmitters, including GABA (Supplemental Table 6).

To investigate in detail the nature of cells generated by Noggin-treated ESCs, at the end of Step III, we analyzed at the cellular level the expression of FoxG1, which labels telencephalic neuronal progenitors [54], and Tbr1, the

Fig. 6 Effects of BMP inhibition on ESCs neural conversion and cell fate acquisition: **a–c** double immunocytodetection of Nestin (*green*) and FoxG1 (*red*) at the end of step II in ESCs cultured in CDMM (**a**) or in CDMM + Noggin (150 nM, **b**). FoxG1-positive cells were always co-labeled by Nestin. Numbers in (**c**) show ratios of Nestin-positive cells among total cells (*light blue bars*), or ratios of FoxG1-positive cells among Nestin-positive cells (*red bars*). **d–f** VGlut2 (*red* in **e**), *β*-III-Tubulin (*green* in **f**), and Gad65 (*red* in **f**) immunocytodetection and cell counts in Noggin-treated ESCs at step III + 4 days. *Arrow* in (**f**) indicates a *β*-III-Tubulin/Gad65 double positive cell. **d** The ratios of cells positive for the markers in (**e** and **f**). **g–o** Immunocytodetection of FoxG1 (*red* in **g–j**), Tbr1 (*red* in **k–n**) and acetylated-Tubulin (*green* in **g–n**) in ESCs cells at the end of step III after differentiation in CDMM (control; **g**, **k**), CDMM plus Noggin (400 nM; **h**, **l**, **j**, **n**) and Dorsomorphin (5 uM; **i**, **m**). **o** Cell ratios of FoxG1-positive and Tbr1-positive cells from culture conditions as in (**g–n**), and for ESCs treated with SAG, RA or 150 nM Noggin (not shown). **p** A group of neurons almost all positive for Satb2 nuclear staining. **q** Numbers show the ratios of Tbr1 or Satb2 positive cells over time in 150 nM Noggin-treated ESC cultures. *Error bars* standard error; $*p < 0.05$, $**p < 0.01$ (two-tailed Student's *t* test)

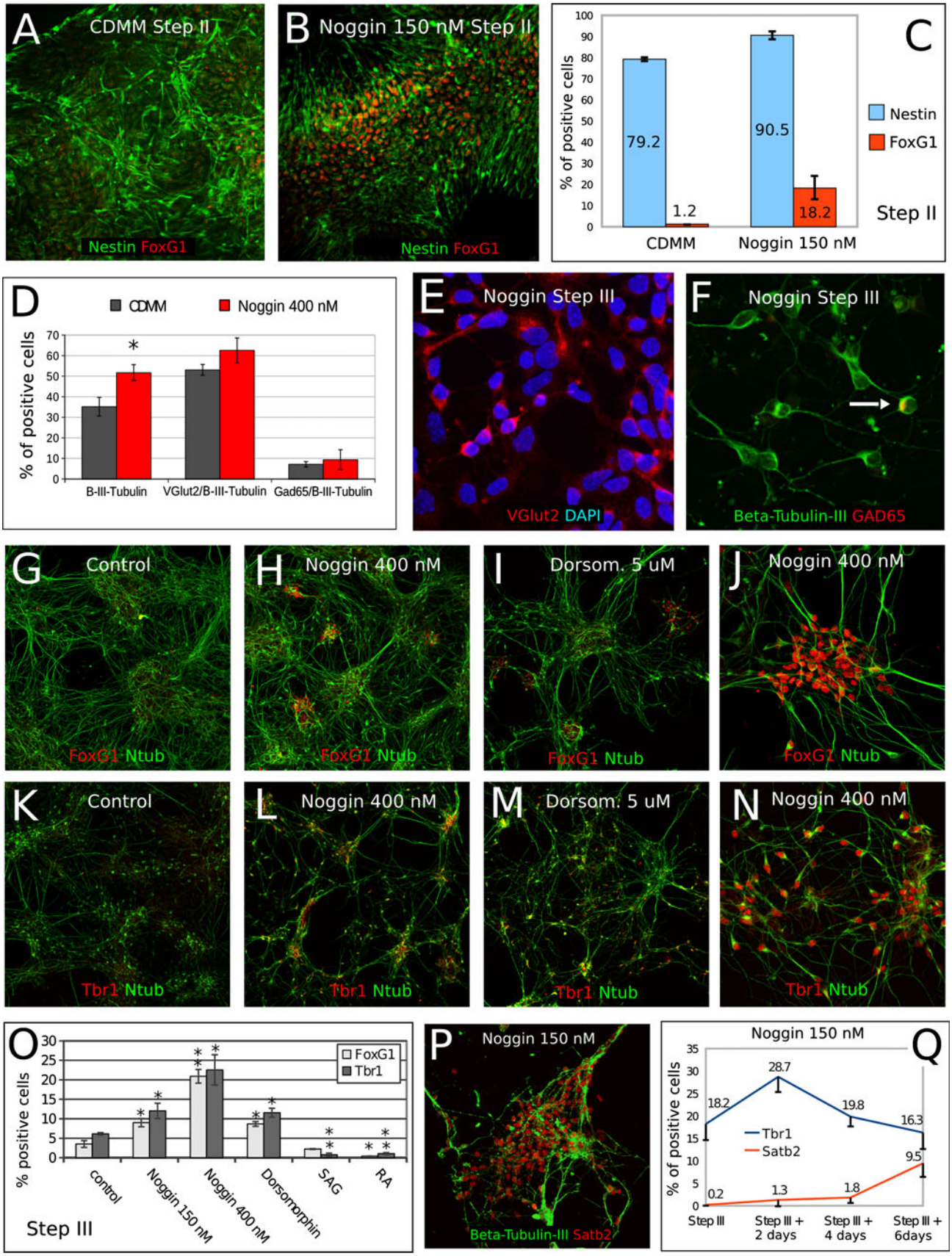
A
CDMM Step II
Nestin FoxG1
B
Noggin 150 nM Step II
Nestin FoxG1
C
% of positive cells
79.2
1.2
90.5
18.2
CDMM
Noggin 150 nM
Nestin
FoxG1
Step II
D
CDMM
Noggin 400 nM
% of positive cells
B-III-Tubulin
VGlut2/B-III-Tubulin
Gad65/B-III-Tubulin
E
Noggin Step III
VGlut2 DAPI
F
Noggin Step III
Beta-Tubulin-III GAD65
G
Control
FoxG1 Ntub
H
Noggin 400 nM
FoxG1 Ntub
I
Dorsom. 5 uM
FoxG1 Ntub
J
Noggin 400 nM
FoxG1 Ntub
K
Control
Tbr1 Ntub
L
Noggin 400 nM
Tbr1 Ntub
M
Dorsom. 5 uM
Tbr1 Ntub
N
Noggin 400 nM
Tbr1 Ntub
O
% positive cells
FoxG1
Tbr1
control
Noggin 150 nM
Noggin 400 nM
Dorsomorphin
SAG
RA
Step III
P
Noggin 150 nM
Beta-Tubulin-III Satb2
Q
Noggin 150 nM
% of positive cells
18.2
28.7
19.8
16.3
0.2
1.3
1.8
9.5
Tbr1
Satb2
Step III
Step III + 2 days
Step III + 4 days
Step III + 6days

expression of which specifically identifies a sub-set of cortical neurons (Cajal-Retzius cells, subplate cells and glutamatergic neurons of the deep layers of the cerebral cortex; [29]). We compared the expression of the two proteins in control cells and in cells differentiated in the presence of Noggin (150 and 400 nM), Dorsomorphin (5 μM), SAG (100 nM) or of RA (10 μM) during step II. We found that, compared to control (Fig. 6g, k), ESCs treated at Step II with Noggin produced a higher ratio of both FoxG1-positive (Fig. 6h, j, o) and Tbr1-positive cells at step III (Fig. 6l, n, o). Consistently, the expression of both proteins was induced by Dorsomorphin and repressed by RA (Fig. 6i, m, o). Ventralization induced by SAG inhibited Tbr1 expression and left Foxg1 expression almost unchanged (Fig. 6o).

Notably, Noggin-induced expression of Tbr1, which marks earlier cortical neurons, was followed by the activation of Satb2 (Fig. 6p), which labels late-generated cortical neurons of layers 2/3. This suggests that Noggin-treated ESCs follow a differentiation schedule similar to that of in vivo cortical neurons (Fig. 6q).

We considered the possibility that Noggin acts by selecting cells committed to a cortical identity, which might be already present in ESC cultures maintained in serum + LIF. We thus assayed the effect of Noggin on ESCs selected in the absence of signals that might influence their differentiation potential. ESCs in which mitogen-activated protein kinase signaling and glycogen synthase kinase-3 (GSK3) are double-inhibited are homogeneous and pluripotent when cultured in a medium containing LIF but devoid of serum (2i ESCs; [57, 71]). In our protocol, 2i ESCs neuralization was slightly faster than the neuralization of ESC maintained in serum + LIF (Supplemental Figure SF7A, B). However, the expression of A/P and D/V markers in neural cells obtained by 2i ESCs was comparable to the expression in neural cells obtained by ESCs cultured in serum (Supplemental Figure SF7C–J). For this reason, we can exclude that our results might be influenced by some heterogeneity of the starting ESC population due to culture in serum-containing medium.

We characterized the identity of Noggin-treated ESCs in more detail by comparing their global gene expression profiles to the profiles of ESCs differentiated in other culture conditions, or to the profiles of embryonic brain regions. To this purpose, we performed microarray hybridization (see "Materials and methods").

As RA is a potent inducer of neuronal differentiation [24], we compared its action to that of Noggin on ESCs differentiation. We analyzed gene expression profiles using Gene Set Enrichment Analysis (GSEA). GSEA is a computational method which allows to identify, within predefined groups of genes (gene sets associated with particular cellular functions) whether a significant enrichment of regulated genes occurs when comparing two conditions [61]. Figure 7a shows gene ontology categories implicated in neuronal function/differentiation and cell cycle control. The color heat map displays gene set enrichment scores for Noggin-treated (400 nM) versus control ESCs (first column) and for RA-treated (10 uM) versus control ESCs (second column). Comparing Noggin to RA reveals that both molecules induce highly concordant effects, as seen by the upregulation of gene sets associated to neuronal differentiation and by the repression of gene sets related to cell proliferation and cell cycle progression.

We then investigated the effect of Noggin on positional identity. Noggin induced the expression of a number of dorsal–telencephalic markers and left almost unchanged the expression of intermediate-lateral or ventro-basal markers. This was evaluated by comparing the mRNA expression profile of ESCs treated with Noggin (400 nM) to that of control (CDMM-differentiating ESCs; Fig. 7b).

To study the effects of Noggin and RA on anterior/posterior (A/P) identity of ESCs, we selected a predefined subset of developmental genes known to pattern the A/P axis of the CNS, and we analyzed their expression, using RA treatment as a control for posteriorization of ESCs. A number of these genes were coherently regulated in Noggin-treated ESCs and E16 cortex, or in RA-treated ESCs and E16 hindbrain, suggesting a certain similarity of treated ESCs and corresponding brain regions (Supplemental Figure SF8A).

To further characterize ESCs positional identity, we extracted a list of genes that are differentially expressed along the A/P axis of developing brain. We chose 592 genes that were differentially expressed between E16 cortex and E16 hindbrain with absolute fold-change greater than, or equal to, 10-fold. This gene set (Supplemental Table 5) was first analyzed by principal component analysis (PCA) to assay the effect of Noggin on ESC positional identity. PCA is an unbiased method of analysis that projects data variability on a reduced number of orthogonal axes, such that the first axis captures the highest degree of variance in gene expression (Component 1), and subsequent axes (Component 2…n) correspond to successively decreasing variance. The components capturing the highest degrees of variance identify the qualities mostly discriminating among data populations.

Figure 7c shows a plot of the first two principal components, which account for 64.15 % (component 1) and for 18.64 % (component 2) of variance between samples. Component 2 discriminates ESCs (cyan items) from brain tissues (orange items). As expected by the nature of gene set selection, component 1 discriminates the A/P identity (dashed lines in Fig. 7c). Notably, Noggin-treated ESCs

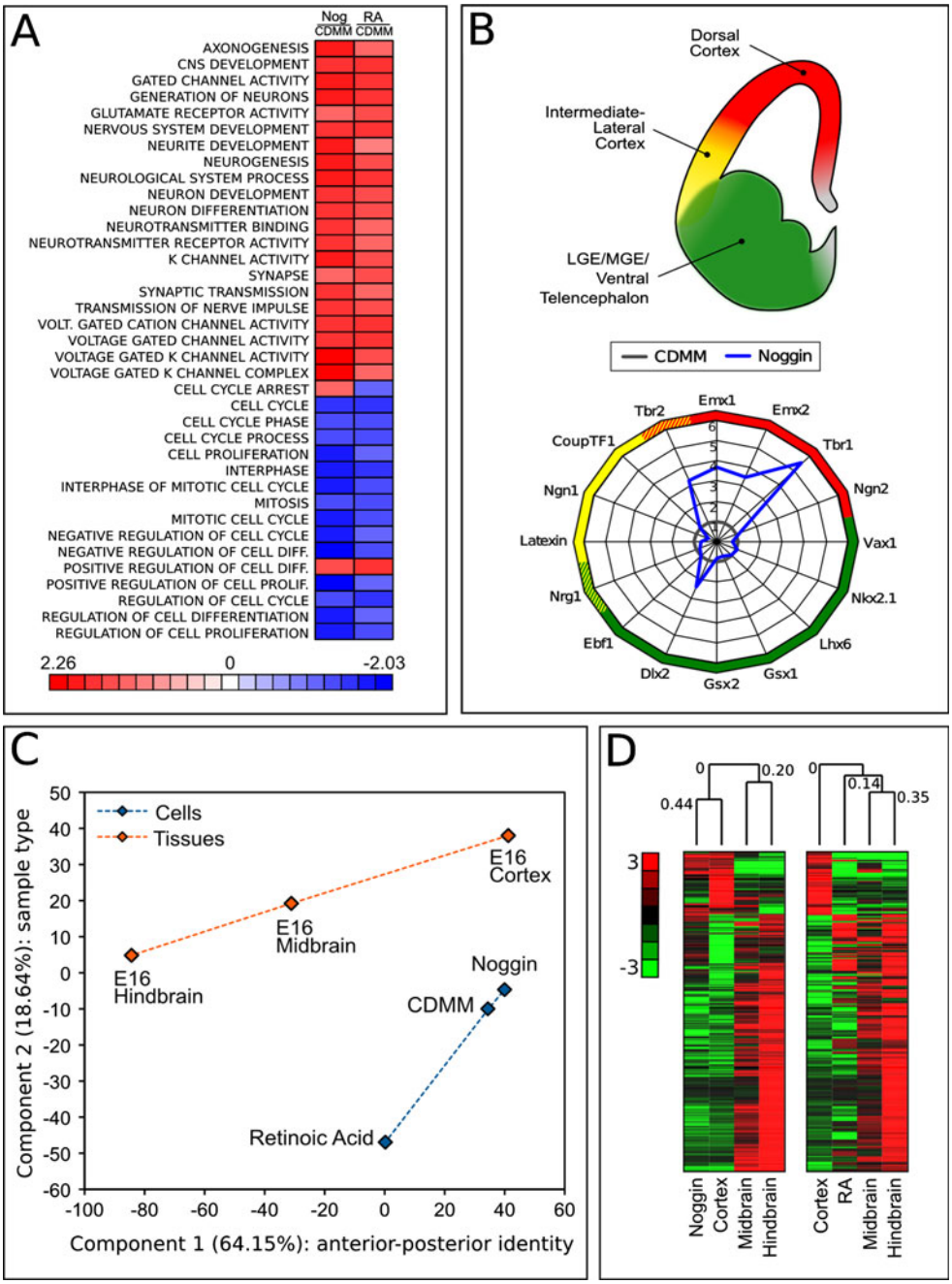

Fig. 7 Gene expression profiling of differentiated ESCs: **a** Gene Set Enrichment Analysis of 400 nM Noggin-treated versus control ESCs (Nog/CDMM, first column) and 10 μM RA-treated versus control ESCs (RA/CDMM, second column), filtered for neuronal function/differentiation and control of cell cycle. Heat map color scale indicates gene set enrichment scores. **b** Gene expression fold change of selected forebrain markers (see Supplemental Table 7 for references) at step III in Noggin-treated ESCs compared to control (CDMM). **c** Principal component analysis of ESCs and E16 brain regions (see text for details). **d** Hierarchical gene clustering analysis of ESCs and E16 brain regions. The first 390 genes are shown (complete clustering is displayed in Supplemental Figure SF7B–D). Numbers over the branching report Euclidean distance correlation. Heat map color scale indicates normalized gene expression

have more positive values on component 1 than control ESCs, confirming the anteriorizing effect of BMP inhibition. As an internal control of the analysis, RA-treated ESCs show an opposite trend, consistently with RA posteriorizing effect.

The same gene selection of 592 genes was used for hierarchical gene clustering analysis (see "Materials and Methods") of either Noggin-treated or RA-treated ESCs, with the three brain regions (Fig. 7d; Supplemental Figure SF8B–D). We found that the gene expression profile of Noggin-treated ESCs clustered with that of cerebral cortex (0.44 correlation factor), whereas the RA profile clustered with midbrain/hindbrain profile, although with a lower extent (0.14 correlation factor). Regions of high concordance between the differentiated ESCs and the corresponding brain region are shown in Supplemental Figure SF8B–D and correspond to known genes of A/P patterning, including those genes whose expression was analyzed by RT-PCR.

We concluded that Noggin, in addition to its known role as neural inducer, plays a major role in establishing an anterior, cortical fate.

Discussion

We have addressed the direct role of BMPs in anterior–posterior neural patterning. A role for BMP in inhibiting an anterior identity was suggested by many observations. Classical studies in lower vertebrates showed that BMP antagonism on *Xenopus* animal caps generates anterior neural structures [26, 38, 56]. In mouse, specific forebrain defects in mice mutant for BMP antagonists were shown [3]. However, this is to our knowledge the first study that directly addresses this issue in a systematic way in neuralized ESCs. We have established an original method of ESCs neuralization that permits to obtain fully differentiated neurons in a short time through the use of a chemically defined, minimal medium. These cells respond to RA and Shh by activating posterior and ventral pathways of differentiation, respectively. This is a strong evidence that in vitro they follow and respond the same signals found during in vivo embryonic development. We assayed the effect of BMP endogenously produced by neuralized ESCs on their own positional identity. The use of this in vitro differentiation method has allowed us to convincingly show that BMP signaling can influence the anterior–posterior neural patterning independently of signals from other germ-layers. In fact, neuralized ESCs spontaneously acquire a dorsal–telencephalic identity when deprived of endogenous BMPs. An important significance of our finding in the stem cells field consists in the possibility to obtain in vitro cortical neurons from pluripotent ESCs very rapidly and easily, without the need of any external signaling.

We found that ESCs cultured as adherent cells in a minimal medium without any added exogenous factors (CDMM), differentiated as neurons more efficiently than ESCs cultured in serum-containing medium (SCM) during the early phase of differentiation (step I). This is consistent with similar observations reported in the literature ([15, 20, 22, 65, 66]) and confirms the notion that a default program of neuronal differentiation of ESCs exists and can be inhibited by factors contained in serum. We do not know to what extent BMPs, which are present in serum [37], may account for its inhibitory effects.

Neurons generated by ESCs in CDMM express midbrain markers, but we cannot exclude that a portion of them acquired a diencephalic identity. In fact, these neurons express Otx2 and Irx3, which are also expressed in caudal regions of the developing diencephalon. Moreover, BMP antagonists nearly completely repressed En1 but not Otx2 and Irx3, suggesting that some degree of diencephalic specification may be retained even following BMP inhibition. In any instances, an accurate comparison of their global gene expression profile to the global gene expression profile of dissected embryonic diencephalon is necessary to definitely address this point.

Noggin inhibited the action of endogenously produced, secreted BMPs and its action was specific, as confirmed by control experiments using BMPR1A-Fc and Dorsomorphin, which specifically block BMP pathway.

Noggin acted at two distinct levels of ESCs differentiation: it strengthened their spontaneous neural differentiation in a minimal medium and induced a telencephalic identity. Zfp521 (see "Introduction") expression was highest in Noggin-treated cultures compared to any other culture conditions (Fig. 4b), confirming the crucial role of Noggin in ESCs neural conversion. However, Noggin induced only a slight increase of neural progenitor ratio compared to control, while supporting a dramatic increase of cells expressing the telencephalic marker FoxG1 (Fig. 6). This indicates that: (1) the removal of serum from our culture is per se sufficient to induce a high degree of neuralization, (2) although significant, the small increase in neural progenitors induced by high doses of Noggin cannot explain the dramatic increase of telencephalic cells, and (3) these results suggest a novel mechanism, whose molecular nature is still unknown, by which BMPs endogenously produced by differentiating ESCs directly act on the positional identity of the neural progenitors they spontaneously generate in a minimal medium.

Notably, we have induced comparable cortical commitment in ESCs which were propagated in chemically-defined conditions in the absence of serum (2i ESCs; [57, 71]) before using them for differentiation assays. Thus, the effect of Noggin on the positional identity of ESC-generated neurons is not due to the selection of cells committed to a cortical identity, which might be already present in ESC cultures maintained in serum + LIF.

We speculate that the induction of the telencephalic transcription factors FoxG1 and Emx2 is sufficient to inhibit the expression of more posterior patterning genes as En1 and Otx2 through intrinsic molecular mechanisms, but the nature of such mechanisms has yet to be investigated.

To induce a cortical fate, some procedures make use of a feeder layer of stromal cells [32], or cell aggregation [15]. In these studies, the factors that were endogenously produced by cells in culture and that might have influenced ESCs differentiation were not identified. In one of these studies, ESCs cultured in a minimal medium at a very low density generated cells with morphological, electrophysiological, and molecular features of anterior neurons. These could be directed toward a cortical fate by treatment with the SHH antagonist Cyclopamine, although neither SHH secretion nor autocrine action of SHH were directly investigated [19]. We did not observe any effect of Cyclopamine on ESCs dorsoventral fate. However, we can confirm that ESCs can activate SHH signaling, as shown by the ventralizing effect we describe when adding a SHH agonist during step II. We hypothesize that, under the low

density culture conditions employed by Gaspard et al. [19], an endogenous production of SHH that was not present in our culture condition was induced. In any case, ESCs differentiating as a monolayer of adherent cells in a minimal medium devoid of external signals were never able, to our knowledge, to induce a genuine cortical gene expression profile, as we on the contrary observed in our Noggin-treated cells.

The analysis of multiple markers is required to correctly determine CNS regional identity and exclude possible alternative fates in ESC-derived neural precursor cells [25]. To this purpose, we carried out a large-scale gene expression analysis of differentiated ESCs, using principal component analysis (PCA) and hierarchical clustering. Our main finding is that Noggin has a profound effect on the positional identity of ESCs-generated neurons, as it up-regulated the global gene expression of cortical genes and down-regulated that of midbrain and hindbrain genes. Thus, we reasoned that a telencephalic, possibly cortical, fate might be the default, intrinsic differentiation program of pluripotent cells when endogenous BMP signaling is inhibited. This finding reinforces the evidence obtained by the immunocytodetection of cortical cells markers such as Tbr1 and Satb2 (cortical neurons of deep and upper layers, respectively).

The molecular and embryological bases of neural tissue induction and brain patterning are beginning to emerge, indicating BMPs as key linking molecules [41, 63]. In our experimental model, endogenous BMPs were able to inhibit the expression of telencephalic genes, while at the same time allowing ESCs neuronal differentiation and high levels of expression of more posterior markers such as En1 and Otx2. We speculate that BMP activity, which is finely tuned in mouse developing prosencephalon [17], might regulate regional differences in embryonic fore-midbrain as well as it does in ESCs differentiating in a culture dish.

A revisited analysis of mammalian neural induction points to a model in which neural inducing signals called "activators" are proposed to impart both neural and anterior identity to the ectoderm. In this view, events that posteriorize the anterior neural tissue to generate the full range of CNS structures would occur later, by "tranformer" molecules [41, 67]. According to such a classical model, we speculate that a primitive neuronal-telencephalic fate of ESCs might be further transformed in midbrain or hindbrain fate by a secondary signaling of BMP or RA "transformers", respectively.

Inhibition of BMP signaling appears to be a crucial step in forebrain induction, as shown by the severe defects in the development of the prosencephalon of mice double mutants of the BMP inhibitors chordin and noggin [3]. However, dual inhibition of Wnt and BMP signals has been proposed to be necessary to confer head organizer activity both in zebrafish [31], *Xenopus* [21, 42] and mouse [14]. Although we observed a robust activation of cortical markers and a strong repression of midbrain genes with the sole inhibition of BMP, we cannot exclude that differentiating ESCs produce and are sensitive to Wnts and that Wnt inhibition might be synergistic with BMP inhibition in inducing a cortical fate in ESCs. Endogenous Wnt activity might explain why the ratios of ESCs treated with high doses of Noggin that express markers of cortical progenitors (FoxG1, 22 %) and of cortical neurons (Tbr1 and Satb2, 30 % in total) at the end of step III do not account for the total number of Sox1-positive cells neuralized at step II (90.5 %). Our model of ESCs neuralization might allow us to experimentally address this point and to dissect the role of other pathways involved in neural patterning better than other in vivo systems.

A crucial role for BMP in patterning neural structures has been recently suggested in vitro, as pluripotent cells of *Xenopus* animal caps acquired anterior neural fate when treated with high doses of Noggin [39, 64]. In fact, our results are consistent with this observation and point to the existence of a default, intrinsic program of differentiation of pluripotent cells that has been conserved through vertebrate evolution and is both neuronal and anterior.

Acknowledgments We are indebted with Diana Boraschi for providing RAW 264.7 and with Cristina Magli for supplying MS cells. We thank Paola Italiani for advice on RAW 264.7 cell culture, Cristina Di Primio and Valentina Quercioli for confocal imaging, Valentina Adami for microarray hybridization and analysis, Maria Antonietta Calvello for technical assistance and Tania Incitti for FACS protocol. We are grateful to Austin Smith for the use of the Sox1-GFP mouse ESCs and to Mario Costa for generously providing FoxG1 antibody. We thank Elena Cattaneo and Marco Onorati for their advice on 2i + LIF culture. We also thank Massimiliano Andreazzoli, Antonino Cattaneo, Paolo Malatesta, Roberto Marangoni, Massimo Pasqualetti and Robert Vignali for discussion and critical reading of the manuscript. A special mention is due to Alessandro Vanni who contributed to compare SCM/CDMM ESC cultures. The Authors acknowledge NHLBI-BayGenomics and NCRR-MMRRC (UC Davis) for the E14Tg2A cell line. This work was supported by Grant for Ricerca Interna of Scuola Normale Superiore and by Fondazione Cassa di Risparmio di Livorno to F.C., by University of Trento Startup Grant to S.C., and by Grant n. 2011.0251 of Cassa di Risparmio di Trento e Rovereto to F.C. and S.C.

Conflict of interest We declare that we have no conflicts of interest in the authorship or publication of this contribution.

References

1. Abe E, Yamamoto M, Taguchi Y, Lecka-Czernik B, OBrien CA, Economides AN et al (2000) Essential requirement of BMPs-2/4

for both osteoblast and osteoclast formation in murine bone marrow cultures from adult mice: antagonism by noggin. J Bone Miner Res 15(4):663–673
2. Acampora D, Avantaggiato V, Tuorto F, Briata P, Corte G, Simeone A (1998) Visceral endoderm-restricted translation of Otx1 mediates recovery of Otx2 requirements for specification of anterior neural plate and normal gastrulation. Development 125(24):5091–5104
3. Bachiller D, Klingensmith J, Kemp C, Belo JA, Anderson RM, May SR et al (2000) The organizer factors Chordin and Noggin are required for mouse forebrain development. Nature 403:658–661
4. Bayramov A, Eroshkin FM, Martynova NY, Ermakova GV, Solovieva EA, Zaraisky AG (2011) Novel functions of Noggin proteins: inhibition of Activin/Nodal and Wnt signaling. Development 138(24):5345–5356
5. Bibel M, Richter J, Lacroix E, Barde YA (2007) Generation of a defined and uniform population of CNS progenitors and neurons from mouse embryonic stem cells. Nat Protoc 2:1034–1043
6. Bosse A, Zülch A, Becker MB, Torres M, Gómez-Skarmeta JL, Modolell J et al (1997) Identification of the vertebrate Iroquois homeobox gene family with overlapping expression during early development of the nervous system. Mech Dev 69(1–2):169–181
7. Briscoe J, Pierani A, Jessell TM, Ericson J (2000) A homeodomain protein code specifies progenitor cell identity and neuronal fate in the ventral neural tube. Cell 101(4):435–445
8. Bulfone A, Smiga SM, Shimamura K, Peterson A, Puelles L, Rubenstein JL (1995) T-brain-1: a homolog of Brachyury whose expression defines molecularly distinct domains within the cerebral cortex. Neuron 15(1):63–78
9. Chambers SM, Fasano C, Papapetrou EP, Tomishima M, Sadelain M, Studer L (2009) Highly efficient neural conversion of human ES and iPS cells by dual inhibition of SMAD signaling. Nature 27(3):275–280
10. Chatzi C, Brade T, Duester G (2011) Retinoic acid functions as a key GABAergic differentiation signal in the basal ganglia. PLoS Biol 9(4):e1000609
11. Chen F, Capecchi MR (1997) Targeted mutations in hoxa-9 and hoxb-9 reveal synergistic interactions. Dev Biol 181(2):186–196
12. Chiba S, Kurokawa MS, Yoshikawa H, Ikeda R, Takeno M, Tadokoro M et al (2005) Noggin and basic FGF were implicated in forebrain fate and caudal fate, respectively, of the neural tube-like structures emerging in mouse ES cell culture. Exp Brain Res 163(1):86–99
13. DeCamp DL, Thompson TM, de Sauvage FJ, Lerner MR (2000) Smoothened activates Galphai-mediated signaling in frog melanophores. J Biol Chem 275(34):26322–26327
14. del Barco Barrantes I, Davidson G, Gröne H-J, Westphal H, Niehrs C (2003) Dkk1 and noggin cooperate in mammalian head induction. Genes Dev 17:2239–2244
15. Eiraku M, Watanabe K, Matsuo-Takasaki M, Kawada M, Yonemura S, Matsumura M et al (2008) Self-organized formation of polarized cortical tissues from ESCs and its active manipulation by extrinsic signals. Cell Stem Cell 3(5):519–532
16. Eisen MB, Spellman PT, Brown PO, Botstein D (1998) Cluster analysis and display of genome-wide expression patterns. Proc Natl Acad Sci USA 95(25):14863–14868
17. Furuta Y, Piston DW, Hogan BL (1997) Bone morphogenetic proteins (BMPs) as regulators of dorsal forebrain development. Development 124(11):2203–2212
18. Gaspard N, Vanderhaeghen P (2010) Mechanisms of neural specification from embryonic stem cells. Curr Opin Neurobiol 20(1):37–43
19. Gaspard N, Bouschet T, Hourez R, Dimidschstein J, Naeije G, Passante L et al (2008) An intrinsic mechanism of corticogenesis from embryonic stem cells. Nature 455:351–358
20. Gaspard N, Bouschet T, Herpoel A, Naeije G, van den Ameele J, Vanderhaeghen P (2009) Generation of cortical neurons from mouse embryonic stem cells. Nat Protoc 4(10):1454–1463
21. Glinka A, Wu W, Onichtchouk D, Blumenstock C, Niehrs C (1997) Head induction by simultaneous repression of Bmp and Wnt signalling in Xenopus. Nature 389(6650):517–519
22. Gratsch TE, O'Shea KS (2002) Noggin and chordin have distinct activities in promoting lineage commitment of mouse embryonic stem (ES) cells. Dev Biol 245(1):83–94
23. Groppe J, Greenwald J, Wiater E, Rodriguez-Leon J, Economides AN, Kwiatkowski W, Affolter M, Vale WW, Belmonte JC, Choe S (2002) Structural basis of BMP signalling inhibition by the cystine knot protein Noggin. Nature 420(6916):636–642
24. Guan K, Chang H, Rolletschek A, Wobus AM (2001) Embryonic stem cell-derived neurogenesis. Retinoic acid induction and lineage selection of neuronal cells. Cell Tissue Res 305(2):171–176
25. Hansen DV, Rubenstein JLR, Kriegstein AR (2011) Deriving excitatory neurons of the neocortex from pluripotent stem cells. Neuron 70(4):645–660
26. Hawley SH, Wunnenberg-Stapleton K, Hashimoto C, Laurent MN, Watabe T, Blumberg BW, Cho KW (1995) Disruption of BMP signals in embryonic Xenopus ectoderm leads to direct neural induction. Genes Dev 9:2923–2935
27. Hébert JM, Mishina Y, McConnell SK (2002) BMP signaling is required locally to pattern the dorsal telencephalic midline. Neuron 35:1029–1041
28. Hendrickx M, Van XH, Leyns L (2009) Anterior-posterior patterning of neural differentiated embryonic stem cells by canonical Wnts, Fgfs, Bmp4 and their respective antagonists. Dev Growth Differ 51(8):687–698
29. Hevner RF, Shi L, Justice N, Hsueh Y, Sheng M, Smiga S et al (2001) Tbr1 regulates differentiation of the preplate and layer 6. Neuron 29(2):353–366
30. Hollnagel A, Oehlmann V, Heymer J, Rüther U, Nordheim A (1999) Id genes are direct targets of bone morphogenetic protein induction in embryonic stem cells. J Biol Chem 274(28):19838–19845
31. Houart C, Caneparo L, Heisenberg C, Barth K, Take-Uchi M, Wilson S (2002) Establishment of the telencephalon during gastrulation by local antagonism of Wnt signaling. Neuron 35:255–265
32. Ideguchi M, Palmer TD, Recht LD, Weimann JM (2010) Murine embryonic stem cell-derived pyramidal neurons integrate into the cerebral cortex and appropriately project axons to subcortical targets. J Neurosci 30(3):894–904
33. Kamiya D, Banno S, Sasai N, Ohgushi M, Inomata H, Watanabe K et al (2011) Intrinsic transition of embryonic stem-cell differentiation into neural progenitors. Nature 470:503–509
34. Keller S, Nickel J, Zhang JL, Sebald W, Mueller TD (2004) Molecular recognition of BMP-2 and BMP receptor IA. Nat Struct Mol Biol 11(5):481–488
35. Kinney JW, Davis CN, Tabarean I, Conti B, Bartfai T, Behrens MM (2006) A specific role for NR2A-containing NMDA receptors in the maintenance of parvalbumin and GAD67 immunoreactivity in cultured interneurons. J Neurosci 26(5):1604–1615
36. Knoth R, Singec I, Ditter M, Pantazis G, Capetian P, Meyer RP et al (2010) Murine features of neurogenesis in the human hippocampus across the lifespan from 0 to 100 years. PLoS ONE 5(1):e8809
37. Kodaira K, Imada M, Goto M, Tomoyasu A, Fukuda T, Kamijo R et al (2006) Purification and identification of a BMP-like factor from bovine serum. Biochem Biophys Res Commun 345(3):1224–1231
38. Lamb T, Knecht A, Smith W, Stachel S, Economides A, Stahl N et al (1993) Neural induction by the secreted polypeptide noggin. Science 262:713–718

39. Lan L, Vitobello A, Bertacchi M, Cremisi F, Vignali R, Andreazzoli M et al (2009) Noggin elicits retinal fate in Xenopus animal cap embryonic stem cells. Stem Cells 27(9):2146–2152
40. Lee SH, Lumelsky N, Studer L, Auerbach JM, McKay RD (2000) Efficient generation of midbrain and hindbrain neurons from mouse embryonic stem cells. Nat Biotechnol 18(6):675–679
41. Levine AJ, Brivanlou AH (2007) Proposal of a model of mammalian neural induction. Dev Biol 308(2):247–256
42. Lupo G, Harris WA, Barsacchi G, Vignali R (2002) Induction and patterning of the telencephalon in *Xenopus laevis*. Development 129:5421–5436
43. McNeish J, Roach M, Hambor J, Mather RJ, Weibley L, Lazzaro J et al (2010) High-throughput screening in embryonic stem cell-derived neurons identifies potentiators of AMPA-type glutamate receptors. J Biol Chem 285(22):17209–17217
44. Nadri S, Soleimani M, Hosseni RH, Massumi M, Atashi A, Izadpanah R (2007) An efficient method for isolation of murine bone marrowmesenchymal stem cells. Int J Dev Biol 51:723–729
45. Niwa H, Miyazaki J, Smith AG (2000) Quantitative expression of Oct-3/4 defines differentiation, dedifferentiation or self-renewal of ES cells. Nat Genet 24(4):372–376
46. Nordgård O, Kvaløy JT, Farmen RK, Heikkilä R (2006) Error propagation in relative real-time reverse transcription polymerase chain reaction quantification models: the balance between accuracy and precision. Anal Biochem 356(2):182–193
47. Okano H, Kawahara H, Toriya M, Nakao K, Shibata S, Imai T (2005) Function of RNA-binding protein Musashi-1 in stem cells. Exp Cell Res 306(2):349–356
48. Oliver G, Mailhos A, Wehr R, Copeland NG, Jenkins NA, Gruss P (1995) Six3, a murine homologue of the sine oculis gene, demarcates the most anterior border of the developing neural plate and is expressed during eye development. Development 121(12):4045–4055
49. Parr BA, Shea MJ, Vassileva G, McMahon AP (1993) Mouse Wnt genes exhibit discrete domains of expression in the early embryonic CNS and limb buds. Development 119(1):247–261
50. Pera EM, Kessel M (1997) Patterning of the chick forebrain anlage by the prechordal plate. Development 124(20):4153–4162
51. Pfaffl MW, Horgan GW, Dempfle L (2002) Relative expression software tool (REST) for group-wise comparison and statistical analysis of relative expression results in real-time PCR. Nucleic Acids Res 30(9):e36
52. Ralph P, Nakoinz I (1977) Antibody-dependent killing of erythrocyte and tumor targets by macrophage-related cell lines: enhancement by PPD and LPS. J Immunol 119(3):950–954
53. Ramfrez-Solis R, Zheng H, Whiting J, Krumlauf R, Bradley A (1993) Hoxb-4 (Hox-2.6) mutant mice show homeotic transformation of a cervical vertebra and defects in the closure of the sternal rudiments. Cell 73(2):279–294
54. Regad T, Roth M, Bredenkamp N, Illing N, Papalopulu N (2007) The neural progenitor-specifying activity of FoxG1 is antagonistically regulated by CKI and FGF. Nat Cell Biol 9(5):531–540
55. Saldanha AJ (2004) Java Treeview—extensible visualization of microarray data. Bioinform 20(17):3246–3248
56. Sasai Y, Lu B, Steinbeisser H, De Robertis EM (1995) Regulation of neural induction by the Chd and Bmp-4 antagonistic patterning signals in *Xenopus*. Nature 376:333–336
57. Silva J, Barrandon O, Nichols J, Kawaguchi J, Theunissen TW, Smith A (2008) Promotion of reprogramming to ground state pluripotency by signal inhibition. PLoS Biol 6(10):e253
58. Simeone A, Gulisano M, Acampora D, Stornaiuolo A, Rambaldi M, Boncinelli E (1992) Two vertebrate homeobox genes related to the Drosophila empty spiracles gene are expressed in the embryonic cerebral cortex. EMBO J 11(7):2541–2550
59. Smukler SR, Runciman SB, Xu S, van der Kooy D (2006) Embryonic stem cells assume a primitive neural stem cell fate in the absence of extrinsic influences. J Cell Biol 172(1):79–90
60. Stoykova A, Gruss P (1994) Roles of Pax-genes in developing and adult brain as suggested by expression patterns. J Neurosci 14(3 Pt 2):1395–1412
61. Subramanian A, Tamayo P, Mootha VK, Mukherjee S, Ebert BL, Gillette MA et al (2005) Gene set enrichment analysis: a knowledge-based approach for interpreting genome-wide expression profiles. Proc Natl Acad Sci USA 102(43):15545–15550
62. Taipale J, Chen JK, Cooper MK, Wang B, Mann RK, Milenkovic L et al (2000) Effects of oncogenic mutations in Smoothened and Patched can be reversed by cyclopamine. Nature 406(6799): 1005–1009
63. Tropepe V, Hitoshi S, Sirard C, Mak TW, Rossant J, Toronto T et al (2001) Direct neural fate specification from embryonic stem cells: a primitive mammalian neural stem cell stage acquired through a default mechanism. Neuron 30:65–78
64. Viczian AS, Solessio EC, Lyou Y, Zuber ME (2009) Generation of functional eyes from pluripotent cells. PLoS Biol 7(8): e1000174
65. Watanabe K, Kamiya D, Nishiyama A, Katayama T, Nozaki S, Kawasaki H et al (2005) Directed differentiation of telencephalic precursors from embryonic stem cells. Nat Neurosci 8(3):288–296
66. Wataya T, Ando S, Muguruma K, Ikeda H, Watanabe K, Eiraku M et al (2008) Minimization of exogenous signals in ES cell culture induces rostral hypothalamic differentiation. Proc Nat Acad Sci USA 105(33):11796–11801
67. Wilson SW, Houart C (2004) Early steps in the development of the forebrain. Dev Cell 6(2):167–181
68. Wurst W, Auerbach AB, Joyner AL (1994) Multiple developmental defects in Engrailed-1 mutant mice: an early mid-hindbrain deletion and patterning defects in forelimbs and sternum. Development 120(7):2065–2075
69. Xuan S, Baptista CA, Balas G, Tao W, Soares VC, Lai E (1995) Winged helix transcription factor BF-1 is essential for the development of the cerebral hemispheres. Neuron 14(6):1141–1152
70. Ying QL, Nichols J, Chambers I, Smith A (2003) BMP induction of Id proteins suppresses differentiation and sustains embryonic stem cell self-renewal in collaboration with STAT3. Cell 115(3):281–292
71. Ying QL, Wray J, Nichols J, Batlle-Morera L, Doble B, Woodgett J, Cohen P, Smith A (2008) The ground state of embryonic stem cell self-renewal. Nature 453:519–523
72. Yu PB, Hong CC, Sachidanandan C, Babitt JL, Deng DY, Hoyng SA et al (2008) Dorsomorphin inhibits BMP signals required for embryogenesis and iron metabolism. Nat Chem Biol 4(1):33–41
73. Zhang SC, Wernig M, Duncan ID, Brüstle O, Thomson JA (2001) In vitro differentiation of transplantable neural precursors from human embryonic stem cells. Nat Biotechnol 19(12):1129–1133

The Double Inhibition of Endogenously Produced BMP and Wnt Factors Synergistically Triggers Dorsal Telencephalic Differentiation of Mouse ES Cells

Michele Bertacchi,[1] Luca Pandolfini,[1] Mara D'Onofrio,[2,3] Rossella Brandi,[2,3] Federico Cremisi[1,4]

[1] Scuola Normale Superiore, Classe di Scienze, Pisa, Italy

[2] Genomics Facility, European Brain Research Institute, Roma, Italy

[3] Istituto di Farmacologia Traslazionale, Consiglio Nazionale dell Ricerche, Roma, Italy

[4] Istituto di Tecnologie Biomediche, Consiglio Nazionale delle Ricerche, Pisa, Italy

Received 28 February 2014; revised 5 July 2014; accepted 7 July 2014

ABSTRACT: **Embryonic stem (ES) cells are becoming a popular model of *in vitro* neurogenesis, as they display intrinsic capability to generate neural progenitors that undergo the known steps of *in vivo* neural development. These include the acquisition of distinct regional fates, which depend on growth factors and signals that are present in the culture medium. The control of the intracellular signaling that is active at different steps of ES cell neuralization, even when cells are cultured in chemically defined medium, is complicated by the endogenous production of growth factors. However, this endogenous production has been poorly investigated so far. To address this point, we performed a high-throughput analysis of the expression of morphogens during mouse ES cell neuralization in minimal medium. We found that during their neuralization, ES cells increased the expression of members of Wnt, Fibroblast Growth Factor (FGF), and BMP families. Conversely, the expression of Activin/Nodal and Shh ligands was low in early steps of neuralization. In this experimental condition, neural progenitors and neurons generated by ES cells expressed a gene expression profile that was consistent with a midbrain identity. We found that endogenous BMP and Wnt signaling, but not FGF signaling, synergistically affected ES cell neural patterning, by turning off a profile of dorsal/telencephalic gene expression. Double BMP and Wnt inhibition allowed neuralized ES cells to sequentially activate key genes of cortical differentiation. Our findings are consistent with a novel synergistic effect of Wnt and BMP endogenous signaling of ES cells in inhibiting a cortical differentiation program.** © 2014 Wiley Periodicals, Inc. Develop Neurobiol 75: 66–79, 2015

Keywords: **Wnt; BMP; mouse embryonic stem cells; cortical fate; *in vitro* neurogenesis**

INTRODUCTION

The dissection of diffusible signals that orchestrate neural induction and regulate regional brain patterning has recently been made easier by the study of embryonic stem (ES) cell *in vitro* differentiation. Mouse and human ES cells acquire neural identity in the absence of external signals (Tropepe et al., 2001; Muñoz-Sanjuán and Brivanlou, 2002; Bouhon et al.,

Additional Supporting Information may be found in the online version of this article.

Correspondence to: F. Cremisi (f.cremisi@sns.it).

Contract grant sponsor: Flagship Project InterOmics PB.05.

Contract grant sponsor: Cassa di Risparmio di Trento e Rovereto; contract grant number: 2011.0251.

Published online 15 July 2014 in Wiley Online Library (wileyonlinelibrary.com).
DOI 10.1002/dneu.22209

2005; Smukler et al., 2006). ES cell neurogenesis *in vitro* in chemically defined culture media allows to perform either gain or loss of function assays with many molecules at different times, which is currently not feasible or extremely cumbersome with *in vivo* approaches. Thus, ES cell neuralization is becoming a useful tool to functionally assay the role of growth factors and morphogens that have distinct roles in specific regions of the embryonic brain at precise times of development.

According to the "Activation-Transformation" model, ectodermal cells initially acquire an anterior fate on neural induction (Activation), but they can subsequently be transformed into more caudal cell fates (Transformation) to obtain all of the different subdomains along the A/P axis, a process referred to as caudalization (Wilson and Houart, 2004). In many assays, whenever neural tissue is induced, it expresses transcripts that are later restricted to forebrain and midbrain territories. Expression of these "anterior markers" raises the possibility of an obligate link between induction of neural identity and acquisition of anterior character (Foley and Stern, 2001). Wnts, Retinoic acid (RA), and Fibroblast Growth Factors (FGFs) are thought to convert neuroepithelial cells from an anterior default state to a more posterior identity along the neuraxis.

The patterning events that define A–P and D–V identities *in vivo* can be mimicked performing ES cell differentiation in a minimal medium devoid of growth factors and morphogens. The effects of RA, BMPs, Wnts, FGFs, and Sonic Hedgehog (SHH) on the identity of neurons generated by ES cells have been described (Watanabe et al., 2005; Eiraku et al., 2008; Gaspard et al., 2008; Chatzi et al., 2011). Addition of caudalizing signals, such as RA or FGF2 can promote a spinal cord identity and subsequent production of motor neurons (Wichterle et al., 2002), whereas addition of Wnt and Nodal antagonists promotes production of telencephalic progenitors (Watanabe et al., 2005). These observations are consistent with a close parallelism between *in vivo* and *in vitro* molecular mechanisms of neural patterning and support the advantage of ES cells as *in vitro* model for the dissection of signaling involved in neural patterning.

Although the effect of growth factors and morphogens on ES neural patterning can be anticipated by their known role *in vivo*, the use of ES cultures for studies aimed to steer their neural patterning toward distinct fates, or to investigate *in vitro* the signaling controlling neuronal fate acquisition, is complicated by the possible production of growth factors and morphogens inside the neuralizing culture. Many studies reported that natural or chemical inhibitors/antagonists of Wnts (Bouhon et al., 2006; Kirkeby et al., 2012), BMPs (Surmacz et al., 2012; Lupo et al., 2013; Ozair et al., 2013), FGFs (Chambers et al., 2009; Kriks et al., 2011; Lupo et al., 2013), Activin/Nodal (Lupo et al., 2013), or Shh (Gaspard et al., 2008; Li et al., 2009; Nicoleau et al., 2013) affect the differentiation fate of neurons cultured in chemically defined media. These studies implicate that such factors were endogenously produced by ES differentiating cells. However, few of them went into the detail of the endogenous expression of these signals and their role in ES neural patterning has been somehow neglected. This approach limited stem cell studies, especially when addressing the concept of default ES cell differentiation fate and of the exact role of distinct morphogens during neuralization.

We have recently established a protocol of mouse ES neuralization in chemically defined minimal medium (CDMM) in which the generated neurons acquire a dorsal midbrain identity. We found that neuralizing ES cells produce BMPs and that inhibiting BMP signaling turns on a global profile of gene expression that is consistent with a dorsal telencephalic identity (Bertacchi et al., 2013). We hypothesized that in our protocol other signals than BMPs could be produced. To identify them, we performed a global analysis of gene expression at different times of ES neuralization. Here, we show that different forms of BMP, Wnt, and FGF were expressed by ES neural progenitors, whereas the expression level of Activin/Nodal and Shh ligands was low until late stages of neuronal differentiation in our protocol. Although FGF signaling inhibition had no gross effects on neural patterning, Wnt signaling inhibition induced massive expression of dorsal telencephalic markers. This effect was higher than the effect obtained by BMP inhibition. BMP/Wnt double inhibition exerted a synergistic effect resulting in time-specific and robust expression of key genes of corticogenesis.

METHODS

ES Cell Neuralization

Murine ES cell lines E14Tg2A (passages 25–38) and 46C (transgenic Sox1-GFP ES cells, kindly provided by A. Smith, University of Cambridge, UK; passages 33–39) were cultured on gelatin-coated tissue culture dishes at a density of 40,000 cells/cm^2. ES cell medium, which was changed daily, contained GMEM (Sigma), 10% Fetal Calf Serum, 2 m*M* Glutamine, 1 m*M* sodium Pyruvate, 1 m*M* nonessential amino acids, 0.05 m*M* β-mercaptoethanol, 100 U/mL Penicillin/Streptomycin, and 1000 U/mL recombinant mouse LIF (Invitrogen).

CDMM for neural induction consisted of DMEM/F12 (Invitrogen), 2 m*M* Glutamine, 1 m*M* sodium Pyruvate, 0.1 m*M* nonessential amino acids, 0.05 m*M* β-mercaptoethanol, 100 U/mL Penicillin/Streptomycin supplemented with N2/B27 (no vitamin A; Invitrogen). The protocol of ES neuralization consisted of three steps. In Step-I, dissociated ES cells were washed with DMEM/F12, aggregated in agar-coated culture dishes (65,000 cells per cm^2), and cultured as floating aggregates in CDMM for 2 days. The second day, 75% of CDMM was renewed. In Step-II, ES cell aggregates were dissociated and cultured in adhesion (65,000 cells per cm^2) on Poly-ornithine (Sigma; 20 μg/mL in sterile water, 24 h coating at 37°C) and natural mouse Laminin (Invitrogen; 2.5 μg/mL in PBS, 24 h coating at 37°C) for 4 days, changing CDMM daily. In Step-III, after a second dissociation, ES cells were cultured four additional days in CDMM devoid of B27 supplement to drive terminal differentiation, using the same type of seeding density and coated surface described for Step-II. Serum used for Trypsin inactivation was carefully removed by several washes in DMEM/F12.

Growth Factor and Morphogen Treatments

The following factors were tested by addition during Step-II: Dorsomorphin (BMP signaling inhibitor; Sigma-Aldrich; 5 μM), Shh agonist (SAG; Santa Cruz Biotechnology; 100/150 n*M*), IWR-1-Endo (Wnt inhibitor; Calbiochem; 5/10 μM), PD0325901 (MEK/ERK-inhibitor; Calbiochem; 10–100 n*M*), PD173074 (FGF-receptor -inhibitor; Calbiochem; 200 n*M*).

Semiquantitative Real-Time PCR

Total RNA was extracted from ES cell or tissue samples with NucleoSpin RNA II columns (Macherey-Nagel). ES cells from at least two-three different wells of 24-well plates were always pooled together to compensate for variability in cell seeding. RNA quantity and RNA quality were assessed with Nanodrop and gel electrophoresis. For each sample, 200/500 ng of total RNA were reverse-transcribed. Amplified cDNA was quantified using GoTaq qPCR Master Mix (Promega) on Rotor-Gene 6000 (Corbett). Amplification take-off values were evaluated using the built-in Rotor-Gene 6000 relative quantitation analysis function, and relative expression was calculated with the $2^{-\Delta\Delta Ct}$ method, normalizing to the housekeeping gene β-Actin. Standard errors were obtained from the error propagation formula as described in (Nordgård et al., 2006) and statistical significance was probed with randomization test, taking advantage of REST Software (Pfaffl et al., 2002).

Immunocytodetection

Cells prepared for immunocytodetection experiments were cultured on Poly-ornithine/Laminin coated round glass coverslips. Cells were fixed using 2% paraformaldehyde for 10–15 min, washed twice with PBS, permeabilized using 0.1% Triton X100 in PBS, and blocked using 0.5% BSA in PBS. Primary antibodies used for microscopy included Oct3/4 (1:200; Santa Cruz DBA), Nanog (1:300; Novus Biologicals), acetylated N-Tubulin (1:500; Sigma), Neuronal Class III β-Tubulin (1:500; Covance), Musashi-1 (1:200; Cell Signaling), Nestin (1:200; Millipore), FoxG1 (1:200; Abcam), Tbr1 (1:400; Millipore), Satb2 (1:200; Abcam), Ctip2 (1:400; Abcam), vGlut2 (1:300; Abcam), GAD65 (1:500; Chemicon), Pax6 (1:400; Covance), and Nkx2.1 (1:400; Abcam). Primary antibodies were incubated 2 h at room temperature; cells were then washed three times with PBS (10′ each). Alexa Fluor 488 and Alexa Fluor 568 anti-mouse, anti-rabbit or anti-chicken IgG conjugates (Molecular Probes, 1:500) were incubated 1 h at RT in PBS containing 0.1% Triton X100 and 0.5% BSA for primary antibody detection, followed by three PBS washes (10′ each). Nuclear staining was obtained with DAPI. The protocol varied for Tbr1, Satb2, Ctip2, and FoxG1, which antibodies were incubated over-night at 4°C using 0.3% Triton X100.

Microarray Hybridization and Data Analysis

Total RNA was extracted with NucleoSpin RNA II columns (Macherey-Nagel). RNA from three different sets of experiments/embryos was pooled. RNA quality was assessed with Agilent Bioanalyzer RNA 6000 Nano kit; 200 ng of RNA were labeled with One Color (Agilent), purified and hybridized overnight onto an Agilent Mouse Gene Expression Microarray chip (8 × 60K, grid ID 028005), according to the manufacturer's instructions. Agilent Microarray scanner G2564C was used for slide acquisition and spot analysis was performed with Feature Extraction software (Agilent). Data were background-corrected and normalized between arrays by means of Bioconductor package limma (Smyth, 2005). Principal component analysis (PCA) was performed on normalized whole-gene expression dataset using software Cluster 3 (Eisen et al., 1998).

RESULTS

Mouse ES Cells Quickly Neuralize in Minimal Culture Medium

We followed a protocol of ES neuralization in three steps [Fig. 1(A)], minimizing the activation of morphogen signaling by the use of CDMM, see Methods; (Bertacchi et al., 2013). Undifferentiated mouse ES cells (E14 Tg2A ES cell line) were positive for pluripotency markers Oct4 and Nanog when expanded in the presence of LIF and serum before neuralization (Supporting Information Fig. 1A). Priming to neuralization was initiated by a first step in aggregation on agar-coated surface (Step-I, 2 days);

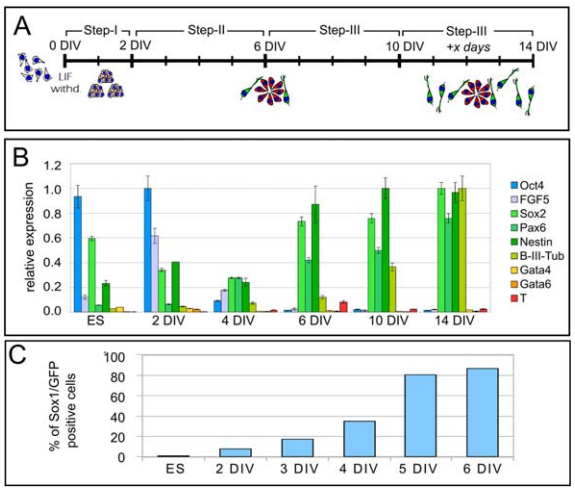

Figure 1 Time course of ES cells neural conversion. (A) scheme of the differentiation steps. (B) Expression of mRNAs coding for markers of pluripotency (Oct4, Sox2), priming to differentiation (FGF5), early neural progenitors (Nestin, Pax6, Sox2), postmitotic neurons (B-III-Tub), and endomesoderm (Gata4–6; Brachyury, T). Expression was evaluated by RT-PCR as relative to Beta-actin. Values were normalized to maximum expression, except those of Gata4–6 and T, which were normalized to the average relative expression of the other markers. (C) flow-cytometry analysis of Sox1-GFP ES cells at different DIV as indicated. Error bars show standard error. [Color figure can be viewed in the online issue, which is available at wileyonlinelibrary.com.]

at the end of this first step (2 days of *in vitro* differentiation, 2 DIV) cells already turned off most of Nanog expression (Supporting Information Fig. 1B). At 2 DIV, aggregates were dissociated and cells were left to spontaneously neuralize in a second step as adherent cultures (Step-II, 4 days). At 4 DIV, cells had turned off Oct4 expression (not shown), already expressed the early neural progenitor marker nestin and formed rosette-like structures typical of neural progenitors (Zhang et al., 2001; Supporting Information Fig. 1C). Nestin expression increased and few B-III-tubulin neurons appeared at 6 DIV (Supporting Information Fig. 1D). The ratio of B-III-Tubulin-positive and N-Tubulin-positive neurons increased at DIV 10 (Supporting Information Fig. 1E) and became considerable at DIV14 (Supporting Information Fig. 1F). Gene expression analysis by RT-PCR confirmed the immunocytodetection analysis. Moreover, cells showed very low expression of endomesodermal markers Gata4, Gata6, and Brachyury (T), which was consistent with a high degree of neuralization [Fig. 1(B)]. To validate the occurrence of robust neuralization, we used a transgenic Sox1-GFP ES cell line (46C; Ying et al., 2003), in which GFP expression identifies early Sox1-positive neural progenitors. As determined by flow cytometry, neural progenitor ratio rapidly increased over the first days of neuralization, reaching 87% at 6 DIV [Fig. 1(C)]. A progressive process of ES cell differentiation through known steps of embryonic development was suggested also by the analysis of markers of pluripotency, priming to differentiation, neuralization, and differentiated neurons, using gene expression arrays (Supporting Information Fig. 2).

Mouse ES Cells Express Wnts, BMPs, and FGFs During *In Vitro* Neural Differentiation

To investigate the endogenous production of ligands of growth factor and morphogen families that are known to orchestrate neural patterning *in vivo*, we performed a high-throughput analysis of gene expression by microarray hybridization at different steps of ES cell neuralization.

In neuralizing cells at Step-II (6 DIV, Fig. 2), distinct members of Wnt, BMP and FGF families were highly expressed as compared to members of TGF-beta and Shh families. Wnt7b, Wnt8b, Wnt9a, Wnt1, BMP4, BMP7, and FGF23 showed the highest levels of expression. Notably, during Step-II neural progenitors are formed and previous studies indicated that they are competent to be patterned by BMP, RA, or Shh signaling (Bertacchi et al., 2013). According to the literature, FGF4, which is known to be expressed by mouse ES cells (Ying et al., 2008), showed the highest expression level at 0 DIV, whereas the expression of FGF5, which is a marker of priming to differentiation (Nichols and Smith, 2009), peaked at 2 DIV. The FGF member with the highest expression at 6 DIV was FGF23, whose expression reached its maximum at 10 DIV. Compared to Wnt, BMP, and FGF, members of TGF-beta and Shh familes were poorly expressed throughout all ES cell differentiation. In particular, Shh expression was very low until 10 DIV.

To get insights into the cell type that was responsible for the expression of ligands, we performed Aracytin (AraC) treatment, which is known to kill cycling cells (Orr and Smith, 1988). AraC treatment from 12 DIV to 14 DIV [Fig. 3(A)] negatively selected nestin-positive progenitor cells, leaving viable postmitotic neurons [Fig. 3(B–D)]; this diminished the level of expression of most members of Wnt, BMP, and FGF families, suggesting that cycling neural progenitors were responsible for the expression of these factors. BMP7, Wnt4, FGF5, and FGF7 were the exception, because their expression increased after AraC treatments, implying that they were produced preferentially by postmitotic neurons [Fig. 3(E–G)].

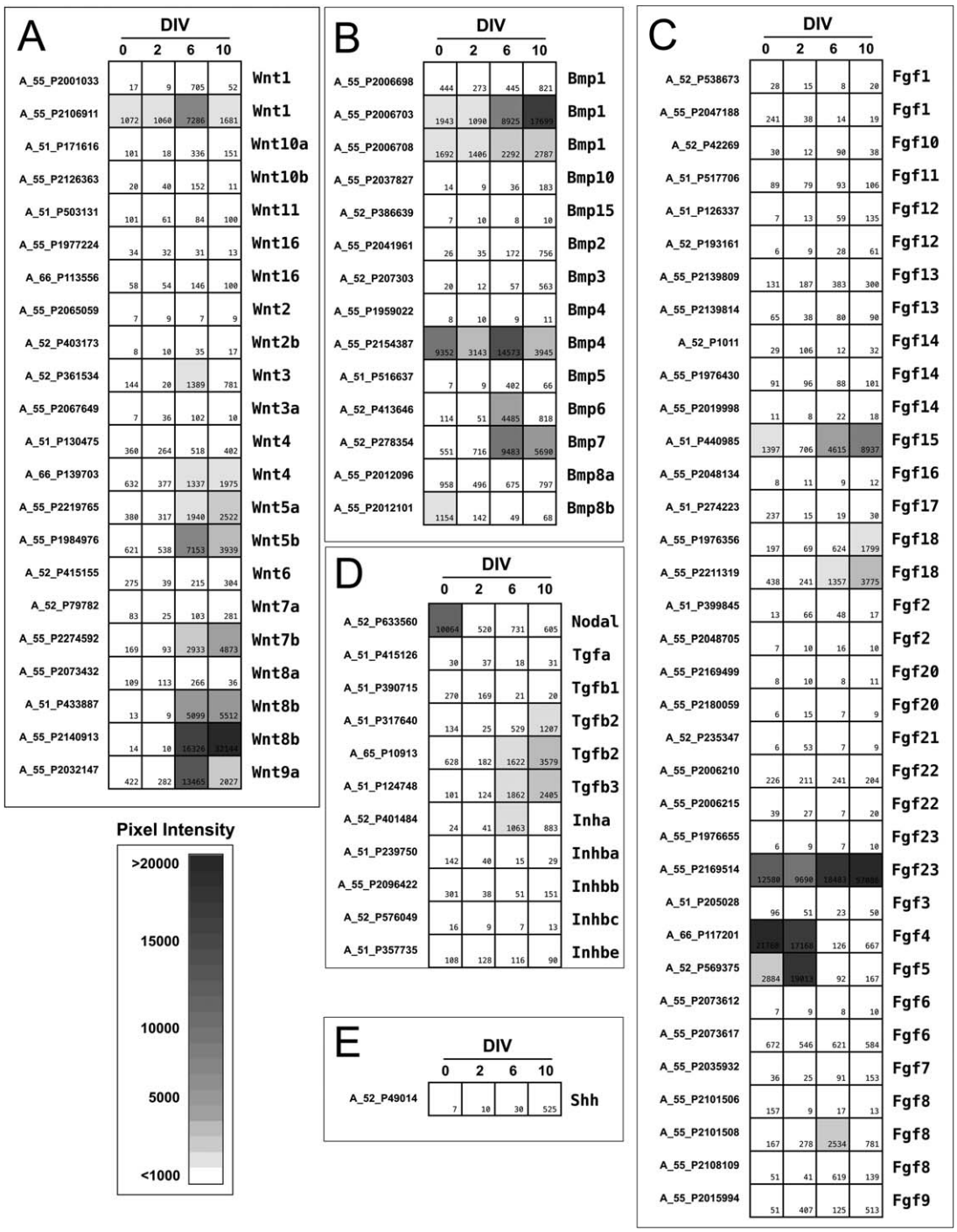

Figure 2 Endogenous signaling of neuralizing ES cells. (A–E) expression of different members of growth factor and morphogen families at different DIV: Wnts (A), BMPs (B), FGFs (C), Activin/Nodal (D), Shh (E). Values are expression levels in linear scale, obtained by the analysis of Agilent gene expression microarrays. Gray-scale indicates intensity degree, from minimum (white) to maximum (dark gray). Agilent probe annotation and gene name are indicated in the most left and right column of each panel, respectively.

Taken all together, these data suggest that mouse ES cells express different morphogens during neural differentiation *in vitro*, especially BMPs, Wnts, and FGFs. Thus, the concept of CDMM must be carefully addressed: even when using a morphogen-free culture medium, differentiating cells might be expressing

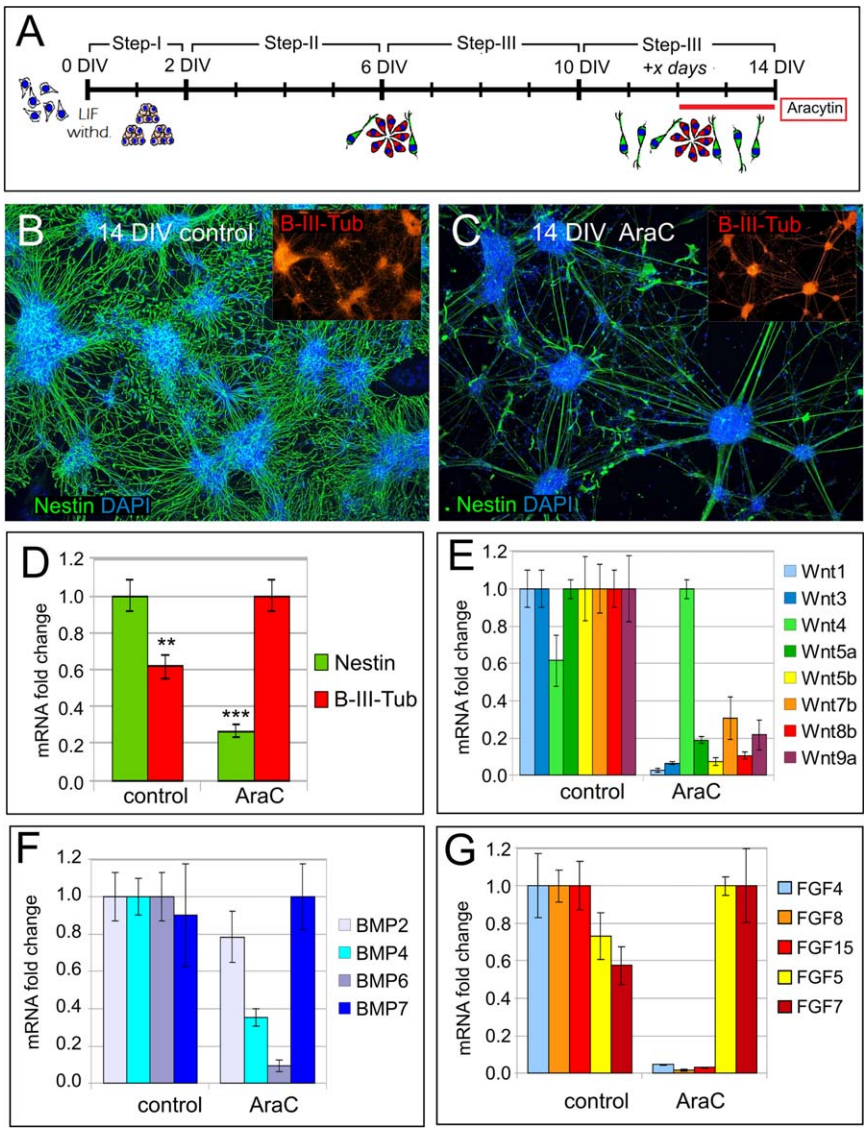

Figure 3 Effect of AraC treatment on the morphogen production of neuralizing ES cells. (A) experimental protocol of Aracytin (AraC) treatment. (B,C) Nestin and Beta-III-Tubulin (B-III-Tub) immunocytodetection in control (B) and AraC-treated (C) cells. (D) RT-PCR analysis of Nestin and Beta-III-Tubulin. (E–G) RT-PCR analysis of Wnts (E) BMPs (F) and FGFs (G) in control or AraC-treated (Ara C) cultures. Error bars show standard error; **p\0.01, ***p\0.001 (two-tailed Student's t test). [Color figure can be viewed in the online issue, which is available at wileyonlinelibrary.com.]

by themselves high amounts of different active molecules.

We postulated that endogenous Wnt, BMP, and FGF could affect the positional identity of progenitors generated by ES cells in CDMM.

Effect of BMP, Wnt, and FGF Inhibition on ES Cell Neural Patterning

BMPs produced by neuralizing ES cells were already proved to inhibit telencephalic identity in neural progenitors (Bertacchi et al., 2013). We, thus, assayed if also endogenous Wnts and FGF affected the patterning of ES-derived progenitors. ES cells neuralized in CDMM express midbrain markers starting from Step-II (Bertacchi et al., 2013). When Wnt signaling was inhibited by IWR-1-Endo treatment during Step-II [10 μM, Fig. 4(A)], the midbrain markers En1, Irx3, and Otx2 were downregulated and the forebrain and cortical markers Emx2, Six3, FoxG1 were upregulated at 6 DIV (not shown). We tested whether a double inhibition of BMP and Wnt pathways could

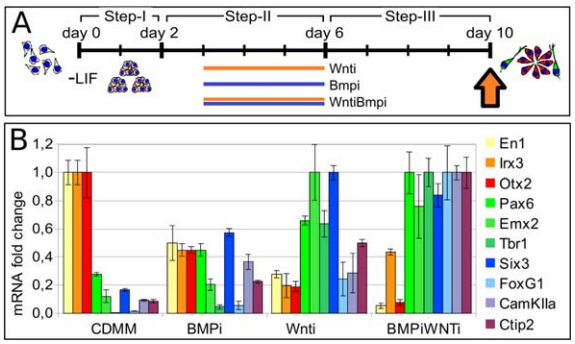

Figure 4 Effect of BMP and Wnt inhibition on ES cell neural patterning. (A) scheme of treatments. Wnti, Wnt inhibition; BMPi, BMP inhibition. The arrow shows the time of analysis. B, RT-PCR analysis of markers of dorsal/neural differentiation (Pax6) or anterior/posterior patterning. Forebrain markers: Emx2 (Simeone et al., 1992b), Tbr1 (Bulfone et al., 1995), Six3 (Oliver et al., 1995), FoxG1 (Xuan et al., 1995), CamKIIa (Arimatsu et al., 1999), Ctip2 (Arlotta et al., 2005). Midbrain markers: En1 (Davis et al., 1988), Irx3 (Bellefroid, 1998), and Otx2 (Simeone et al., 1992a).Values report fold changes. Error bars show standard error. [Color figure can be viewed in the online issue, which is available at wileyonlinelibrary.com.]

strengthen the expression of forebrain markers. Cells were treated during Step-II with antagonist of BMP (Dorsomorphin, 5 μM; Bertacchi et al., 2013), of Wnt (IWR-1-Endo,10 μM), or with a combination of both. Wnt-inhibition was able to upregulate anterior/cortical markers (Emx2, Six3, FoxG1, CamKII-α, Tbr1,and Ctip2) more efficiently than BMP-inhibition, while the double inhibition showed a synergistic effect on the expression of A/P markers at Step-III [10 DIV; Fig. 4(B)]. Notably, positional memory of these changes was further maintained when prolonging the culture without treatment (14 DIV; Supporting Information Fig. 3A). The majority of Wnt/BMP double inhibited cells at 10 DIV were positive for the dorsal pan-neuronal marker Pax6 (66.4%,) and the telencephalic marker FoxG1 [69%, Fig. 5(A–F)], whereas the ratio of double BMP-Wnt inhibited cells expressing the ventral marker Nkx2.1 was very low (0.2%, Supporting Information Fig. 3B), according to the modest expression of Shh (see earlier). However, BMP/Wnt inhibited cells were competent to be ventralized by Shh signaling, as treatment with a SAG (150nM at Step-II) induced Nkx2.1 expression in 84% of cells (Supporting Information Fig. 3C).

The induction of a telencephalic identity was quite rapid, since at 6 DIV 55% of cells were already FoxG1 positive [Fig. 5(G)]. Treatments at Step-I or Step-III, either by Wnt-inhibition alone, or by double Wnt/BMP inhibition, were much less effective than treatments at Step-II on the expression of early markers of A/P patterning (Supporting Information Fig. 4). This is consistent with previous results obtained by BMP inhibition (Bertacchi et al., 2013) and indicates that Step-II is the time when early A/P patterning occurs in our *in vitro* protocol of ES cell differentiation.

To investigate the specificity of action of the treatments, we quantified by RT-PCR the expression of ID1, a downstream effector of the BMP-responsive pathway, and the expression of LEF1, a *bona fide* marker of the canonical Wnt pathway activity. Cells were treated during Step-II (starting at the beginning of day 2) and analyzed 72 h after, at 6 DIV. Dorsomorphin-mediated BMP-inhibition, both in single and in double treatment, resulted in a strong decrease of ID1 expression, compared to control cells. Similarly, LEF1 expression decreased when cells were treated with IWR-1-Endo (both in single Wnt-inhibition and in double BMP/Wnt-inhibition). Surprisingly, LEF1 expression showed a marked decrease also in Dorsomorphin-treated cells, [Fig. 5(H)]. This suggested a cross-talk mechanism between the two pathways. However, when culturing ES cells until 6 DIV and then performing an acute treatment of 12 h with chemical drugs, LEF1 and ID1 levels decreased in cells treated with IWR-1-Endo and Dorsomorphin, respectively, but LEF1 expression level in Dorsomorphin-treated cells was comparable to that of control cells [Fig. 5(I)]. Thus, the acute treatment demonstrated the specificity of the two antagonists on their respective pathways. We concluded that Dorsomorphin affects BMP signaling but is able to inhibit the Wnt canonical signaling as a secondary/late effect.

We investigated the effect of endogenous FGFs by treating the cell culture with PD0325901 (10 to 100 nM during Step-II or during Step-III), which blocks FGF signaling pathway by inhibiting MEK/ERK kinases. At each of the concentrations used, FGF depletion caused high level of cell death (not shown). This effect was likely due to a strict requirement of FGF signaling for cell survival during Step-II, or to high toxicity following MEK/ERK-inhibition. The lack of viability impeded an analysis of the patterning of neural progenitors. Better results were obtained with a specific inhibitor of FGF-receptor, PD173074 (200 nM during Step-II), which slowed-down cell proliferation (not shown) but allowed neural conversion (Supporting Information Fig. 5A–C). FGF-activation by exogenous FGF8b at Step-II significantly induced FoxG1 expression, while treatment at Step-III induced Gbx2 and En2. FGF-inhibition left

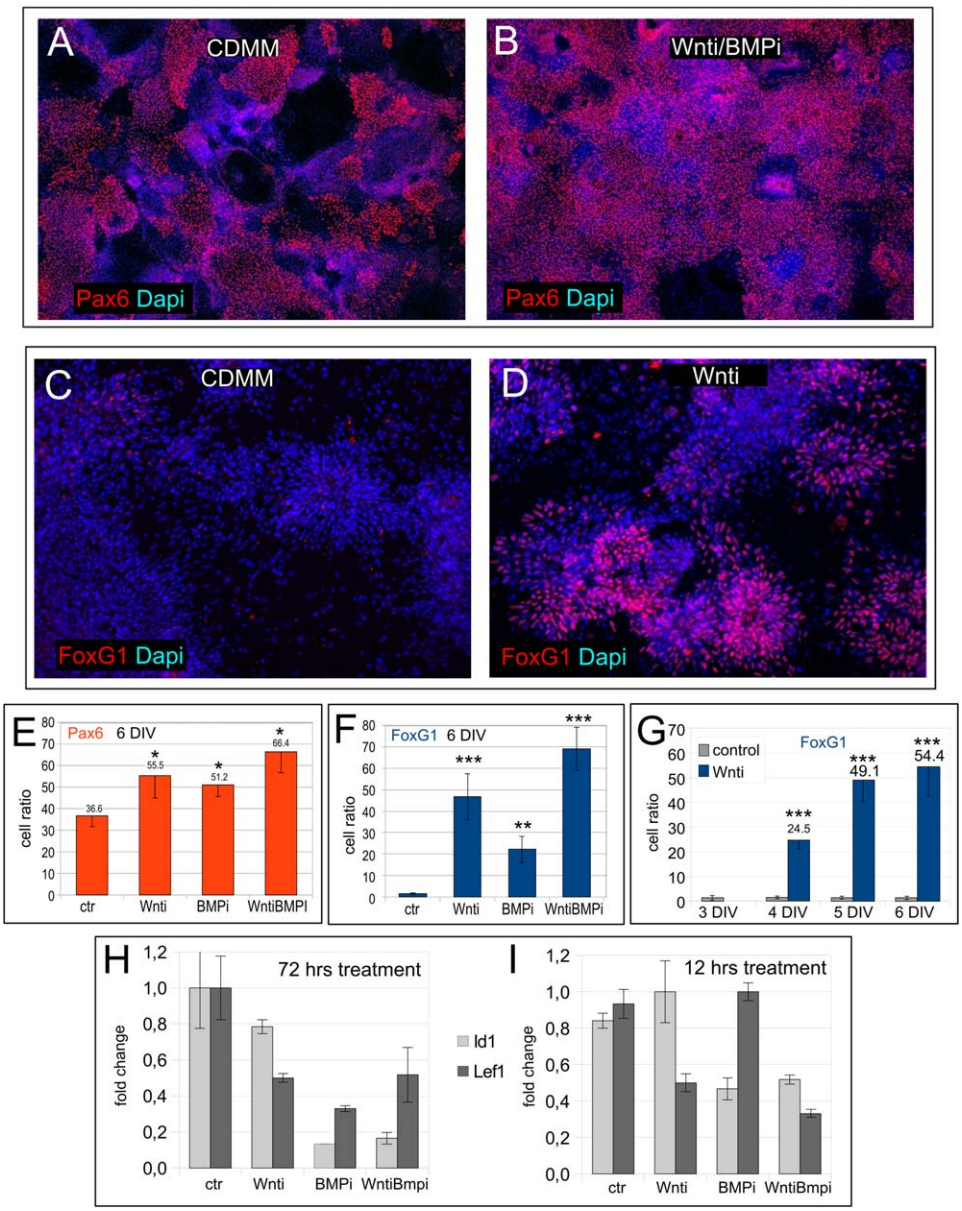

Figure 5 Effects of Wnt/BMP double inhibition of neuronal cell identity. (A–D) immunocytodetection of dorsal neural marker Pax6 (A,B) and forebrain marker FoxG1(C,D) in control (CDMM) or Wnt/BMP double inhibited ES cultures at 10 DIV. E,F, Ratio of Pax6 (E) and FoxG1 (F) positive cells at 10 DIV. (G) ratio of FoxG1positive cells at different DIV. H,I, RT-PCR analysis of Lef1 and ID1, reporters of Wnt and BMP signaling pathways, respectively, after 72 h (H) or 12 h (I) of inhibition of Wnt and/or BMP signaling. Values are expressed as fold change. Error bars show standard error; **p*\0.05, ***p*\0.01, ****p*\0.001 (two-tailed Student's *t* test). [Color figure can be viewed in the online issue, which is available at wileyonlinelibrary.com.]

the expression level of A/P markers almost unaffected (Supporting Information Fig. 5D). The double nature of FGF8b as a modulator of both anterior/telencephalic and midbrain markers is consistent with its expression pattern *in vivo*, as FGF8b can be found in the anterior telencephalon and in the midbrain/hindbrain boundary (Rhinn and Brand, 2001; Shimogori et al., 2004). As a control of specificity of our treatments, FGF depletion/activation was confirmed by the regulation of the FGF signaling targets Spry2 and Sp8 (Supporting Information Fig. 5E). As little or no difference in the expression level of A/P

markers was found by comparing control cells with FGF-depleted cells, we concluded that the endogenous FGF signaling of neural progenitors during Step-II is necessary to neural differentiation and cell survival but it is not affecting in a relevant way the A/P identity of neural precursors in this window of treatments. However, we cannot exclude that the activation/inhibition of specific subsets of receptors by different FGF ligands could exert discordant effects on patterning.

Double Wnt/BMP Inhibition Turns on a Gene Expression Program that is Comparable to that of Cortical Progenitors

BMP and Wnt inhibition increased the ratio of cells expressing Tbr1, which specifically identifies a subset of early-generated cortical neurons, and Ctip2, which labels medium/early-generated cortical neurons of cortical layer 5, with the double inhibition exerting a synergistic effect [Fig. 6(A–E); Leone et al., 2008). We asked if the BMP-Wnt double inhibition could induce a neurogenic program similar to that of *in vivo* telencephalic development. We, thus, assayed if the expression of the markers of early, medium-late and late projecting neurons (Tbr1, Ctip2, and Satb2, respectively), was activated following a temporal sequence as during *in vivo* corticogenesis. The analysis of cells expressing the three markers [Fig. 6(F,G)] showed that a sequential onset of Tbr1-Ctip2-Satb2 expression *in vitro* occurs similarly to embryonic cortical development (Leone et al., 2008). Moreover, BMP/Wnt inhibited ES cultures at 18 DIV showed a robust labeling with B-III-tubulin and vGlut2 (87%), but were poorly labeled by GAD2 (8%; Supporting Information Fig. 6A–I), which was instead induced by the activation of Shh signaling with SAG (Supporting Information Fig. 6H,I), These observations suggest that BMP/Wnt inhibition induced a glutamatergic fate and are consistent with a cortical identity of the neurons generated by ES cells.

To better characterize neuronal identity, we compared the global gene expression profile of control or BMP/Wnt inhibited ES cultures at 15 DIV to the profile of isocortex, hippocampus, ventral telencephalon, or midbrain dissected from E15 embryo. We first compared gene expression profiles by PCA (see Methods). The first component, which accounts for 29.8% of variability, separated embryonic tissues from ES cell cultures. The second and third components, accounting for 19.4% and 17.6% of variability, respectively, distinguished the different embryonic brain regions. A 3D plot of these first three components, accounting in total for 66.8% of gene expression variability, is shown in Figure 7(A). Compared to control cells differentiated in CDMM, Wnt/BMP-inhibited cells (WiBi) are closer to isocortex and hippocampus than to midbrain or ventral telencephalon, indicating that Wnt/BMP-inhibition steers ES cell identity toward a general telencephalic identity. This observation is consistent with the results obtained when comparing the gene expression fold change between WiBi and CDMM to the gene expression fold change between isocortex and midbrain [Fig. 7(B)], isocortex and hippocampus [Fig. 7(C)] or isocortex and ventral telencephalon [Fig. 7(D)]. In fact, there is a pretty high coherence between WiBi/CDMM gene expression fold-change (gray bar plot) and Isocortex/Midbrain or Isocortex/Ventral Telencephalon gene expression fold change (black dot plot). All in all, these data support the ability of Wnt/BMP double inhibition to steer the identity of ES cells toward a dorsal/telencephalic identity rather than toward the identity of other brain regions.

DISCUSSION

Endogenous Production of Growth Factors

By adopting an *in vitro* neuralization protocol of mouse ES cells that makes use of minimal medium, we were able to investigate the endogenous activation of BMP, Wnt, and FGF signaling and their effects on neural patterning. In a previous work, we demonstrated that neuralizing ES cell cultures produce and are sensitive to BMPs, and that BMP signaling inhibition was permissive to the activation of a gene expression program consistent with a dorsal telencephalic identity (Bertacchi et al., 2013). In this study, we performed a high-throughput analysis to characterize, at distinct times of our neuralization protocol, the expression of ligands of the main growth factor and morphogen pathways known to act during early neural development. We found that members of BMP, Wnt and FGF, but not of Shh and TGFb families, were endogenously produced at high level in early neuralized ES cultures. Many previous studies described the effects of growth factor and morphogen antagonists on ES cells neuralization and patterning (see Introduction). This indirectly supported evidence of endogenous production of growth factors and morphogens, but no particular attention was addressed to characterize when and which particular ligand was produced. With our observations, we contributed to fill in this gap and highlighted the

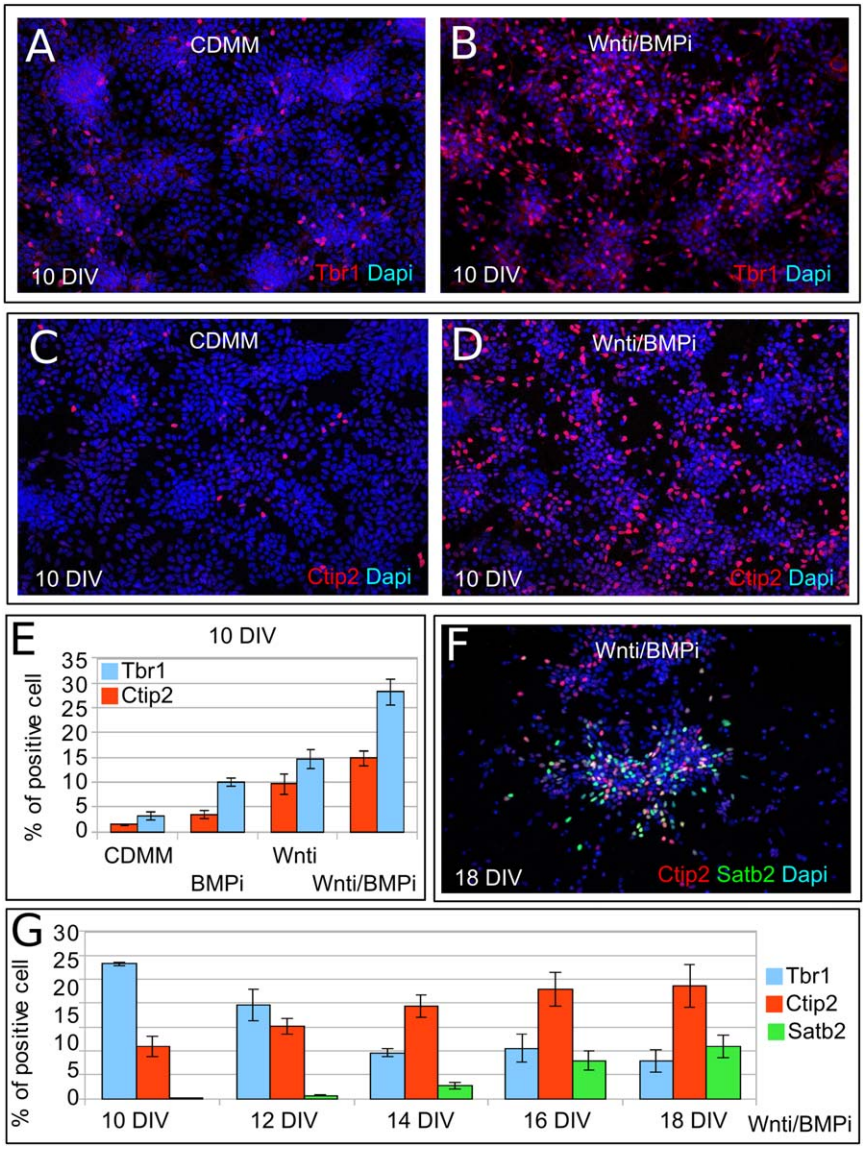

Figure 6 ES cells corticalization by double Wnt/BMP inhibition. (A–D,F) Tbr1, Ctip2, and Satb2 immunocytodetections at the indicated DIV in control cells (CDMM) or in cells treated by Wnt/BMP double inhibition (Wnti/BMPi). (E) ratio of cells positive for Tbr1 and Ctip2 at 10 DIV. (G) ratio of Wnt/BMP double inhibited cells positive to Tbr1, Ctip2, and Satb2 at different DIV as indicated. Error bars show standard error. [Color figure can be viewed in the online issue, which is available at wileyonlinelibrary.com.]

importance of knowing which is the endogenous contribution of signaling when steering the neural patterning of ES cultures. The novelty of our approach is to relate the final fate of ES-derived neurons with the role of specific morphogens, whose endogenous production in neuralizing ES cells was characterized by global gene expression profiling.

We found that endogenous FGF signaling acted mainly on cell viability and proliferation, whereas both endogenous Wnts and BMPs worked as posteriorizing signals, inhibiting the expression of forebrain markers and supporting midbrain identity. Comparing to BMP inhibition, whose effect on ES cells neural patterning was previously described (Bertacchi et al., 2013), Wnt inhibition was more effective in inducing the expression of dorsal/telencephalic genes. We found that BMP inhibition was able to inhibit also Wnt signaling as a secondary, later

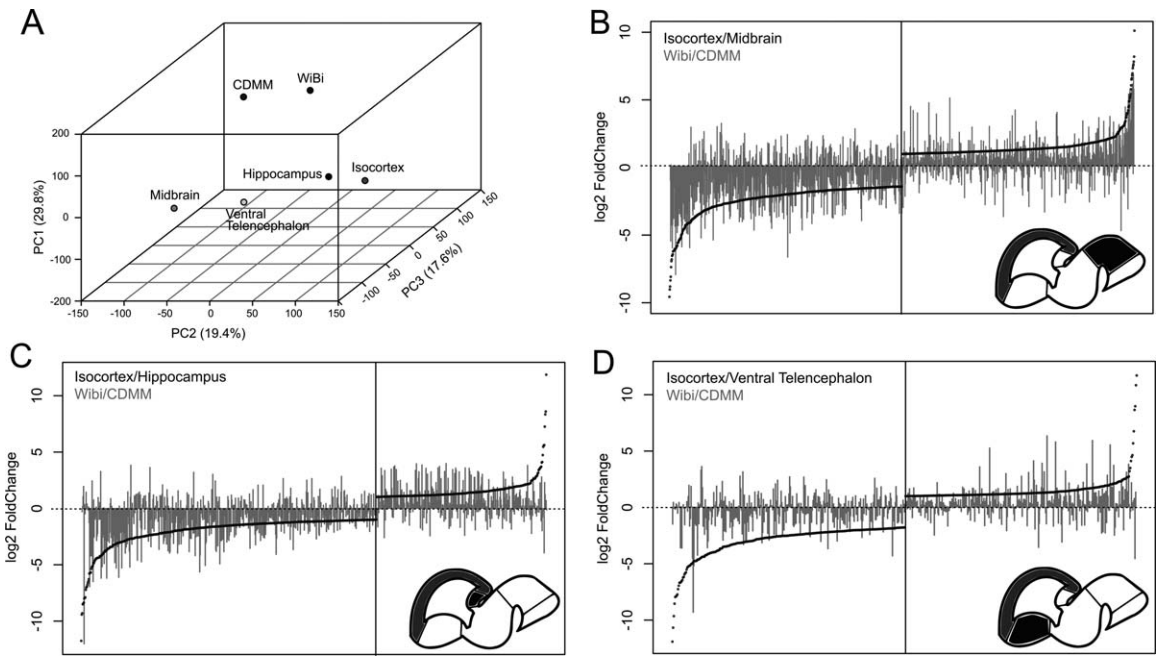

Figure 7 Global gene expression profiles of neuralized ES cells and embryonic brain regions. (A) PCA of the gene expression profiles of 15 DIV ES cells and E15 brain regions. The first three components, whose values are indicated in brackets, were plotted in *X*, *Y*, and *Z* axis, respectively. (B–D) show the gene expression fold-change between cell culture conditions (gray bars) or between brain regions (black dots), as indicated in labels and in schematic drawings. Comprehensive lists of genes showing fold-change higher than 2 in the different brain regions are reported in Supporting Information Table 1.

effect [see Fig. 5(H,I)]. The exact mechanism by which the two signals act in a cooperative manner on the genetic program of telencephalic specification remains to be elucidated.

Identitity of Neurons Generated by ES Cells

BMP/Wnt double inhibition was capable to induce massive anteriorization of ES-derived neural progenitors, since 69% of cells were FoxG1 positive at 10 DIV [Fig. 5(F)]. The nature of these telencephalic cells was mainly dorsal, as 66.4% of them were Pax6-positive [Fig. 5(E)] and 87% of them differentiated at 18 DIV as glutamatergic neurons labeled by vGlut2 (Supporting Information Fig. 5), which *in vivo* derive from the dorsal telencephalic aspect. Accordingly, ventral Nkx2.1-positive cells at 10 DIV were almost absent (0.2%, Supporting Information Fig. 3B) and the ratio of GAD2-positive neurons at 18 DIV, which *in vivo* originate from the ventral developing pallium, was low (8%, Supporting Information Fig. 6). These observations are consistent with very low expression of Shh until 10 DIV (Fig. 2) and suggest a dorsal default identity of ES-generated neural progenitors. Nonetheless, progenitors were competent to respond to Shh signaling, as SAG treatment at Step-II induced Nkx2.1 expression in 84% of cells (Supporting Information Fig. 3C). It is still to be established why 8% of cells became GAD2-positive GABAergic neurons. We speculate that this fraction derived from late neurogenesis occurring after 10 DIV and induced to a ventral identity by endogenous Shh signaling, which starts at 10 DIV (Fig. 2). In fact, after 10 DIV a fraction of cycling progenitors still remains in our cultures [see Fig. 3(B)], which might have been responsible for the generation of GAD2-positive neurons due to the effect of late Shh signaling.

Ventral default identity of ES-derived neural progenitors was described by Gaspard et al. (Gaspard et al., 2008). In their work, mouse ES cells cultured at low density in a minimal medium spontaneously neuralized and turned on ventral telencephalic markers. The inhibition of Shh signaling by Cyclopamine treatment was sufficient to shift the expression from ventral to dorsal markers and induced a cortical fate. The acquisition of a telencephalic identity is in line with similar reports of monolayer cultures at low

density (Tropepe et al., 2001; Smukler et al., 2006). Moreover, it may be still consistent with our findings, if we consider that the dilution of posteriorizing ligands such as BMP and Wnt, due to low plating density in minimal culture medium used by Gaspard et al., might have highly weakened their signaling. However, the need of Shh signaling inhibition to support dorsal identity is apparently inconsistent with our observations. We assume that this divergence is due to different culture conditions. In fact, compared to our protocol, the protocol of neuralization followed by Gaspard et al. used a low seeding density of the initial ES cell plating (5000 vs. 40,000 cells per square cm), which might be responsible of a higher and earlier Shh expression. We thus hypothesize that in the protocol of Gaspard et al. most of neural patterning occurred in the presence of high endogenous Shh signaling, thus resulting in ventral identity.

All in all, our observations suggest that inhibiting BMP and Wnt signaling in mouse ES cells neuralizing in minimal medium is sufficient to initiate a program of dorsal /telencephalic differentiation. This is consistent with the "Activation-Transformation" model in which, during neural induction (Activation), cells would acquire an anterior fate that would be maintained in the absence of signals inducing posterior Transformation (see Introduction). In addition, we propose that Activation would specify dorsal identity as default, unless ventralizing signals such as Shh are expressed (see earlier). This view is coherent with a genuine parallelism between early steps of ES cells neuralization *in vitro* and neural patterning *in vivo*.

In Vitro Corticogenesis

To induce cortical fate, some procedures made use of a feeder layer of stromal cells (Ideguchi et al., 2010), or cell aggregation (Eiraku et al., 2008). In these studies, the factors that were endogenously produced by cells in culture and that might have influenced ES cell differentiation were not identified. In fact, the multicellular and multidimensional nature of these cultures might complicate the study of the signals involved in the acquisition of a particular neuronal identity. Gaspard et al. showed that ES cell cultured in minimal medium at low density in the presence of Shh inhibitor Cyclopamine generated cells with morphological, electrophysiological and molecular features of cortical projection neurons (Gaspard et al., 2008). Notably, Gaspard et al. showed that the sequential activation of key transcription factors specifying early neurons of deep layers first (Tbr1 and Ctip2), and then late neurons of superficial layers (Cux1 and Satb2), occurs as observed *in vivo*. This result suggested that neural progenitors specified toward a cortical identity require neither a tridimensional environment nor spatially organized signaling to orchestrate the production of distinct types of cortical cells. The same conclusion came from pivotal works demonstrating that isolated cortical progenitors seeded at clonal density in primary cultures generated lineages whose composition, in terms of different types of cells and their respective birthdates, were mimicking those of cortical lineages *in vivo* (Qian et al., 2000; Shen et al., 2006; Slater et al., 2009).

Working with monolayer cultures of ES cells at subconfluent density, we confirmed the capability of ES-derived progenitors with a dorsal/telencephalic identity to express *in vitro* markers of cortical development. In fact, Wnt-BMP double-inhibited ES cells undergo sequential activation of Tbr1-Ctip2-Satb2 transcription factors [Fig. 6(G)]. Moreover, they differentiate predominantly as vGlut2-positive projection neurons. Global gene expression profiling of 15 DIV neurons derived from ES cells helped to investigate cell identity more in deep. PCA analysis indicated that the profile of neurons derived from ES cell cultures is quite distant from the profiles of the embryonic regions. We think that this is an expected result for two reasons: (i) neuronal cultures are much less complex cell populations than embryonic brain tissues; (ii) as it is difficult to know the exact correspondence between cell cultures and embryonic tissues in terms of developmental time, a gross part of gene expression diversity between them might by due to difference in proliferation, terminal differentiation, and maturation of differentiated cells. Nonetheless, PCA indicates that Wnt-BMP double inhibition steers ES cell identity more toward isocortex and hippocampus than toward ventral telencephalon or midbrain. Moreover, the analysis of gene expression fold-change shows a robust coherence between Wnt-BMP double inhibited cells and isocortex. Although an exact isocortical or hippocampal identity cannot be ascertained, our findings suggest a general cortical identity of Wnt-BMP double inhibited cells.

Further experiments, including assays of neuronal activity and *in vivo* grafting, are required to confirm real identity and potentials of the neurons generated by ES cells after BMP/Wnt double inhibition. However, due to the shorter time required for differentiation and the higher amount of neurons produced compared to the approaches discussed earlier, our method might be preferable for studies aimed to elucidate the molecular mechanisms regulating the production of different types of cortical projection neurons, and to produce cortical projection neurons suited for experiments of cell therapy.

We thank Antonino Cattaneo for his support in many aspects of this work, including critical discussion of the mechanisms of endogenous signaling in ES neuralizing cultures.

REFERENCES

Arimatsu Y, Ishida M, Takiguchi-Hayashi K, Uratani Y. 1999. Cerebral cortical specification by early potential restriction of progenitor cells and later phenotype control of postmitotic neurons. Development 126:629–38.

Arlotta P, Molyneaux BJ, Chen J, Inoue J, Kominami R, Macklis JD. 2005. Neuronal subtype-specific genes that control corticospinal motor neuron development in vivo. Neuron 45:207–221.

Bellefroid EJ. 1998. Xiro3 encodes a Xenopus homolog of the Drosophila Iroquois genes and functions in neural specification. EMBO J 17:191–203.

Bertacchi M, Pandolfini L, Murenu E, Viegi A, Capsoni S, Cellerino A, Messina A, Casarosa S, Cremisi F. 2013. The positional identity of mouse ES cell-generated neurons is affected by BMP signaling. Cell Mol Life Sci 70: 1095–1111.

Bouhon IA, Joannides A, Kato H, Chandran S, Allen ND. 2006. Embryonic stem cell-derived neural progenitors display temporal restriction to neural patterning. Stem Cells 24: 1908–1913.

Bouhon IA, Kato H, Chandran S, Allen ND. 2005. Neural differentiation of mouse embryonic stem cells in chemically defined medium. Brain Res Bull 68:62–75.

Bulfone A, Smiga SM, Shimamura K, Peterson A, Puelles L, Rubenstein JL. 1995. T-brain-1: A homolog of Brachyury whose expression defines molecularly distinct domains within the cerebral cortex. Neuron 15:63–78.

Chambers SM, Fasano CA, Papapetrou EP, Tomishima M, Sadelain M, Studer L. 2009. Highly efficient neural conversion of human ES and iPS cells by dual inhibition of SMAD signaling. Nat Biotechnol 27:275–280.

Chatzi C, Brade T, Duester G. 2011. Retinoic acid functions as a Key GABAergic differentiation signal in the basal ganglia. PLoS Biol 9:e1000609.

Davis CA, Noble-Topham SE, Rossant J, Joyner AL. 1988. Expression of the homeo box-containing gene En-2 delineates a specific region of the developing mouse brain. Genes Dev 2:361–371.

Eiraku M, Watanabe K, Matsuo-Takasaki M, Kawada M, Yonemura S, Matsumura M, Wataya T, Nishiyama A, Muguruma K, Sasai Y. 2008. Self-organized formation of polarized cortical tissues from ESCs and its active manipulation by extrinsic signals. Cell Stem Cell 3:519–32.

Eisen MB, Spellman PT, Brown PO, Botstein D. 1998. Cluster analysis and display of genome-wide expression patterns. Proc Natl Acad Sci USA 95:14863–14868.

Foley AC, Stern CD. 2001. Evolution of vertebrate forebrain development: How many different mechanisms? J Anat 199:35–52.

Gaspard N, Bouschet T, Hourez R, Dimidschstein J, Naeije G, Passante L, Schiffmann SN, Gaillard A, Espuny-camacho I, Vanderhaeghen P. 2008. An intrinsic mechanism of corticogenesis from embryonic stem cells. Nature 455:351–357.

Ideguchi M, Palmer TD, Recht LD, Weimann JM. 2010. Murine embryonic stem cell-derived pyramidal neurons integrate into the cerebral cortex and appropriately project axons to subcortical targets. J Neurosci 30:894–904.

Kirkeby A, Grealish S, Wolf DA, Nelander J, Wood J, Lundblad M, Lindvall O, Parmar M. 2012. Generation of regionally specified neural progenitors and functional neurons from human embryonic stem cells under defined conditions. Cell Rep 1:703–714.

Kriks S, Shim J-W, Piao J, Ganat YM, Wakeman DR, Xie Z, Carrillo-Reid L, Auyeung G, Antonacci C, Buch A, Yang L, Beal MF, Surmeier DJ, Kordower JH, Tabar V, Studer L. 2011. Dopamine neurons derived from human ES cells efficiently engraft in animal models of Parkinson's disease. Nature 480:547–551.

Leone DP, Srinivasan K, Chen B, Alcamo E, McConnell SK. 2008. The determination of projection neuron identity in the developing cerebral cortex. Curr Opin Neurobiol 18:28–35.

Li X-J, Zhang X, Johnson MA, Wang ZB, Lavaute T, Zhang SC. 2009. Coordination of sonic hedgehog and Wnt signaling determines ventral and dorsal telencephalic neuron types from human embryonic stem cells. Development 136:4055–4063.

Lupo G, Novorol C, Smith JR, Vallier L, Miranda E, Alexander M, Biagioni S, Pedersen RA, Harris WA. 2013. Multiple roles of Activin/Nodal, bone morphogenetic protein, fibroblast growth factor and Wnt/β-catenin signalling in the anterior neural patterning of adherent human embryonic stem cell cultures. Open Biol 3: 120167.

Muñoz-Sanjuán I, Brivanlou AH. 2002. Neural induction, the default model and embryonic stem cells. Nat Rev Neurosci 3:271–280.

Nichols J, Smith A. 2009. Naive and primed pluripotent states. Cell Stem Cell 4:487–492.

Nicoleau C, Varela C, Bonnefond C, Maury Y, Bugi A, Aubry L, Viegas P, Bourgois-Rocha F, Peschanski M, Perrier AL. 2013. Embryonic stem cells neural differentiation qualifies the role of Wnt/β-Catenin signals in human telencephalic specification and regionalization. Stem Cells 31:1763–1774.

Nordgård O, Kvaløy JT, Farmen RK, Heikkilä R. 2006. Error propagation in relative real-time reverse transcription polymerase chain reaction quantification models: the balance between accuracy and precision. Analytical Biochemistry 356:182–193.

Oliver G, Mailhos A, Wehr R, Copeland NG, Jenkins NA, Gruss P. 1995. Six3, a murine homologue of the sine oculis gene, demarcates the most anterior border of the developing neural plate and is expressed during eye development. Development 121:4045–4055.

Orr DJ, Smith RA. 1988. Neuronal maintenance and neurite extension of adult mouse neurones in non-neuronal cell-reduced cultures is dependent on substratum coating. J Cell Sci 91 (Pt 4):555–561.

Ozair MZ, Noggle S, Warmflash A, Krzyspiak JE, Brivanlou AH. 2013. SMAD7 directly converts human embryonic stem cells to telencephalic fate by a default mechanism. Stem Cells 31:35–47.

Pfaffl MW, Horgan GW, Dempfle L. 2002. Relative expression software tool (REST) for group-wise comparison and statistical analysis of relative expression results in real-time PCR. Nucleic Acids Research 30:e36.

Qian X, Shen Q, Goderie SK, He W, Capela A, Davis AA, Temple S. 2000. Timing of CNS cell generation: A programmed sequence of neuron and glial cell production from isolated murine cortical stem cells. Neuron 28:69–80.

Rhinn M, Brand M. 2001. The midbrain–hindbrain boundary organizer. Curr Opin Neurobiol 11:34–42.

Shen Q, Wang Y, Dimos JT, Fasano CA, Phoenix TN, Lemischka IR, Ivanova NB, Stifani S, Morrisey EE, Temple S. 2006. The timing of cortical neurogenesis is encoded within lineages of individual progenitor cells. Nat Neurosci 9:743–51.

Shimogori T, Banuchi V, Ng HY, Strauss JB, Grove EA. 2004. Embryonic signaling centers expressing BMP, WNT and FGF proteins interact to pattern the cerebral cortex. Development 131:5639–5647.

Simeone A, Acampora D, Gulisano M, Stornaiuolo A, Boncinelli E. 1992a. Nested expression domains of four homeobox genes in developing rostral brain. Nature 358: 687–690.

Simeone A, Gulisano M, Acampora D, Stornaiuolo A, Rambaldi M, Boncinelli E. 1992b. Two vertebrate homeobox genes related to the Drosophila empty spiracles gene are expressed in the embryonic cerebral cortex. EMBO J 11:2541–2550.

Slater JL, Landman KA, Hughes BD, Shen Q, Temple S. 2009. Cell lineage tree models of neurogenesis. J Theor Biol 256:164–179.

Smukler SR, Runciman SB, Xu S, van der Kooy D. 2006. Embryonic stem cells assume a primitive neural stem cell fate in the absence of extrinsic influences. J Cell Biol 172:79–90.

Smyth GK. 2005. Limma: Linear models for microarray data. Bioinformatics. In: Gentleman R, et al., editors. Bioinformatics and Computational Biology Solutions using R and Bioconductor. New York: Springer; 2005. p. 397–420.

Surmacz B, Fox H, Gutteridge A, Fish P, Lubitz S, Whiting P. 2012. Directing differentiation of human embryonic stem cells toward anterior neural ectoderm using small molecules. Stem Cells 30:1875–1884.

Tropepe V, Hitoshi S, Sirard C, Mak TW, Rossant J, van der Kooy D. 2001. Direct neural fate specification from embryonic stem cells: A primitive mammalian neural stem cell stage acquired through a default mechanism. Neuron 30:65–78.

Watanabe K, Kamiya D, Nishiyama A, Katayama T, Nozaki S, Kawasaki H, Watanabe Y, Mizuseki K, Sasai Y. 2005. Directed differentiation of telencephalic precursors from embryonic stem cells. Nat Neurosci 8:288–296.

Wichterle H, Lieberam I, Porter JA, Jessell TM. 2002. Directed differentiation of embryonic stem cells into motor neurons. Cell 110:385–397.

Wilson SW, Houart C. 2004. Early steps in the development of the forebrain. Dev Cell 6:167–181.

Xuan S, Baptista CA, Balas G, Tao W, Soares VC, Lai E. 1995. Winged helix transcription factor BF-1 is essential for the development of the cerebral hemispheres. Neuron 14:1141–1152.

Ying Q-L, Stavridis M, Griffiths D, Li M, Smith A. 2003. Conversion of embryonic stem cells into neuroectodermal precursors in adherent monoculture. Nat Biotechnol 21: 183–186.

Ying Q-L, Wray J, Nichols J, et al. 2008. The ground state of embryonic stem cell self-renewal. Nature 453:519–523.

Zhang SC, Wernig M, Duncan ID, Brüstle O, Thomson JA. 2001. In vitro differentiation of transplantable neural precursors from human embryonic stem cells. Nat Biotechnol 19:1129–1133.

Stem Cell Reports
Article

OPEN ACCESS

Activin/Nodal Signaling Supports Retinal Progenitor Specification in a Narrow Time Window during Pluripotent Stem Cell Neuralization

Michele Bertacchi,[1,10,11,12] Giuseppe Lupo,[2,3,4] Luca Pandolfini,[1] Simona Casarosa,[5] Mara D'Onofrio,[6,7] Roger A. Pedersen,[8] William A. Harris,[4] and Federico Cremisi[1,9,*]

[1]Laboratorio di Biologia, Scuola Normale Superiore di Pisa, Piazza dei Cavalieri 7, 56124 Pisa, Italy
[2]Department of Chemistry, Sapienza University of Rome, Piazzale A. Moro 5, 00185 Rome, Italy
[3]Istituto Pasteur-Fondazione Cenci Bolognetti, Sapienza University of Rome, Piazzale A. Moro 5, 00185 Rome, Italy
[4]Department of Physiology, Development and Neuroscience, University of Cambridge, Downing Street, Cambridge CB2 3DY, UK
[5]Centre for Integrative Biology, University of Trento, Via delle Regole 101, 38123 Mattarello (Trento), Italy
[6]Genomics Facility, European Brain Research Institute "Rita Levi-Montalcini," Via del Fosso di Fiorano 64, 00143 Rome, Italy
[7]Istituto di Farmacologia Traslazionale, CNR, Via del Fosso del Cavaliere 100, 00133 Rome, Italy
[8]Department of Surgery and The Anne McLaren Laboratory for Regenerative Medicine, Wellcome Trust-Medical Research Council Cambridge Stem Cell Institute, West Forvie Building, Robinson Way, Cambridge CB2 0SZ, UK
[9]Institute of Biomedical Technologies (ITB), National Research Council (CNR) of Pisa, Via Moruzzi 1, 56124 Pisa, Italy
[10]Present address: University of Nice Sophia-Antipolis, iBV, UMR 7277, 06108 Nice, France
[11]Present address: Inserm, iBV, U1091, 06108 Nice, France
[12]Present address: CNRS, iBV, UMR 7277, 06108 Nice, France
*Correspondence: federico.cremisi@sns.it
http://dx.doi.org/10.1016/j.stemcr.2015.08.011

SUMMARY

Retinal progenitors are initially found in the anterior neural plate region known as the eye field, whereas neighboring areas undertake telencephalic or hypothalamic development. Eye field cells become specified by switching on a network of eye field transcription factors, but the extracellular cues activating this network remain unclear. In this study, we used chemically defined media to induce in vitro differentiation of mouse embryonic stem cells (ESCs) toward eye field fates. Inhibition of Wnt/β-catenin signaling was sufficient to drive ESCs to telencephalic, but not retinal, fates. Instead, retinal progenitors could be generated from competent differentiating mouse ESCs by activation of Activin/Nodal signaling within a narrow temporal window corresponding to the emergence of primitive anterior neural progenitors. Activin also promoted eye field gene expression in differentiating human ESCs. Our results reveal insights into the mechanisms of eye field specification and open new avenues toward the generation of retinal progenitors for translational medicine.

INTRODUCTION

The vertebrate retina originates from the eye field, an anterior neural plate region identified by coexpression of a network of eye field transcription factors (EFTFs) including, among others, *Rax* and *Pax6* (Viczian, 2013).

In vertebrate embryos, downregulation of the bone morphogenetic protein (BMP) and Activin/Nodal signaling pathways is responsible for the specification of forebrain progenitors (Andoniadou and Martinez-Barbera, 2013). Anterior-posterior gradients of Wnts, fibroblast growth factors, and retinoic acid impose diencephalic, midbrain, hindbrain, or spinal cord identities on posteriorly located neural precursors. Rostral forebrain fates, instead, are preserved in anterior regions by shielding them from these signals (Andoniadou and Martinez-Barbera, 2013; Wilson and Houart, 2004).

Although diversification of the secondary prosencephalon into telencephalon, eye field, and hypothalamus has been difficult to dissect in vivo, it can be modeled in vitro using mouse and human embryonic stem cells (mESCs and hESCs, respectively). In these culture systems, both endogenous and exogenous signals contribute to cell-fate specification. Previous reports have shown induction of hypothalamic fates by minimizing ESC exposure to exogenous signals (Wataya et al., 2008), whereas culture in minimal media in the presence of transforming growth factor β and Wnt pathway inhibitors causes telencephalic specification (Bertacchi et al., 2015; Lupo et al., 2014). Extracellular cues, instead, appear to be critical for the induction of eye field fates, because production of retinal progenitors was generally inefficient in ESC systems with reduced extracellular signaling (Lupo et al., 2014).

Previous studies suggested that Activin/Nodal signaling promotes eye field fates, as shown by enhanced retinal progenitor generation in mESCs treated with exogenous Activin (Ikeda et al., 2005) and by repression of eye field gene expression in hESCs differentiating in the presence of Activin/Nodal pathway inhibitors (Lupo et al., 2013). The contribution of Activin/Nodal signaling to eye field specification, however, remains poorly understood (Lupo et al., 2014; Viczian, 2013). Here, building on previous studies (Ikeda et al., 2005; Lupo et al., 2013), we provide much more extensive evidence that Activin supports retinal identity in ESCs. Notably, we show that this function is restricted to a narrow time window coincident with the emergence of early

forebrain progenitors from pluripotent cells. These findings suggest the feasibility of efficiently mimicking retinal progenitor formation in vitro using purely defined reagents.

RESULTS

Activin Supports Expression of Eye Field Genes in mESCs Differentiating to Anterior Neural Progenitors

We recently described a protocol of mESC neuralization using a chemically defined minimal medium (CDMM) (Bertacchi et al., 2013). mESCs are prompted to differentiate by floating aggregate culture (step I, 2 days) and then allowed to spontaneously neuralize as adherent cultures (step II, 4–6 days). In these conditions, mESCs efficiently convert to neural progenitors, which can undergo neuronal differentiation following long-term culture (Bertacchi et al., 2013, 2015).

With this protocol, we found that the endogenous levels of extracellular signaling pathways in early differentiating mESCs are permissive for neural conversion. Emerging neural progenitors, however, produce BMP and Wnt signals that repress rostral forebrain specification and promote caudal forebrain/midbrain fates (Bertacchi et al., 2013, 2015). Because BMP-dependent caudalization is, at least in part, indirectly due to activation of Wnt signaling, treatments with Wnt/β-catenin inhibitors during step II are sufficient to elicit rostral forebrain character in mESCs (Figures 1A–1C; Bertacchi et al., 2015). In this study, we used this experimental system and a *Rax*-GFP knockin mESC line (K/l EB5), driving eGFP expression under control of the *Rax* promoter (Wataya et al., 2008), to investigate the signals promoting eye field fates in early anterior neural progenitors. mESCs were differentiated to neuroectoderm with or without the Wnt/β-catenin signaling inhibitor IWR-1-Endo (Wnti) applied from 3 days of in vitro differentiation (3 DIV) (Figure 1A). Cells were harvested every 12 hr between 3.5 and 10 DIV, and GFP-positive cells were detected by flow cytometry or immunostaining. Cells treated with Wnti showed a transient activation of GFP expression between 5 and 6 DIV (Figures 1B and 1D). GFP-positive cells then decreased, reaching the very low numbers seen in control cultures by 8 DIV (Figures 1B and 1E). By quantitative RT-PCR (qRT-PCR), a peak of eye field marker (*Rax*, *Six6*) transcription was detectable at 5 DIV, but it rapidly declined (Figure 1C). Instead, telencephalic markers (*Emx2*, *FoxG1*, *Tbr1*, *Ctip2*) were steadily upregulated from 5 DIV onward (Figure 1C). Thus, differentiation in the presence of Wnt/β-catenin inhibitors converts mESCs to early forebrain progenitors that are competent to express both eye field and telencephalic genes. In the absence of appropriate signals, however, eye field gene transcription is not maintained and telencephalic fates prevail.

Previous work described repression of eye field genes in adherent hESC cultures differentiating in the presence of inhibitors of Activin/Nodal signaling (Lupo et al., 2013). Furthermore, exogenous Activin enhances generation of retinal progenitors in mESCs cultured as floating aggregates in serum-containing media (Ikeda et al., 2005). Notably, bioinformatic analysis of chromatin immunoprecipitation sequencing datasets obtained in mouse and human ESCs indicate that both SMAD2/3 and FOXH1, key components of the Activin/Nodal pathway (Yamamoto et al., 2001), can bind to a highly conserved region located within 2 kb upstream of the *Rax* transcription start site (Figure S1; Kim et al., 2011; Mullen et al., 2011). Thus, the instability of eye field gene transcription in our differentiation system may be due to insufficient activation of Activin/Nodal signaling.

mESCs differentiating to neuroectoderm with our protocol show very low expression of Activin/Nodal ligands, suggesting that Activin/Nodal signaling remains quiescent in these conditions (Bertacchi et al., 2015). Confirming these data, we found that *FoxH1* was barely expressed in either control differentiation conditions or in the presence of Wnti and/or the BMP pathway inhibitor dorsomorphin (BMPi) at 6 DIV but was upregulated by treatments with exogenous Activin (10–100 ng/ml; Figures S2A and S2B). In these assays, weaker upregulation of *FoxH1* in the presence of BMPi (Figure S2B) is likely due to the previously described partial interference of BMPi with the Activin/Nodal pathway (Zhou et al., 2010). As previously described (Besser, 2004), high doses of Activin (50–100 ng/ml) also upregulated *Lefty1/2*, which encode for feedback inhibitors of Activin/Nodal signaling (Meno et al., 1999; Perea-Gomez et al., 2002), whereas genes encoding for other antagonists of this pathway (*Fst*; Hemmati-Brivanlou et al., 1994) were not affected (Figure S3B).

In support of the idea that Activin/Nodal signaling needs to be active for stable eye field gene transcription, simultaneous delivery of both Activin (10 ng/ml) and Wnti during mESC forebrain differentiation (Figure 1A; Figure S1C) increased the fraction of *Rax*-GFP-positive cells at 8–10 DIV compared to cultures treated with Wnti alone (Figures 1B and 1D–1F). Costaining with PAX6 suggested that *Rax*-GFP-positive cells had a retinal progenitor identity (Figures 1G and 1G′). By qRT-PCR at 8 DIV, cultures treated with both Activin and Wnti showed upregulation of eye field markers (*Otx2*, *Six3*, *Rax*, *Six6*, *Tbx3*, *Vsx2*) and downregulation of telencephalic markers (*FoxG1*, *Emx2*, *Tbr1*, *Ctip2*) in comparison with Wnti-treated samples (Figure 1H).

In time course assays, the percentage of *Rax*-GFP-positive cells in Activin-treated cultures, compared to samples treated with Wnti only, was lower at 5–6 DIV and became similar at 6.5 DIV (Figure 1B). From 6.5 DIV, however,

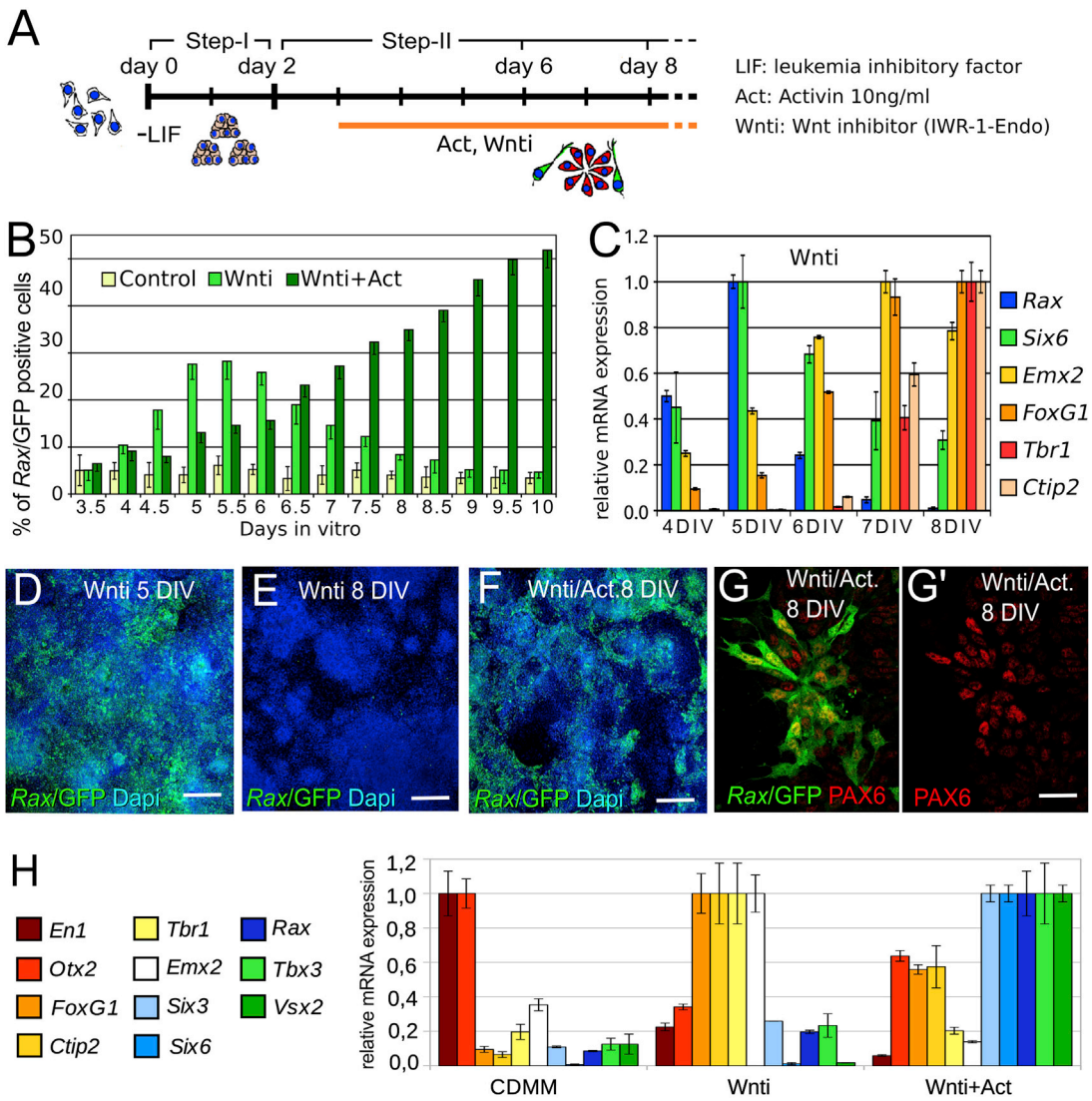

Figure 1. Activin Supports *Rax* Expression in mESC-Derived Early Anterior Neural Progenitors

(A) Scheme of mESC neuroectoderm differentiation with or without Wnti and Activin. Days show the time of mouse ESC differentiation after LIF (−LIF) and serum withdrawal.

(B) Flow cytometry of K/l EB5 cells harvested at different time points showing the percentage of *Rax*-GFP-positive cells during differentiation in plain CDMM (control) or in the presence of Wnti or Wnti and Activin (Wnti+Act), as indicated. Error bars represent SEM (n = 4 independent experiments with n = 3 in vitro technical replicates per experiment; technical replicates were pooled together and analyzed by n = 3 flow cytometry acquisitions).

(C) qRT-PCR quantification of telencephalic (*Emx2*, *FoxG1*, *Tbr1*, *Ctip2*) and eye field (*Rax*, *Six6*) gene expression in cells differentiated in the presence of Wnti and harvested every 24 hr between 4 and 8 DIV. For each analyzed gene, the sample with maximal transcription levels was chosen for normalization, and relative expression levels in all the other samples are shown. Error bars were obtained from the error propagation formula (n = 3 independent biological replicates were pooled together and analyzed by qRT-PCR).

(D–F) GFP immunodetection of cells differentiated in the presence of Wnti or Wnti and Activin (Wnti/Act.). The scale bars represent 50 μm. Dapi, 4′,6-diamidino-2-phenylindole.

(G and G′) Double immunodetection at 8 DIV in cultures treated with Wnti and Activin. The scale bar represents 10 μm.

(H) qRT-PCR of mesencephalic (*En1*, *Otx2*), telencephalic (*Emx2*, *FoxG1*, *Ctip2*, *Tbr1*), and eye field (*Rax*, *Six6*, *Vsx2*, *Six3*, *Otx2*, *Tbx3*) marker expression at 8 DIV in cultures differentiated in control medium (CDMM) or in medium supplemented with Wnti (Wnti) or both Wnti and Activin (10 ng/ml; Wnti+Act). Error bars were obtained from the error propagation formula (n = 3 independent experiments were pooled together and analyzed by qRT-PCR; each experiment contained n = 2 in vitro technical replicates).

See also Figures S1 and S2.

Rax-GFP-positive cells rapidly disappeared in Wnti-treated cultures, whereas their fraction progressively increased in the presence of Activin, nearly reaching 50% at 10 DIV (Figure 1B). Activin treatment delayed mESC neuralization, as shown by enhanced expression of the epiblast markers *Oct4* and *Fgf5* and repression of the neuroectoderm markers *Pax6* and *NCAM* at 6 DIV compared to controls (Figure S2D), thus explaining the later appearance of *Rax*-GFP-positive cells in Activin-treated cultures. Nonetheless, *Oct4* and *Fgf5* were downregulated at 8 DIV (Figure S2D) and neural progenitors expressing *Rax*-GFP, *Pax6*, and other eye field markers (e.g., *Six3*, *Six6*, *Tbx3*) became evident (Figures S2E–S2H). Thus, low doses of Activin can transiently delay neural differentiation in mESCs but, once cells convert to neural progenitors, Activin signaling can steer them toward eye field fates.

We systematically analyzed the effects of Activin/Nodal signaling on neural induction and patterning in mESCs, starting by treating differentiating cells with exogenous Activin at different concentrations. We delivered Activin and Wnti simultaneously from 3 DIV using 10, 50, and 100 ng/ml Activin (Figure S3). Activin caused dose-dependent inhibition of neural progenitor markers (*Sox2*, *Nestin*, *Pax6*, *Musashi*) and upregulation of pluripotency (*Oct4*, *Fgf5*) and mesendoderm (*Gata4*, *Gata6*) markers at 6 DIV (Figures S3B–S3L). The ability of Activin to upregulate expression of eye field markers (*Otx2*, *Six3*, *Rax*, *Six6*, *Vsx2*, *Tbx3*) decreased at higher doses, consistent with a stronger inhibition of neural differentiation (Figure S3M), whereas transcription of the telencephalic markers *Foxg1* and *Emx2* was always repressed (Figure S3M). Activin delivery in the absence of Wnti caused a stronger upregulation of mesendoderm markers (Figure S3B) and a weaker upregulation of eye field markers (Figure S3M) in comparison with treatments with both Wnti and Activin, suggesting that Activin elicits eye field fates specifically in anterior neural progenitors, which form more efficiently when the Wnt/β-catenin pathway is inhibited (Bertacchi et al., 2015). The effects of Activin in the presence of both Wnti and BMPi were similar to those of treatments without BMPi (Figures S3B–S3M), indicating that endogenous BMP signaling does not hinder eye field specification in this system. Treatments with the Activin/Nodal inhibitor SB431542 did not affect expression of eye field or telencephalic markers (Figure S3N), in agreement with the very low endogenous activation of Activin/Nodal signaling in these conditions (Bertacchi et al., 2015). Although these data suggest that Activin can steer pluripotent stem cells differentiating to anterior neuroectoderm toward eye field fates, their interpretation is complicated by the fact that early Activin treatments, in line with previous studies (Lupo et al., 2014; Vallier et al., 2004), interfere with mESC neuralization.

Activin Promotes Eye Field Fates within a Specific Time Window during Differentiation of mESCs to Anterior Neural Progenitors

To distinguish an earlier role of Activin/Nodal signaling in opposing neuroectoderm differentiation from a later role in anterior neural patterning, we focused on a moderate dose of Activin (10 ng/ml), which is more permissive toward mESC neuralization compared to higher doses (Figures S2C and S3), but started the treatments at different time points during anterior neural differentiation. Cultures were treated with Wnti from 3 DIV with or without Activin, which was added starting at the same time point or with increasing delays of 12, 24, 36, or 48 hr (Figure 2A); the percentage of the total cell count that was positive for *Rax*-GFP or OCT4 was then analyzed at 8 DIV. Cultures treated with Wnti alone differentiated efficiently to neuroectoderm (as shown by very few OCT4-positive cells), but they were refractory to eye field specification (5% *Rax*-GFP-positive cells; Figures 2B and 2C). When Activin was added together with Wnti (3 DIV), it promoted eye field specification (26.9% of *Rax*-GFP-positive cells; Figures 2B and 2D) but delayed neuroectoderm differentiation (18.9% of OCT4-positive cells persisting at 8 DIV; Figures 2B and 2D). Delaying the start of Activin treatment by 12–36 hr after Wnti delivery (3.5–4.5 DIV; Figure 2A) nearly doubled the percentage of *Rax*-GFP-positive cells (up to 45.2% *Rax*-GFP-positive cells at 8 DIV; Figures 2B–2G) without delaying differentiation (3% OCT4-positive cells at 8 DIV following Activin treatment from 4 DIV; Figures 2B–2G). No induction of *Rax*-GFP-positive cells was observed when cultures were treated with Activin starting from 5 DIV (5.5% *Rax*-GFP-positive cells at 8 DIV; Figures 2B and 2H). qRT-PCR analyses confirmed that transcription of *Six3*, *Rax*, *Six6*, and *Vsx2* peaked when Activin treatments were started between 12 and 36 hr after Wnti delivery (Figure 2I) but was similar to control (Wnt inhibition alone) levels when applying Activin 48 hr after Wnti (Figure 2I).

Activin treatment conditions causing optimal upregulation of eye field genes were also more effective at downregulating expression of telencephalic markers (Figure 2I). Activin efficiently enhanced eye field gene expression only in cultures treated with Wnti (Figures 2B and 2I), supporting the idea that Activin promotes eye field fates in anterior neural progenitors.

Higher Activin doses (50 ng/ml), even when delivered at 3.5 DIV (Figure S4A), decreased the fraction of *Rax*-GFP-positive cells at 8 DIV, probably due to maintenance of *Oct4* expression and delayed neuroectoderm differentiation (Figures S4B–S4M). Altogether, these results suggest that Activin plays different roles at different stages of mESC differentiation. At early stages (up to 3 DIV), Activin opposes neuroectoderm specification by promoting expression of pluripotency and mesendoderm genes. In

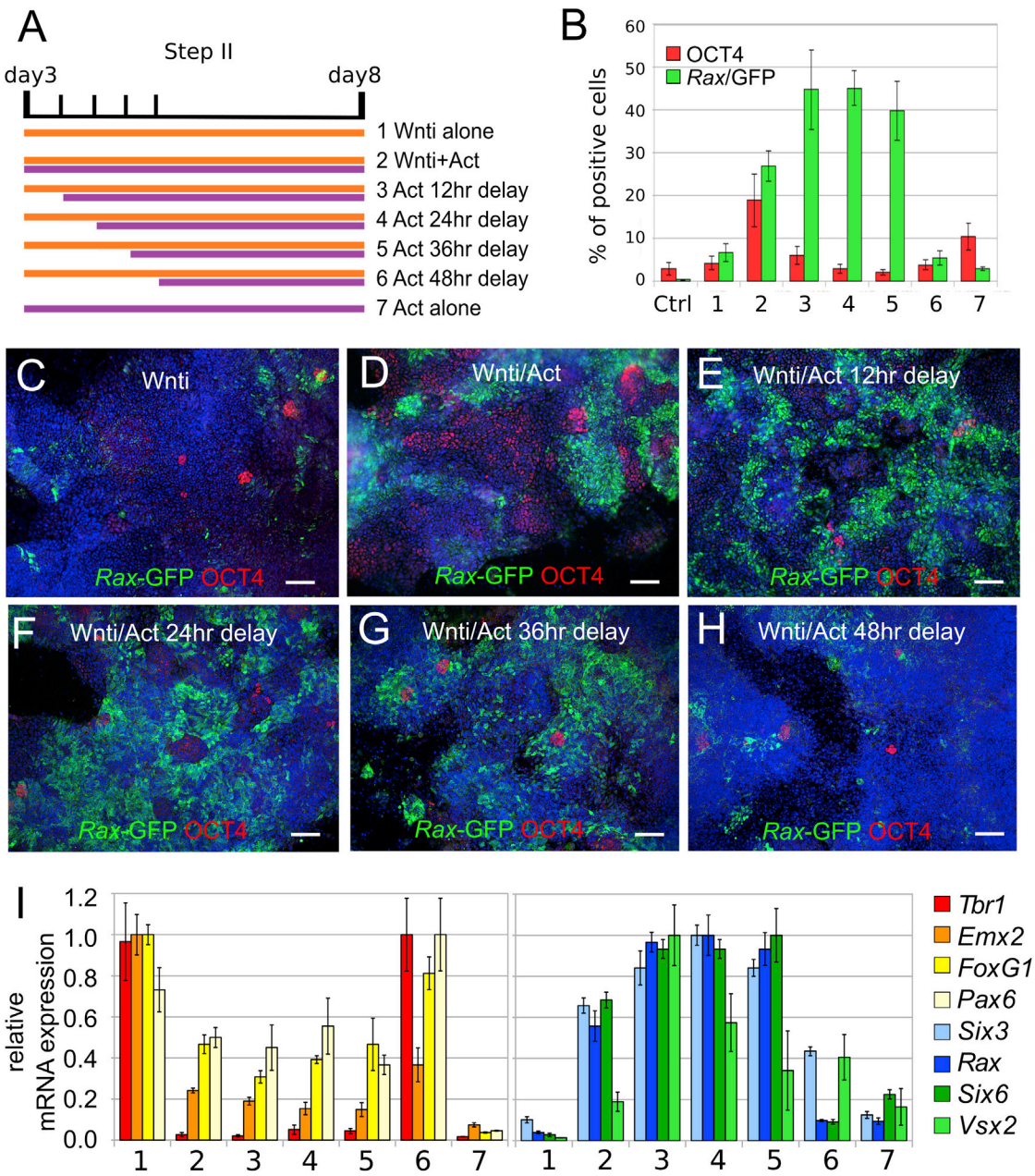

Figure 2. Activin Promotes *Rax* Expression within a Restricted Time Window during mESC Differentiation to Anterior Neuroectoderm

(A) Scheme of temporally controlled Activin treatments.

(B) Percentage of the total K/l EB5 cell count that was positive for OCT4 or *Rax*-GFP. Culture conditions were as in (A). Ctrl, control (CDMM). Error bars represent SEM (n = 3 independent experiments).

(C–H) Representative images of K/l EB5 cells differentiated in the conditions indicated in (A) and immunostained for both GFP and OCT4 at 8 DIV. The scale bars represent 50 μm.

(I) qRT-PCR of neuroectoderm (*Pax6*), telencephalic (*Tbr1*, *Emx2*, *FoxG1*), and eye field (*Six3*, *Rax*, *Six6*, *Vsx2*) gene expression in the conditions indicated in (A). Values are normalized to samples with maximal expression levels. Error bars were obtained from the error propagation formula (n = 3 independent experiments were pooled together; each experiment contained n = 2 technical replicates).

See also Figures S3 and S4.

early anterior neural progenitors, which emerge at 3.5–4.5 DIV in conditions of low Wnt signaling, moderate Activin levels promote eye field fates.

Activin Promotes Formation of *Rax*-Expressing Progenitors Bearing Retinal-Specific Regional Identities

In mouse embryos, strong *Rax* expression is found both in the developing retina and ventral hypothalamus (Wataya et al., 2008). Retinal progenitors express *Rax* and *Pax6*, whereas ventral hypothalamic progenitors express *Rax* and *Nkx2.1* (Ikeda et al., 2005; Wilson and Houart, 2004). Because Wnt inhibition and Activin/Nodal signaling have been implicated in hypothalamic development (Kapsimali et al., 2004; Mathieu et al., 2002), we investigated whether *Rax*-expressing progenitors generated in the presence of Wnti and Activin acquired retinal and/or hypothalamic identities. Sonic Hedgehog (SHH) signaling has a well-established role in promoting hypothalamic development (Ikeda et al., 2005; Wataya et al., 2008). Therefore, to better distinguish *Rax*-positive retinal fates from *Rax*-positive hypothalamic fates, we compared the identity of *Rax*-expressing progenitors forming in Activin-treated cultures with that of *Rax*-positive cells generated in cultures treated with SHH pathway agonists.

Rax-GFP-positive progenitors induced by treating differentiating mESC cultures with both Wnti (from 3 DIV) and Activin (from 3.5 DIV) were mostly PAX6 positive and NKX2.1 negative at 8 DIV (up to 40.7% *Rax*-GFP-positive cells, 32.4% *Rax*-GFP/PAX6 double-positive cells, 2.2% *Rax*-GFP/NKX2.1 double-positive cells; Figure 3), suggesting that they had acquired a retinal identity.

Previous studies indicated that activation of SHH signaling in mESCs differentiating to anterior neuroectoderm led to the specification of ventral hypothalamic progenitors expressing *Rax* and *Nkx2.1* (Wataya et al., 2008). To further confirm that *Rax*-positive cells generated in Activin-treated cultures acquired a retinal, rather than hypothalamic, identity, we generated *Rax*-positive ventral forebrain progenitors by means of treatments with a Smoothened agonist (SAG; 100 nM). SAG was added to differentiating mESC cultures from 3 DIV with or without Wnti. Some of these cultures were also treated with Activin from 3.5 DIV (Figure 3A). SAG robustly increased the percentage of *Rax*-GFP-positive cells (up to 61.6% of the total cell count) at 8 DIV, but only in cultures treated with Wnti (Figures 3B–3D). In contrast to Activin treatments, however, the vast majority of these cells were PAX6 negative and NKX2.1 positive (0.6% *Rax*-GFP/PAX6 double-positive cells, 60% *Rax*-GFP/NKX2.1 double-positive cells; Figures 3B and 3D), indicating acquisition of a ventral hypothalamic identity. NKX2.1-expressing cells were increased by SAG also in the absence of Wnti (65.3% NKX2.1-positive cells), but they were mostly *Rax*-GFP negative (Figures 3B and 3C). Activin and SAG treatments together did not show collaborative effects in the generation of *Rax*-GFP-positive cells, which were mostly PAX6 negative and NKX2.1 positive (Figures 3B–3D). Similar results were obtained when cultures were treated with Activin and different doses of SAG (1, 10, 100 nM; Figures S5A–S5D). Inhibition of SHH signaling with cyclopamine (5 μM) in cultures treated with Activin did not enhance either the generation of *Rax*-GFP-positive cells or the fraction of cells coexpressing *Rax*-GFP and PAX6 (Figures 3B–3D), in agreement with the observation that endogenous SHH signaling is inactive during the early stages of our differentiation protocol (Bertacchi et al., 2015).

Treatments with Wnti and Activin could promote formation of *Rax*-GFP/PAX6-positive (NKX2.1-negative) retinal progenitors even when cells were maintained as floating aggregates until harvesting at 10 DIV (Figures S5E and S5F). Treatments of floating aggregate cultures with Wnti and SAG led to formation of *Rax*-GFP/NKX2.1-positive (PAX6-negative) progenitors. Retinal progenitors were mainly present within superficial layers of Activin-treated cell aggregates, whereas hypothalamic progenitors could be found throughout SAG-treated aggregates. This may be explained by more limited diffusion of exogenous signaling proteins (as compared to small molecules) within cell aggregates.

We further characterized the positional identity of adherent cultures treated with either Wnti and Activin or Wnti and SAG by global transcriptomic analyses. We sorted *Rax*-positive (*Rax*$^+$) or *Rax*-negative (*Rax*$^-$) cells from these cultures at 10 DIV (Figures S6A–S6E) and used them, along with unsorted cells from cultures treated only with Wnti, for microarray-based comparative gene expression profiling with respect to eye, cortex, or hypothalamus/diencephalon explanted from embryonic day 12.5 mouse embryos (Figure 4; Figures S6F–S6H). Pearson correlation analysis indicated that cell cultures and embryonic tissues clustered separately, with high values of correlation among samples of the same category (Figure S6F). Principal component analysis (PCA) confirmed that cultures and tissues formed well-separated groups (Figure S6G). Moreover, it indicated that the large majority of genes whose expression varies among different samples (principal component 1, accounting for 92.7% of variance) is actually not separating them and that only a small ratio of gene expression variance (principal component 2, accounting for 2.2% of variance) is responsible for the difference between cell-culture sample and tissue sample groups (Figure S6G). These analyses suggested that the genes whose expression accounts for differences among different brain regions, and different cell-culture conditions, are few, and that the

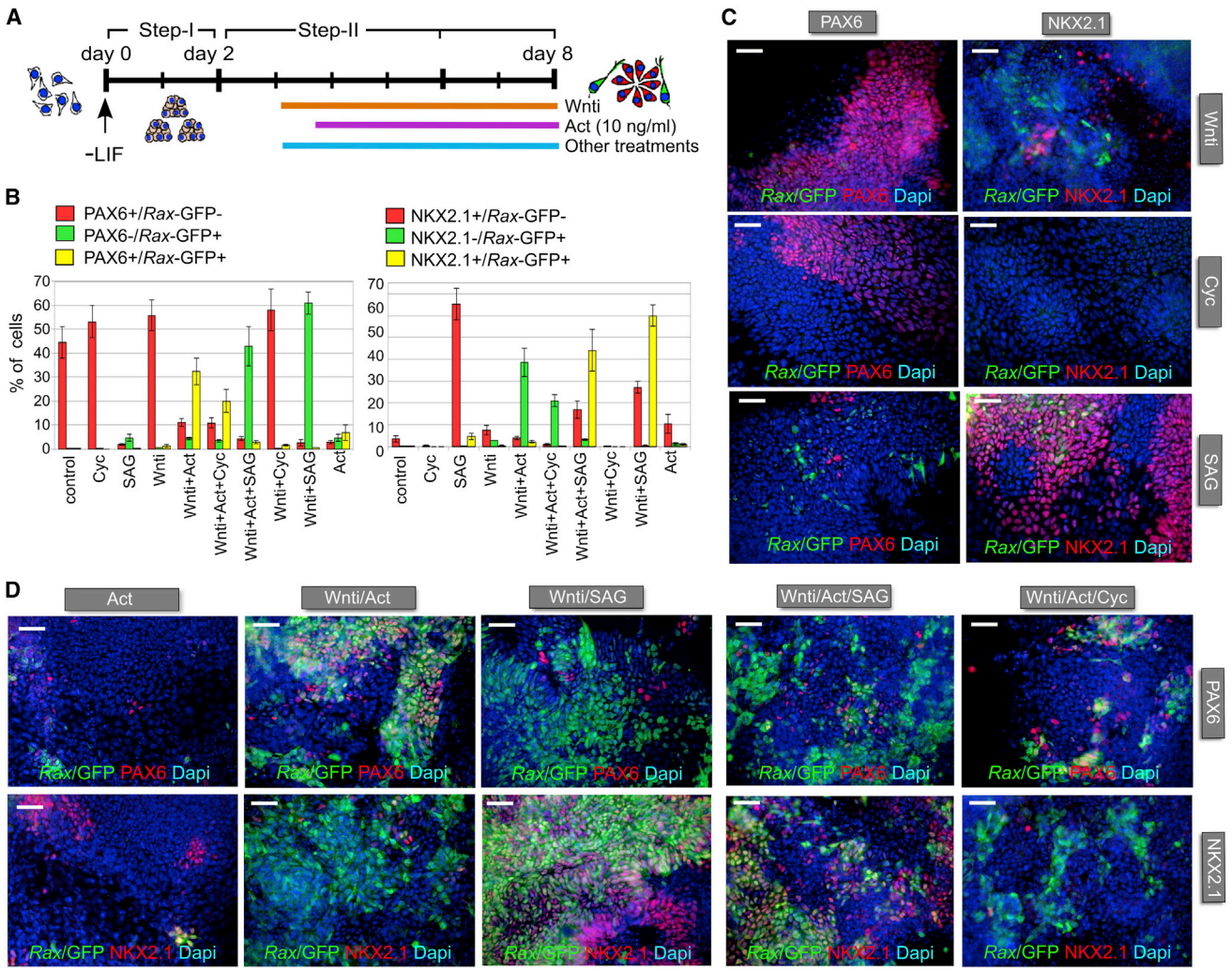

Figure 3. Activin and SHH Signaling Promote Retinal Progenitor or Ventral Forebrain Progenitor Identity, Respectively, in mESCs Differentiating to Anterior Neuroectoderm

(A) Scheme of anterior neural differentiation of mESCs in the presence of different signaling molecules. Activin was applied 12 hr after the start of Wnti treatments, whereas SAG or cyclopamine (Cyc) was delivered simultaneously with Wnti.

(B) Quantification of the percentage of the total K/l EB5 cell count that was positive for *Rax*-GFP and/or PAX6 (left chart) or for *Rax*-GFP and/or NKX2.1 (right chart), as detected by immunodetection at 8 DIV, following differentiation in the indicated conditions. Error bars represent SEM (n = 3 independent experiments).

(C and D) Representative images of K/l EB5 cells differentiated in the indicated conditions at 8 DIV. The scale bars represent 30 μm. See also Figure S5.

variance of their expression is masked by the variance of the rest of the genes. We then performed clustering and PCA on a transcriptome subset, including genes with highest variance among tissues or cultures (see the Experimental Procedures). Analysis of this subset indicated that cells treated with Wnti and Activin clustered with embryonic eye tissue and cells treated with Wnti and SAG clustered with embryonic hypothalamus/diencephalon, whereas control cultures treated with Wnti only clustered with embryonic cortex (Figures 4A and 4B). Notably, the values of correlation among samples of the same category (cell culture or tissue) were quite low, indicating that this subset of genes can discriminate different positional identities in both cell culture and tissue samples, regardless of their in vitro or in vivo origin (Figure 4A). Accordingly, the first two principal components of the PCA, together accounting for 49.8% and 19.3% of variance, respectively, divided the samples into the same three major clusters (corresponding to eye, hypothalamus/diencephalon, and cortex identities) identified by Pearson correlation analysis

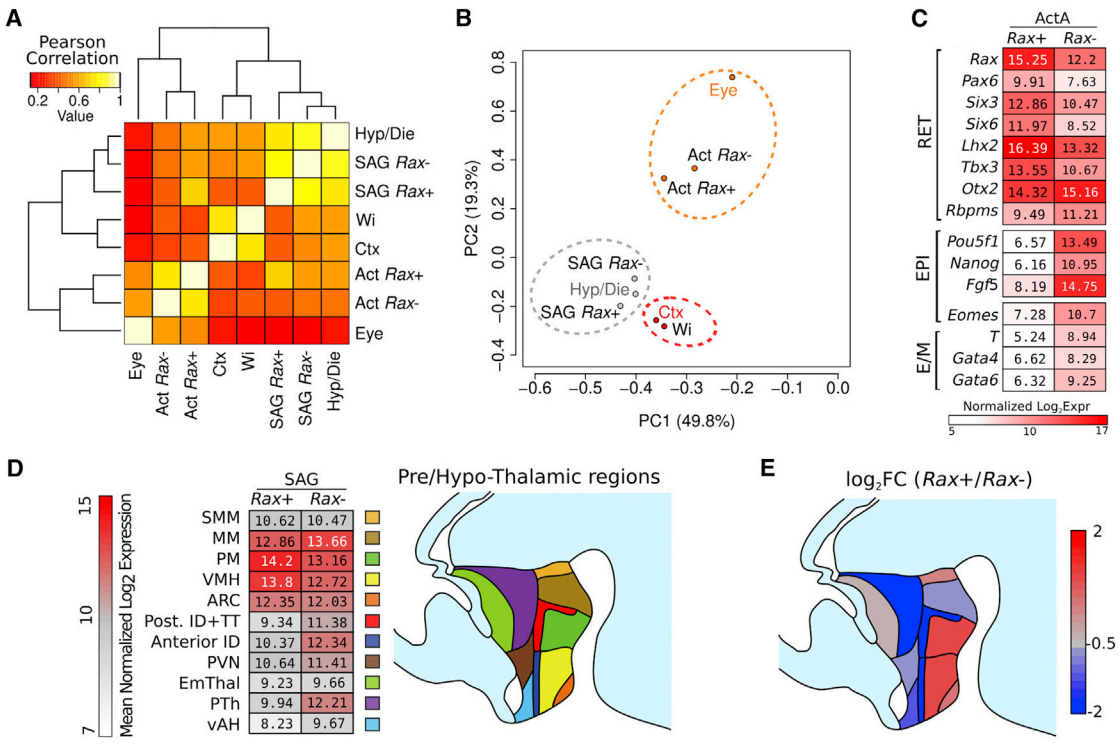

Figure 4. Cultures Treated with Activin or SAG Display Eye or Hypothalamic/Diencephalic Gene Expression Profiles, Respectively

(A) Clustering analysis, showing the distribution of Pearson correlation among transcriptome subsets of different cell cultures and embryonic brain regions. The subset of transcriptome analyzed consists of the 414 gene with the highest variance among cell cultures or tissues (top 2%; see the Experimental Procedures). Hyp/Die, hypothalamus/diencephalon; SAG, SHH agonist; *Rax*$^{+}$ and *Rax*$^{-}$, K/l EB5 cells positive or negative for GFP expression, respectively; Wi, Wnt inhibition; Ctx, cortex; Act, Activin.

(B) PCA of samples as in (A). PC1 and PC2 indicate the first and second principal component, respectively, with percentages of explained variance in parentheses.

(C) Color heatmap showing $\log_2$ mean normalized expression of selected gene subsets, marking retina (RET), epiblast (EPI), or endomesoderm (E/M) cell identity in Activin-treated *Rax*$^{+}$ and *Rax*$^{-}$ cells.

(D) Color heatmap showing $\log_2$ mean normalized expression of selected gene subsets in SAG-treated *Rax*$^{+}$ and *Rax*$^{-}$ cells. Each gene subset marks a specific prethalamic (purple and dark brown) or hypothalamic (other colors) region, as described in Shimogori et al. (2010).

(E) Color heatmap showing the $\log_2$ fold change (FC) ratio of the mean normalized expression values in (D). SMM, supramamillary nucleus; MM, mamillary nucleus; PM, premamillary region; VMH, ventromedial hypothalamic nucleus; ARC arcuate nucleus; ID, intrahypothalamic diagonal region; TT, tuberomamillary terminal region; PVN, paraventricular nucleus; EmThal, eminentia thalami; PTh, prethalamus; vAH, ventral anterior hypothalamus. Tissue samples were obtained from n = 3 embryos (wild-type, Sv129s6 mouse strain, Taconic) and pooled together before RNA extraction. In vitro samples were produced with n = 3 technical replicates; cells were dissociated and pooled together before processing.

See also Figure S6.

(Figure 4B). Unexpectedly, neither analysis was able to neatly separate *Rax*$^{+}$ from *Rax*$^{-}$ cells in cultures treated with Activin or SAG. A closer inspection of each transcriptome contributed to explaining why *Rax*$^{+}$ and *Rax*$^{-}$ cells seemed more homogeneous than expected when compared to embryonic tissues. In cultures treated with Activin, *Rax*$^{-}$ cells expressed higher levels of both epiblast and endo/mesoderm markers in comparison to *Rax*$^{+}$ cells but also appreciable levels of retinal markers, including *Rax*. This suggests that a fraction of these cells had activated *Rax* expression and started retinal differentiation, even if they had not yet accumulated enough GFP fluorescence, and that the ratio of GFP-positive cells at DIV 10 represents an underestimation of the fraction of cells with a retinal gene expression profile. In cultures treated with SAG, both *Rax*$^{+}$ and *Rax*$^{-}$ cells expressed a substantial number of hypothalamic and prethalamic markers (Figure 4C and data not shown). We then extrapolated small subsets of markers that identify distinct hypothalamic and/or prethalamic regions, as previously described (Shimogori et al., 2010; Figure 4C; Figure S6H). This analysis indicated that *Rax*$^{+}$ cells preferentially express markers of ventral

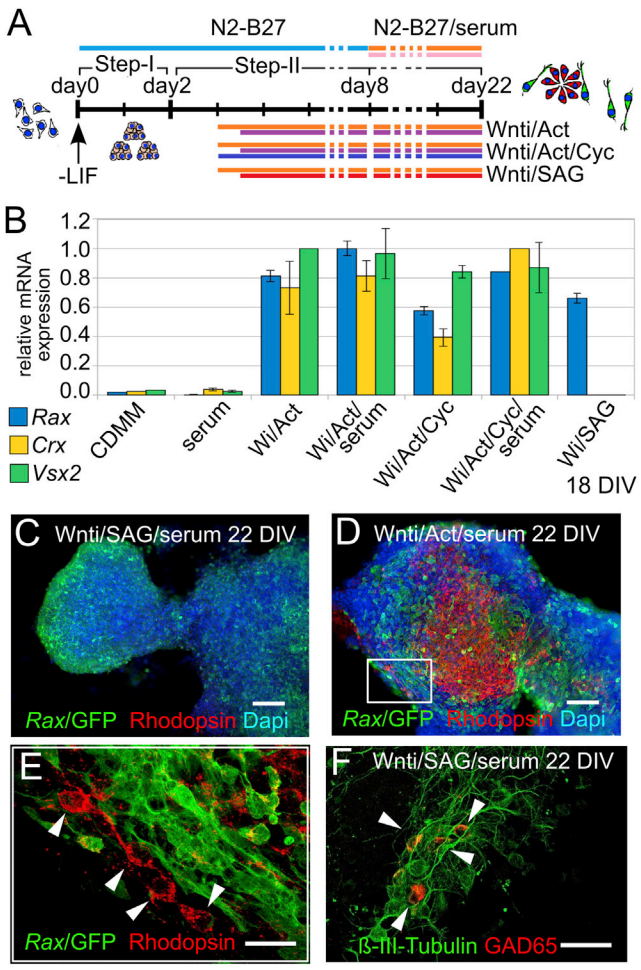

Figure 5. Terminal Differentiation of Activin-Treated Cells or SAG-Treated Cells Generates Rhodopsin-Positive Neurons or Gad65-Positive Neurons, Respectively

(A) Scheme of long-term mESC differentiation in the presence of Wnti and Activin (Wnti/Act), with or without Cyc, or with Wnti and SAG (Wnti/SAG). Activin and SAG were applied 12 hr after the start of Wnti treatments, whereas Cyc was delivered simultaneously with Wnti.

(B) qRT-PCR of retinal marker (*Rax*, *Crx*, *Vsx2*) expression 18 DIV. Results are normalized to samples with maximal expression levels for each marker. Error bars were obtained from the error propagation formula (n = 3 independent experiments).

(C–F) Representative images of K/l EB5 cells differentiated in the indicated conditions at 22 DIV. Rhodopsin-positive cells are indicated by arrowheads in (E). Gad65-positive neurons (27.6% GAD65-positive cells among B-III-Tub-positive neurons) are indicated by arrowheads in (F). The boxed area in (D) is shown at higher magnification in (E). The scale bars represent 30 μm (C and D), 10 μm (E), and 15 μm (F).

See also Figure S7.

hypothalamic regions, whereas *Rax*$^{-}$ cells tend to express markers of more dorsal hypothalamic regions or prethalamic areas (Figure 4D), in agreement with the distribution of *Rax* expression in the developing hypothalamus and diencephalon (Wataya et al., 2008).

Our results suggest that both Activin and SHH signaling are able to drive *Rax* expression in early anterior neural progenitors, but that they work independently of each other promoting alternative cell fates. Different from SHH signaling, Activin supports formation of retinal progenitors coexpressing *Rax* and PAX6, rather than *Rax*-NKX2.1-positive ventral hypothalamic progenitors. To further support these conclusions, we evaluated the ability of *Rax*$^{+}$ progenitors induced by Activin or SAG treatments to undertake a retinal neuron differentiation program in long-term cultures (up to 22 DIV; Figure 5A). Besides *Rax*, cells treated with Wnti and Activin (10 ng/ml, 12-hr delayed treatment), but not SAG, transcribed *Crx*, a marker of immature photoreceptor cells, *Vsx2*, a marker of differentiating bipolar cells, and *Brn3b*, a marker of differentiating retinal ganglion cells, at 18–22 DIV (Figure 5B; Figure S7F). At 22 DIV, cells positive for Rhodopsin, a marker of more mature photoreceptors, were evident in these cultures (Figures 5D and 5E) but not in control or SAG-treated cultures (data not shown). Rhodopsin-positive cells were preferentially located in close proximity to clusters of *Rax*-GFP-positive retinal progenitors, but they showed weak *Rax*-GFP signal themselves (Figures 5D and 5E). This is consistent with the fact that retinal progenitors switch off *Rax* expression when they undergo terminal differentiation (Furukawa et al., 1997a, 1997b). In contrast, SAG-treated long-term cultures produced GAD65-positive neurons (27.6%; Figure 5F). At 22 DIV, cells treated with both Wnti and Activin also upregulated other markers of retinal neuron differentiation in comparison with Wnti-treated samples. In addition to Rhodopsin, Cone Opsin (cones), BRN3 (ganglion cells), VSX2 (bipolar cells), and Recoverin (pan-photoreceptor) were detected in significant percentages of cells (Figures S7A–S7E and S7G). These results suggest that *Rax*-expressing progenitors generated in the presence of Activin mainly acquire a retinal identity, which can be distinguished from SHH-dependent hypothalamic fates.

Activin Promotes Eye Field Gene Expression in Differentiating hESCs

Culture of hESCs as floating aggregates in a chemically defined minimal medium (CDMM) (Vallier et al., 2004) is permissive, to some extent, for differentiation to neural progenitors expressing early anterior neural markers such as *OTX2* and *PAX6* (Patani et al., 2009; Smith et al., 2008; Vallier et al., 2004). We therefore used this straightforward experimental system to address whether Activin

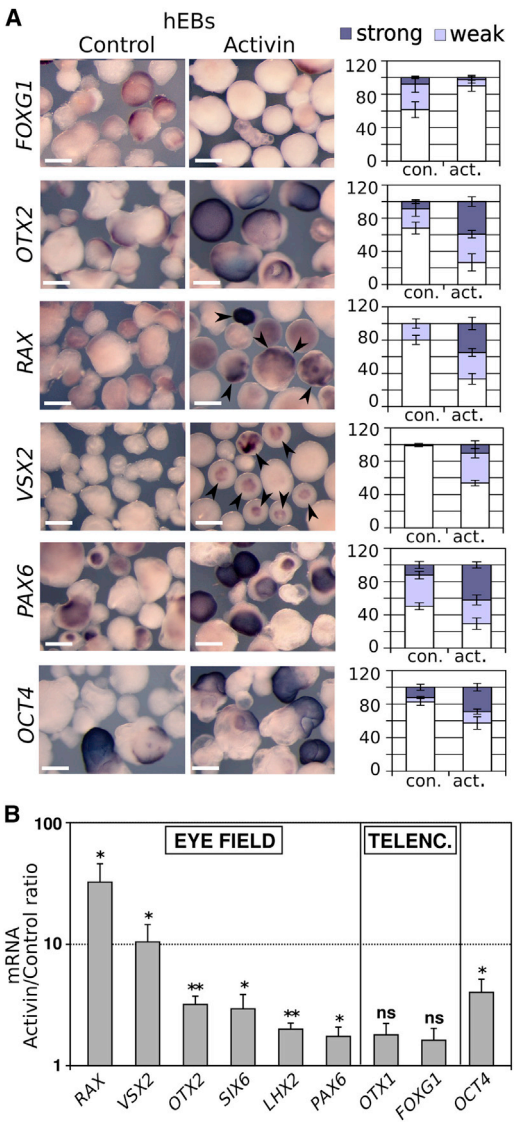

Figure 6. Activin Promotes Eye Field Gene Expression in Differentiating hESCs

(A) In situ hybridization on floating aggregates obtained following a 12-day differentiation of hESCs in nonadherent conditions either in plain CDMM or in the presence of Activin, as indicated. Arrowheads point to *RAX*-positive or *VSX2*-positive aggregates. Bar histograms show the percentage of aggregates displaying strong (dark purple), weak (light blue), or absent (white) signal. The scale bars represent 0.8 mm. Error bars represent SEM. (At least 100 aggregates for each culture condition and probe from one representative experiment were used for these analyses.) hEBs, human embryoid bodies.

(B) qRT-PCR of gene expression in hESCs differentiated as floating aggregates for 12–14 days with or without Activin. Results are shown as the mean ratio between Activin and control conditions. Error bars represent SEM. *$p < 0.05$; **$p < 0.01$; ns, nonsignificant ($p \geq 0.05$) according to Student's t test performed between Activin and control conditions ($n = 8$ independent experiments).

treatments could promote eye field gene expression in differentiating hESCs. hESCs were differentiated as floating aggregates for 12–14 days in basic CDMM or CDMM supplemented with 50 ng/ml Activin. These doses of Activin were chosen to compensate for limited diffusion of exogenous growth factors within hESC aggregates, as previously described (Vallier et al., 2004). Cell aggregates were then harvested for molecular marker analyses by in situ hybridization and qRT-PCR. As detected by in situ hybridization, Activin treatments increased the number of *OCT4*-positive aggregates, although the majority of the aggregates were *OCT4* negative (Figure 6A). Thus, Activin could delay, but not prevent, hESC differentiation in these conditions. Nonetheless, compared with controls, Activin-treated cultures showed stronger expression of eye field markers (*OTX2*, *RAX*, *VSX2*, *PAX6*), but not of the telencephalic marker *FOXG1*, both in terms of percentage of positive aggregates and staining intensity (Figure 6A). qRT-PCR analysis confirmed a significant increase in transcription levels of several eye field markers (*RAX*, *VSX2*, *SIX6*, *OTX2*, *LHX2*, *PAX6*) following Activin treatments, whereas telencephalic markers (*OTX1*, *FOXG1*) were not significantly affected (Figure 6B). These data suggest that Activin can support the expression of eye field genes during differentiation of both mESCs and hESCs.

DISCUSSION

The extracellular signals that induce the EFTF network in retinal progenitors are poorly understood. Although inhibition of BMP and Wnt/β-catenin signaling has been implicated in eye field formation (Cavodeassi et al., 2005; Lan et al., 2009), transient downregulation of these pathways appears to be a prerequisite for the initial specification of the entire secondary prosencephalon. How the telencephalon, eye field, and hypothalamus are then diversified within this prosencephalic tissue remains unclear.

In ESC in vitro systems, culture conditions devoid of exogenous signals or supplemented with inhibitors of endogenous signals were not sufficient for efficient generation of retinal progenitors and they drove instead hypothalamic or telencephalic specification (Bertacchi et al., 2015; Lupo et al., 2013; Nicoleau et al., 2013; Wataya et al., 2008). To date, efficient acquisition of retinal identity has been achieved via poorly defined exogenous cues, including complex extracellular matrices (ECMs) and biological supplements (Lupo et al., 2014; Viczian, 2013; Boucherie et al., 2013; Eiraku et al., 2011; Gonzalez-Cordero et al., 2013; Zhu et al., 2013)

Previous work suggested that Activin/Nodal signaling promotes eye field fates in ESCs. In particular, supplementation of serum and serum replacement media with Activin

increased the production of retinal progenitors from mESCs (Ikeda et al., 2005). Subsequently, a combination of the Nodal and ECM molecules entactin and laminin was found to mimic retinal progenitor induction by Matrigel (Eiraku et al., 2011). Finally, inhibitors of the Activin/Nodal pathway repressed eye field gene expression during neuroectoderm differentiation of hESCs (Lupo et al., 2013). These studies, however, did not clarify the role of Activin/Nodal signaling in retinal progenitor specification.

In this study, we show that Activin promotes eye field fates in mESCs differentiating to anterior neuroectoderm in chemically defined minimal media. Activin effectively upregulated eye field gene expression only when delivered at moderate doses and within a narrow 24-hr time window during early steps of neuroectoderm differentiation. In agreement with previous literature (Lupo et al., 2014; Smith et al., 2008; Vallier et al., 2004), treatments at higher doses and/or earlier time points promoted pluripotency and mesendoderm differentiation and repressed neuroectoderm differentiation, whereas later treatments could not support retinal identity. Moreover, Activin efficiently enhanced eye field specification only in cultures treated with inhibitors of Wnt/β-catenin signaling, which promote anterior neural fates at the expense of posterior fates in differentiating ESCs (Bertacchi et al., 2013; Lupo et al., 2013, 2014; Nicoleau et al., 2013). Hence, the effects of Activin are dependent on the competence of the responding cells: we speculate that Activin can upregulate eye field genes in primitive forebrain progenitors, but not in pluripotent cells, later forebrain progenitors, or posterior neural progenitors. We observed Activin-dependent upregulation of eye field genes in either adherent or floating aggregate cultures. Activin enhanced eye field gene expression also in hESCs differentiating as floating aggregates in chemically defined medium devoid of ECM components and serum replacement, indicating that the ability of Activin to promote eye field fates is not limited to mouse ESCs or to a specific cell line or culture method.

In mouse embryos, both the developing retina and the ventral hypothalamus show strong *Rax* expression (Ikeda et al., 2005; Wataya et al., 2008; Wilson and Houart, 2004). Consistent with previous studies (Ikeda et al., 2005; Wataya et al., 2008), we confirmed that SHH agonists upregulated *Rax* in mESCs but in the context of ventral hypothalamic specification, because *Rax*-expressing cells were positive for NKX2.1 and negative for PAX6. Upon terminal differentiation, these cultures generated GAD65-positive neurons. Side-by-side comparison of Activin and SAG treatments confirmed that the effects of these molecules were clearly distinguishable. Activin, but not SAG, supported specification of *Rax*-PAX6-positive retinal progenitors, which were endowed with transcriptomic profiles clustering with those of embryonic eye tissue and were capable of undertaking retinal neuron differentiation in long-term cultures.

Activin/Nodal signaling controls early vertebrate development at multiple levels, and it is difficult to distinguish direct roles in eye development from indirect effects. Forebrain and eye formation are affected in fish and mouse mutants with defective Activin/Nodal signaling (Lu and Robertson, 2004; Varlet et al., 1997; Wilson and Houart, 2004), but these effects are likely due to the disruption of mesendodermal signaling centers required for rostral neuroectoderm formation (Wilson and Houart, 2004). Excessive Activin/Nodal signaling, however, can repress anterior neural fates by maintaining pluripotency and/or promoting mesendoderm differentiation within the ectoderm (Thisse et al., 2000; Vallier et al., 2004). Anterior neural induction occurs prematurely in the epiblast of *Nodal* mouse mutants (Camus et al., 2006), but although telencephalic genes are upregulated in Nodal-deficient anterior neuroectoderm, eye field markers (*Six3* and *Pax6*) are not properly expressed (Camus et al., 2006). Furthermore, during eye morphogenesis, eye field cells migrating laterally to form the optic vesicles become exposed to Activin-like signals released by extraocular tissues. Although these signals are involved in retinal pigment epithelium and anterior eye segment specification (Fuhrmann et al., 2000; Ittner et al., 2005), they might also support retinal progenitor identity. Highlighting the complex functions of Activin/Nodal signaling in eye development, recent studies in *Xenopus* found opposite effects of Nodal signaling inhibition on the specification of retinal identity using different experimental assays (Messina et al., 2015; Wong et al., 2015). Clearly, the roles of Activin/Nodal signaling in eye formation are much more difficult to dissect in vivo than they are in vitro, and further investigations in animal model organisms are warranted.

The results described in this and previous studies using ESC in vitro systems (Bertacchi et al., 2013, 2015; Lupo et al., 2013, 2014) lead to a model of the role of the Activin/Nodal pathway in the specification of retinal identity (Figure 7). In this model, downregulation of Activin/Nodal signaling in pluripotent cells leads to the emergence of early anterior neural progenitors, which can acquire rostral forebrain fates (corresponding to progenitors of the secondary prosencephalon in vivo) or caudal forebrain fates (corresponding to progenitors of the diencephalic/mesencephalic regions in vivo) depending on the levels of Wnt/β-catenin signaling, as previously described (Lupo et al., 2014 and references therein). Without further signaling, primitive rostral forebrain progenitors spontaneously evolve toward a default cortical identity (Bertacchi et al., 2013; Lupo et al., 2014), whereas they can be steered to retinal fates under the influence of Activin. As in

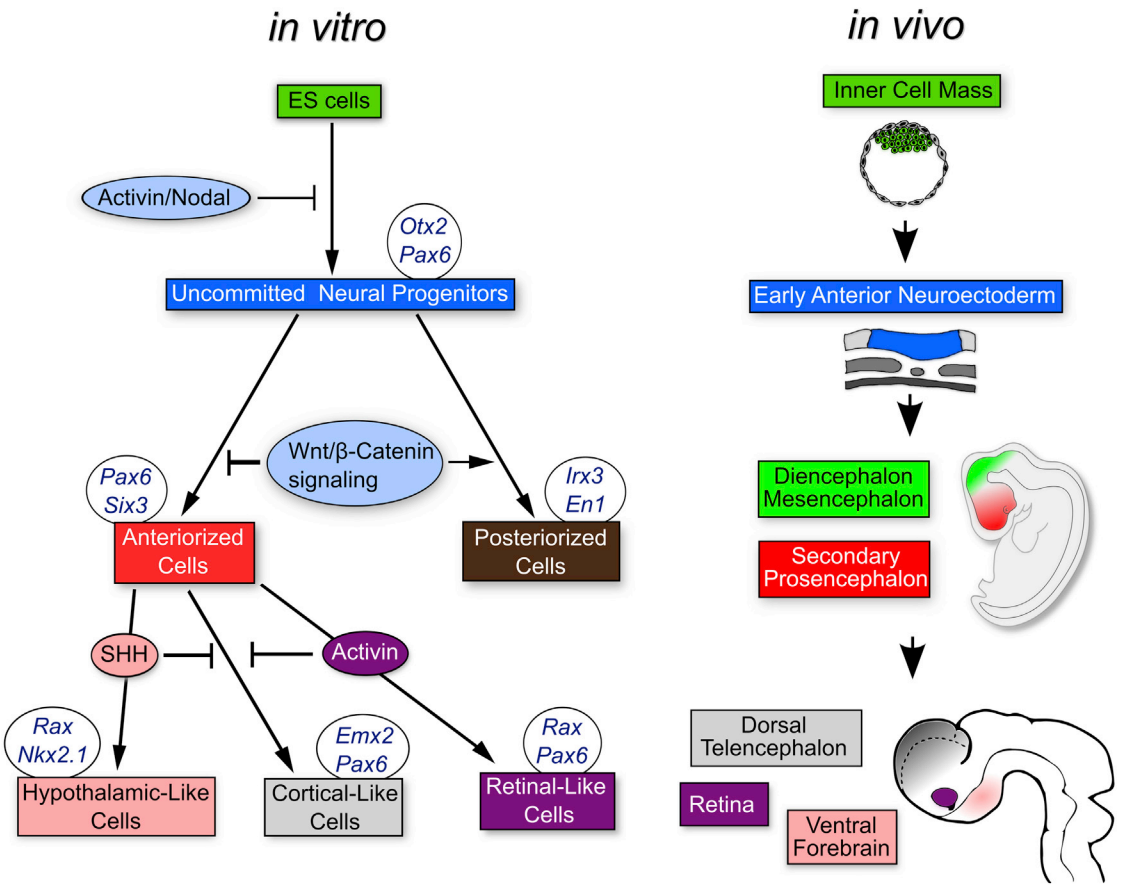

Figure 7. Model of the Roles of the Activin/Nodal, Wnt/β-Catenin, and SHH Signaling Pathways in the Induction of Rostral Forebrain Precursors

Embryonic structures and stages of mouse development in vivo corresponding to the progressively more fate-restricted progenitors emerging during ESC differentiation in vitro are shown. See text for details.

previous studies (Ikeda et al., 2005; Wataya et al., 2008), SHH signaling instead promotes ventral hypothalamic fates. Although more work is needed to address the function of Activin/Nodal signals during early eye development in vivo, this model provides a framework for future studies aimed at clarifying the mechanisms of eye field formation and producing retinal progenitors for basic research or therapy.

EXPERIMENTAL PROCEDURES

Murine ESC lines E14Tg2A (passages 25–38) and K/l EB5 (transgenic Rax-GFP ESCs, used with the kind permission of Y. Sasai, RIKEN Center) and H9 hESCs (WiCell) were cultured as described (Bertacchi et al., 2013; Lupo et al., 2013). All animal protocols were reviewed and approved by the Animal Protocol Review Committee at ITB-CNR of Pisa.

Detailed experimental procedures are available in Supplemental Information.

ACCESSION NUMBERS

The accession number for the microarray gene expression data reported in this paper is GEO: GSE71830.

SUPPLEMENTAL INFORMATION

Supplemental Information includes Supplemental Experimental Procedures and seven figures and can be found with this article online at http://dx.doi.org/10.1016/j.stemcr.2015.08.011.

ACKNOWLEDGMENTS

We are grateful to Morgan Alexander for help with hESC culture. We thank Kawssar Harb and Joséphine Parisot for their kind help with confocal imaging, and Elena Chiavacci for her hints about in situ hybridization. This work was supported by the Biotechnology and Biological Sciences Research Council (W.A.H., G.L.), Wellcome Trust (W.A.H.), Italian Ministry of Education, University and Research programme "Rientro dei Cervelli" and a start-up grant from Istituto Pasteur-Fondazione Cenci Bolognetti (G.L.),

Medical Research Council (R.A.P.), Flagship Project InterOmics PB.05, and Italian Ministry of Education, University and Research grant PRIN-2102 (F.C.).

Received: March 19, 2015
Revised: August 21, 2015
Accepted: August 21, 2015
Published: September 17, 2015

REFERENCES

Andoniadou, C.L., and Martinez-Barbera, J.P. (2013). Developmental mechanisms directing early anterior forebrain specification in vertebrates. Cell. Mol. Life Sci. *70*, 3739–3752.

Bertacchi, M., Pandolfini, L., Murenu, E., Viegi, A., Capsoni, S., Cellerino, A., Messina, A., Casarosa, S., and Cremisi, F. (2013). The positional identity of mouse ES cell-generated neurons is affected by BMP signaling. Cell. Mol. Life Sci. *70*, 1095–1111.

Bertacchi, M., Pandolfini, L., D'Onofrio, M., Brandi, R., and Cremisi, F. (2015). The double inhibition of endogenously produced BMP and Wnt factors synergistically triggers dorsal telencephalic differentiation of mouse ES cells. Dev. Neurobiol. *75*, 66–79.

Besser, D. (2004). Expression of Nodal, Lefty-A, and Lefty-B in undifferentiated human embryonic stem cells requires activation of Smad2/3. J. Biol. Chem. *279*, 45076–45084.

Boucherie, C., Mukherjee, S., Henckaerts, E., Thrasher, A.J., Sowden, J.C., and Ali, R.R. (2013). Brief report: self-organizing neuroepithelium from human pluripotent stem cells facilitates derivation of photoreceptors. Stem Cells *31*, 408–414.

Camus, A., Perea-Gomez, A., Moreau, A., and Collignon, J. (2006). Absence of Nodal signaling promotes precocious neural differentiation in the mouse embryo. Dev. Biol. *295*, 743–755.

Cavodeassi, F., Carreira-Barbosa, F., Young, R.M., Concha, M.L., Allende, M.L., Houart, C., Tada, M., and Wilson, S.W. (2005). Early stages of zebrafish eye formation require the coordinated activity of Wnt11, Fz5, and the Wnt/beta-catenin pathway. Neuron *47*, 43–56.

Eiraku, M., Takata, N., Ishibashi, H., Kawada, M., Sakakura, E., Okuda, S., Sekiguchi, K., Adachi, T., and Sasai, Y. (2011). Self-organizing optic-cup morphogenesis in three-dimensional culture. Nature *472*, 51–56.

Fuhrmann, S., Levine, E.M., and Reh, T.A. (2000). Extraocular mesenchyme patterns the optic vesicle during early eye development in the embryonic chick. Development *127*, 4599–4609.

Furukawa, T., Kozak, C.A., and Cepko, C.L. (1997a). rax, a novel paired-type homeobox gene, shows expression in the anterior neural fold and developing retina. Proc. Natl. Acad. Sci. USA *94*, 3088–3093.

Furukawa, T., Morrow, E.M., and Cepko, C.L. (1997b). Crx, a novel otx-like homeobox gene, shows photoreceptor-specific expression and regulates photoreceptor differentiation. Cell *91*, 531–541.

Gonzalez-Cordero, A., West, E.L., Pearson, R.A., Duran, Y., Carvalho, L.S., Chu, C.J., Naeem, A., Blackford, S.J.I., Georgiadis, A., Lakowski, J., et al. (2013). Photoreceptor precursors derived from three-dimensional embryonic stem cell cultures integrate and mature within adult degenerate retina. Nat. Biotechnol. *31*, 741–747.

Hemmati-Brivanlou, A., Kelly, O.G., and Melton, D.A. (1994). Follistatin, an antagonist of activin, is expressed in the Spemann organizer and displays direct neuralizing activity. Cell *77*, 283–295.

Ikeda, H., Osakada, F., Watanabe, K., Mizuseki, K., Haraguchi, T., Miyoshi, H., Kamiya, D., Honda, Y., Sasai, N., Yoshimura, N., et al. (2005). Generation of Rx+/Pax6+ neural retinal precursors from embryonic stem cells. Proc. Natl. Acad. Sci. USA *102*, 11331–11336.

Ittner, L.M., Wurdak, H., Schwerdtfeger, K., Kunz, T., Ille, F., Leveen, P., Hjalt, T.A., Suter, U., Karlsson, S., Hafezi, F., et al. (2005). Compound developmental eye disorders following inactivation of TGFbeta signaling in neural-crest stem cells. J. Biol. *4*, 11.

Kapsimali, M., Caneparo, L., Houart, C., and Wilson, S.W. (2004). Inhibition of Wnt/Axin/beta-catenin pathway activity promotes ventral CNS midline tissue to adopt hypothalamic rather than floorplate identity. Development *131*, 5923–5933.

Kim, S.W., Yoon, S.-J., Chuong, E., Oyolu, C., Wills, A.E., Gupta, R., and Baker, J. (2011). Chromatin and transcriptional signatures for Nodal signaling during endoderm formation in hESCs. Dev. Biol. *357*, 492–504.

Lan, L., Vitobello, A., Bertacchi, M., Cremisi, F., Vignali, R., Andreazzoli, M., Demontis, G.C., Barsacchi, G., and Casarosa, S. (2009). Noggin elicits retinal fate in *Xenopus* animal cap embryonic stem cells. Stem Cells *27*, 2146–2152.

Lu, C.C., and Robertson, E.J. (2004). Multiple roles for Nodal in the epiblast of the mouse embryo in the establishment of anterior-posterior patterning. Dev. Biol. *273*, 149–159.

Lupo, G., Novorol, C., Smith, J.R., Vallier, L., Miranda, E., Alexander, M., Biagioni, S., Pedersen, R.A., and Harris, W.A. (2013). Multiple roles of Activin/Nodal, bone morphogenetic protein, fibroblast growth factor and Wnt/β-catenin signalling in the anterior neural patterning of adherent human embryonic stem cell cultures. Open Biol. *3*, 120167.

Lupo, G., Bertacchi, M., Carucci, N., Augusti-Tocco, G., Biagioni, S., and Cremisi, F. (2014). From pluripotency to forebrain patterning: an in vitro journey astride embryonic stem cells. Cell. Mol. Life Sci. *71*, 2917–2930.

Mathieu, J., Barth, A., Rosa, F.M., Wilson, S.W., and Peyriéras, N. (2002). Distinct and cooperative roles for Nodal and Hedgehog signals during hypothalamic development. Development *129*, 3055–3065.

Meno, C., Gritsman, K., Ohishi, S., Ohfuji, Y., Heckscher, E., Mochida, K., Shimono, A., Kondoh, H., Talbot, W.S., Robertson, E.J., et al. (1999). Mouse Lefty2 and zebrafish antivin are feedback inhibitors of nodal signaling during vertebrate gastrulation. Mol. Cell *4*, 287–298.

Messina, A., Lan, L., Incitti, T., Bozza, A., Andreazzoli, M., Vignali, R., Cremisi, F., Bozzi, Y., and Casarosa, S. (2015). Noggin-mediated retinal induction reveals a novel interplay between bone morphogenetic protein inhibition, transforming growth factor β, and Sonic Hedgehog signaling. Stem Cells *33*, 2496–2508.

Mullen, A.C., Orlando, D.A., Newman, J.J., Lovén, J., Kumar, R.M., Bilodeau, S., Reddy, J., Guenther, M.G., DeKoter, R.P., Young, R.A.,

et al. (2011). Chromatin and transcriptional signatures for Nodal signaling during endoderm formation in hESCs. Cell *147*, 492–504.

Nicoleau, C., Varela, C., Bonnefond, C., Maury, Y., Bugi, A., Aubry, L., Viegas, P., Bourgois-Rocha, F., Peschanski, M., and Perrier, A.L. (2013). Embryonic stem cells neural differentiation qualifies the role of Wnt/β-catenin signals in human telencephalic specification and regionalization. Stem Cells *31*, 1763–1774.

Patani, R., Compston, A., Puddifoot, C.A., Wyllie, D.J.A., Hardingham, G.E., Allen, N.D., and Chandran, S. (2009). Activin/Nodal inhibition alone accelerates highly efficient neural conversion from human embryonic stem cells and imposes a caudal positional identity. PLoS ONE *4*, e7327.

Perea-Gomez, A., Vella, F.D.J., Shawlot, W., Oulad-Abdelghani, M., Chazaud, C., Meno, C., Pfister, V., Chen, L., Robertson, E., Hamada, H., et al. (2002). Nodal antagonists in the anterior visceral endoderm prevent the formation of multiple primitive streaks. Dev. Cell *3*, 745–756.

Shimogori, T., Lee, D.A., Miranda-Angulo, A., Yang, Y., Wang, H., Jiang, L., Yoshida, A.C., Kataoka, A., Mashiko, H., Avetisyan, M., et al. (2010). A genomic atlas of mouse hypothalamic development. Nat. Neurosci. *13*, 767–775.

Smith, J.R., Vallier, L., Lupo, G., Alexander, M., Harris, W.A., and Pedersen, R.A. (2008). Inhibition of Activin/Nodal signaling promotes specification of human embryonic stem cells into neuroectoderm. Dev. Biol. *313*, 107–117.

Thisse, B., Wright, C.V., and Thisse, C. (2000). Activin- and Nodal-related factors control antero-posterior patterning of the zebrafish embryo. Nature *403*, 425–428.

Vallier, L., Reynolds, D., and Pedersen, R.A. (2004). Nodal inhibits differentiation of human embryonic stem cells along the neuroectodermal default pathway. Dev. Biol. *275*, 403–421.

Varlet, I., Collignon, J., and Robertson, E.J. (1997). nodal expression in the primitive endoderm is required for specification of the anterior axis during mouse gastrulation. Development *124*, 1033–1044.

Viczian, A.S. (2013). Advances in retinal stem cell biology. J. Ophthalmic Vis. Res. *8*, 147–159.

Wataya, T., Ando, S., Muguruma, K., Ikeda, H., Watanabe, K., Eiraku, M., Kawada, M., Takahashi, J., Hashimoto, N., and Sasai, Y. (2008). Minimization of exogenous signals in ES cell culture induces rostral hypothalamic differentiation. Proc. Natl. Acad. Sci. USA *105*, 11796–11801.

Wilson, S.W., and Houart, C. (2004). Early steps in the development of the forebrain. Dev. Cell *6*, 167–181.

Wong, K.A., Trembley, M., Abd Wahab, S., and Viczian, A.S. (2015). Efficient retina formation requires suppression of both Activin and BMP signaling pathways in pluripotent cells. Biol. Open *4*, 573–583.

Yamamoto, M., Meno, C., Sakai, Y., Shiratori, H., Mochida, K., Ikawa, Y., Saijoh, Y., and Hamada, H. (2001). The transcription factor FoxH1 (FAST) mediates Nodal signaling during anterior-posterior patterning and node formation in the mouse. Genes Dev. *15*, 1242–1256.

Zhou, J., Su, P., Li, D., Tsang, S., Duan, E., and Wang, F. (2010). High-efficiency induction of neural conversion in human ESCs and human induced pluripotent stem cells with a single chemical inhibitor of transforming growth factor beta superfamily receptors. Stem Cells *28*, 1741–1750.

Zhu, Y., Carido, M., Meinhardt, A., Kurth, T., Karl, M.O., Ader, M., and Tanaka, E.M. (2013). Three-dimensional neuroepithelial culture from human embryonic stem cells and its use for quantitative conversion to retinal pigment epithelium. PLoS ONE *8*, e54552.